LCH Laboratoire de Constructions Hydrauliques
Laboratory of Hydraulic Constructions

ÉCOLE POLYTECHNIQUE
FÉDÉRALE DE LAUSANNE

Communication 68

Development of a methodology for extreme flood estimations in alpine catchments for the verification of dam safety

Fränz Zeimetz

Editeur : Prof. Dr A. Schleiss

Lausanne, 2017

Communications du Laboratoire de Constructions Hydrauliques ISSN 1661-1179
Ecole Polytechnique Fédérale de Lausanne
Editeur: Prof. Dr A. Schleiss

Preface

Dams are critical infrastructures which may be endangered by natural hazards as extreme foods. The water release structures especially the spillways must be designed in such a way that they can ensure the safe passage of extreme floods. Uncontrolled overtopping of the dam cannot be accepted since it may result in its failure. The estimation of the design and the safety flood to take into account for the determination of the spillway capacity is a complex and difficult task in alpine regions. Dr. Fränz Zeimetz proposes a new and validated methodology for the estimation of extreme floods in alpine catchment based on several scientific developments which could close some relevant gaps of knowledge. The first question addressed by Dr. Zeimetz concerns the temporal rainfall distribution based on the existing Swiss PMP maps. The candidate could show by a comprehensive analysis that a unique rainfall mass curve (RMC) can be adopted for the entire territory of Switzerland. Another open question is the temperature gradient in the atmosphere to take to into account for extreme flood simulations. Regarding a coherent combination of temperature and extreme precipitations, Dr. Zeimetz could develop linear relations between the duration of the precipitation event and the zero-degree isothermal altitude. When using hydrological modelling, the influence of the initial conditions for extreme flood simulations has to be assessed. Based on an extensive analysis of the model state variables, Dr. Zeimetz could develop methodological recommendations for the choice of the initial conditions for extreme flood simulations. Furthermore, he could define the maximum admissible area of the catchment area for which the PMP events derived from the Swiss PMP maps can be still applied. Dr. Zeimetz could also show that the combination of the simulation results with the approach of upper bounded statistical extrapolations has the advantage that the sample sensitivity can be reduced and that the plausibility of the extrapolations is enhanced compared to conventional statistical distributions. Finally, Dr. Zeimetz could formulate a new holistic methodology for extreme flood estimations which he illustrated with three application examples. Based on the PMP-PMF approach the methodology allows to estimate extreme flood hydrographs using hydrological simulation and to attribute a return period to the simulated peak discharge using deterministically determined upper discharge limit.

We would like to thank the members of the jury, Dr. Georges Darbre from the Swiss Federal Office of Energy (SFOE), Prof. Bettina Schaefli, from the University of Lausanne, Switzerland and Prof. Peter Molnar from IFU-ETH Zurich, Switzerland for their helpful suggestions. Finally, we also thank gratefully the Swiss Federal Office of Energy (SFOE) – Supervision of dams for their financial support under contract No. SI/500804-1.

Lausanne, 23rd February 2017 Prof. Dr. Anton Schleiss

Words cannot lend impressiveness to the simple statement that only nine or ten families in Woodvale (a suburb of Johnstown) were not deprived of a father, mother, brother, or sister... Two hundred and fifty-five habitations were swept away, leaving not one house in Woodvale proper.. Woodvale had ceased to exist!

—J.J. McLaurin, Survivor of the Johnstown Flood of 1889

To my family.


CRUEX
++

Abstract

In the context of dam safety, reliable safety flood estimation methods are necessary to guarantee a sufficiently designed spillway capacity. Today's state of the art allows to approach this topic under different angles. Statistical extrapolations are common practice, but do not grant to address all needs of dam safety verifications. Due to the evolution of informatics in the last years, computational power has been pushed to a level where hydrological modelling can be performed under optimal conditions. Practitioners are, however, not yet very familiar with hydrological modelling and its potential is not completely exploited.

The present research work develops an approach combining statistics and hydrological modelling techniques to propose an innovative ready-to-use methodology to address the complex issue of extreme flood estimations. In order for this to be successful, some lacks of scientific knowledge had to be addressed before dwelling on the combination between statistics and simulations. Concerning the temporal rainfall distribution, it could be shown that a unique rainfall mass curve is admissible for the entire territory of Switzerland. Regarding a coherent combination of temperature and extreme precipitations, linear relations between the duration of the precipitation event and the zero degree isothermal altitude could be determined. In the context of hydrological modelling, the influence of initial conditions for extreme flood simulations have been assessed and methodological recommendations for the choice of initial conditions for extreme flood simulations could be formulated. Furthermore, the maximum admissible spatial expansion of the PMP events derived from the Swiss PMP maps, elaborated during the CRUEX project, could be estimated to be 230 km^2. Finally, the combination of the simulation results with the approach of upper bounded statistical extrapolations could be shown to be advantageous: the sample sensitivity is reduced and the plausibility of the extrapolations is enhanced compared to conventional statistical distributions.

Besides these scientific challenges, the methodology has to be pragmatic and ready-to-use as it is destined to engineers. The methodology was developed to be easily communicable. Therefore, its development has been undertaken under respect of common practices.

Ultimately, a holistic methodology for extreme flood estimations could be formulated. The main advantage of the methodology is that it allows to estimate extreme flood hydrographs using hydrological simulation and to plausibly attribute a return period to the simulated peak discharge taking a deterministically determined upper discharge limit into account by referring to the PMP-PMF approach. The methodology combines thus the possibility of flood routing estimations with the knowledge of the occurrence probability of the peak discharge of the event, that is normally a reference quantity in flood safety guidelines.

The application of the developed methodology to three catchments with different characteristics could prove its ease of utilization and, more importantly, its advantages compared to conventional approaches. A computer tool could be developed to make the CRUEX++ methodology accessible and readily applicable.

Keywords

dam safety, alpine catchments, safety flood, statistical distributions, hydrological modelling, temporal rainfall distribution, precipitation-temperature scaling, initial model conditions, PMP-PMF, upper bounded statistical distributions, extreme flood estimation methodology

Résumé

Dans le cadre de la sécurité des barrages, des méthodes fiables pour l'estimation des crues de sécurité sont une nécessité afin de garantir une capacité suffisante des évacuateurs de crues. L'état de l'art actuel permet d'aborder ce sujet sous différents angles. Les extrapolations statistiques sont une pratique commune, mais ne sont pas suffisantes pour satisfaire tous les besoins des vérifications de sécurité des barrages. Grâce à l'évolution des ressources informatiques lors de dernières années, la puissance de calcul des ordinateurs a pu être amenée au degré où la modélisation hydrologique peut être effectuée dans des conditions de calcul optimales. Cependant, les praticiens n'ont souvent pas l'habitude de la modélisation hydrologique. Il s'en suit que le potentiel de la modélisation hydrologique n'est pas complètement exploité par les ingénieurs.

Ce projet de recherche a permis de développer une approche combinant les statistiques et la modélisation hydrologique afin de formuler une méthodologie innovatrice et prêt à l'emploi pour adresser la problématique complexe des estimations de crues extrêmes. De sorte à ce que ce développement puisse être réussi, la résolution d'un certain nombre de lacunes de connaissance scientifiques a due être abordée avant d'insister sur la combinaison entre statistiques et simulations. Concernant la distribution temporelle des précipitations, il a été possible de montrer qu'une structure unique est admissible pour l'entité du territoire suisse. Au sujet d'un couple cohérent précipitation-température, une relation linéaire entre le durée de la précipitation et l'altitude de l'isotherme 0°C a pu être déterminée. Dans le contexte de la modélisation hydrologique, l'influence des conditions initiales a pu être évaluée et des recommandations méthodologiques pour le choix des conditions initiales pour des estimations de crues extrêmes ont pu être formulées. En outre, l'expansion maximum admissible pour un événement de PMP dérivé des cartes PMP suisses, élaborées au cours du projet CRUEX, a pu être estimé à 230 km^2. Enfin, l'avantage de la combinaison des résultats de simulations et des distributions statistiques à borne supérieure a pu être démontré: la sensibilité des extrapolations aux échantillons est réduite et les résultats d'extrapolation sont plus plausibles comparés aux distributions conventionnelles non bornées.

A part ces défis scientifiques, la méthodologie doit être pragmatique, prêt à l'emploi et aisément communicable vu qu'elle est destinée aux ingénieurs. Par conséquent, le développement s'est déroulé sous respect de pratiques communes.

Finalement, une méthodologie holistique pour l'estimation de crues extrêmes a été formulées. L'avantage principal de cette dernière et qu'elle permet de générer un hydrogramme de crue et d'attribuer plausiblement une période de retour à son débit de pointe en prenant en compte une limite supérieure déterminée a priori en s'appuyant sur la méthode PMP-CMP (pluie maximale probable - crue maximale probable). De cette manière, la méthodologie combine la possibilité

de prendre en compte l'estimation du laminage de la crue avec la connaissance de la probabilité d'occurrence du débit de crue, une gradeur de référence dans la majorité des directives pour la sécurité contre les crues.
L'application de la méthodologie à trois bassins versants avec des caractéristiques différentes était favorable à la démonstration de la facilité d'utilisation de la méthodologie et, plus important encore, de ses avantages vis-à-vis des approches conventionnelles. Un outil informatique a été développé pour rendre accessible la méthodologie CRUEX++ de manière à ce qu'elle soit prêt à l'emploi.

Mots clés
sécurité des barrages, bassins versants alpins, crues de sécurité, distributions statistiques, modélisation hydrologique, distribution temporelle des précipitations, relation précipitation-température, conditions initiales de simulation, PMP-CMP, distributions statistiques à borne supérieure, méthodologie d'estimation de crues extrêmes.

Zusammenfassung

Im Rahmen der Staudammsicherheit kann von einer zuverlässigen Methode zur Abschätzung extremer Hochwasser nicht abgesehen werden da diese eine Notwendigkeit zur Gewährleistung einer ausreichenden Kapazität der Hochwasserentlastung darstellt. Der heutige Stand der Technik erlaubt es auf verschiedene Art und Weisen an dieses Thema heran zu gehen. Statistische Extrapolationen sind sehr gebräuchlich im Rahmen der Abschätzung extremer Hochwasser, allerdings ermöglichen es letztere nicht allen notwendigen Anforderungen der Staudammsicherheit gerecht zu werden. Die Abschätzung des Hochwasserdämpfung im Stausee kann nur mittels hydrologischer Simulation bewerkstelligt werden. Dank der schnellen technischen Entwicklung der Datenrechner in den letzten Jahren können hydrologische Simulationen unter optimalen Gegebenheiten ablaufen. Allerdings sind Praktiker oft nicht mit hydrologischer Modellierung vertraut. Daraus folgt ein nicht komplett ausgeschöpftes Potenzial letzterer.

Im Laufe dieses Forschungsprojektes konnte eine innovative und einsatzbereite Methodologie zur Abschätzung extremer Hochwasser entwickelt werden, die durch die Kombinierung statistischer und simulationsbasierter Ansätze zustande kam. Um diese Entwicklung erfolgreich umzusetzen, mussten einige offene wissenschaftliche Fragen beantwortet werden bevor die Kombinierung von Statistik und Simulation bewerkstelligt werden konnte. So konnte in Bezug auf die zeitliche Niederschlagverteilung nachgewiesen werden, dass eine zeitliche Struktur für die ganze Schweiz gültig gemacht werden kann. Was eine plausibles Niederschlag-Temperatur Paar angeht konnte mittels meteorologischer Ballonmessungen ein lineares Verhältnis zwischen der Niederschlagsdauer und der Höhe der Nullgradgrenze abgeleitet werden. Bezüglich der Anfangsbedingungen für die Simulierung extremer Hochwasserereignisse war es möglich methodische Empfehlungen zu deren Bestimmung zu geben. Des weiteren wurde festgestellt, dass die maximale räumliche Ausdehnung eines PMP-Event (probable maximum precipitation) bei 230 km^2 liegt, wenn das Event von den Schweizer PMP-Karten abgeleitet wurde, die im Rahmen des Cruex Projektes erstellt worden sind. Schließlich konnte nachgewiesen werden, dass die Verbindung von simulierten Abflüssen mit begrenzten Verteilungen, im Vergleich zu herkömmlichen Verteilungen, zu gesteigerter Stabilität und Plausibilität der Extrapolierung systematischer Datenreihen führt.

Neben diesen wissenschaftlichen Herausforderungen sollte die Methodologie pragmatisch, einsatzbereit und gut vermittelbar sein. Aus diesem Grund fand die Entwicklung unter Berücksichtigung gängiger Ansätze statt.

Schlussendlich konnte eine holistische Methodologie zur Abschätzung extremer Hochwasser verfasst werden. Der größte Vorteil der Methodologie ist, dass sie es ermöglicht eine plausible Verbindung zwischen simulierten Hochwasserereignissen und der statischen Ermittlung von

Wiederkehrperioden unter Anbetracht der PMP-PMF Methode herzustellen. Sie erlaubt es also Hochwasserdämpfung im Stausee mit der Abschätzung der Wiederkehrperiode des zugrunde liegenden Hochwassers zu verbinden, wobei wohl bemerkt werden soll dass letztere eine gängige Referenzgröße in Richtlinien zur Hochwassersicherheit ist.
Die Anwendung der Methodologie auf drei verschiedene Einzugsgebiete erlaubte es die leichte Handhabung der Methodologie zu veranschaulichen. Des weiteren war es möglich die Vorteile gegenüber konventionellen statistischen Methoden aufzuzeigen. Eine Computertool, das die einfache Zugänglichkeit und Anwendung der CRUEX++ Methodologie ermöglicht konnte ebenfalls erstellt werden.

Stichwörter
Staudammsicherheit, alpine Einzugsgebiete, Sicherheitshochwasser, statistische Verteilungen, hydrologische Modellierung, zeitlich Niederschlagsverteilung, Niederschlag-Temperatur Beziehung, Modellrandbedingungen, PMP-PMF, begrenzte statistische Verteilungen, Methodologie zur Abschätzung extremer Hochwasser

Riassunto

In campo di sicurezza delle dighe è necessario avere dei metodi affidabili per per stimare gli eventi di piena in modo da poter garantire la progettazione di una adeguata capacità di sfioro. La bibliografia ad oggi esistente permette di avvicinarsi a questo argomento secondo diversi fronti. Estrapolazioni statistiche sono pratica comune, ma non garantiscono di rispondere a tutti i bisogni richiesti dalle verifiche di sicurezza delle dighe. Negli anni passati, lo sviluppo informatico e il conseguente incremento delle risorse di calcolo hanno permesso di adoperare modelli idrologici in condizioni ottimali. Purtroppo questi modelli non sono ancora molto diffusi tra gli operatori nel settore e il loro potenziale è dunque solo parzialmente utilizzato.

Questo lavoro di ricerca sviluppa un approccio che permette di combinare statistiche con tecniche di modellazione idrologica e propone un'innovativa metodologia "pronta all'uso" per risolvere il complicato problema della stima degli eventi di piena estremi. Per portare a compimento questo progetto è stato necessario innanzitutto colmare alcune lacune scientifiche per poi potersi occupare della combinazione tra statistiche e simulazioni. Riferendosi alla distribuzione temporale delle precipitazioni, è stato possibile dimostrare la validità di un'unica struttura per l'intero territorio svizzero. Si è inoltre determinata una relazione lineare tra durata di precipitazione e temperatura (altitudine dell'isoterma a 0°C). In merito alla modellizzazione idrologica, è stata valutata l'influenza delle condizioni iniziali e sono state fornite delle raccomandazioni, delle linee guida metodologiche, per la scelta delle condizioni iniziali nella stima degli eventi estremi di piena. Si è stiamata l'espansione massima ammissibile per un evento di PMP derivato dalle carte PMP svizzere, elaborate durante il progetto CRUEX, che risulta essere di 230 km^2. Infine, la combinazione dei risultati ottenuti da simulazioni e distribuzioni statistiche a limite superiore si è dimostrata favorevole: la sensibilità al campione delle estrapolazioni è ridotta e i risultati sono più plausibili rispetto alle distribuzioni generalmente utilizzate.

Oltre alle sfide in campo scientifico, la necessità è di avere una metodologia pragmatica, pronta ad essere utilizzata e facilmente trasmissibile ai destinatari ultimi: gli ingegneri. Per questo motivo lo sviluppo é stato fortemente influenzato da questo aspetto pratico.

È stata dunque formulata una metodologia olistica per la stima di eventi di piena estremi. Il vantaggio principale è quello di permettere di generare un idrogramma di piena e di attribuire un tempo di ritorno alla portata di punta considerando il limite superiore, determinato a priori attraverso la metodologia PMP-PMF (pioggia massima probabile – piena massima probabile). In questo modo la metodologia combina la possibilità di prendere in conto la stima della laminazione della piena con la conoscenza della probabilità di accadimento di una portata di piena, che è di solito un valore di riferimento nelle direttive per la sicurezza contro le piene.

L'applicazione della metodologia a tre bacini d'invaso con caratteristiche tra loro diverse è stato utile per dimostrare la sua semplicità d'utilizzo e, ancora più importante, i suoi vantaggi rispetto agli approcci convenzionali. È stato sviluppato uno strumento informatico che rende accessibile la metodologia CRUEX++, ora pronta ad essere utilizzata.

Parole chiave

Sicurezza delle dighe, bacini d'invaso alpini, piene di sicurezza, distribuzione statistica, modello idrologico, distribuzione temporale di precipitazione, relazione precipitazione-temperatura, condizioni iniziali di simulazione, PMP-PMF, distribuzioni statistiche superiormente limitate, metodo di stima di eventi di piena estremi.

Traduzione: J. Z.

Contents

List of Figures

List of Tables

Introduction and literature review Part I

1 Introduction

1.1 Background

In Switzerland, 162 large dams (h > 15 m according to the definition adopted by the International Commission on Large Dams) have been constructed in the past. Knowing that Switzerland has a surface of 41285 km^2, this roughly corresponds to 20 dams per 5000 km^2. This is among the highest dam densities in the world. In comparison to the European leading hydroelectricity producer, Norway, the large dam density is approximately 4 dams per 5000 km^2 . In China, the world leading hydroelectricity producer, the dam density raises to 11.5 dams per 5000 km^2. Due to the high dam density in Switzerland combined with a high population density, flood safety is a critical topic for Swiss engineers and the knowledge of guaranteeing it is a necessity.

In the early nineties, the technological and scientific progresses allowed to initiate a research project on the topic of extreme flood estimations with the probable maximum precipitation-probable maximum flood (PMP-PMF) approach. This project was called CRUEX and was funded by the formerly called Federal Office for Water and Geology (FOWG), currently named Federal Office for the Environment (FOEN). Besides the elaboration of PMP maps for Switzerland, different models and methods have been developed. However, in the year 2012, the methodological developments in the domain of extreme flood estimations for dam safety verifications are still not totally completed. This led the Swiss Federal Office of Energy (SFOE) to the decision to initiate the CRUEX++ research project in 2012. The goal was to develop a clear and reliable methodology for the estimation of extreme floods for dam safety verifications that can compensate for the current lacks.

The CRUEX++ project was interdisciplinary and could profit from the collaboration of different actors from various fields who were already involved in earlier developments phases at EPFL. Thanks to the funding of the Swiss Federal Office of Energy (SFOE), the competences of the *Centre de recherche sur l'environnement alpin (CREALP)* as well as of the consulting firms *e-dric.ch* and *Hertig & Lador SA* could be assembled under the lead of the Laboratory of Hydraulic Constructions (LCH) at EPFL.

1.2 Motivation and Objectives

In mountainous regions, flood estimations and the estimation approaches have to be adapted to the particular topography. For obvious reasons, this is the case for Switzerland. Hydrology in alpine catchments faces additional difficulties compared to the lowland. Considerable snow cover and the presence of glaciers induce the hydrological processes to differ substantially from those observed in non alpine regions. Rain-on-snow events (liquid water falling on a pre-existing snow pack) are known to be at the origin of disastrous flood events (Rössler et al., 2014; Beniston and Stoffel, 2016). Recent research in this field showed that such events tend to increase in the Alps with a warming climate (Beniston and Stoffel, 2016). In Switzerland, rain-on-snow events have been observed three times in the last 17 years and led to substantial damages. Other researchers also found evidence for increasing flood risk in the Alps. Giorgi et al. (2016), for example, found that precipitations can increase over high Alpine elevations due to climate change. In their research letter, Jongman et al. (2014), stated that extreme flood losses could more than double in frequency by 2050. Considering these latest findings, research in the domain of dam safety in alpine catchments for flood events gains on importance.

In Switzerland, dam construction started in the 19^{th} century. Obviously, the flood estimations that were undertaken for the design of the dams were performed according to the state of the art and the data available at the time of planning. Today, more data with better quality, in terms of time series length and spatial repartition, is available. Technology and science have evolved and led to more efficient flood estimation methods. Due to the high concern about dam safety, the consideration of current knowledge can only be beneficial.

Over the last years, some dam operators have faced situations that led them to the conclusion that the spillway capacity has to be increased. This was, for example, the case of the Mattmark (Boillat and Schleiss, 2002) and the Contra (Bremen and Bertola, 1994) dams, two major constructions among the Swiss dams. Their required spillway capacity was re-evaluated and construction works have been undertaken to increase the capacity. The flood estimation approaches applied in these cases are however very different. The revision of the Mattmark dam spillway was based on the findings of the CRUEX project (Boillat and Schleiss, 2002). This means that the estimation took into account the PMP-PMF approach with hydrological simulation to derive the inflow hydrograph and the flood peak attenuation due to the lake. According to Bremen and Bertola (1994), the flood estimate for the Contra dam was based on statistical extrapolations on 29 years of discharge observation data. The two approaches applied in the case of Mattmark and Contra are very different and it may be concluded that the development for a more uniform flood estimation approach is needed. It seems that in practice outdated flood estimation approaches are still used. This is probably due to a lack of communication between scientists and practitioners. Consequently, a quite large gap between the flood estimation approaches used by practitioners and those which could be applied according to the latest scientific developments, is existing.

The ultimate aim of this research project was to develop a holistic flood estimation methodology to verify dam safety in terms of spillway capacity, adapted to alpine catchments. Such a methodology

forms the frame that is fundamental to compensate for the current discrepancies in extreme flood estimations. The developed methodology allows to estimate extreme flood hydrographs using hydrological simulation. The combination of the simulation based and statistical approaches allows to attribute a return period to the simulated peak discharge by taking the PMP-PMF approach into account to expand the systematic data set used for the statistical extrapolations. The work carried out during this research project focusses on the hydrology of Switzerland and targets the combination and completion of existing modern flood estimation methods with the following challenges:

- the developed methodology should be pragmatic and ready-to-use as the end users are not scientists but engineers;
- the communication of the final methodology is primordial;
- the methodology should not neglect common practices in order to facilitate the transfer of knowledge to the practitioners.

The developed methodology, described in Chapter 8, is supposed to be valid under current climatic conditions. The conclusions reached by ongoing research in climate change and its consequences are not yet ready to be applied by practitioners. Flood estimations with climate projections still enrol too much uncertainty for the formulation of a pragmatic approach as it is targeted here; expert knowledge is currently unavoidable in this domain. However, for extreme flood estimations, climate change effects can be supposed to be significantly smaller than other methodological uncertainties. Even if the methodology achieved in this research project does not allow to perform climate change projections, it's development is a necessary step towards an extreme flood estimation approach valid in a changing climate. In fact, the present safety of Swiss dams should first be validated. The expertise gained over time by practitioners and scientists forms a solid base for achieving a more general approach accounting for the latest findings in climate change and its consequences.

Finally, an extreme flood estimation tool has been developed. This tool, named CRUEX++ after the title of this research project, is freely available for practitioners. The tool has been embedded in a hydrological modelling software. Its development has been carried out in collaboration with *Centre de recherche sur l'environnement alpin (CREALP)* as well as *e-dric.ch*, *Hertig & Lador SA* who were involved in earlier development phases at EPFL. It allows not only to simulate extreme floods and to perform its routing through the dam reservoir, but it also incorporates statistical distributions and allows to combine the simulation results with the latter. In order to guarantee an efficient knowledge transfer, workshops with adapted documentation are foreseen to present the CRUEX++ methodology and the flood estimation tool.

1.3 General description and structure of the document

This document is structured in three parts (Introduction and literature review, Scientific developments for extreme flood estimations and Application procedure of the methodology and conclusions) and ten chapters. The literature review allowed to set the state of the art in the domain of extreme flood estimation. The identification of the lack of knowledge that needed to be addressed was conducted as well. Different research questions have been formulated and subjected to further analysis in the following chapters. The document structure is illustrated in Figure 1.1 and detailed in the following:

Part I: Introduction and literature review:

- Chapter 2 provides an overview of the state of the art in extreme flood estimation. A classification of the methods is proposed. The discussion of the different approaches, evaluating their advantages and disadvantages in the context of extreme flood estimations, led to the research questions treated in the following chapters.
- Chapter 3 describes the analysis of temporal rainfall structures in the context of Switzerland through rainfall mass curves, taking regional, seasonal and precipitation duration related considerations into account.

Part II: Scientific developments for extreme flood estimations:

- Chapter 4 is devoted to the analysis of precipitation-temperature scalings. The analysis makes use of meteorological soundings as well as precipitation and temperature data from meteorological stations.
- Chapter 5 focuses on the importance of initial conditions for extreme flood simulations in the context of hydrological modelling. The prediction intervals of the flood discharge and related lake level related to the initial conditions are estimated. A comparison between a deterministic and stochastic approach is undertaken. A sensitivity analysis allows to enhance the understanding of the influence of the different initial conditions and to discuss which approach (deterministic and/or stochastic) the final methodology should take into account.
- Chapter 6 dwells on the maximum admissible spatial expansion of PMP events derived from the Swiss probable maximum precipitation maps (Hertig et al., 2005; Hertig and Fallot, 2009), developed during the CRUEX project. The determination of the maximum catchment area, above which the PMP maps should not be used any more, is aimed.
- In Chapter 7, the robustness of extrapolations using upper bounded and unbounded statistical distributions is compared in order to discuss the advantages of the bounded distributions in the context of the CRUEX++ methodology. In a second step, the sensitivity of bounded

distribution extrapolations to the deterministically determined upper bound, estimated in this case with the PMP-PMF approach, is addressed in order to solidify or possibly contradict the previously reached conclusions on the advantages of upper bounded distributions.

- Chapter 8 provides a step by step explanation on the extreme flood estimation methodology CRUEX++, developed under consideration of the previously gained knowledge from the literature review and the analyses conducted in the previous chapters.

Part III: Application procedure of the methodology and conclusions:

- Chapter 9 describes the application of the CRUEX++ methodology to three catchments differing in size, geographical situation and glacier cover.
- Finally, conclusions and prospects for future works are summarized in Chapter 10 .

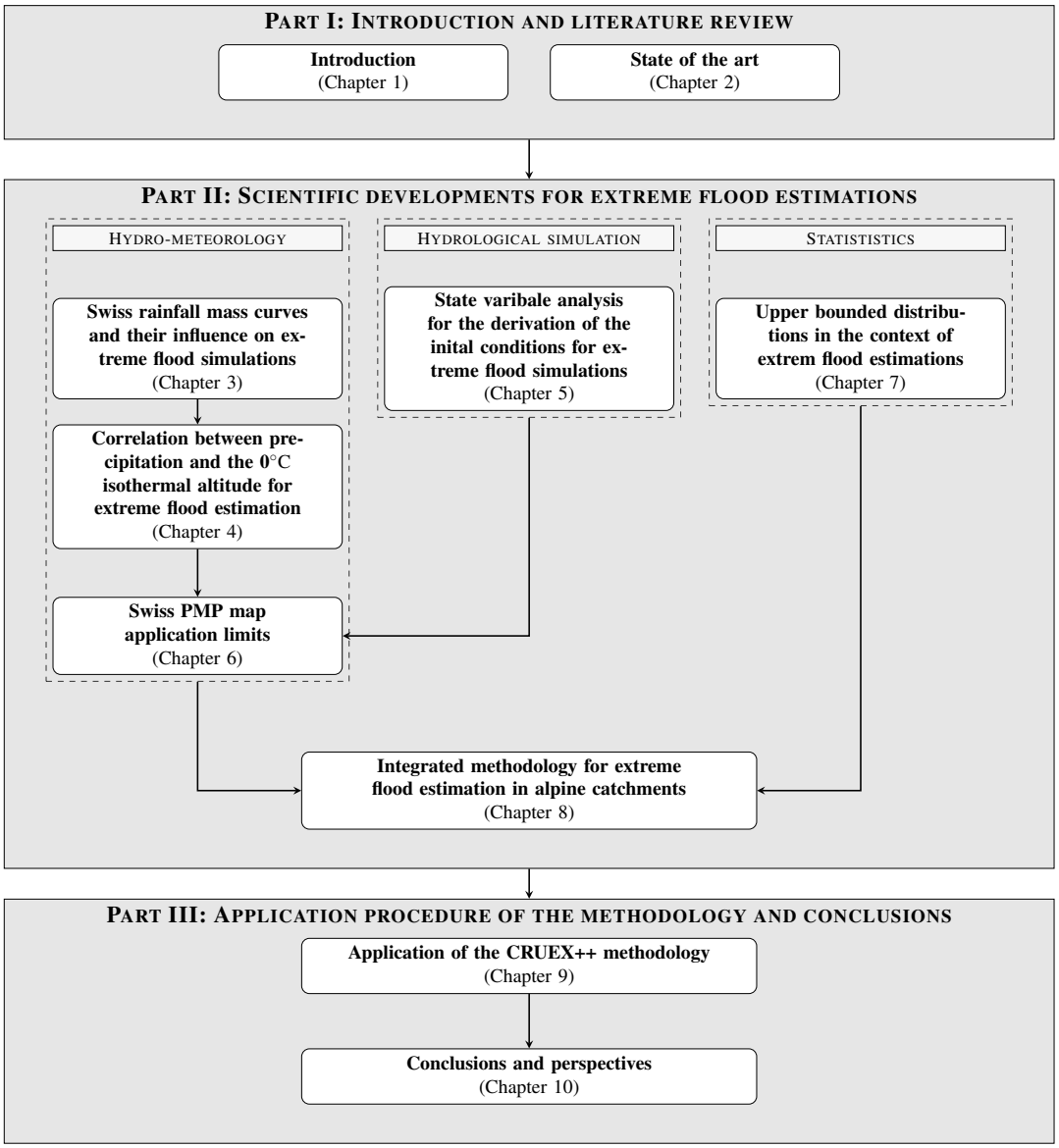

Figure 1.1: Schema of the document structure divided in three Parts and ten Chapters.

2 State of the art

2.1 Classification of flood estimation methods

The evolution of hydrological science is conditioned by the evolution of the resources for hydrological research, i.e. discharge data, meteorological data and computing power. Over the years, these resources have evolved and led to numerous approaches for discharge estimations. They differ in many aspects but can be classified by different approaches. Based on the classification proposed by Hingray et al. (2009), the organizational chart shown on Figure 2.1 has been elaborated. For this chart, the informations of Hingray et al. (2009) have been completed according to the detailed literature review developed in Sections 2.2, 2.3 and 2.4. These three sections treat the three main categories: observation based methods, simulation based methods and mixed methods. A discussion about their suitability for extreme flood estimations has been led in this chapter.

Before the literature review could be engaged, it was essential to define the "extreme flood" in the context this research project is conducted, i.e. the development of a methodology for extreme flood estimation in order to verify dam safety. The Swiss Guidelines for dam safety (SFOE, 2008a) define the extreme flood as a flood with a return period larger than 1000 years.

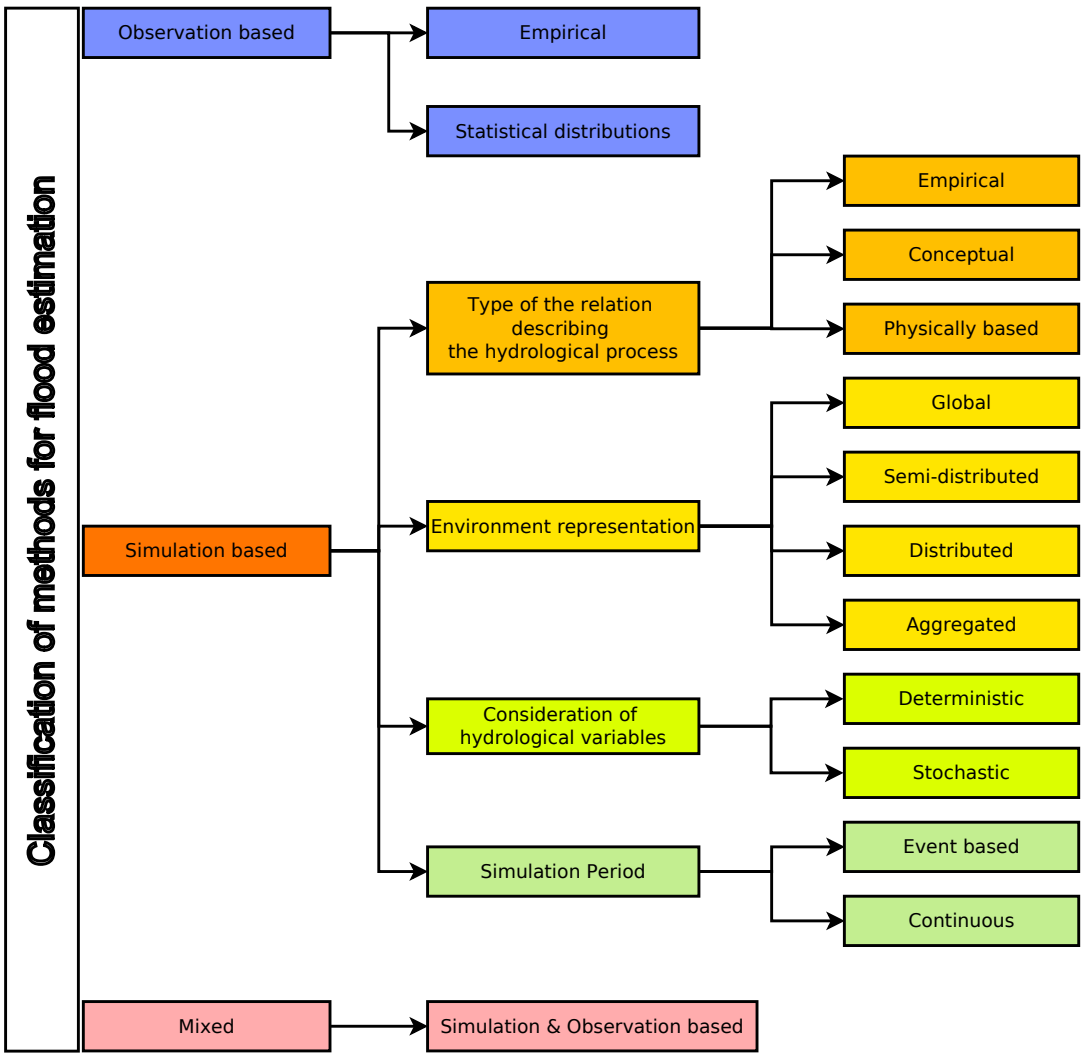

Figure 2.1: Classification of hydrological flood estimation methods/models, based on the classification of Hingray et al. (2009).

2.2 Observation based methods

Observation based methods got their name from the fact that the extreme flood estimation is derived directly from the observations, i.e. with a statistical distribution or based on a generalized approach leading to empirical formulas.

2.2.1 Empirical methods

In Switzerland, empirical formulas have been developed in the context of the elaboration of inundation maps and sewer design. These formulas, i.e. Müller-Zeller (Müller (1943), Zeller (1975)),Kürsteiner (1917) and Melli (1924) are the most known Swiss empirical formulas. Others like BaD7 Barben (2003), GIUB'96 (Kan (1995), Weingartner (1999)) and Kölla meso Kölla (1987) have been developed. These methods and formulas are listed and explained in FOWG (2003). They provide empirical estimations of the hundred year flood or of an estimation of Q_{max}, based on the largest observed floods. Consequently, their usage is limited. Thus, these methods are not suitable for extreme flood estimations in the context of dam safety. For this reason, they are not further discussed here.

2.2.2 Extreme value theory

> *Extreme value theory is unique as a statistical discipline in that it develops techniques and models for describing the unusual rather than the usual.* (Coles, 2001)

Statistical distributions are used in hydrology to extrapolate measured data. The extreme value theory was developed in the early 20^{th} century (Coles, 2001). The first statistical models in the domain of the extreme value theory for hydrological applications were developed to describe the statistical behaviour of annual maximum (AM) discharge values. Through the extremal types theorem (also called Fisher-Tippet-Gnedenko theorem) it could be proven that the maxima of a sequence of independent random variables from a common distribution function F, follow one of three distribution families, i.e. Gumbel, Fréchet or Weibull. These three distribution can be combined in one formula, called the General Extreme Value distribution (Jenkinson, 1955) . The extremal types theorem has been described in detail by Coles (2001). In Switzerland, other distributions like, log-normal, Pearson Type 3, log-Pearson Type 3, Gamma, Gumbel and Weibull are also used for the use of data extrapolations (FOWG, 2003). For the latter distributions, a mathematical justification could not be found in literature. The annual maxima approach is still used in hydrology because of its simplicity. However, it is often neglected that the extrapolation should not go beyond a return period corresponding to 2 to 3 times the time series used to fit the distribution (FOWG, 2003; DWA, 2012).

In order to extend the data used for the extrapolation, the Peak Over Threshold (POT) method can be used. It has been widely discussed by Davison and Smith (1990) and Coles (2001). For this approach, the time series, used to fit the General Pareto distribution is determined by conserving the independent events of the complete time series, the events being above an a priori determined threshold (Coles, 2001; Meylan et al., 2008). Pickands (1975) was the first on to illustrate the arguments for the use of the generalized Pareto distribution in threshold modelling. The mathematical justification for the generalized Pareto distribution has also been exposed by Coles (2001).

Compared to the GEV, the POT method is a bit more difficult to use as it involves the estimation of a threshold. Concerning the performance of the POT, Cunnane (1973) found that the AM approach is outperformed by the POT when the truncated series has an average number of at least 1.65 events per year. Tavares and Da Silva (1983) discussed the threshold level and conclude that it should be as low as possible and that the flood estimation is significantly over or underestimated by the POT method compared to the AM approach if the average number of exceedances per year is around 2. They also state that the estimated flood variance is significantly decreasing with an increasing average number of exceedances per year. Davison and Smith (1990) also obtained better results with the POT compared to the AM approach. Madsen et al. (1997) stated that it cannot be generally concluded if it is better to chose the AM or the POT approach. According to Madsen (1996); Madsen et al. (1997), it depends on the shape parameter, whether the POT or the AM method performs better. In addition, the parameter estimation method is influencing the performance of the two methods. Madsen (1996) concluded that the POT method gives better results for a minimum number of 2-5 events per year, depending on the shape parameter and the parameter estimation method. Two main advantages of the POT compared to the AM method were highlighted by Madsen et al. (1997): (1) due to the larger amount of data considered for the POT approach, the estimates are more robust; (2) the POT method can better represent the structure and hydrological processes of the considered time series. The analyses of Bhunya et al. (2012) and Bezak et al. (2014) confirmed that the POT method performs better than the AM method, however, in the study of Bhunya et al. (2012) the differences were small.

If historical flood data are available, it is possible to extend the continuous time series of discharge measurements with this additional information in order to enhance the flood estimations (DWA, 2012; Bodoque et al., 2014; Brázdil et al., 2012; Benito et al., 2015; Machado et al., 2015; Swain et al., 2006). Beside this temporal expansion, Merz and Blöschl (2008a,b), argue that the spatial and causal information expansion improve the flood estimates.

A spatial or regional information expansion consists in using data from the same region than the location of interest under the assumption that an apparent regional trend allows to transpose data from different observation stations to the location of interest. Merz and Blöschl (2008a,b) illustrated the benefits of such an approach. Lima et al. (2016) also showed how regional information can reduce the uncertainty of flood estimations with high return periods. This approach seems, however, to be hardly applicable to mountainous catchments due to the high regional variability of meteorological and hydrological conditions.

A causal information expansion can be performed when using upper bounded statistical distributions with a priori determined bounds (Botero and Francés, 2010). These distributions have major advantages for the estimation of floods with return periods higher than 2 to 3 times the underlying time series length. Botero and Francés (2010) compared the results from upper bounded statistical distribution extrapolations when the upper bound is considered as a parameter to be estimated to the results obtained when the upper bound is a priori deterministically determined , with a PMP-PMF (probable maximum precipitation - probable maximum flood). When the PMF is estimated using a hydrological model, the approach referring to upper bounded statistical

distributions would fit the "mixed methods" class. As Botero and Francés (2010) advised the deterministic estimation of the upper bound, the upper bounded distributions have been further discussed in the section concerning the mixed methods (Section 2.4).

If the hydrological processes are not stationary but encounter changes in time, a non-stationary model should be used. Non-stationary processes could for example be due to climate change. Coles (2001) describe the usage of the GEV in a non-stationary case: the distribution parameters are represented by functions in order to account for their temporal dependences.

When flood estimates are performed in the context of dam safety, not only the flood peak plays an important role but also the flood volume. Therefore, bivariate flood frequency analyses are very interesting to combine both the peak discharge and the flood volume (Brunner et al., 2016; Dung et al., 2015; Genest and Favre, 2007). Such an approach allows to attribute a probability to the couple "peak discharge - flood volume".

2.2.3 Synthesis of the statistical methods

Finally, it can be summarized that the statistical methods allow to attribute a return period to the flood estimations. This is an important quantity for risk analysis. Different approaches (AM, POT and bounded distributions) have been exposed and their advantages and disadvantages have been discussed. The bounded statistical distributions could be identified as most interesting in the context of this research project. However, the complete hydrograph cannot be estimated with these methods. Therefore, the deterministic methods based on flood simulations with a hydrological model are necessary when the complete hydrograph has to be known, as it is the case for spillway capacity verifications when flood damping estimations are performed.

2.3 Simulation based flood estimation methods

The simulation based methods need meteorological events (synthetic or observed) to derive extreme floods by routing these events through a calibrated hydrological model.

Simulation based models can be divided into four sub-categories, depending on the type of the relation describing the hydrological process (empirical, conceptual, physically based), the representation of the environment (global, semi-distributed, distributed, aggregated), the consideration of the hydrological variables (deterministic, stochastic) and the consideration of the simulation period (event based or continuous simulation) of the model. Figure 2.1 graphically shows this classification.

2.3.1 Type of hydrological process description

The first category, distinguishing the approaches by the type of the relation describing the hydrological process, can be subdivided into 3 sub-categories, i.e. empirical, conceptual and physically based models. Concerning the empirical models, they act like a black box. Hingray et al. (2009) cite three well known empirical methods, the SCS-CN approach (USDA-SCS, 2007) for the precipitation estimation coupled to the method of the unit hydrograph for the estimation of the resulting discharge. They also classify the ARX (autoregressive statistical model with exogenous inputs) or ARMAX (autoregressive moving average model with exogenous inputs) (Box and Jenkins, 1970; Stoffer, 1986; Marco et al., 1989) methods in this category. These methods relate the generating quantities of a process to the response of the system by fitting a linear black box model to the measured time series. Hingray et al. (2009) mention two important limitations of these models: the data series needs to be generated by a stationary process and the relationship between the input variables and the model responses have a linear behaviour, what is not the case in a lot of hydrological applications. Hingray et al. (2009) underline in particular the fact that the flood discharge is not necessarily related directly to the precipitation. The saturation of the basin, the snow fall and melt as well as the glacier evolution have a strong influence on the flood discharge. The artificial neural networks, also mentioned by Hingray et al. (2009) are used to express in a non-linear way the relationship between the inputs and the outputs. These empirical models are however not recommended for the estimation of extreme floods. The extreme flood estimation would be very uncertain because the estimation is way beyond the domain of the measured data on which the model has been trained. In addition, Hingray et al. (2009) do not advise the usage of these models in ungauged basins, because the models need to be calibrated on a gauged basin and cannot be transposed to an ungauged basin. This is due to the fact that the calibration parameters have neither a physical nor a conceptual meaning.

Regarding the conceptual models, Hingray et al. (2009) defined them as follows: "Conceptual hydrological models are designed to represent the main hydrological processes in a reasonable manner without requiring parametrization of the physical laws that govern them." Due to the ease of implementation of these models, hydrologists like to use them. A main advantage is that a relatively small amount of data is necessary. The number of parameters to calibrate is normally small. The computation time of these models is also quite limited, making them very attractive. These models have, however, some limitations when it comes to the representation of realistic hydrological processes. The intermediate results, like the evolution of the state variables only make sense in the context of the model and may not represent the quantities that would be measured on the field.

The physically based models allow to get rid of these limitations. Hingray et al. (2009) defined the physically based models as follows: "Physically based models represent the hydrological operation of the hydrosystem by coupling different sub-models, each dedicated to certain hydrological processes." The perfect physically based model would not need calibration and would perfectly model all the hydrological processes. Such a model is, however, not existing (Hingray et al., 2009). The real hydrological behaviour is too complex and not yet well enough understood

to build the perfect physically based model. The complexity of these models makes their usage difficult and time consuming. The immense amount of data necessary for the description of the environment and the related precesses cannot yet be handled or the data are simply not available.

Conceptual and physical models allow to account for non stationarity and non linearity. This leads to a better flood estimation outside of the calibration domain according to Hingray et al. (2009). They also stated that these models are much easier transposable to ungauged catchments. A particular advantage of conceptual and physically based models is that they can incorporate the modelisation of hydraulic structures such as reservoirs and spillways. This is obviously a very important advantage when it comes to dam safety verifications in terms of spillway capacity.

2.3.2 Representation of the environment

The second category of the simulation based methods is depending on the representation of the environment by the model structure. The model can be lumped, semi-distributed or distributed.

The first type of simulation models, the so-called global or lumped models, represent the catchment by only one hydrological model unit returning the discharge at the outlet of the catchment. They assume that the characteristics of the catchment can be considered to be the same for the whole area. Thus they have the lowest level of information requirements and output.

Semi distributed models also use physically based functions to estimate the discharge, but they do not take into account the spatial distribution of the physical parameters. They employ conceptual schemes, modelling the main characteristics of a catchment by gathering zones with similar physical characteristics and altitudes. Programs entering this category are Mordor (Garçon, 1996 and Paquet, 2004), IHACRES (Jakeman et al., 1990 and Croke and Jakeman, 2004), CASC2D, described by Singh and Frevert (2002b) in Singh and Frevert (2002a), SWMM described by Gironás et al. (2010), SAC (Burnash, 1995) and GR4J (Perrin et al., 2003) and the Integrated Hydrological Modelling System HBV (Bergström, 1992 cited by Krysanova et al., 1999), IHW (Plate et al., 1988) and the GSM-Socont (Schaefli et al., 2005; Schaefli and Zehe, 2009; Jordan et al., 2012) for glacial alpine catchments. The GSM compound for glacial modelling cannot only be combined with the Socont model but also with other non glacial models.

A distributed model takes into account the spatial distribution of the physical parameters describing the modelled environment. The catchments are represented by a grid of points, making it possible to estimate the discharge at each grid point using physically based functions. However, these models have the disadvantage that it is difficult to introduce hydraulic elements for the simulation of a hydro-electric power plant. Frequently used programs allowing a distributed modelling of the catchment are listed hereafter. Topmodel, developed by Beven and Kirkby (1979) (originally reported by Beven, 2012), is an open source model. A detailed description of TOPMODEL has been provided by Beven et al. (1994) (cited by Singh and Frevert, 2002a). The latest version of TOPMODEL, called Dynamic TOPMODEL, has been described by Beven and Freer (2001). Other models are MIKE SHE (DHI, 1993 cited by Singh and Frevert, 2002a),

Larsim (Bremicker, 2000), Wasim (Schulla, 2012), Nasim (Rothe and Wolf-Schumann, 2013), MPF (Receanu, 2013; Receanu et al., 2013), Modular Modeling System PRMS/MMS (Singh and Frevert, 2005), TOPOG (Vertessy et al., 1993), SLURP Hydrological Model (Kite, 1995 cited by Beven, 2012).

A fourth type can theoretically be imagined, the aggregated model. It is a composition of the three types described above. This type can be developed for huge catchments where sub-catchments are modelled using different approaches and put together later.

2.3.3 Consideration of the hydrological variables

The methods can, as shown on Figure 2.1, also be classified by distinguishing between the ways in which the hydrological variables are considered. A deterministic method assumes that for one input there is only one output. For stochastic methods, the output is not unique under a given input. This is due to the fact that in these methods, the output depends at a certain moment from a random variable. According to Hingray et al. (2009), stochastic methods are only rarely used in hydrology.

2.3.4 Simulation period

The last category of the simulation based methods is the one that differs the models by their simulation period, i.e. event based or continuous. An event based model derives the resulting discharge from one particular meteorological event. The initial conditions need to be previously fixed for every simulated event. This approach is very interesting when safety floods are estimated (Hingray et al., 2009) based on design storms as it is the case for the PMP-PMF method (further exposed in Section 2.6). Continuous simulations are of a much longer duration than event based simulations. The determination of the initial conditions is not necessary if a warming period is considered for updating the state variables of the hydrological model. According to Hingray et al. (2009) the initial conditions become negligible for continuous simulations after a period (called the warming period) of some days to some months, depending on the case. When a long time series is available for the calibration of a model, and the calibrated model is then used to route design storms in order to determine a safety flood, the simulation period can be considered to be semi-continuous if the initial conditions are derived from the longer continuous calibration period.

2.4 Mixed methods

The third category, the mixed methods, uses simulation based methods in order to generate input data for a statistical analysis. Two types of mixed methods can be found in literature.

2.4.1 Type 1: Generation of a synthetic time series by continuous simulations

The first possibility is to generate discharge time series by continuous simulations using as input synthetic meteorological events generated a priori. In this way, the measured discharge time series can be extended and more data is available for the statistical analysis.

In France, two mixed methods with continuous simulations are currently used: The SHYPRE/SHYREG method and the SCHADEX.

The SHYPRE method has been developed by IRSTEA[1] (Cernesson et al., 1996, Arnaud et al., 1999 and Arnaud and Lavabre, 2000 originally cited by Roche et al., 2012). SHYPRE generates hourly hyetographs that are used to rainfall-runoff simulations using the GR3H hydrological model (Fourmigué and Lavabre, 2005). Thousands of years of synthetic precipitations can be generated and transformed in flood data.

According to Aubert (2012) the development of precipitation generators took 15 years (4 thesis's) and leaded to the model SHYREG, that is the regionalisation of the SHYPRE method.

The SCHADEX (climatic-hydrological simulation of extreme floods[2]) method is the result of improvements of the GRADEX method Paquet et al. (2006). Since 2007 SCHADEX is the official method used by EDF (Electricité de France) to estimate the design flood in order to design spillways (Paquet et al., 2013). This method has been conceived to estimate extreme floods by a stochastic simulation combining a probabilistic rain model and an hydrological rainfall runoff model (Garavaglia, 2011). SCHADEX takes into account the atmospheric circulations in order to analyze the seasonal risk of precipitations. Consequently, the weather situations with heavy rainfall events can be isolated and thus the probability of extreme rainfall increases (Paquet et al., 2006). The hydrological conceptual model MORDOR is then used to simulate the runoff resulting from generated synthetic precipitation events, considering a huge number (several million) of initial saturation conditions of the catchment (Paquet et al., 2013). The initial conditions observed during a continuous simulation of the catchment are used for the simulation with the generated precipitation. This leads to a semi-continuous model, as it mixes continuous (to get the initial conditions) and event-based (to simulate runoff from generated synthetic precipitations) simulations (Garavaglia, 2011 and Paquet et al., 2013). The resulting flood events can then be analyzed by statistical methods (Roche et al., 2012).

According to Paquet et al. (2013), the SCHADEX method is suitable for large catchments, up to $10^4\ km^2$, and can be used to estimate floods in mountainous regions. Paquet et al. (2006) qualify the SCHADEX method to be adapted for the estimation of floods with a return period of 10 000 years.

In Switzerland, the project CONSECRU 1 (Niggli et al., 1997), and later the project CONSECRU

[1] Institue national de recherche en science et technologie pour l'environnement et l'agriculture; former CEMAGREF.

[2] simulation climato-hydrologique pour l'appréciation des débits extrêmes

2 (Hingray et al., 2006) have been realized by HYDRAM. It is based on a stochastic multi-evenemential methodology. The precipitation series are generated by a stochastic precipitation model (NRSPM, Neyman-Scott Rectangular Pulses Model (Cowpertwait, 1991 originally reported by FOWG, 2003) and introduced in a rainfall-runoff model using a continuous simulation. The CONSECRU methodology leads to a large number of flood scenarios that are subjected to usual statistical analysis in order to conclude. Nevertheless, this method has not been developed in order to estimate PMF. Furthermore, when the generated precipitations events are not numerous enough, or if by chance they did not generate the critical precipitation, the simulated floods are not sure to be extraordinary floods.

2.4.2 Type 2: Event based or semi-continuous methods

The second possibility is to use the simulation based method in an event based or semi-continuous manner, in order to extend the information sources of the statistical methods, as described by Merz and Blöschl (2008a,b); Botero and Francés (2010). As mentioned earlier in Section 2.2.2, the combination between the simulated PMF and the annual maxima method can be done through the usage of upper bounded distribution functions. Due to the appealing character of this approach for the current research project, contextualized in the introduction of this report, the upper bounded distribution functions as well as the PMP-PMF method have been attributed the two following Sections 2.5 and 2.6.

2.5 Upper bounded statistical distributions

Recently, Botero and Francés (2010) have presented a paper comparing three upper-bounded distributions, i.e. the Extreme Value with four parameters distribution function EV4 (Kanda, 1981), the Slade-type four parameter Log-Normal distribution function LN4 (Slade Jr, 1936; Takara and Loebis, 1996) and the transformed extreme value type distribution function TDF (Elíasson, 1994).

The EV4 and LN4 distributions have an upper and a lower bound, whereas the TDF distribution is only upper bounded. In the works of Kanda (1981), Takara and Tosa (1999), Botero and Francés (2010) and Fernandes et al. (2010), the lower bound for EV4 and LN4 are assumed to be larger or equal to zero in order to get a more parsimonious model. These authors even mention to fix the lower bound to zero. However, the sensitivity analysis of Fernandes et al. (2010) that addressed the influence of the lower bound on the upper fitted distribution tail, showed that the influence is very small in their case.

The main hypothesis underlying the usage of one of these distributions is that a physical upper limit is existing (Enzel et al., 1993). They discuss the estimation of this upper limit using conventional distribution fitting methods, i.e. Maximum Likelihood Method, and using a deterministic approach. In this case, the upper limit should be estimated with the PMP-PMF method and

according to Merz and Blöschl (2008a), the PMF could be seen as a causal information expansion.

Upper bounded distributions have successfully been applied for extreme flood estimations by Takara and Tosa (1999); Fernandes et al. (2010) Botero and Francés (2010) and to extreme precipitation estimates by Takara and Loebis (1996) and Elíasson (1997). All authors conclude that the inclusion of an upper bound is valuable for extreme flood estimations. The choice of of the best fitting distribution has rarely been addressed in literature. The Akaike and Bayesian information criterion, a least squared error approach and a correlation coefficient have been used by Takara and Loebis (1996) and Takara and Tosa (1999). Takara and Tosa (1999) finally came up with the recommendation to use the EV4 distribution when the sample skewness γ, estimated by Equation 2.1, is larger than 2 and the LN4 distribution when the sample skewness γ is smaller than 1.5. The TDF distribution did not enter their analysis.

$$\gamma = \frac{1}{Ns^3} \sum_{i=1}^{N} (x_i - \bar{x})^3 \tag{2.1}$$

where x_i is an observation value, $\bar{x}$ is the mean value of the observations x_i and s is the estimate of the standard deviation of the observations.

The reason the TDF distribution was not considere by Takara and Tosa (1999) may be the following explanation of Elíasson (1994). In fact, he stated that the parameter k (see Equations 2.6 and 2.7) has a negligible effect for small return periods. In order to estimate k properly, a large sample is necessary. In the application of Elíasson (1994), more than 5000 data points aggregated from different pluviometers have been used. For discharge measurements, such a large time series is impossible to have as the systematic discharge measurements generally started later than the precipitation measurements and the regionalization of discharge data is not possible. Consequently, an aggregation of the data as it can be done for precipitation data (as performed by Elíasson (1994)) is not possible. Due to the resulting questionable parameter k estimation in the case of small time series, the TDF distribution has been neglected for further investigations in this research project.

It is interesting to notice that the Canadian guidelines on extreme flood analysis (Hogg et al., 2004) accept the PMF as upper limit for the statistical applications. In the Canadian guidelines it has been proposed to derive the 1000 year flood by interpolating the statistically estimated 100 year flood with the deterministically estimated PMF by assuming a return period of 100 000 years for the PMF. This approach is empirical, very pragmatic and certainly easy to criticize, but illustrates the will of hydrologists to combine the PMF estimates with statistical extreme value theory.

2.5.1 EV4 distribution

The EV4 distribution was derived from the GEV distribution by Kanda (1981). The cumulative distribution function is provided by Equation 2.2.

$$F(x) = \exp\left[-\left\{\frac{g-x}{\nu(x-a)}\right\}^{k}\right] \tag{2.2}$$

where g is the upper bound and a is the lower bound, ν is the scale parameter and k characterizes the shape of the distribution.

The probability densitiy function of the EV4 distribution is given by Equation 2.3.

$$f(x) = \exp\left[-\left\{\frac{g-x}{\nu(x-a)}\right\}^{k}\right] \frac{(g-x)^{k-1}k(g-a)}{\nu^{k}(x-a)^{k+1}} \tag{2.3}$$

2.5.2 LN4 distribution

The two parameters log-normal distribution has been modified by Slade Jr (1936) to derive the LN4 distribution. The cumulative distribution function is presented by Equation 2.4.

$$F(x) = -\frac{1}{2}\Phi\left[\frac{\sigma_Y - Y}{\sqrt{2}\sigma_Y}\right] \tag{2.4}$$

where g is the upper bound and a is the lower bound, μ_Y and σ_Y are the mean and standard deviation of Y and Y is given by the Slade-type transformation $Y = \ln\left(\frac{x-a}{g-x}\right)$ (Slade Jr, 1936). Φ stands for the cumulative density function of the standard normal distribution.

The probability density function of the LN4 distribution is given by Equation 2.5

$$f(x) = \frac{g-a}{(x-a)(g-x)\sigma_Y\sqrt{2\pi}} \exp\left[-\frac{1}{2}\left\{\frac{Y-\mu_Y}{\sigma_Y}\right\}^{2}\right] \tag{2.5}$$

2.5.3 TDF distribution

The TDF distribution has been derived by Elíasson (1994) from the Gumbel distribution (Extreme value type 1 distribution). The cumulative distribution function is given by Equation 2.6

$$F(x) = \exp\left[-\exp\left(\frac{-x}{\alpha} + \frac{\alpha k}{g-x} - b\right)\right] \tag{2.6}$$

where g is the upper bound and α is the scale parameter, b is the location parameter and k is a negative constant.

The probability density function of the TDF distribution is given by Equation 2.7

$$f(x) = \exp\left[-\exp\left(\frac{-x}{\alpha} + \frac{\alpha k}{g-x} - b\right)\right] \exp\left(\frac{-x}{\alpha} + \frac{\alpha k}{g-x} - b\right)\left(\frac{1}{\alpha} + \frac{\alpha k}{(g-x)^2}\right) \tag{2.7}$$

2.6 PMP-PMF method

2.6.1 Introduction

The use of design storms and related design flows is a key tool for the design of hydraulic infrastructures (Niemi et al., 2015; Swain et al., 2006; Salas et al., 2014). In the case of dam design, spillways are frequently designed to withstand the probable maximum flood (PMF) (Swain et al., 2006; Salas et al., 2014). The PMF is defined as "the theoretical maximum flood that poses extremely serious threats to the flood control of a given project in a design watershed. [...]" (WMO, 2009). The PMF definition of the Bureau of Reclamation, USBR (1974), is less severe; it is considered to be the "largest flood that can reasonably be expected to occur on a given stream at a selected point. Furthermore, the World Meteorological Organization (WMO, 2009) specified that the PMF is "converted from the probable maximum precipitation (PMP) over a design watershed". The PMP is defined as "the theoretical maximum precipitation for a given duration under modern meteorological conditions [...]" (WMO, 2009). The conversion from PMP into PMF is generally done by routing the PMP through a rainfall-runoff model (Swain et al., 2006; WMO, 2009). A key issue in PMF estimation is the choice of the modelling method and the uncertainty quantification (Jothityangkoon et al., 2013; Beauchamp et al., 2013; Lagos-Zúñiga and Vargas M, 2014; Salas et al., 2014; Brigode et al., 2015; Haddad and Rahman, 2016). Depending on the availability of data, among other criteria, event-based or continuous simulations can be used for the rainfall-runoff routing (e.g. Jasper et al., 2002; Zeimetz et al., 2015). Data availability constraints frequently impose the choice of event-based approaches, as it is for example the case for the analysis carried out by Zhang and Smith (2003).

Concerning the main assumption the PMP-PMF approach is based on, i.e. the existence of an upper limit, some authors claim that such an upper bound cannot be justified (Koutsoyiannis, 2004; Papalexiou and Koutsoyiannis, 2006). For this reason, these authors reject the PMP-PMF method and thus also upper bounded statistical distributions. However, at the current state of the art, the advantages the assumption of an upper limit induces are much more valuable than the acceptance of its reject. The reason is because the results are much more consistent and reasonable than current unbounded approaches. The usage of bounded approaches is thus justifiable in the context of dam safety, where current unbounded approaches provide clearly more often unsatisfactory results than unbounded methods.

2.6.2 Where is the PMP-PMF method applied ?

Hydrologists speak of the PMP-PMF (Probable maximum precipitation-probable maximum flood) method when PMP is transformed into PMF using a rainfall-runoff model (WMO, 2009). This method is frequently used in the United States of America (Bérod et al., 1992a) where it has been developed in the 1930^{th} by Roche et al. (2012) , Australia (Nathan et al., 2001), Canada (Beauchamp et al., 2013), Spain (Casas et al., 2011) and Austria (Nobilis et al., 1991). The PMP-PMF method has also been introduced in the guidelines for dam design and dam safety in countries like India, Turkey and the United Kingdom (ICOLD, 2016). The main assumption of the method is that an upper limit of the precipitation volume is existing (Bérod et al., 1992a). The Swiss guidelines for dam safety verification in term of spillway capacity SFOE (2008b) mention the PMP-PMF method for the estimation of the safety flood [3].

The first time the PMP has been used to estimate PMF in Switzerland was during a project of the Laboratory of Hydrology and Facilities HYDRAM at EPFL (Bérod et al., 1992a). The collaboration of the engineering companies Bonnard et Gardel Ingénieurs Conseils SA Lausanne and SA Ufficio d'ingenieria MAGGIA from Lucarno was helpful in the estimation of the PMF of the two catchments Dischma (Canton of Graubünden / Grisons) and Carrassina (Canton of Ticino / Tessin). The project was founded by the *Commission pour l'encouragement de la recherche scientifique* (CERS).

The second project undertaken on this subject was the CRUEX project (Bérod et al., 1992a). The CRUEX[4] project has been financed by the Swiss Federal Office of Energy (SFOE)[5]. Three EPFL research laboratories were involved in the project: the Laboratory of Hydraulic Constructions (LCH), the Laboratory of Energy Systems (LASEN) and the Laboratory of Hydrology and Facilities (HYDRAM[6]) (Schleiss and Pougatsch, 2011).

[3]It should be mentioned that the flood discharge estimated by $Q = 1.5 \cdot Q_{1000}$ is also eligible for the estimation of the safety flood according to SFOE (2008b)

[4]The abbreviation CRUEX is derived from the french expression "Crues Extrêmes", that means "extreme floods".

[5]Office fédérale de l'énergie (OFEN)

[6]This laboratory has been replaced in 2008 by the Laboratory of Ecohydrology ECHO at EPFL.

2.6.3 The Swiss PMP maps

During the CRUEX project, PMP maps have been developed (SFOE, 2008b) for the entire surface of Switzerland, with a resolution of 5 km for precipitation durations of 3 and 24 hours. The approach aimed to make the link between climate analysis and weather conditions. Then a maximization of the precipitation has been performed in order to approach the worst case without obtaining unrealistic values (Hertig et al., 2005; Audouard et al., 2006).

The development and the application of the set of programs, used for the estimation of the PMP, have been based on theoretical approaches as well as on various special studies in Switzerland and abroad. For Switzerland, studies realized for the watersheds Mattmark, Reuss, the Oberalp, Mauvoisin and Toules (Pérez and Hertig, 1998) and basins outside the Alps, i.e. the dams Deriner in Turkey and Krasnodar in Russia (Dubois and Boillat, 2000; Dubois and Pirotton, 2002; Boillat and Schleiss, 2002), were included.

The methodology used for the mapping of extreme precipitation in Switzerland took into account the mechanisms of orographic, frontal and convective precipitation. For orographic and frontal precipitation, a meteorological meso-scale model was first used to estimate a wind field over the topography for given weather conditions specifying the initial conditions of wind, temperatures and humidity. The wind field has then used to solve the equations of the rain model by Kessler (1969) to obtain a spatial distribution of rainfall intensity, which has then been associated to a precipitation duration. The physical atmospheric conditions, such as temperature profiles, wind direction, wind profiles and speeds, humidity,...etc, have been varied in the meteorological model in order to maximize the precipitation intensity for a certain precipitation duration concerning the orographic events. According to Receanu (2013), the main challenge was to estimate plausible physical parameter values entering the precipitation maximization calculations. Finally, for the wind speed, values from 23 m/s (wind from the North) to 54 m/s (wind from the East) have been considered. These values have been estimated statistically by assuming that a return period of 50 years is plausible for the PMP estimation. Concerning the wind profile, a logarithmic profile has been admitted for the boundary layer. Above the boundary layer a constant profile was used. Concerning the temperature gradient, the atmospheric temperature has been assumed to vary by 0.55°C per 100 m. At the ground, a temperature of 20°C has been taken into account. Due to the complex topography of Switzerland with highly variable altitudes inducing considerably different temperatures at different locations, this assumption may not be realistic but can be assumed to be conservative.

The convective precipitation estimates have not been calculated using a meteorological model, but were based on the method proposed by Haiden (Haiden et al., 1992 and Haiden, 1991), which parametrizes the latter depending on local slopes, humidity conditions and surface radiation.

In 2007, the engineering company Hertig & Lador SA, recalculated the Swiss PMP maps using similar models with a horizontal resolution of 2 km for a surface area of 350 x 240 km in order to cover the whole area of Switzerland for different wind sectors (North, South, West-North-west).

The recalculation has been necessary because the confrontation of the first maps with field measurements showed that a horizontal resolution of 5 km is not sufficient to take into account all the effects of Swiss topography on extreme precipitation (Hertig et al., 2008; Hertig and Fallot, 2009). An example of a PMP map is shown on Figure 2.2. The meteorological model has been used to estimate the PMPs for precipitation durations of 3h and 24h. The other maps for precipitation durations of 1, 6, 9 and 12 hours have been deduced from the findings of Bérod et al. (1992b) who showed that the PMP data fit a straight line on an intensity duration frequency plot in a log-log space. Logically intermediate durations can be derived from this linear interpolation. An example of interpolated PMP map data at (694 000,121 510), in the Swiss national coordinate system CH1903/LV03), close to the city of Maggia in Ticino is shown on Figure 2.3.

The calculation model of PMP has been validated on the basis of in situ measurements. For this validation, 429 Swiss rainfall gauges and meteorological stations have been used. A ratio between extreme precipitation, estimated with the simulation model, and a Gumbel-extrapolation of in situ measurements to a return period of 500 years has been calculated for each measurement station. The obtained mean ratio for a 3h-precipitation was 2.2 and for a 24h-precipitation the mean was estimated at 1.9 (Hertig et al., 2005; Audouard et al., 2006 and Hertig and Fallot, 2009). According to Hertig and Fallot (2009), the mean ratio of 1.9 found for 24h-precipitations lets conclude that the mean return period of the PMP values is larger than 10^4 years. Their argument is based on the statement that a ratio of 1.5 between the 10^4 and 500 years precipitations is a common observation. However, their analysis lets also conclude that at some locations, the PMP values may be underestimated, the ratio between the estimated PMP values and the 500 year-precipitation extrapolations (using a Gumbel distribution) has be found to be smaller than 1.

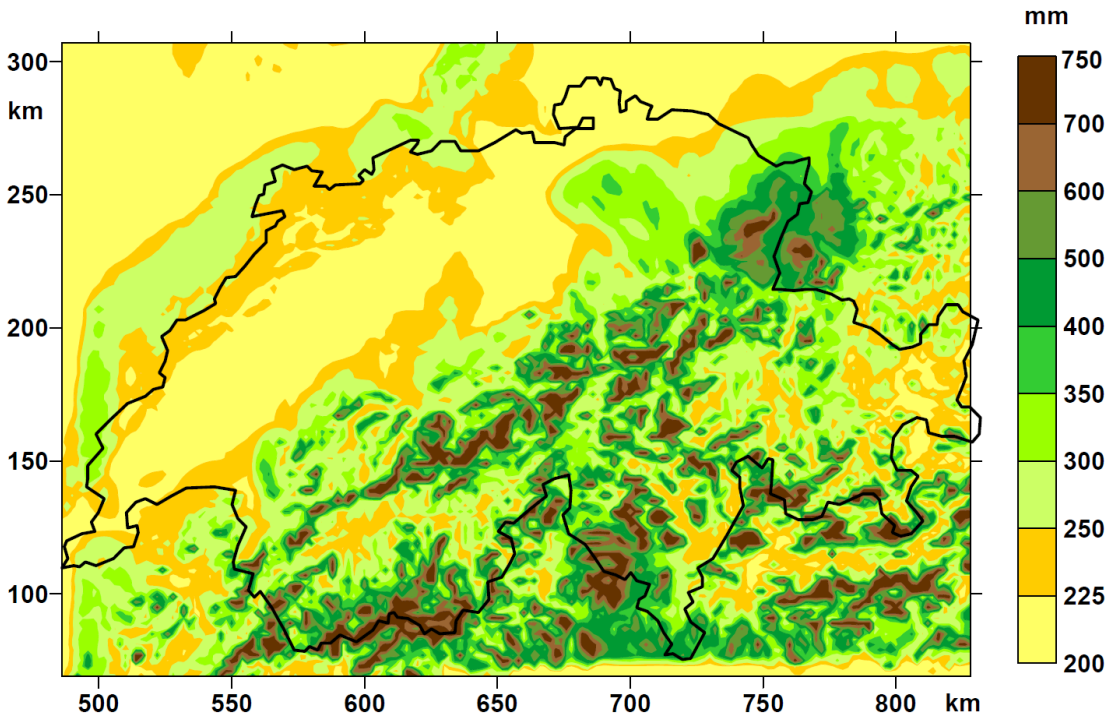

Figure 2.2: Simulated probable maximum precipitation (PMP) map for a precipitation duration of 24h and a horizontal resolution of 2km. The three wind sectors (North, south and west) are confounded on this map. The data was mapped by Hertig and Fallot (2009).

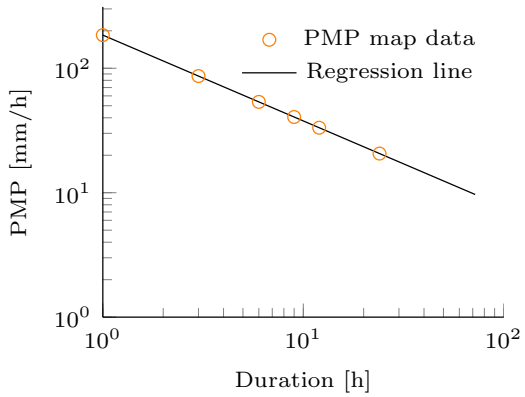

Figure 2.3: PMP values for location (694 000,121 510), in the Swiss national coordinate system CH1903/LV03, plotted in a log-log space on an intensity duration frequency like curve.

2.6.4 Conversion from PMP to PMF

The conversion from PMP to PMF can be performed with two different methods (WMO, 2009): (1) the unit hydrograph method or (2) with hydrological process models. According to (Bérod et al., 1992a), the estimation of the PMF using the unit hydrograph method is not recommended in

mountainous regions because the assumption of a linear catchment response is not verified. The method is too simple because it does not take into account the physical phenomena. Hydrological rainfall-runoff methods are recommended in this case.

When using a hydrological model, some additional information are required: spatial and temporal rainfall structure, the initial terrain conditions (soil saturation, snow, snow saturation, ...)[7] According to Cohen et al. (2009), improvement of the PMP-PMF method is needed in order to apply it for the safety verifications of dams because to much uncertainties are remaining in terms of initial conditions and model configurations, such as model complexity.

2.6.5 Spatial structure

Bérod et al. (1992b) defined the spatial variability as being the description of the variability of the precipitation depth at different locations at a given moment. The spatial distribution of the PMP is mainly depending on the scale of the event and on the topography of the concerned region (Bérod et al., 1992b).

The World Meteorological Organization (WMO, 2009) proposes PMP depth-duration-area curves to which a geographical reduction factor is applied. When a distribution of the PMP in space is required, elliptical isohyetal curves are considered to synthetically structure the event in space.

Hingray et al. (2009) described precipitation depth reduction factors depending on the storm area as well as its duration. These factors have been defined for the transformation of point rain estimated using intensity duration frequency curves for a given meteorological station under the assumption that the meteorological station is at the centre of the event.

For Switzerland, PMP depth-area-curves, geographical reduction factors or synthetic spatial distribution shapes have not been developed yet. The complex Swiss topography makes it a necessity to account for the Alps when PMP data are estimated. Therefore, PMP maps have been developed with a meteorological model that can consider the Swiss topography. This has, however, the drawback that the depth-area relation could not be considered. Consequently, the spatial extension of the PMP event is not reported on the maps, returning only the probable maximum precipitation for each pixel (2km x 2km). According to Bérod et al. (1992b), the area covered by the event can highly influence the precipitable water amount. In fact, when the distance to the centre of the precipitation event increases, the precipitation amount can considerably decrease. Bérod et al. (1992b) also claim that the spatial decrease can be neglected when the basin is sufficiently small. Consequently there is an area below which the usage of the PMP map data does not need to account for a reduction factor linked to the storm extension area. On the other hand, above this area, the PMP maps do not represent a realistic amount of simultaneously precipitable water and lead to an overestimation of the PMF. However, no studies have been done yet to determine the maximum surface above which the PMP cannot by

[7]The initial conditions needed for an event based simulation are depending on the number of state variable the used model is estimating.

considered without reduction factor.

2.6.6 Temporal structure

For a realistic hydrological simulation, information about the hyetograph of the rainfall event, meaning the distribution of the precipitated water volume (extracted from the PMP maps) over time, are necessary. For the estimation of the temporal rainfall distribution, different methods have been developed. A summary of existing methods for the generation of synthetic hyetographs has been exposed by Prodanovic and Simonovic (2004). They classified the methods according to Veneziano and Villani (1999) in 4 categories: (1) Specification of simple geometrical shapes anchored to a single point of the intensity duration frequency (IDF) curve, (2) Use of the entire IDF curve, (3) use of standardized profiles obtained directly from rainfall records and (4) simulation from stochastic models. The fourth category has not been further discussed here. The aim is to come up with a conservative temporal structure for the PMP event. The stochastic approach would be wasteful of computation time because all non-conservative configurations would be generated too.

The first category regroups the most basic methods attributing a temporal structure to the volume derived from the IDF curves. The easiest hyetograph that one could imaging is the rectangular hyetograph as it is used often in the so called rational method (Pilgrim and Cordery, 1993, e.g.). The method of Yen and Chow (1980) structures the rainfall event by attributing a triangular shape to the hyetograph. Watt et al. (1986) refine the shape by adding an exponential decay (and linear increase) for early peaking storms and an exponential increase (linear decrease) for late peaking storms. These approaches are easy to apply but Veneziano and Villani (1999) criticize the absence of a strong conceptual bias and add that these methods may lead to biased flow estimates.

The Chicago method (Keifer and Chu, 1957) fits the second category. This method takes into account the entire IDF curve based on the Talbot equation (exposed in Hingray et al. (2009)). Veneziano and Villani (1999) criticize this method because it overestimates the peak flow due the fact that it produces in the generated precipitation event the T-year event for all the durations shorter than the aimed event.

The methods of the third category reduce the precipitation events to a dimensionless curve by adimensionalizing the total duration of the event and the cumulative rainfall depth, the so-called rainfall mass curves. These curves have first been mentioned in literature by Huff (1967). Therefore, later authors also refer to these curves by calling them *Huff curves*.

For the application in the context of the PMP-PMF method, Bérod et al. (1992b) cites two methods, i.e. the Chicago method (Keifer and Chu, 1957) and the rainfall mass curve method (Huff, 1967). These curves are frequently recommended in literature for the temporal distribution of the PMP (WMO, 2009; Walland et al., 2003). Also Bérod et al. (1992b) retains this approach as most appropriate. In their study, the estimated discharge was less sensitive to the model parameters when the rainfall mass curve approach was used to distribute the PMP in time.

Veneziano and Villani (1999), Bérod et al. (1992b) and Prodanovic and Simonovic (2004) justify the preference for this type of temporal distribution with the argument that it attributes the most realistic shape to the hyetographs. As the rainfall mass curves are very appealing in the context of the present project, they deserve a more detailed description.

2.6.7 Rainfall mass curves

Rainfall mass curves have been introduced 50 years ago, but are still of interest in hydrological science when dealing with temporal rainfall distributions (Caballero and Rahman, 2013; Vernieuwe et al., 2015; Ghassabi et al., 2016). Different characteristics of the curves have been issued in the last years, as is elucidated hereafter.

Huff (1967) distinguished between four different types of curves by separating them according to 4 quartiles depending on the moment the precipitation burst occurred. In the events in the first quartile, for example, the precipitation burst occurs in the first 25% of the total precipitation duration. For the second quartile, the burst occurs between 25% and 50% of the total duration. Huff (1967) found that short events (less than 6h) were mostly associated with the first quartile, storms with a duration between 6 and 24 h with the second quartile, events during between 12 and 24 h with the third quartile and events during longer than 24 h with the fourth quantile. However, Guo and Hargadin (2009), Bonta (2004) and NERC (1975) could show that the curves do not depend on the rainfall duration. Bonta (2004) criticized the approach of separating the curves into burst quartiles, because an analyst could also use a different number of quartiles. Therefore, they did not use quartiles for their study. They supposed that the dependence between event duration and precipitation burst timing was due to the fact that Huff (1967) was not distinguishing between seasons. They stated that a seasonal analysis would lead to the conclusion that the storm durations within a season tend to be similar and that the Huff curves would be independent from storm quartiles. The results of Back (2011) partially confirmed the suppositions of Bonta (2004) for Brazil. They concluded that first and second quartile storms are more likely to occur in summer, whereas third and fourth quartile storms are distributed throughout the entire year.

Shaw et al. (1984) analyzed the regional variability of the rainfall mass curves in Virginia and concluded that only very small regional variability could be found. Regional variability of the Huff curves has also been found by Kimoto et al. (2011) for the state of Arizona. They argue that topography has a significant influence on the temporal rainfall distribution. Bonta (2004) did not find any regional variability for the North Appalachian Experimental Watershed in Ohio. In his case, the three used rain gauges were located only 1.5 km far from each other. He concluded that regionalization of Huff curves is possible. Furthermore, he stated that regions with different climatic conditions should have different Huff curves. Regionalization over large areas has been proved to be consistent by Azli and Rao (2010), determining one set of Huff curves for entire Peninsular Malaysia. In addition, the original Huff curves were developed by Huff (1967) based on 49 gauges spread over 1037 km^2, a topographically homogeneous region (as reported by Azli and Rao (2010)). In the United Kingdom, the study of NERC (1975) led to curves useful across

the entire country due to no or only very small regional variability. In the study of Garcia-Guzman and Aranda-Oliver (1993), it has been shown that, in Southern Spain, the rainfall mass curves depended on duration, depth and season, but the dependence is small. It can be retained that regional variability is small if the considered scale is not too large and the topography is similar within the considered region. Furthermore, heterogeneous climatic zones should be distinguished.

For the temporal distribution of design storms, NRCS (1986) proposed design curves. However, these curves have been shown to overestimate real floods leading to unrealistic results (Kimoto et al., 2011; Guo and Hargadin, 2009; Ghassabi et al., 2016). Guo and Hargadin (2009) concluded that the design Huff curve given by NRCS (1986) do not represent statistical average values. They should be seen as the worst distribution to form a severe storm. The comparison of synthetic temporal distribution models, performed by Prodanovic and Simonovic (2004), let conclude that the design Huff curve given by NRCS (1986) are returning hyetographs with a shape close to the hyetographs produced by the Chicago method (Keifer and Chu, 1957).

Furthermore, Bonta (2004) reported that in an earlier study, Bonta and Rao (1992) could show that Huff curves from hourly data can be used to estimate floods for small watersheds having times of concentration of the order of minutes.

It can be retained, that rainfall mass curves are widely used for temporal storm distribution. Regional and seasonal variability has been proved to exist in some cases. However, the above cited authors do not agree on the dependence of the Huff curves on event duration. Furthermore, to the best of the author's knowledge, Huff curves have not yet been studied on a national scale in Switzerland.

2.6.8 Non-stationary Spatio-temporal distribution

In 2013, the distributed hydrological model MPF was developed for small alpine basins without glaciers by Receanu (2013). This model is divided into a hydrological and a meteorological module. The meteorological module is a cloud-model to distribute the precipitation data from the PMP maps in time and in space. This model provides a dynamic evolution of the rain on a very fine scale over a watershed, or even across an entire region. At the heart of the calculation model is an advection-diffusion equation, which models the behaviour of the cloud, both spatially and temporally. The spatio-temporal distribution is performed by attributing precipitation intensity clouds to the considered event. The spatio-temporal distribution tool was validated by Receanu (2013) for a 6h storm and could be shown to accurately estimate the spatio-temporal distribution of a precipitation event. A disadvantage for its usage in the context of PMF estimations is that this model needs to be calibrated and initialized. Receanu (2013) did this calibration based on radar records of a measured storm event. For PMP events, such records do not exist, making it very difficult to apply it in this context.

The guidelines proposed by The World Meteorological Organization admit stationary PMP storms (WMO, 2009) for the determination of the PMF. In the mentioned manual, it has been explained

that the most extreme observed rainfall events did almost not move. This assumption has been adopted for the present research project as the above mentioned spatio-temporal precipitation distribution tool can not be considered for a reliable use in the context of PMP structuring. Therefore, the spatio-temporal evolution is not adopted for this research project. Space and time variability have been considered separately.

2.6.9 Hydrological model initialization

As exposed above, the PMP-PMF concept is based on an event based approach. This makes the initialization of the hydrological model very important as its influence on the result is remarkable (Hingray et al., 2009; Chen et al., 2016). Harris and Brunner (2011) stated that the initial conditions should be "reasonably possible". The World Meteorological Organization (WMO, 2009) doesn't give any details on model initialization for the determination of the PMF based on the PMP.

Bérod et al. (1992b) have summarized some of the most conventional initialization assumptions for the PMP-PMF approach in terms of antecedent precipitation event. Below is the summary as given by Bérod et al. (1992b) (some elements of this summary can also be found in Hogg et al. (2004)):

- 40 % of the PMP (America Nuclear Standard)
- 15 to 50 % of the PMP depending on the catchment size. (Tennessee Valley Authorities). Stallings (1987) indicated that this organization proposed another antecedent precipitation: the one that produces a 100 year flood followed by a dry period of 3 days.
- Precipitation leading to the 100 years flood followed by a dry period of 1 to 5 days (Bureau of Reclamation).
- Precipitation leading to the 100 years flood in the reservoir, 10 days before the PMP (Soil Conservation Service).
- 40% of the PMP, followed by a dry period of 3 to 5 days (National Research Council).

The Canadian Guidelines on Extreme Flood Analysis (Hogg et al., 2004) proposed to initialize the model with an "antecedent flood [...] based on 100-year precipitation." The dry period between the end of the antecedent rainfall and the beginning of the PMP should be 3 days (Cudworth, 1992).

In mountainous regions, snow from the winter can remain in high altitudes and snowfall is possible even during summer. The initial snow height should also be taken into account as it can have major influence on the generated flood (Chen et al., 2016). However, the above described approach of initializing the model with an antecedent precipitation does not allow to account for

antecedent snow fall, as the snow is resulting from a different season as the one the design storm is supposed to occur.

Hogg et al. (2004) summarized the propositions of FERC (2001) and CDA (1999) for initializations taking snow into account:

- A 100-year snowmelt runoff occurs during and somewhat prior to the PMP (Cudworth, 1992).
- A maximum historical temperature sequence is applied to a 100-year snowpack (FERC, 2001).
- Probable Maximum Snow Accumulation (PMSA) combined with rainstorm not exceeding 100-year severity and prevailing storm temperature (CDA, 1999).
- PMP combined with snow accumulation not exceeding 100-year depth (CDA, 1999).
- PMSA combined with a critically severe temperature sequence (CDA, 1999).

A considerable disadvantage of the antecedent precipitation approach is that this antecedent event also needs to be initialized and one cannot be sure that the duration of the antecedent event is sufficiently long in order to neutralize the influence of the initial conditions. As mentioned earlier, Hingray et al. (2009) stated that in the best cases, the initial conditions become negligible after some days. Consequently, the antecedent precipitation event approach is in most cases sub-optimal. This problem is partially solved by conditioning the initial PMP conditions on the antecedent flood as this induces the calibration of the initial model conditions. However, more combinations between precipitation and initial conditions are possible to lead to the same flood. Thus, the resulting initialization for the PMP-PMF simulation would not be unique.

A more reliable, less severe but realistic and reasonable initialization is described by Beauchamp et al. (2013). They proposed to insert the PMP in a continuous simulation, what leads to the semi-continuous approach, where a lot of different initializations are tested for a given event storm.

The semi-continuous approach of Beauchamp et al. (2013) is however in line with the simultaneity of the possible values for all state variables that need to be initialized. Clearly, this approach leads to less severe initializations if the very severe events have not been simulated, but they remain coherent and no contradiction occurs. This approach has recently been applied by Chen et al. (2016).

It can be retained that for the initialization of the hydrological model, a lot of different propositions could be found in literature. The different approaches differ a lot. A clear consensus could not be asserted. Also were they often vaguely formulated letting space for subjective reasoning. The semi-continuous approach led to the most coherent initializations that could easily be justified by good calibration results.

2.6.10 Temperature conditions

When dealing with PMF estimations, it is important to consider PMP and temperature conditions as a coherent couple (Chen et al., 2016). When looking for a coherent PMP-Temperature couple, the question of precipitation-temperature scaling arises as such a couple cannot be deduced from measured data.

In snow-influenced environments, a key factor for the estimation of event runoff volumes is the aggregation state of the event precipitation (rainfall or snowfall) and the amount of event runoff that is due to the meltwater outflow from a potentially pre-existing snowpack. As discussed e.g. in the work of Schaefli (2016), both quantities can be assumed to strongly depend on air temperature. A precise estimation of the aggregation state of precipitation at a given altitude (of the snowfall limit) would require knowledge of the wet-bulb temperature (e.g. Tobin et al., 2012), but air temperature has been shown to be a good proxy for hydrological purposes (Rohrer et al., 1994). Air temperature is also a dominant driver for melt processes in most alpine environments, since long wave radiation and sensible heat (two of the three dominant energy sources for melt) are strongly influenced by air temperature (Ohmura, 2001).

Accordingly, the relation between precipitation intensity (P) and temperature (T) and the effective runoff and snow melt are key factors for flood estimations. This P-T relationship is generally studied in the context of climate change research, where an often raised question is how strongly the precipitation intensity is likely to increase with increasing temperature (Pall et al., 2006).

Brandsma and Buishand (1997) pointed out that in Switzerland an increase of the mean daily precipitation with temperature was detectable and was also dependent upon the direction and the strength of the atmospheric flow. Lenderink and Van Meijgaard (2008, 2010) could show similar results for Europe. They stated that precipitation extremes can raise twice as fast as expected by the Clausius-Clapeyron relation for hourly precipitation. Hardwick Jones et al. (2010) pointed out that in Australia, extreme precipitation events are more sensitive to a temperature increase and that in this world region, the P-T scaling becomes negative for temperatures beyond 20-26 $^{\circ}C$. Moreover, they showed that the scaling depends on the duration of the precipitation event.

The large scale study of Pfahl and Niedermann (2011) led to the conclusion that at mid-latitude, the correlation between the temperature and the relative humidity of the air mass above the ocean is positive. They confirm the super-Clausius-Clapeyron relation mentioned earlier by Lenderink and Van Meijgaard (2008) for air masses over the ocean. Pfahl and Niedermann (2011) identified advection and meridional transport as main drivers for the correlation between temperature and relative humidity. However, these results cannot readily be transposed to land areas and are therefore not directly applicable in the context of flood estimation.

Later, Westra et al. (2012) performed a large scale analysis taking into account a large dataset of annual maximum precipitation across the globe that allowed them to conclude that at mid-latitudes, the association between temperature and precipitation is significant. They showed a clear correlation between the latitude and the percentage increase per degree warming for

the northern hemisphere. Above $50°N$, the strength of the association becomes even stronger. Berg et al. (2009) showed that the dependence between temperature and precipitation was seasonally conditioned. In addition, Berg and Haerter (2011) analyzed the P-T scaling for different precipitation types in Germany. They concluded that for extreme hourly precipitation, super-Clausius-Clapeyron rates are possible for all precipitation types. But both Berg and Haerter (2011) and Lenderink and Van Meijgaard (2008) pointed out that the P-T scaling is less noticeable for daily precipitation.

As mentioned earlier, Hardwick Jones et al. (2010) showed that negative scaling is possible for high temperatures, which has been confirmed in the work of Lenderink et al. (2011) and Utsumi et al. (2011) for temperatures above $\sim 24°C$. However, the analysis of Shaw et al. (2011) showed that for the United States, negative scalings have not been observed during the summer months. Furthermore, they stated that a super-Clausius-Clapeyron behaviour was noticeable but far less important than in the study of Lenderink and Van Meijgaard (2008,2010). Shaw et al. (2011) even raised the question whether temperature of the upper atmosphere can actually be characterized with the surface temperature. They stated that in some cases, the surface temperature may not represent the temperature of the upper atmosphere.

Later, Westra et al. (2014) argue in their detailed review that negative scalings might be due to moisture availability limitations in the case of high temperatures. Panthou et al. (2014) found similar results for Canada and could nuance that "the longer an event was, the less pronounced was the increase of extreme rainfall intensities with temperature". Similarly, Wasko et al. (2015) showed in a study conditioning the scaling on precipitation event duration that, in Australia, moisture availability limitations cannot be found for short events (1h to 2h). In Switzerland, Molnar et al. (2015) concluded that there could be limitations of moisture availability. However, this conclusion was drawn without discussing its dependence on the precipitation duration. Busuioc et al. (2016) also found evidence for limitations in moisture availability for Romania.

According to Drobinski et al. (2016), moisture limitation might however not be the only explanation for negative scaling. They stated that the negative scaling could be overestimated by the fact that the surface temperature is not a reliable quantity to estimate the temperature at higher altitudes in arid conditions. The temperature could be highly overestimated, inducing a too pronounced negative scaling (Drobinski et al., 2016).

To summarize, it can be retained that a dependence between temperature and precipitation has been found in different studies all over the world. The nature of the P-T relationship differs according to latitudes, seasons and precipitation quantiles. There appears to be a stronger dependence for smaller time steps. Furthermore, negative scaling can occur due to moisture availability limitations, but these limitations can depend on the precipitation event duration.

At the time of this writing, the relationship between temperature and precipitation intensity *and* duration has not yet been studied for central Europe. This paper analyzes the relationship between precipitation and temperature taking into account event duration and seasonality for Switzerland.

2.6.11 Synthesis of the PMP-PMF method review

To sum up, it can be said that the research concerning PMP has well progressed in the last years. However there is a great necessity of improvements in the domain of the PMF. The return periods for PMP and PMF are not known, hence it is impossible to use them in a reliable way for risk assessment. However, as the statistical methods cannot furnish a reliable estimation of floods with extreme return periods, it is important to have another method that is able to estimate the extreme floods. As the PMP-PMF method has a lot of potential to be further developed, this method is very interesting in the context of this research project. Currently unanswered questions concern the temporal distribution of the PMP, the temperature conditions related to the PMP and the initialization for the PMP-PMF simulation.

2.7 Approach for Swiss alpine catchments

As it has been exposed above, a lot of different models are existing. The choice of the model should be done depending on the aimed objectives and on the input data availability. Hingray et al. (2009) pretend that a model should not be more complex than necessary and not to easy in a manner that the simplicity of the model would be limiting.

As the title of this research project tells, the aim is to develop a methodology for extreme flood estimation in order to verify dam safety in terms of spillway capacity. As already mentioned, the Swiss guidelines on dam safety (SFOE, 2008b) propose to use the PMP-PMF method for the safety flood estimation or to consider the 1000-year flood after multiplying it by 1.5 for flood safety verifications. As exposed in the state of the art, the PMP-PMF method refers to a simulation based approach, whereas the fact of estimating the flood corresponding to a certain return period leads unavoidably to the application of statistics. Ideally the extreme flood estimation for Swiss alpine catchments should therefore take both approaches into account.

The annual maxima (AM) approach could be identified as not sufficient for the estimation of very high return period floods like a 1000-year flood. The POT method makes better use of the available data by considering more values than the AM method. However, it would be too optimist to assume that the POT method would allow to overcome the extrapolation limitation of the AM method (2 to 3 times the time series length) in a way that the reliability of the 1000-year flood estimation would be significantly increased. Regarding statistical approaches using information expansion, they have been positively evaluated in literature concerning high return periods (Botero and Francés, 2010; Merz and Blöschl, 2008a,b; DWA, 2012; Bodoque et al., 2014; Brázdil et al., 2012; Benito et al., 2015; Machado et al., 2015). Distributions like the EV4 and LN4 allow causal information expansion by using a deterministic estimation of the PMF as upper bound. These distributions lead thus to a parsimonious combination of the statistics with the simulation based PMP-PMF approach. Therefore, they are particularly interesting for this research project.

However, for the moment, no well defined methodology for the derivation of the PMF, based on the PMP maps, is existing in Switzerland. The model chosen for further investigations for this project should therefore be a rainfall-runoff model allowing to route the PMP derived from the Swiss PMP maps. As Switzerland is highly mountainous and most dams are situated in the mountains, the hydrological model should be adapted to this topography. The model GSM-SOCONT (Schaefli et al., 2005; Schaefli and Zehe, 2009; Jordan et al., 2012) has been mentioned to be developed for exactly these regions. It is a conceptual semi-distributed model, requiring a limited amount of input data and with low computation time. Furthermore, the GSM-SOCONT model has been developed for the simulation of Alpine floods and is therefore well adapted to the present study. Hingray et al. (2009) stated that semi-distributed models are generally a good compromise. Furthermore, the conceptual character of the model is sufficient for extreme flood simulations. Other semi-distributed hydrological models could of course be considered for the final methodology. A major advantage of the semi-distributed model in the context of dam design is the ease of the integration of hydraulic elements (lake level, spillway discharge, pump and turbine discharges) in the model.

Different simulation approaches regarding the initial conditions have been exposed in the state of the art. The most realistic and physically justifiable approach in the context of PMP-PMF is the semi-continuous approach. Therefore, using a continuous simulation to derive the initial conditions for the PMP-PMF simulation has been retained as best adapted.

This leads to the final choice of a mixed method with semi-continuous simulation approach using the simulation result (PMF) as causal information expansion in the context of upper bounded statistical distributions. The chosen hydrological model is the GSM-SOCONT model (Schaefli et al., 2005; Schaefli and Zehe, 2009; Jordan et al., 2012). The EV4 and LN4 distributions presented by Botero and Francés (2010) have been considered.

2.7.1 Description of the GSM-Socont hydrological model

GSM-SOCONT is a semi-distributed hydrological model composed by the non-glacial SOCONT model and the glacial GSM model. Both models are briefly exposed here. A detailed description and the underlying mathematical formulas have been presented by Schaefli et al. (2005), Schaefli and Zehe (2009) and Jordan et al. (2012) and have been well summarized by Garcia Hernandez et al. (2016). When using the GSM-SOCONT model, the subdivision of the catchment into altitude bands has to be carried out under distinction of glacial and non glacial parts. The GSM model is than attributed to the glacial altitude bands and the SOCONT model to the non-glacial altitude bands. Garcia Hernandez et al. (2016) have presented a comprehensive schema of the functioning of the two models in form of flowcharts. Their flowcharts are considered to illustrate and explain the models. Figure 2.4 shows the schema of the GSM model. The flowchart SOCONT model is presented on Figure 2.5.

GSM model

The inputs to the GSM model are precipitation and temperature time series. The GSM model is composed by a snow and a glacier model. The snow model allows to account for solid and liquid precipitation. The transition from liquid to solid is linear and depends on the temperature. The transition is commonly admitted to happen for temperatures between 0 and 2°C, which fits well with observed snow and rainfall observations Rohrer et al. (1994). The snowmelt is computed with a degree-day approach (Hogg et al., 2004). Meltwater leaves the snow pack only if a certain saturation threshold of θ_{cr} is reached. The water contained in the snow pack can refreeze in case of negative temperatures. The outflow from the snow pack(Q_{snow}) is simulated with two linear reservoirs, a fast reservoir(part of the snow model) and a slow reservoir(part of the glacier model). If the snow height is zero, the ice melt process starts. The glacier outflow is simulated through a single linear reservoir. The melt process is simulated with a degree-day approach. The total discharge (Q_{tot}) generated by the glacier model corresponds to the sum of the snow (Q_{snow}) and glacier melt ($Q_{glacier}$) discharges.

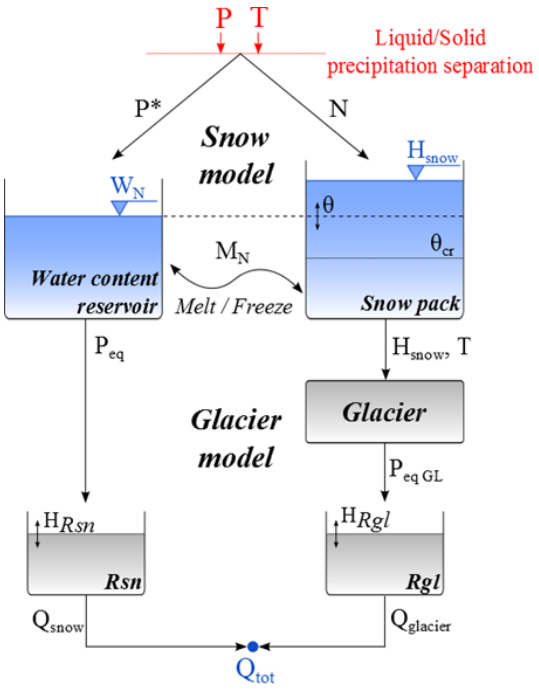

Figure 2.4: Flowchart of the GSM model, taken from Garcia Hernandez et al. (2016).

SOCONT model

The inputs to the SOCONT model are precipitation, temperature and potential evapotranspiration time series. The SOCONT model has the same snow model than the GSM model. The water leaving the snow model (snow melt and liquid precipitation) is supposed to partially infiltrate into the subsoil. One portion of the outflow form the snow model is lost by evapotranspiration.

The degree of infiltration depends on the saturation of the subsoil. A linear reservoir is used to simulated the outflow of the infiltrated water (Q_{GR3}). The portion of the water coming from snow model that does not infiltrate into the subsoil (i_{Net}) is routed as surface runoff with the SWMM model. The total discharge (Q_{tot}) generated by the SOCONT model corresponds to the sum of the discharge leaving the infiltration model (Q_{GR3}) and the runoff discharge (Q_r).

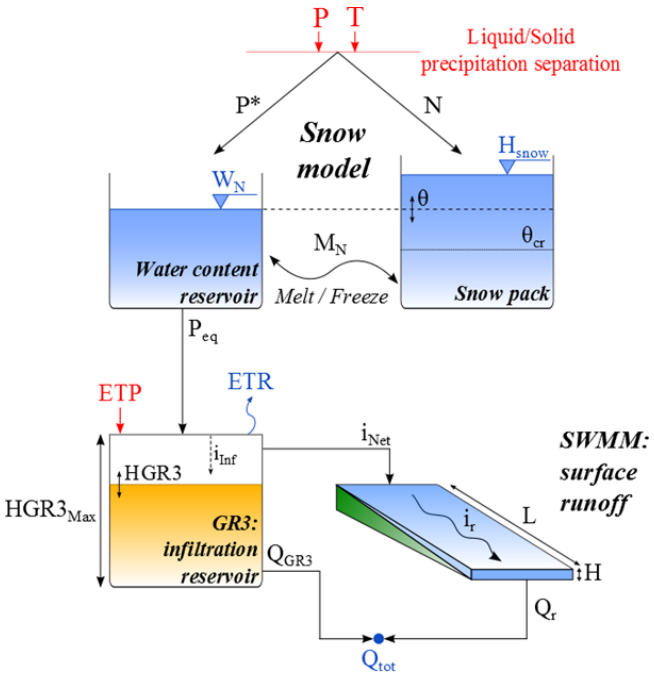

Figure 2.5: Flowchart of the SOCONT model, taken from Garcia Hernandez et al. (2016).

2.8 The largest floods observed around the world and in Europe

When estimating extreme floods, it can be useful to compare the estimations with other approaches or extreme observations in order to verify if a result can be considered to be reasonable. A pragmatic and easy approach to judge estimates would be to compare them to the largest observed floods. Francou and Rodier (1967) have classified the worlds biggest floods and deduced a coefficient K, called Francou coefficient, sometimes called Francou index or Francou-Rodier index, that allows to compare the importance of floods from different basins with different catchment areas. The mathematical expression of K is given by equation 2.8. This coefficient is currently used in the World Catalogue of Maximum Observed Floods (IAHS, 2003) to characterize the importance of the floods from different basins with different areas. According to IAHS (2003), the World's largest known flood has a Francou coefficient of $K = 7.34$. It has been observed in Iceland in 1996. The flood was caused by glacier melt water due to volcanic activity. Of course, this flood cannot be compared with the hydrological risk of the major part of European catchments and the cause is not a heavy rainfall, but it allows the reader to get an idea of the order of magnitude of the Francou coefficient for extreme floods. According to Herschy (2001),

the maximum measured European floods (ignoring the Icelandic flood from 1996) did not exceed $K = 5.65$ until the moment when the analysis was carried out.

$$K = 10\left(1 - \frac{\log(Q) - 6}{\log(A) - 8}\right) \tag{2.8}$$

where Q is the measured discharge in m^3/s and A the surface of the watershed in km^2.

Marchi et al. (2010) classified the euorpean floods and deduced a European maximum observed floods envelope curve (Equation 2.9). They showed, that this envelope curve was mainly defined by the flood measured in the Mediterranean areas. The Alpine floods considered in the study of Marchi et al. (2010) were all smaller than the Mediterranean floods. Unfortunately, an Alpine envelope curve was not exposed by Marchi et al. (2010), but an approximative equation (Equation 2.10) has been derived by analyzing the points corresponding to the alpine floods of the "surface-discharge" graph given by Marchi et al. (2010). A comparison of this curve with PMF estimates for alpine catchments can be interesting in the context of this research project.

$$Q = 97A^{0.6} \tag{2.9}$$

$$Q = 11A^{0.5} \tag{2.10}$$

where Q is the discharge in m^3/s and A the area in km^2 of the catchment.

Equations 2.9 and 2.10 show that the relation between the maximum observed discharge and the catchment area has a linear behaviour in a log-log space. An interesting point to judge on the realistic character of PMF estimates for different basins.

2.9 Objectives and research questions

The objective of the CRUEX++ project is to develop a methodology for the estimation of extreme floods in alpine catchments in order to verify the safety of dams compared to their spillway capacity. After the literature review leading to the exposed state of the art, some lacks of knowledge have been identified, leading to the formulation of the following research questions.

1. Do rainfall mass curves depend on precipitation duration, season and geographical region, in Switzerland or can a single curve be considered as sufficient for the entire Swiss territory

despite its topographic complexity?

2. Is it reasonable to assume a temperature that is high enough to avoid solid precipitation in alpine catchments for extreme precipitation events? Could such a high temperature be related to the precipitation by considering meteorological soundings and precipitation observations?

3. How important is the influence of the initial conditions in the context of PMP-PMF simulations? How large is the prediction interval of the PMF estimates due to various initial conditions and do inter-dependences among the model state variables significantly influence the PMF estimate?

4. What is the maximum admissible spatial expansion of a PMP event, derived from the Swiss PMP maps, for which the spatial intensity decrease can be neglected?

5. Are upper bounded statistical distributions valuable for extreme flood estimations in terms of robustness and sensitivity to the extrapolated sample compared to conventional unbounded distributions? How sensitive are the extrapolations of the upper bounded distributions to the a priori deterministically estimated upper bound?

The above research questions that could be formulated after the literature review are treated and exposed in Part II. Intermediate conclusions are drawn for every treated question. These conclusions allow to compensate for the current lacks of knowledge that prevent performing PMP-PMF simulations, based on the Swiss PMP maps, under justifiable meteorological and terrain conditions. In order to guarantee the formulation of justifiable meteorological and terrain conditions for PMP-PMF simulations, the analyses carried out in this research project are based as much a possible on data analysis rather than theoretical developments in order to assure a maximum of physical coherence prove.

Finally, the different findings will be combined in order to formulate a new methodology for extreme flood estimations and three case studies have been carried out in order to illustrate the application of the methodology.

Part II

Scientific developments for extreme flood estimations

3 Swiss rainfall mass curves and their influence on extreme flood simulations

3.1 Introduction and objectives

The present chapter analyses the regional and seasonal variation of rainfall mass curves in Switzerland. The eventual detected variability is then tested on its influence on the flood and water level simulations.

A rainfall event is defined by the precipitated volume, the spatial and the temporal structure. In the case of stationary events, the spatial and temporal distribution can be analysed separately. For this research project, the Swiss PMP maps developed by Hertig et al. (2005), have been assumed to represent the spatial distribution of a stationary PMP-event. This assumption is in line with the guidelines proposed by The World Meteorological Organization who admit stationary PMP storms (WMO, 2009) for the determination of the PMF. In the mentioned manual, it has been explained that the most extreme observed rainfall events did almost not move. This assumption has been adopted for the present research project and justifies the stationarity hypothesis. The temporal structure of the precipitation event is however not reported on the maps and cannot be directly derived. In the literature review, the state of the art on temporal rainfall structures has been exposed (Section 2.6.6) and different existing approaches have been presented. Is has been retained that the rainfall mass curve approach is the most appropriate as it is by construction the most realistic temporal distribution (Bérod et al., 1992b; Veneziano and Villani, 1999; Prodanovic and Simonovic, 2004). The rainfall mass curve is a the expression of the cumulated precipitated water represented as adimensionalized function expressing the percentage of precipitated water vs the precipitation duration proportion. Figure 3.1 illustrates three schemas of hyetographs with their respective rainfall mass curve. These schemas illustrate the appearance of the rainfall mass curves for early, centred and late burst precipitation events.

Before entering the analysis of seasonal and regional variation, a sensitivity analysis on the storm event definition has been performed in order to chose the most appropriate precipitation event definition. Finally, rainfall mass curve dependence on the precipitation event duration has been issued. The aim of the analysis is to see if regional, seasonal and precipitation duration

related variations of the rainfall mass curves are significant for extreme flood and reservoir level estimates.

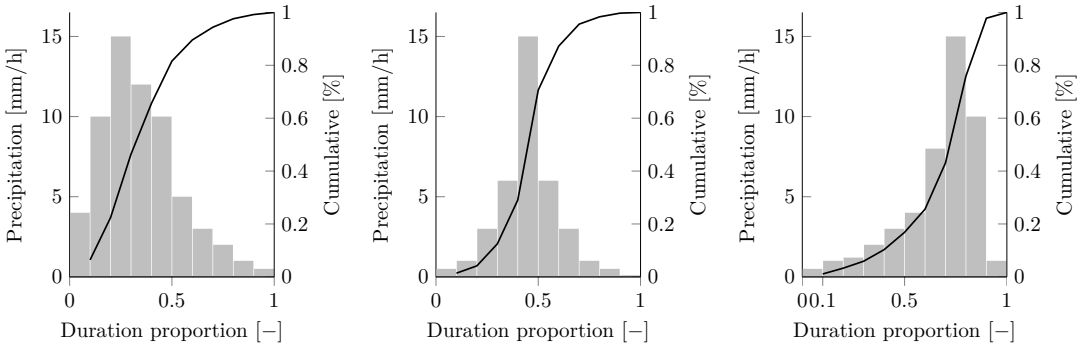

(a) Early bursting event (b) Centrally bursting event (c) Late bursting event

Figure 3.1: Schemas of synthetic rainfall mass curves represented with the related hyetographs.

3.2 Data and methodology of the analysis

3.2.1 Data used for the present study

Hourly precipitation data was provided by MeteoSuisse at 99 locations (Figure 3.2). The hourly precipitation measurement started in 1981 but not all 99 stations were operational since 1981 and some of them have been removed since then. A total of 52 stations have a record of over 30 years. Roughly 18 stations have been added during the period from 1984-2010. From 2011 to 2013, 24 additional stations have been installed. After 2013, until the beginning of 2015, 5 more rain gauges have been built. For this study, all stations have been considered with their respective observation period.

3.2.2 Methodology of the rainfall mass curve analysis

The precipitation data was prepared for the analysis by separating the storm events from the dry periods. The events were than classified by their duration with an hourly time step. Events with durations smaller than 3h have not been taken into account as the few data points due to the hourly time step prevented from drawing representative rainfall mass curves (the 1h-events would lead to a mass curve formed by a single straight line). It has been assumed that, from a precipitation duration of 3h on, the rainfall mass curves can describe the temporal structure of the precipitation, given the hourly temporal resolution of the precipitation observations. Below this minimum duration of 3h, the structure of the rainfall mass curve has been considered to be an artefact of the temporal resolution of the observations and can thus not sufficiently approach the real temporal structure of the precipitation. This is the same approach than the one adopted by Azli and Rao (2010). Nevertheless, the structures observed for longer precipitation durations can

be applied to structure precipitation events with a duration of less than 3h. This could be shown by Bonta and Rao (1992).

The number of events per event duration and season have been plotted in order to assure that the rainfall mass curve calculation was based on sufficiently large samples. For every event duration, only the events with a volume larger than the median volume of the events with a certain duration were retained and subdivided into seasonal sets. A regional classification was then performed according to characteristic Swiss regions. The rainfall mass curves have been calculated for every event and the 95%, 50% and 5% quantiles have been plotted. The differences between two curves induced by eventual regional, seasonal and event duration dependent variations has been quantified by estimating the portion of the precipitated water volume that is displaced in time. For this quantification a check volume of 1 m^3 has been admitted to estimated the displaced volume portion. This calculation has been undertaken for the three quantile curves. Only the most critical case of regional, seasonal or duration dependent variation, i.e. the biggest difference between two curves of the same quantile, has been discussed as an upper limit.

In the next step, a hydrological application on the Mattmark dam catchment allowed to evaluate the influence of the rainfall mass curve shapes on the flood hydrograph in the context of PMP-PMF estimations.

Finally, the rainfall mass curves (5%, 50% and 95% quantiles) are compared to all measured events in order to determine whether the quantile curves are representing realistic events. The measured event curves that are the closest to the quantile rainfall mass curves have been determined and plotted for comparison with the quantile curves. The comparison has been performed considering the root mean square error ϵ defined by equation 3.1.

$$\epsilon = \sqrt{\frac{\sum_{i=1}^{N}(R_q(t) - R_o(t))^2}{N}} \tag{3.1}$$

where R_q stands for the quantile rainfall mass curve, R_o for the rainfall mass curve from observed events and N is the number of values that define the curve.

3.2.3 Event definition

For the purpose of this study, two criteria were used to define a precipitation event. The first one is defines the start and end of an event: an event starts at the moment when $i > 0.1$ mm/h and ends when $i < 0.1$ mm/h, where i stands for precipitation intensity.

The second criterion was introduced to analyze the sensibility of the results to the definition of the precipitation events. It aims at grouping the precipitation amounts of consecutive precipitation events that are separated by less than a certain duration λ. It was defined as follows: If two

events are separated by a time interval λ hours (where $\lambda \in \{0, 1, 2\}$), these consecutive events were considered to be a single event, with the start date of the first event and the end date of the last event. Initially, the value of λ was fixed to 0. Then the analysis was repeated twice for the other two values. A graphical illustration of this third criterion is shown on Figure B.1.

3.2.4 Seasonal and regional subdivision

In order to account for seasonal variability, four seasons were defined: (1) winter (from December to February), (2) spring (from March to May), (3) summer (from June to August) and (4) autumn (from September to November).

Concerning the regional subdivision, the literature review (Section 2.6.7) showed that the topography is supposed to have an impact on the rainfall mass curves. This makes the analysis of rainfall mass curves, accounting for characteristic topographic regions, particularly interesting for Switzerland due to the highly varied topography. The regional subdivision of Switzerland for this study was based on the biogeographical zones of Switzerland (FOEN, 2001). These zones are corresponding to the different topographical regions and subdivide the most heterogeneous region, the Alps, in smaller regions. The subdivision in six different zones is shown on Figure 3.2 and the number of stations per region in Table 3.1.

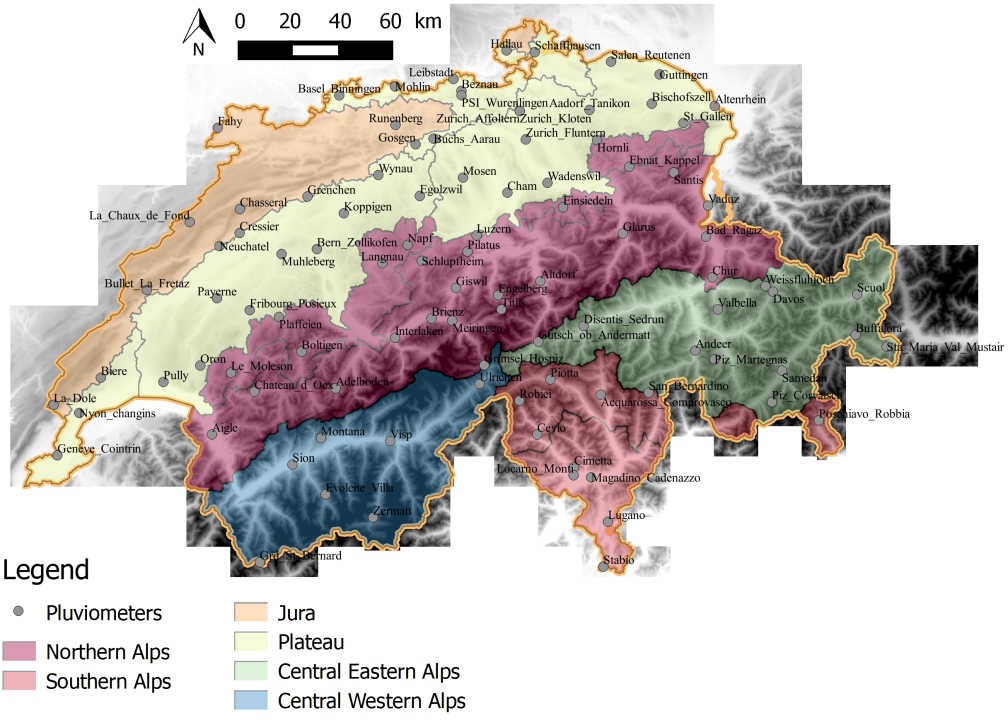

Figure 3.2: Swiss regions and pluviometers considered for the rainfall mass curve analyses.

Table 3.1: Number of pluviometric stations per region.

Region	Number of stations
Central Western Alps	7
Central Eastern Alps	14
Jura	11
Plateau	31
Northern flank of the Alps	26
Southern flank of the Alps	10

3.2.5 Influence of the sample size

The event definition, as exposed in Section 3.2.3, influences the number of events per event duration. As can be seen on Figure 3.3, the number of events is decreasing with the event duration for both definitions (one with a dry period of 1h and one with a dry period of 3h). The two event definitions lead to curves, describing the sample size decrease with the event duration per season, that are approximately parallel. The definitions do thus not influence the shape of the curves but only the sample size. In the following, it is explained how a rough estimation of the minimum sample size for the determination of the rainfall mass curves (RMC) can be made. For this purpose, the relation between the event duration and the number of events (Figure 3.3) and the relation between the event duration and the mean RMC variation $\Delta(d)$ (defined by Equation 3.2 and represented on Figure 3.4) has been considered.

$$\Delta^q(d) = \frac{\sum_{t=1}^{N} R^q_{0,d}(t) - R^q_{2,d}(t)}{N} \tag{3.2}$$

where d stands for the event duration, $R^q_{0,d}$ for the rainfall mass curve with a maximum of 1h dry period corresponding to the event duration d and for quantile q, $R^q_{2,d}$ for the rainfall mass curve of quantile q with a maximum of 3h dry period, and t stands for the dimensionless duration of the mass curve and N stands for the number of values defining the curves.

The reasoning is based on the most constricting season and region for the 5% quantile rainfall mass curve. As can be seen on Figure 3.3, the summer period for the Central Western Alps is the most limiting combination in regard to the minimum sample size. In fact, Figure 3.4 shows that up to an event duration of $d = 24$, the two definitions lead to roughly the same RMC quantile curves. According to Figure 3.4 it can be assumed in agreement with the most constraining region (Central Western Alps) that the number of events ($N = 15$) for the determination of $R^{0.05}_{0,24}$ is sufficiently large to result in practically the same RMC quantiles (mean variation $\Delta^{0.05}(24) \approx 0$) than the larger number of events ($N = 75$) for the determination of $RMC^{0.05}_{2,24}$. Due to the equivalence of the RMCs derived from a small sample of 15 events (1 hour inter event dry period) and a larger

sample of 75 events (3 hour inter event dry period), it is assumed that the number $N = 15$ is sufficient for a reliable RMC quantile determination. Considering the event definition with an inter event dry period of maximum 3h, the necessary minimum sample size (N=15) is reached for an event duration of roughly $d = 35$ (Figure 3.3). The definition with an inter event dry period of maximum 3h has been considered for the following analysis due to the possibility of extending the study to longer events (up to $d = 35$h). The bar plot on Figure 3.5 confirms that for all seasons, enough data ($N \geq 15$) are available for reliable RMC quantile determinations.

The figures showing the mean variation $\Delta^q(d)$ for the 50% and 95% quantiles (Figures A.1 and A.2) are shown in the Appendix A. These curves lead thus to the same conclusion of a minimum sample size of 15 events. Finally it can be retained that the analysis carried out in this chapter is based on the event definition with a dry period of 3h, what allows to analyse event up to a duration of 35h.

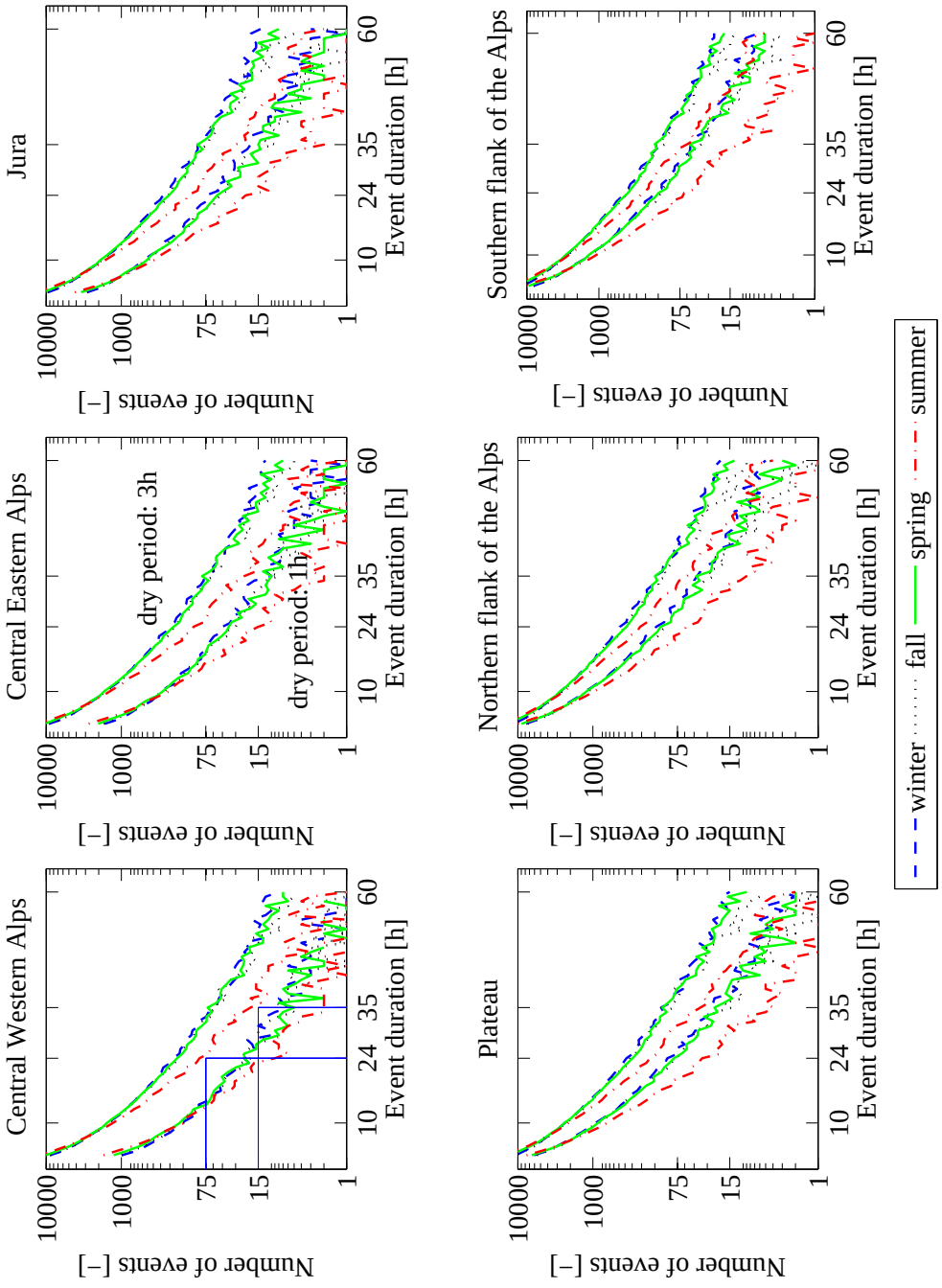

Figure 3.3: Number of measured events per Swiss region (Central Western Alps, Central Eastern Alps, Jura, Plateau, Northern flank of the Alps, Southern flank of the Alps) and season (winter, fall, spring , summer) for the event definitions with 1h and 3h dry inter event periods.

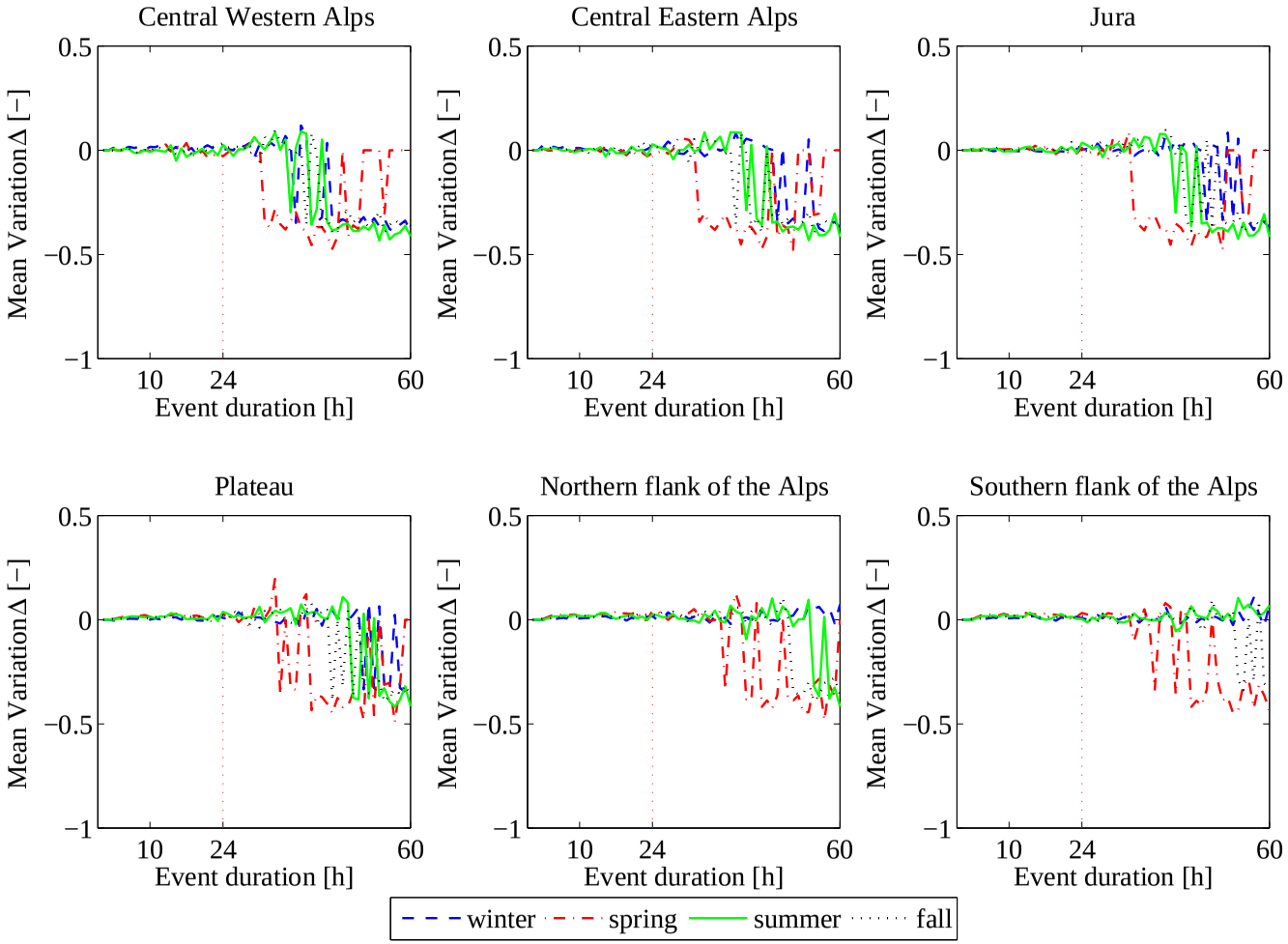

Figure 3.4: Mean variation Δ of rainfall mass curves from event definitions with 1h and 3h dry inter event periods for six Swiss regions (Central Western Alps, Central Eastern Alps, Jura, Plateau, Northern flank of the Alps, Southern flank of the Alps), four seasons winter, fall, spring , summer) of the year and the 5% quantile of the rainfall mass curves.

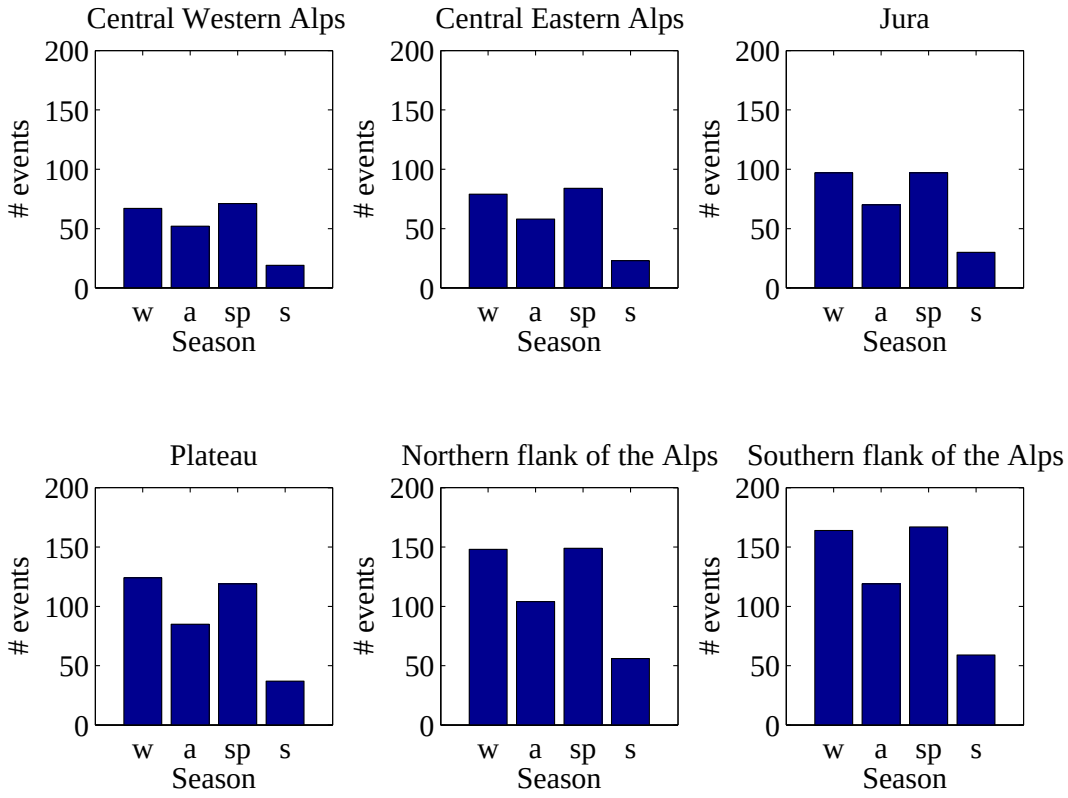

Figure 3.5: Number of events per season for an event duration d = 45h. w=winter, a=autumn, sp=spring, s=summer.

3.3 Results

3.3.1 Regional variability of Swiss rainfall mass curves

The regional variability is discussed here for the two most characteristic seasons (summer as being the hottest and winter as being the coldest season). By doing so, the analysis can be based on two seasons that are marked by considerable climatic differences. For each season, the rainfall mass curves for four event durations were plotted, i.e. 4h, 12h, 24h and 35h. The regional rainfall mass curves are shown on Figures 3.6 and 3.7 for summer and winter. The figures for spring and autumn are shown in Appendix A on Figures A.3 and A.4.

On Figures 3.6 and 3.7, it can be seen that the regional variability is very small but seems more pronounced for summer. In Figure 3.6 it can be observed that for the 95% quantile, the Southern Alps tend to have an earlier burst than the other regions and for the 5% quantile, most of the precipitation volume is released at the end of the event. For the median curve, no big differences can be seen for events lasting up to 24h. For the winter season (Figure 3.7), the regional variations are smaller, but it can also be observed that the events registered in the Southern Alps burst earlier for the 95% quantile whereas the 5% quantile shows rather later bursts. Among the 95%

quantiles, the RMCs of the Central Western Alps led to the latest precipitation burst. In regard to the 5% quantiles, they led to the earliest bursts for the Central Western Alps. These findings hold for durations up to 24h. The biggest rainfall mass curve variation can be observed between the Central Western Alps and the Northern Alps for an event duration of 35h regarding the 50% quantile curve. Indeed the 23% of the volume are displaced in time. By observing Figures 3.7, A.3 and A.4 in Appendix, it can be retained that the differences between the curves are generally smaller than those observed for the summer period. To sum up, regional differences can be observed throughout the seasons. These variations seem to be rather independent on the storm duration. The maximum difference that could be found regarding the portion of temporally displaced volume is 23%.

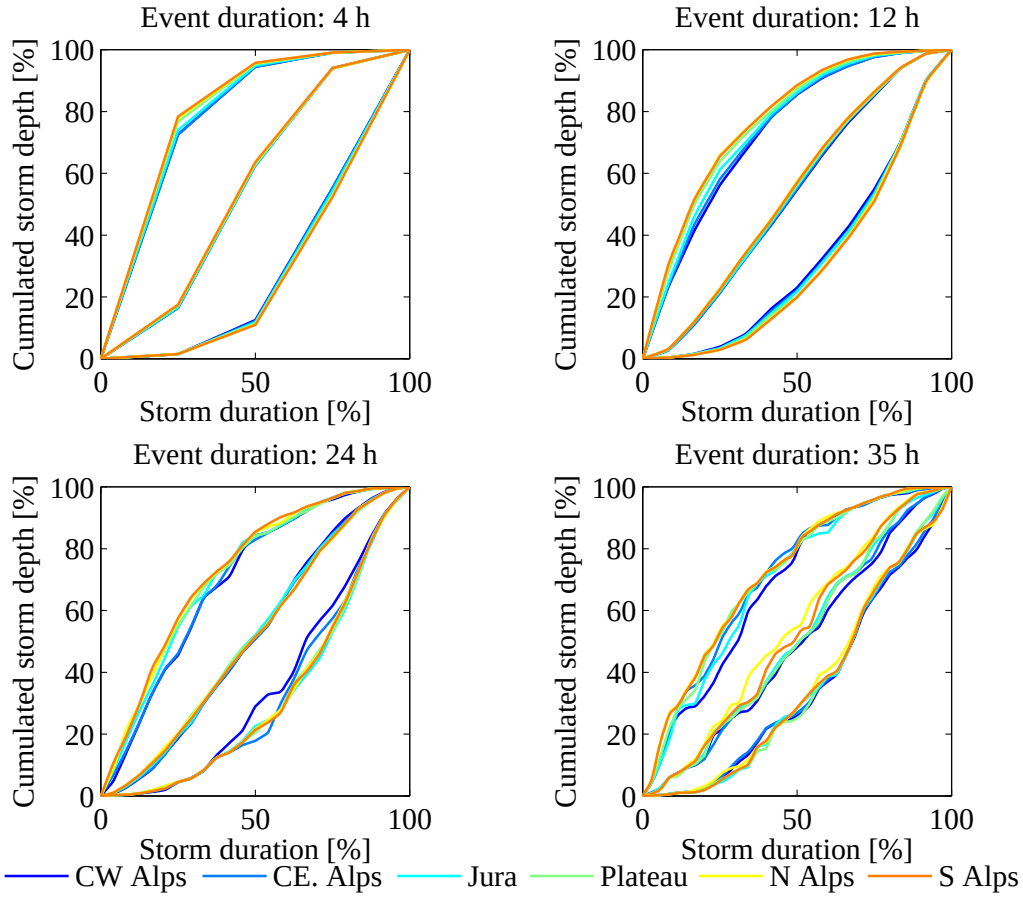

Figure 3.6: Rainfall mass curves for six regions (CW Alps = Central Western Alps, CE Alps = Central Western Alps, N Alps = Northern Alps, S Alps = Southern Alps) during summer for four different event durations (4h, 12h, 24h, 35h).

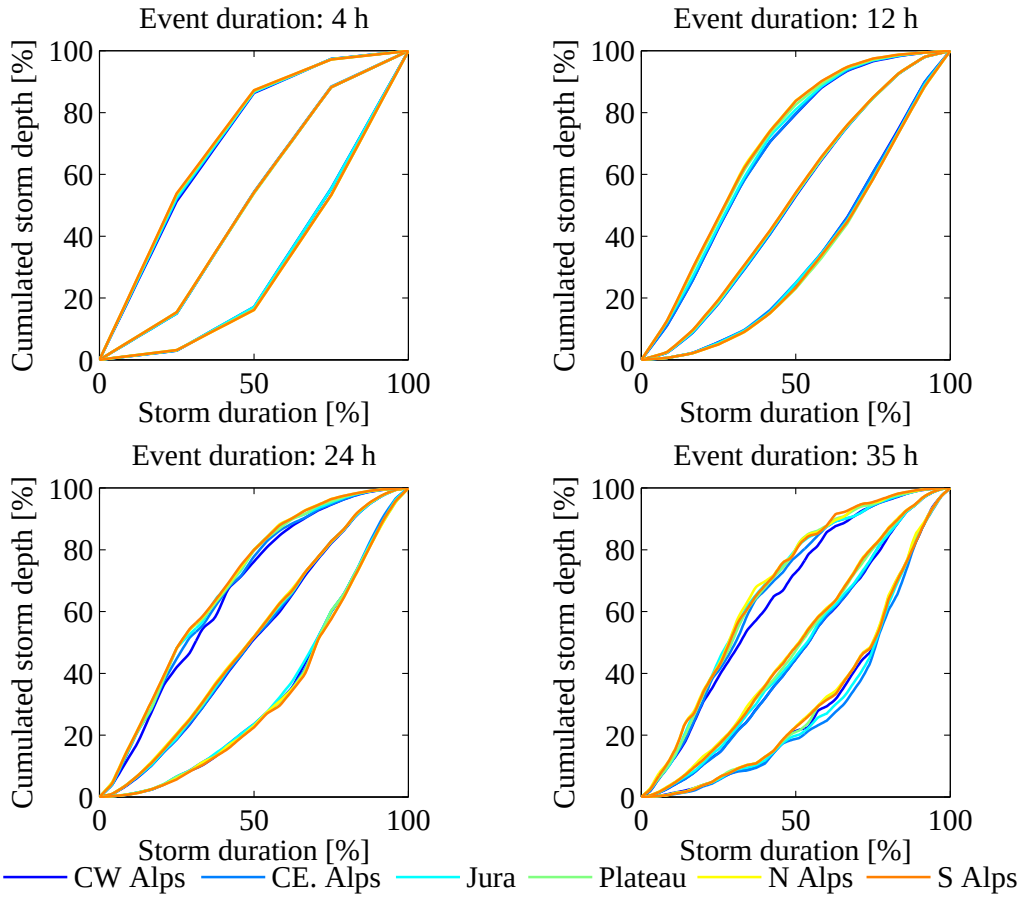

Figure 3.7: Rainfall mass curves for six regions (CW Alps = Central Western Alps, CE Alps = Central Western Alps, N Alps = Northern Alps, S Alps = Southern Alps) during winter for four different event durations (4h, 12h, 24h, 35h).

3.3.2 Seasonal variability of Swiss rainfall mass curves

In this section, the seasonal variability of Swiss rainfall mass curves is exposed. For illustration purposes, two regions have been chosen, i.e. the Southern Alps (high topographic variability) and the Plateau (no mountains). The resulting RMCs are shown on Figures 3.8 and 3.9. The plotted seasonal rainfall mass curves for the four other regions are given in Appendix A on Figures A.5, A.6, A.7 and A.8. Again, four different event durations are considered.

Figures 3.8 and 3.9 indicate a seasonal dependence. The dependence is apparent for all regions, the two exposed here as well as the four others as it can be seen on the Figures shown in Appendix A. The dependence is stronger for the 95% quantile curves and a light dependence on the storm duration is existing for this quantile. Concerning the 4h-events in the Southern Alps, the difference between the summer and the winter for the 95% quantile curve consists in a displacement of 25% of the precipitation volume. For the other curves, the displaced volume percentage is smaller or equal. The median RMCs are in general less influenced by the season. The maximum displaced

volume portion is 20% and is reached for the 35h event. Practically no seasonal variability is apparent for the median curves derived from 24h storms . The 5% quantile curves are only little influenced by the season up to storm durations of 24h (the displaced volume portion is smaller than 14%). The curves derived from 35h storms indicate a higher seasonal dependence for the 5% quantile, indeed the difference between the summer and the winter consists in a displacement of 25% of the precipitation volume for the Southern Alps. Visually, it can be noted that the order of magnitude of the displaced volumes for the different seasons is the same throughout the regions.

The differences between spring and fall curves is hardly noticeable. A clear difference is, however, existing between the winter and summer curves. It can be retained that a seasonal dependence is obviously existing throughout the six Swiss regions and induces a maximum of 25% of the volume to precipitate at a different moment. Figures 3.9, A.5, A.6, A.7 and A.8 prove the resemblance of seasonal behaviour throughout the six regions.

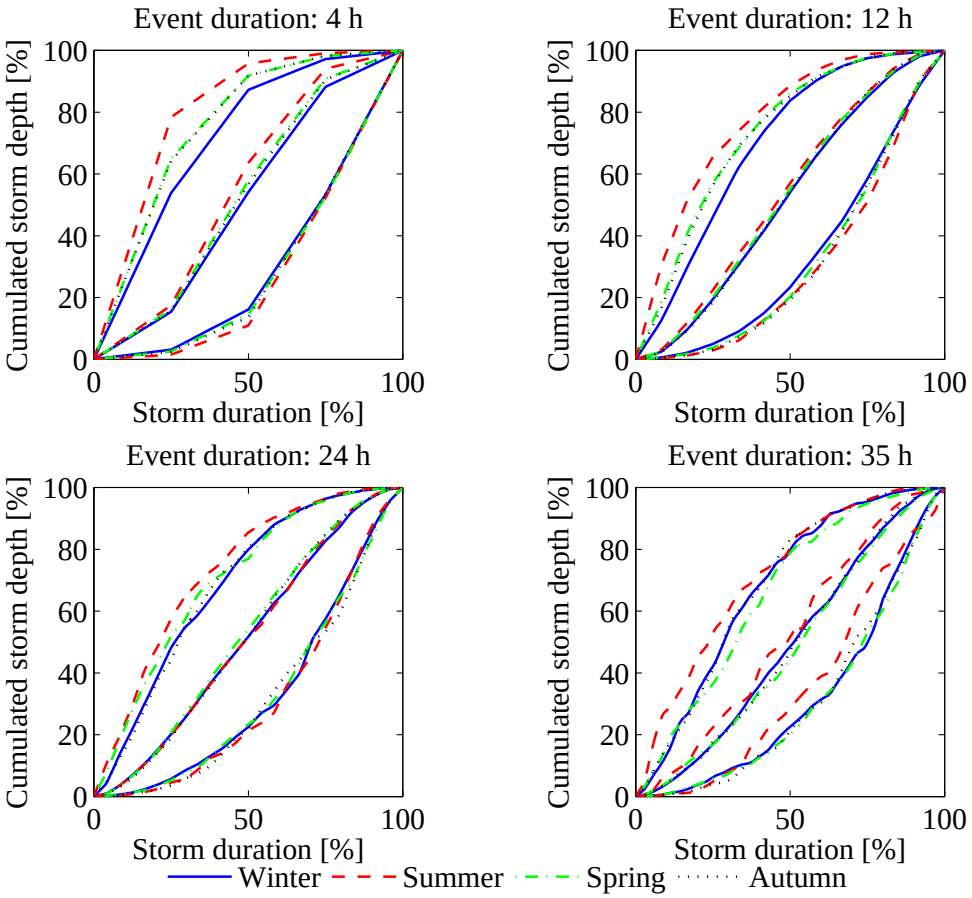

Figure 3.8: Rainfall mass curves for the Southern Alps for four different seasons (winter, summer, spring and autumn) and four event durations (4h, 12h, 24h, 35h).

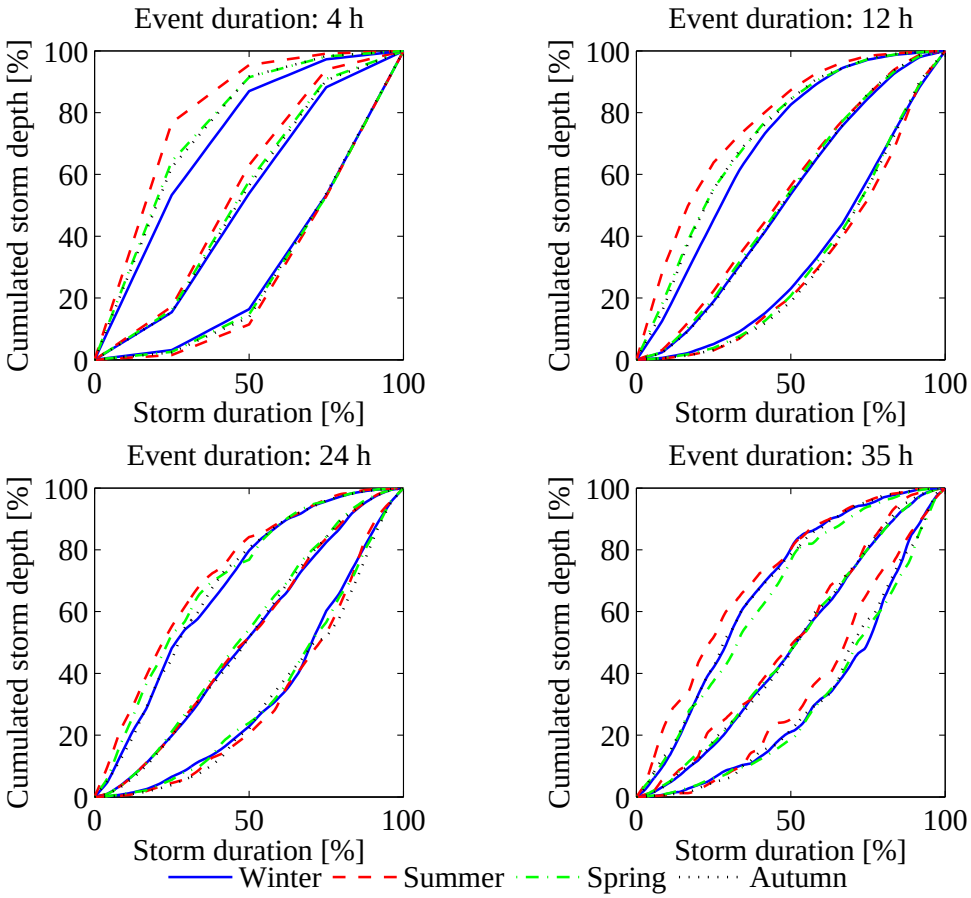

Figure 3.9: Rainfall mass curves for the Plateau for four different seasons (winter, summer, spring and autumn) and four event durations (4h, 12h, 24h, 35h).

3.3.3 Dependence on the event duration

The dependence of the Swiss rainfall mass curves on the storm duration of the events they are derived from is assessed in this section. Two regions have been chosen for the illustration of the event duration influence on the rainfall mass curves, i.e the Southern Alps and the Plateau. The considered durations are reaching from 3h to 35h with an hourly timestep. Figure 3.10 and 3.11 show the duration dependent rainfall mass curves for the four seasons (winter, spring, summer and autumn).

A clear dependence on the event duration can be seen. The variability of the RMCs is the smallest for winter and culminates in summer. It is apparent that the 95% curve is moving towards the median curve with increasing event duration. For the median curve, a difference can only be seen during approximately the last 50% of the storm duration: longer events tend to burst later, especially in summer and autumn. Concerning the 5% quantile curves, summer and spring plots show that longer storms tend to release a higher volume during the first half of the storm

than shorter events and behave similarly from approximately 60% of the storm duration on. The difference between the duration dependent rainfall mass curves has been observed to be maximum for the summer season in the Southern Alps for the 95% quantile curves. In fact, the temporally displaced volume portion reaches 38% comparing the curve corresponding to an event duration of 4h to the one of 33h. The differences between the other curves are smaller for all the six regions throughout the four seasons.

The figures for the other regions are shown in appendix A on Figures A.9 A.10, A.11 and A.12. These figures confirm the duration dependence discussed for the Southern Alps and the Plateau. The duration dependence can thus be detected for the all considered regions (Figure 3.2).

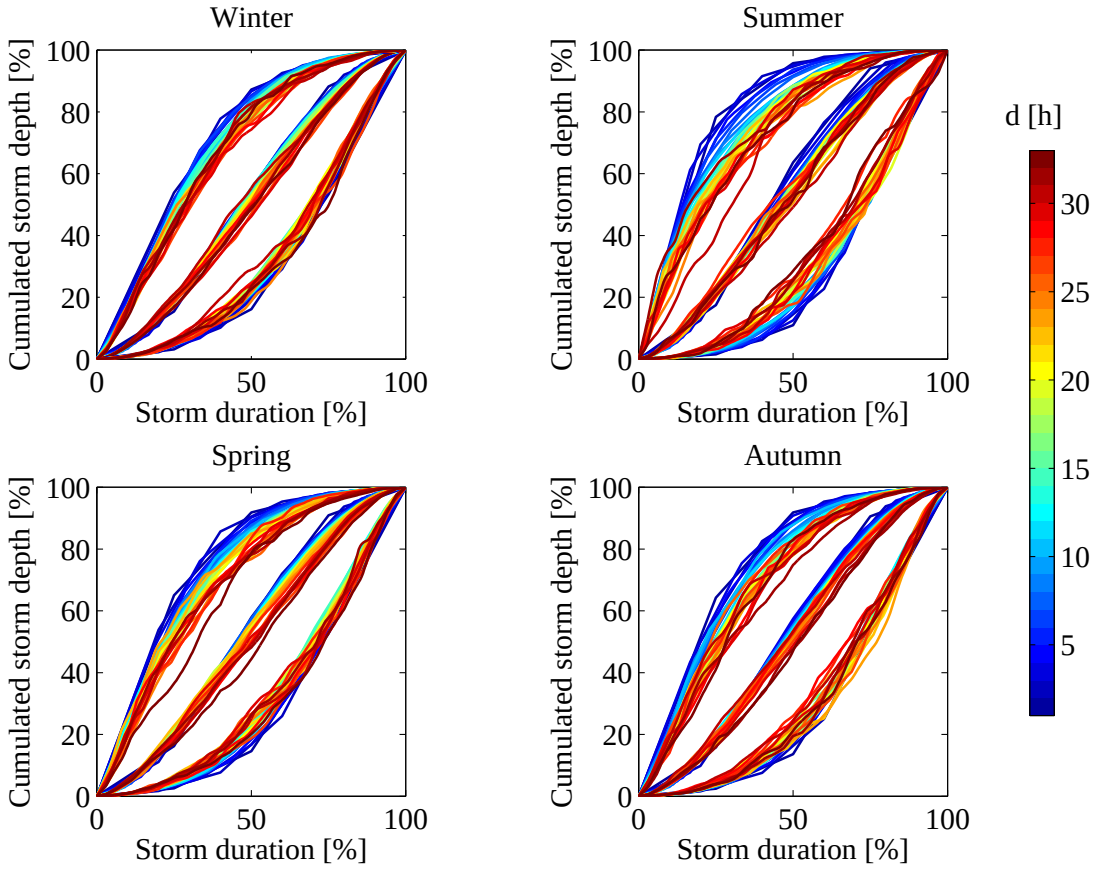

Figure 3.10: Rainfall mass curves for durations from 3 h to 35 h for the Southern Alps for the four seasons (winter, summer, spring and autumn).

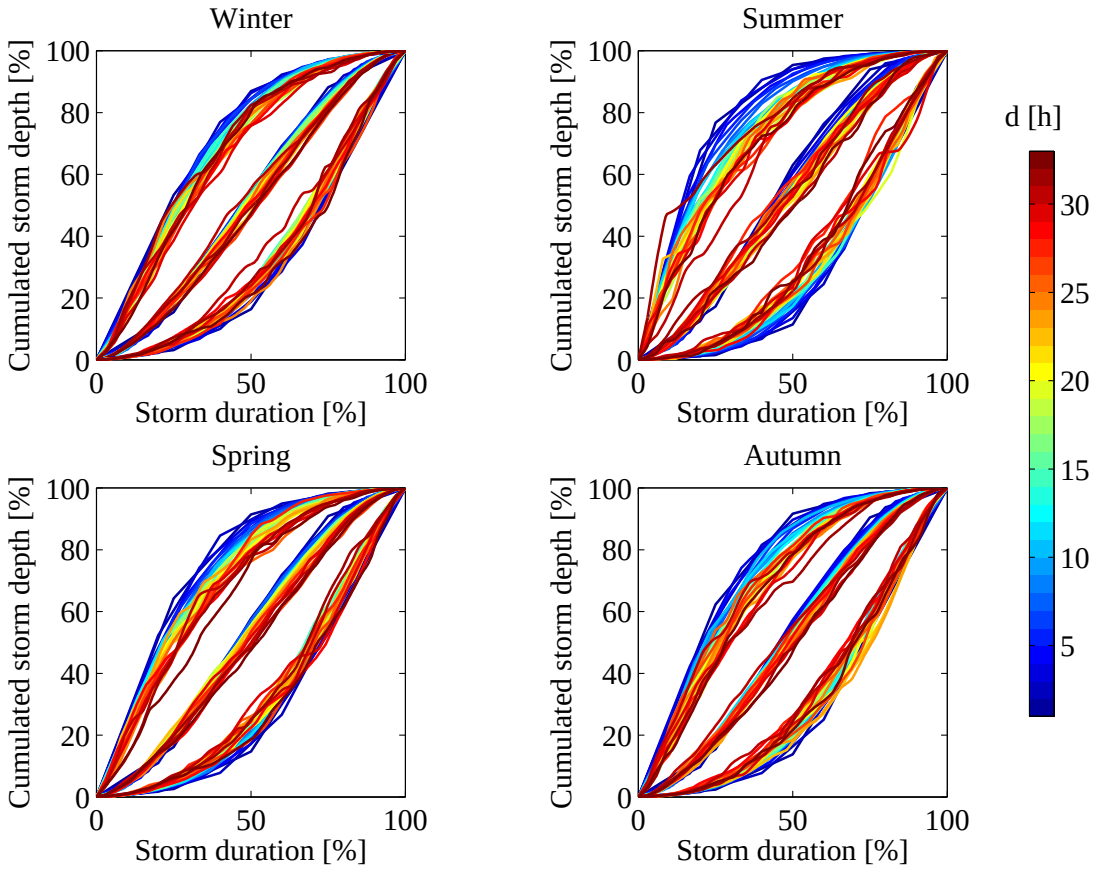

Figure 3.11: Rainfall mass curves for durations from 3 h to 35 h for the Plateau for the four seasons (winter, summer, spring and autumn).

3.4 Relevance of the rainfall mass curve variability for extreme flood estimation

Seasonal, regional and event duration dependences were analysed for rainfall mass curves. The question raised, if the different observed variations were significant for extreme flood estimations. In this section, a hydrological application on the Mattmark dam catchment allowed to conclude on this issue in the context of PMP-PMF simulations.

3.4.1 The case study of the Mattmark dam catchment

The hydrological application on the Mattmark dam catchment was performed to analyze the influence of the seasonality of rainfall mass curves as well as the influence on the event duration. The Mattmark dam catchment is situated in the central western Alps as it can be seen on Figure 3.12. The precipitation-runoff simulation has been performed with the GSM-Socont model (Schaefli et al., 2005; Schaefli and Zehe, 2009; Jordan et al., 2012). This is a semi-distributed

conceptual hydrological model developed for mountainous catchments. Around 28% (10 km^2) of the entire catchment surface, 36 km^2, is covered by glaciers. The basin goes from 2174 m a.s.l. to 3898 m a.s.l. Given the small size of the study catchment, this model does not take into account river routing.

The analysis was done by comparing the hydrographs derived from the regional, seasonal and duration dependent curves and the hydrographs derived from a rainfall mass curve determined for Switzerland but without any subdivision. This curve (Figure 3.13) served as reference curve in order to discuss the relevance of distinguishing between curves derived for a certain region, season and event duration when performing extreme flood estimations with a PMP-PMF approach. For the analysis, the three RMC quantiles 5%, 50% and 95% have been considered.

Figure 3.12: Situation of the Mattmark dam on a map of Switzerland.

Under the assumption that high temperatures are necessary to create a PMP (Hertig and Fallot, 2009), the winter season has been omitted from the following analysis. As the Mattmark dam is situated in the Central Western Alps, the latter region was considered for the analysis of the influence rainfall mass curve on the generated discharge. Thus the influence of the geographical variation could not be directly addressed. However, it could be shown that the regional variation was the smallest among the three analysed variation origins (season, region and event duration). Thus if the seasonal and duration dependent variations do not induce a significant difference regarding the hydrographs and the lake level, it can be assumed that the regional variations can be neglected as well. PMP events with durations of 4h, 8h, 12h, 24h and 35h have been considered and derived from the Swiss PMP maps (Hertig et al., 2005). The choice of these durations has been made in order to analyse the eventual influence of the RMCs on the hydrograph for different durations, sufficiently distant not to overlap each other on the graph and make the latter unreadable. In order to make the comparison as independent as possible from temperature and initial terrain conditions, the hydrological model has been initialized with the same values for all seasons (no snow, 30% of soil saturation) and the temperature has been admitted to be high

enough to avoid snow fall, i.e. 0°C at 4500 m a.s.l..

Besides the influence on the generated hydrographs, the impact of the different rainfall mass curves on the water level in the reservoir of the Mattmark dam was assessed. The H-V relation (water level - water volume relation) as well as the H-Q relation (water level-outflow discharge) are given on Figure 3.14.

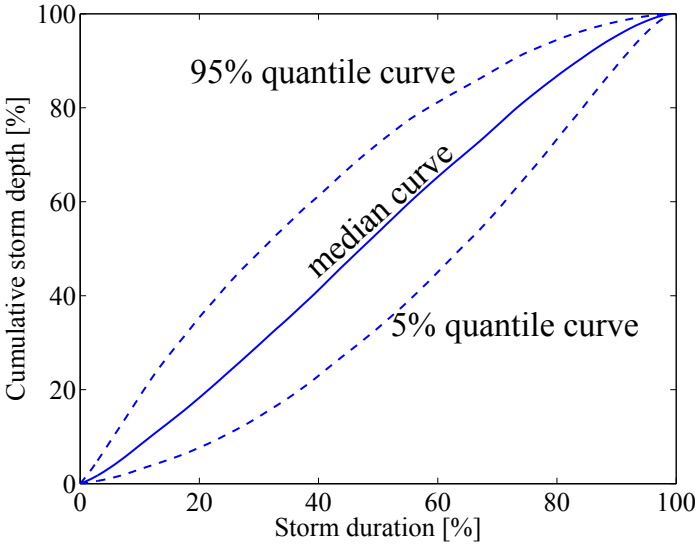

Figure 3.13: Reference rainfall mass curves for Switzerland independent on region, season and event duration.

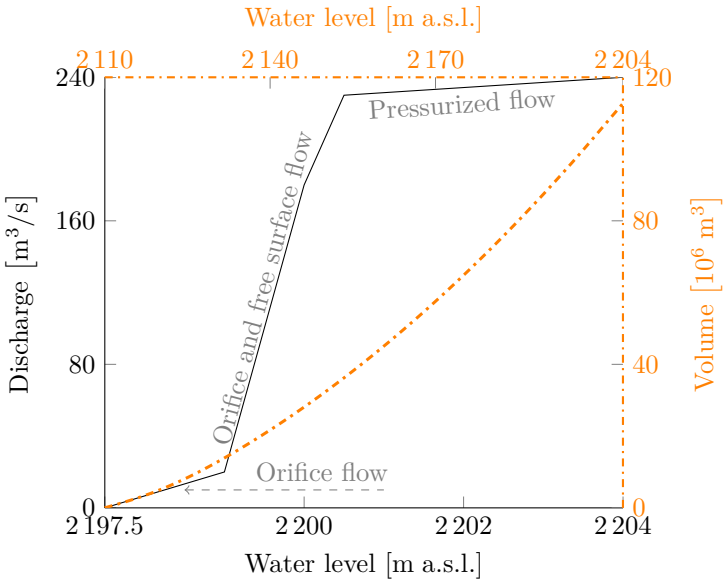

Figure 3.14: Water level-discharge relationship for the spillway of the Mattmark dam and reservoir volume as a function of the water level.

3.4.2 Results

The variability of the flood hydrographs and the reservoir levels has been analysed for the three RMC quantiles 5%, 50% and 95%. The resulting hydrographs are shown on. Figure 3.15, showing the resulting hydrographs, and Figure 3.16, illustrating the evolution of the water level in the reservoir, show that the influence of the seasonal and regional variability as well as the dependence on duration is very small. For the 5% quantile rainfall mass curves, the ratios between the peak discharges, comparing the unique quantile curves to the seasonal and duration dependent scenarios, show that the unique curve returns lower discharge peaks. The ratios show that the 5% quantile curve leads to discharge peak underestimations between 5 and 15.%. For the median curves, the underestimation goes from 3% to 11%, and from 6% to 16% for the 95% quantile rainfall mass curves.

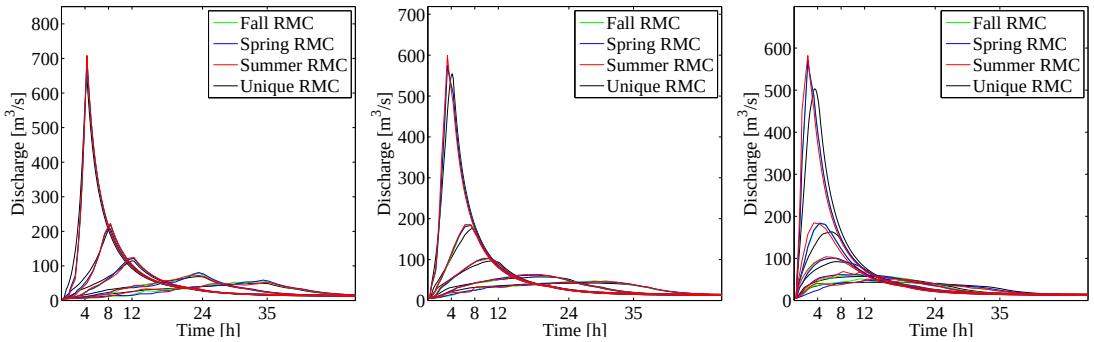

(a) 5% quantile curve (b) 50% quantile curve (c) 95% quantile curve

Figure 3.15: Comparison of the generated PMF discharges for different quantile rainfall mass curves for five different PMP durations (4h, 8h, 12, 24h and 35h).

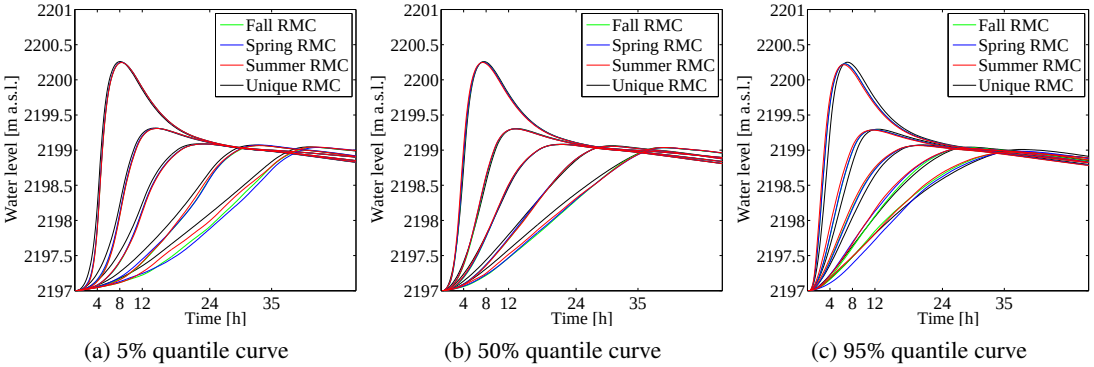

(a) 5% quantile curve (b) 50% quantile curve (c) 95% quantile curve

Figure 3.16: Comparison of the generated PMF reservoir level evolutions for different quantile rainfall mass curves for five different PMP durations (4h, 8h, 12, 24h and 35h).

Interestingly, when estimating these ratios based on the estimated lake levels increases (only

the net increase has been considered for the ratio estimation, the reference level has been put at 2197 m a.s.l.), it can be seen that the unique curve actually returns higher level estimates than the seasonal and duration depend curves. However, the differences are negligible, the rations being smaller than 1.8%. Whereas the different quantile curves have a non negligible influence on the discharge peak, their influence on the maximum lake level is hardly recognizable.

3.5 Do rainfall mass curves represent realistic precipitation events?

The rainfall mass curves have been compared to a reference curve derived from the precipitation events measured at the meteorological stations shown on Figure 3.13. It could be shown that the exposed quantile curves can be reduced to a single curve per quantile valid for the entire region of Switzerland due the very small influence of the supplementary information given by regional, seasonal and duration dependent rainfall mass curves. It remains, however, to prove that this three retained quantile curves (reference curves) are representing realistic events and are not artefacts resulting from a smoothing effect due to the quantile estimation.

Figure 3.17 shows that rainfall mass curves derived from single real events can be similar to the quantile rainfall mass curves. This has been shown to be valid for every considered region. Consequently, the reference rainfall mass curves can be considered to represent realistic temporal rainfall distributions.

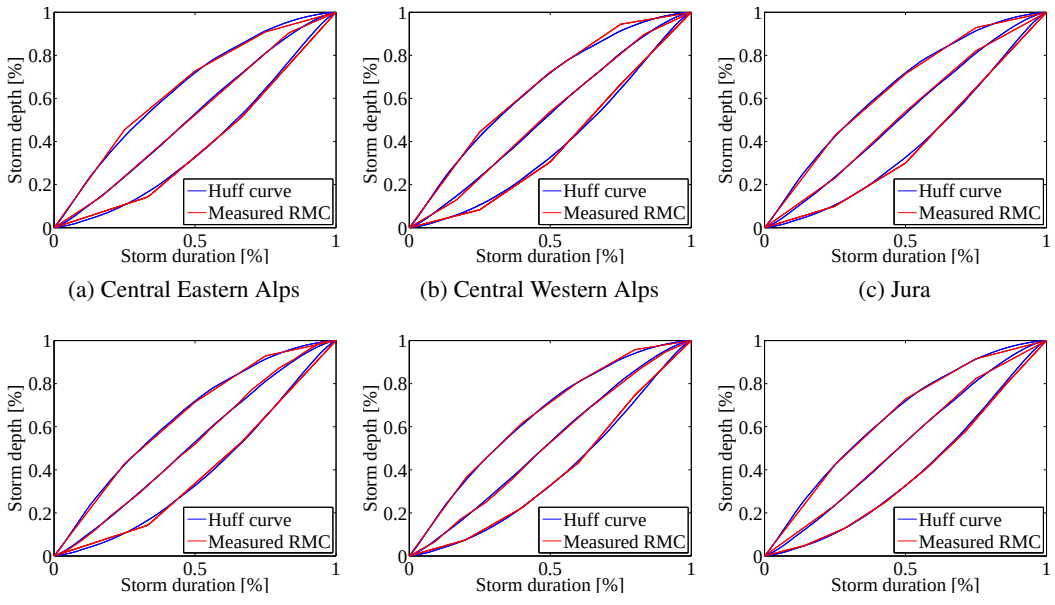

(a) Central Eastern Alps (b) Central Western Alps (c) Jura

(d) Plateau (e) Northern Alps (f) Southern Alps

Figure 3.17: Comparison between the reference quantile rainfall mass curves and most similar measured rainfall mass curves.

3.6 Conclusions

The present study analysed the regional and seasonal variability of rainfall mass curves and investigated on the influence of the event durations on the shape of rainfall mass curves. For all the analysed parameters, i.e. the region, the season and the event duration, dependences could be found. The curve variations expressed in terms of displaced volume can reach 38%. This maximum portion of water volume precipitating at a different moment has been detected for the RMC variation related to the event duration. The lowest variability can be related to the regional dependence of the RMCs and corresponds to a displacement in time of a volume portion of 23%. A comparable portion of 25% could be estimated for the seasonal variability.

The hydrological case study could show that the influence on the hydrographs, and especially on the water level in the reservoir, is small enough to justify the usage of general Swiss curves (the reference curve of Figure 3.13) instead of regional, seasonal and duration dependent curves. The variation of the peak discharges due to the usage of seasonal RMCs compared to the simulated hydrographs using the reference RMC ranges from 3% to 16%. The smallest variations (3%) could be detected for the longest events and for the 5% quantile RMC. The largest variations (16%) have been observed for the 95% RMC and the shortest event.

The 5% quantile curve returns the highest discharge among the three exposed quantiles (5%, 50% and 95%) and is thus the most interesting to distribute design storms in the context of the PMP-PMF approach. Furthermore, it could be shown that the rainfall mass curves do represent realistic temporal rainfall distributions. Thus their usage is close to reality and the synthetic hyetographs derived from rainfall mass curves are physically justified. The initially introduced reference rainfall mass curve (Section 7.3) can thus be used for the entire region of Switzerland independently on the season and event duration.

The regional influence of the RMCs on the hydrographs and the simulated reservoir levels has not been addressed in the hydrological application. The first reason is that the regional variations are the smallest that could be detected in this study. The variations induced by other stronger varying RMCs are thus more intense and of a higher interest. Therefore, the combined effect of the regional RMC variability with seasonal and duration related variability could not be addressed. The second reason is that the situation of the dam is fix whereas events with different durations have to be simulated for the same dam and are thus a variable in the considered case study. In the case seasonal PMP data are available, the season becomes a variable too. Consequently, the seasonal influence is important to be taken into account.

4 Correlation between precipitation and the $0°C$ isothermal altitude for extreme flood estimation

4.1 Introduction and objectives

In this chapter, the correlation between precipitation and temperature is addressed. The context of this study is the estimation of extreme floods within a PMP-PMF (Probable Maximum Precipitation - Probable Maximum Flood) framework for potentially snowfall-influenced environments. PMP events are usually defined independently from air temperature, which, as discussed earlier, is however essential to assess the potential effects of snowfall and melt. This paper thus proposes to use P-T scaling analysis to associate a critical air temperature to PMP events. The basic idea is hereby to identify a potential maximum temperature threshold beyond which precipitation starts decreasing with air temperature. If such a threshold does not exist, the P-T scaling cannot be directly used to associate a temperature to PMP events because PMPs are by construction far beyond observed precipitation amounts. An example of PMP-PMF estimation in the presence of snow accumulation and melt processes is included to underline the importance of a careful selection of the air temperature associated with PMP events. The overall aim of this paper is to come up with recommendations about how to select the initial air temperature for critical precipitation events of different durations.

4.2 Data

4.2.1 Precipitation data

Hourly precipitation data are provided by MeteoSuisse at 104 locations (Figure 4.1). The hourly precipitation measurement started in 1981. However, not all 104 stations were operational since 1981 and some of them have been removed since then. A total of 52% of the stations have a record of over 30 years. Roughly 18% of the stations have been added during the period from 1984-2010. After 2013, 95% of the considered rain gauges were already installed. For the present study, all stations have been considered for the available data length.

Figure 4.1: Situation of the considered meteorological measurement stations and of the meteorological sounding sites on a topographic map.

4.2.2 Temperature: meteorological soundings

In addition to ground-based air temperature (observed at all above mentioned stations), we propose here to use air temperature observations from meteorological soundings, i.e. from weather observation balloons filled with helium that are launched twice a day (at 00:00 and 12:00 UTC) to measure air temperature through the atmosphere. The balloons are surveyed up to an altitude of 30-35 km. The use of such soundings rather than ground-based temperature observations has the main advantage of yielding a direct observation of the atmospheric conditions representative for an entire region. This avoids potentially complicated spatial interpolations of point observations and makes the proposed method more straight-forward for practical applications.

The analyses carried out here are based on meteorological data from Switzerland. This relatively small country (40000 km^2) shows several clearly distinct hydro-climatological regions (Froidevaux, 2014), which can be roughly separated into two major zones (Schiemann and Frei, 2010): north and south of the Alps (Figure 4.1). For this analysis, meteorological soundings from Payerne (CH) and Milan (It) are considered. The situation of the two cities is shown on Figure 4.1. The soundings of Payerne can be assumed to be roughly representative of the climatic conditions for the meteorological stations north of the Alps and the soundings from Milan for

the meteorological stations situated south of the Alps. The subdivision as well as the attribution are shown on Figure 4.1. At Milan, the soundings were available from 1973 to present. For the soundings at Payerne, the measurements started in 1981.

If using temperature soundings, the reconstruction of the ground temperature or the estimation of isothermal altitudes is influenced by the assumption made about how the temperature varies with altitude, i.e. by its gradient or lapse rate. As shown in this paper, the seasonal variation of this gradient is small and extreme precipitations occur mainly during warm periods, for which the gradient is relatively constant (Table 4.1). Therefore, the error induced by the assumption on the gradient remains relatively small.

Table 4.1: Retained temperature gradients Δ for the four validation stations and the mean relative error ϵ of the 0°C isothermal altitude estimation for summer (s) and winter (w).

Sounding	Meteo. station	Δ_s [°C/100m]	Δ_w [°C/100m]	ϵ_s [-]	ϵ_w [-]
Payerne	Bullet la Fretaz	-0.6	-0.4	0.08	0.33
Payerne	Payerne	-0.65	-0.4	0.13	0.57
Milan	Stabio	-0.6	-0.4	0.08	0.36
Milan	Cimetta	-0.6	-0.6	0.07	0.16

4.3 Methodology

The analysis of the relationship between the 0°C isothermal altitude and precipitation characteristics is completed here in two steps: i) an analysis of the correlation between the 0°C isothermal altitude measured before a precipitation event and the precipitation intensity and ii) an analysis of the maximum measured 0°C isothermal altitude before a precipitation event and the duration of the subsequent event. These two analysis steps allow for the determination of whether the precipitation intensity is reaching a maximum for a certain temperature or if a relation between the event duration and the temperature is detectable.

The knowledge of this two relations is important for extreme flood estimation, because the flood estimation is more reliable when the meteorological inputs of a design storm are coherent. Ensuring this coherence is particularly important when the design storm is not obtained with a meteorological model (which would necessarily return temperature and precipitation as a coherent couple), as it is the case for most approaches, i.e. statistical extrapolations (Meylan et al., 2008), frequency duration curves (Meylan et al., 2008), Hershfield method (Hershfield, 1961; WMO, 2009).

Concerning the precipitation data, the following steps are performed. First, the rain gauges are attributed to the geographical classes in order to take into account the climatic regions mentioned above. Then the precipitation events measured at each rain gauge are determined and the precipitation volume and the event duration are derived. The events are then classified in

precipitation duration classes (4.3.2). The next step is to separate the dataset into seasonal sets in order to take into account the meteorological seasonality. Berg et al. (2009) focused on the data of July to characterize the scaling in summer and the data of January for the winter time with the argument that the trends are the strongest for these periods. This paper follows the same approach but extends the period to 3 months in order to increase the amount of considered data and capture the full season. The chosen months for the summer are June to August and December to February for the winter. Spring and autumn are defined by the remaining months.

An essential step is the validation of the coherence of the meteorological soundings and ground-based temperature observations. This was completed by comparing the 0°C isothermal altitude, derived from the meteorological soundings, with the isothermal altitude derived from ground temperature measurements with the temperature gradient approach. Once the meteorological soundings were validated, they were used to determine the 0°C isothermal altitude **before** the precipitation events for each climatological zone. Next the scaling between the altitude and precipitation quantiles (as it was done by Lenderink and Van Meijgaard (2008) and Lenderink and Van Meijgaard (2010)) was analyzed for different precipitation durations. To characterize the antecedent temperature - event duration relation in rare to extreme temperature conditions, the maximum measured 0°C isothermal altitude for the different duration classes was also derived.

4.3.1 Definition and determination of the precipitation events

For the purpose of this study, the following criteria were used to define a precipitation event (where i stands for precipitation intensity). An event starts at the moment when $i > 0.1$ mm/h and ends when $i < 0.1$ mm/h.

In order to analyze the sensibility of the results to the definition of the precipitation events, a third criterion was introduced. It aimed at grouping the precipitation amounts of consecutive precipitation events that were separated by less than a certain duration λ. If the end date of the first precipitation event and the start date of the next event were separated by a time interval of λ hours (where $\lambda \in \{0, 1, 2\}$), these consecutive events were considered to be a single event, with the start date of the first event and the end date of the last event. Initially, the value of λ was fixed to 0. Then the analysis was repeated twice for the other two values. A graphical illustration of this third criterion is available in appendix in Figure B.1.

4.3.2 Classifying the precipitation events in precipitation duration classes

For this analysis, duration classes are defined. The following classes are considered (in hours): $\{[1,2], [3,4], [5,8], [9,12], [13,18], [19,24]$. The classes have been defined in order to be coherent with the available Swiss PMP maps (Hertig et al., 2005) that have been elaborated for 1h, 3h, 6h, 9h, 12h and 24h precipitation durations.

4.3.3 Analysis of the meteorological soundings

Determination of the $0^{\circ}C$ isothermal altitude

The analysis of the meteorological soundings was based on the hypothesis that the temperature varies linearly through the troposphere with an inversion at the tropopause (at approximately 10 000 m a.s.l.). The altitude of the 0°C isothermal altitude was deduced from a linear interpolation of the data corresponding to each sounding.

In order to increase the reliability of the interpolations, the following criteria have been retained for the determination of the 0°C isothermal altitude. (i) The data set of the meteorological soundings had to contain more than two measurements (minimum data for the definition of a line). (ii) The measured temperature during one sounding had to change sign, meaning that the balloon passes through an altitude with 0°C. (iii) The coefficient of determination r^2 of the trendline and the soundings had to be higher than 0.8. Figure 4.2 shows an example of the interpolation and the derived 0°C isothermal altitude. It can be seen that the assumption of a linear behaviour up to 8 000 m a.s.l. was valid.

Validation with ground-based air temperature

Ground-based temperature data from meteorological stations was used to check that the altitude of the 0°C isotherm (derived from soundings) could be reproduced with the use of a simple temperature gradient from a surface air temperature. This was in fact a condition to ensure that the identified precipitation-temperature relationships could be used in a standard hydrological modelling setting where the ground-based air temperature time series are used to identify the aggregation state of precipitation and the melt conditions.

For this validation, it is important to distinguish between meteorological stations located in the mountains or in the valleys because of the thermal inversions that regularly occur in winter times. Two stations have been chosen for each micro-climatic region, Payerne and Bullet La Fretaz for the North and Cimetta and Stabio for the South (see Figure 4.1). The geographical coordinates of these stations are reported in Table 4.2 in the Swiss reference coordinate system CH1903/LV03.

The reconstruction of the 0°C isothermal altitude with the temperature gradient method is completed as follows:

$$H_{iso}(t) = H_{stat}(t) - \frac{T_{stat}(t)}{\Delta}, \tag{4.1}$$

where $H_{iso}(t)$ [m a.s.l.] is the 0°C isothermal altitude at time step t, $H_{stat}(t)$ [m a.s.l.] is the altitude of the meteorological station and $T_{stat}(t)$ $^{\circ}C$ is the measured temperature at this station. $\Delta(t)$ is the temperature gradient for the time step t. For the purpose of the present validation, the

reconstruction was based on two different gradients, one for the winter and one for the summer period, which corresponds to common practice in hydrological modelling (Schaefli and Huss, 2011).

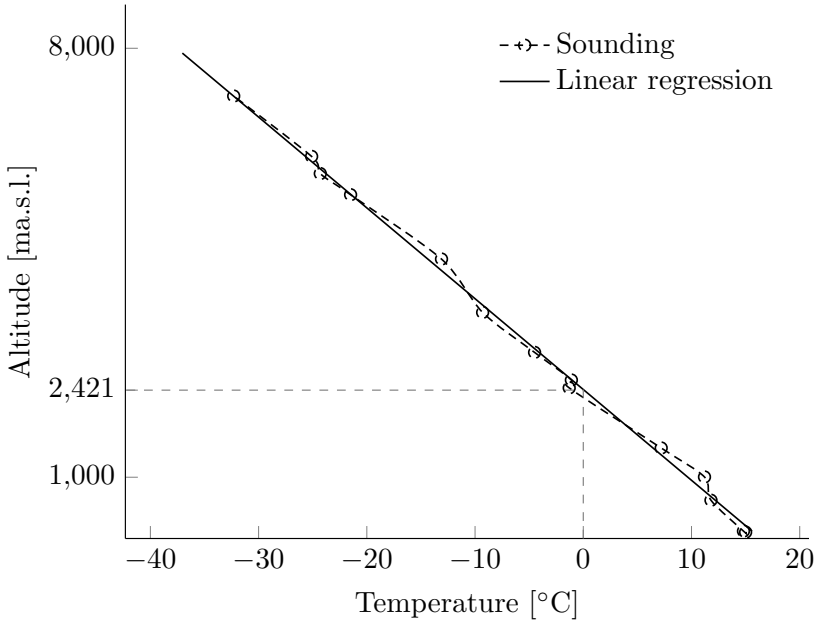

Figure 4.2: Example of meteorological sounding data (Temperatures and corresponding measurement altitudes) and of the linear regression used for the determination of the 0°C isothermal altitude.

The quality of the reconstruction of the 0°C isothermal altitude is measured in terms of the mean relative error ϵ (Eq. 4.2)

$$\epsilon = \frac{1}{N} \sum_{t=1}^{N} \frac{H_{ms}(t) - H_{iso}(t)}{H_{ms}(t)} \tag{4.2}$$

where N is the number of estimation-measurement couples and H_{ms} is the isothermal altitude measured by the meteorological sounding.

Table 4.2: Coordinates X [m], Y[m] and Z [m a.s.l.] (in Swiss national coordinate system CH1903/LV03) of the meteorological stations used for the validation of the gradient approach and of the sites where the meteorological soundings have been undertaken.

Station name	X	Y	Z
Meteorological stations			
Bullet La Fretaz	534 230	188 080	1 202
Payerne	562 150	184 855	490
Cimetta	704 370	117 515	1 672
Stabio	716 040	77 970	353
Meteorological sounding stations			
Payerne	562 200	184 800	491
Milano	743 870	43 708	103

4.4 Results and discussion

4.4.1 Validation of reconstruction

The identified gradients for the reconstruction of the 0°C isothermal altitude as well as the mean relative error ϵ are shown in Table 4.1. The obtained gradients corresponded well to the known range of gradients in the Alps (Damm and Felderer, 2013; Rolland, 2003). It should be mentioned that these gradients have not been determined by minimizing the estimation error. The goal was only to show whether the 0°C isothermal altitude is representative for the ground temperature. For this purpose, the gradients have been determined by trial-and-error. The results are sufficiently good to show the strong link between the ground temperature and the 0°C isothermal altitude. The reconstruction based on equation 4.1 gave reliable results for both regions and both periods, as can be seen from the performance measure in Table 4.1 and from the reconstructed time series of isothermal altitudes (Figures 4.3 and 4.4).

A more detailed inspection showed that the reconstruction of the isothermal altitude (and thus also the back-calculation from the isothermal altitude to ground temperature) was very good during summer (mean relative error $\epsilon_{sum} \leq 0.08$) and good during winter (mean relative error $\epsilon_{win} \leq 0.36$) for the two stations Cimetta and Stabio. For the meteorological stations La Fretaz and Payerne, the reconstruction was also very good for summer (mean relative error $\epsilon_{sum} \leq 0.13$) and slightly less close to the sounding-based isothermal altitude for winter (mean relative error $\epsilon_{win} \leq 0.57$). However, the reconstruction could also be considered very good due to the frequent temperature inversions in winter. Given the good linear relationship between the 0°C isothermal altitude and ground temperature, the remainder of this paper reports all results in terms of the 0°C isothermal altitude.

It is important to mention that the linear relationship between the 0°C isothermal altitude and ground temperature might break down during periods of thermal inversions, but those situations

typically correspond to anticyclonic conditions when no precipitation is occurring. Consequently, the errors induced by thermal inversions are not critical for this analysis because it focused on extreme precipitation.

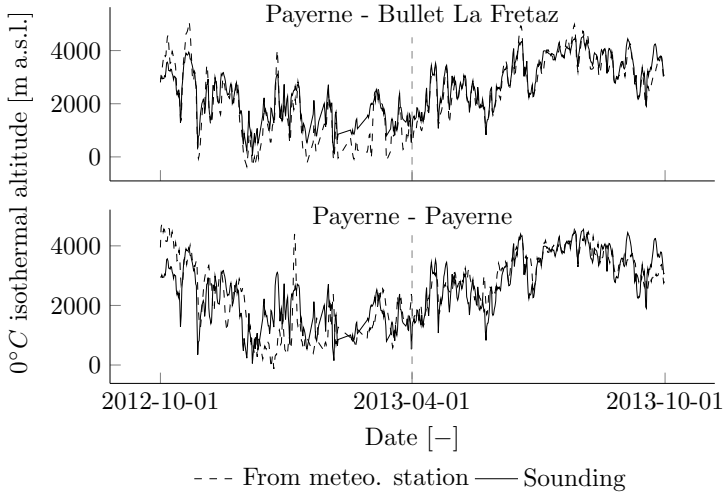

Figure 4.3: Comparison between the 0°C isothermal altitude derived from meteorological soundings of Payerne and from ground temperature measurements at Bullet la Fretaz and Payerne. The dashed line indicates the separation into winter and summer.

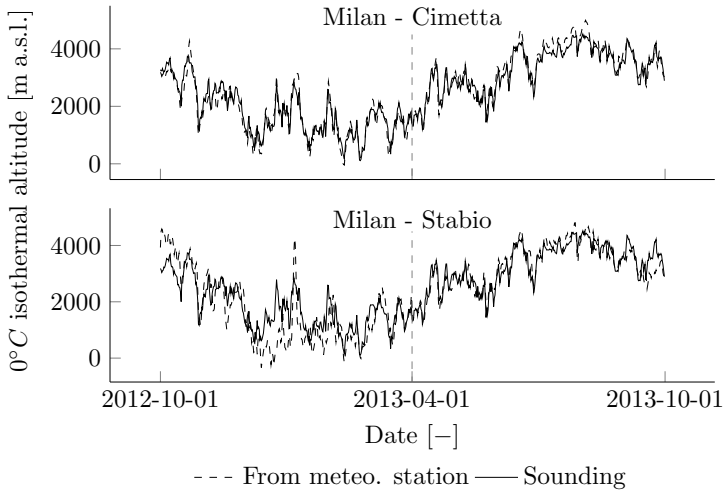

Figure 4.4: Comparison between the 0°C isothermal altitude derived from meteorological soundings of Milan and from ground temperature measurements at Cimetta and Stabio. The dashed line indicates the separation into winter and summer.

4.4.2 Quantile scaling analysis

The precipitation events are classified into the 9 classes discussed in Section 4.3.2. Events of more than 72h have been omitted here because the number of measured events was very small. For each duration class, the 0.5, 0.75, 0.90, 0.95 and 0.99 quantiles have been estimated from all couples of precipitation intensity (P) and of 0°C isothermal altitudes (H_{ms}). Hereby, the mean intensities over the duration of the events were used.

Quantiles were only computed for sample sizes that were large enough for direct quantile identification from the sample. For example, for the quantile 0.99 the sample must have had at least 100 values. It turned out that for longer precipitation durations than those who fell in the class $[19, 24]$, not enough data was available for returning representative results. Therefore, the quantile scaling analysis did not consider precipitation durations longer than 24h.

Figures 4.5 and 4.6 show examples of these $P - H_{ms}$ scalings for the soundings from Payerne and the seasons summer and winter. The results for fall and spring as well as for the soundings from Milan are given in Appendix B. These figures show $P - H_{ms}$ scaling plots (for λ =0) which, as discussed earlier, are equivalent to the more classical precipitation-temperature ($P - T$) scaling plots.

To illustrate the sensitivity of the results to the precipitation event definition, the soundings from Payerne were used as an example. The results for λ =1 and λ =2 were very similar as illustrated in Figure 4.7 for the 99% quantile. The results for the other quantiles are available in Appendix B (Figures B.8, B.9, B.10, B.11). These figures show that the similarity of the results based on the definitions λ =1 and λ =2 compared to those deduced from λ =0 is not dependent on the quantiles. The sensitivity analysis did not show a significant change in the observed trend as a function of the event duration. The sensitivity analysis for the Milan soundings led to the same conclusion (results not shown).

During summer, the $P - H_{ms}$ scaling showed a clear increase in precipitation intensity with increasing 0°C isothermal altitude for the soundings from Payerne (Figure 4.5). No sign of a limitation of moisture availability could be detected up to the precipitation duration class [13,18], for which the scaling was much flatter. This could indicate some limitations of moisture availability. During the summer season, not enough events fit the duration class [19,24] to warrant inclusion in the analysis.

Concerning the soundings from Milan (available appendix, Figure B.4), the same trend can be observed for the duration classes [1,2] and [3,4]. For the duration class [5,8], moisture availability limitations could cause the decrease of the scaling rate for the 99% quantile line for high 0°C isothermal altitudes. The more erratic behaviour of the 99 % quantile of the duration class [9,12] made it hard to draw a conclusion. However, a clear increase was not detectable for the mentioned quantile. The scaling of the events that fitted the class [13,18] was positive over the entire range of 0°C isothermal altitudes. For the class [19,24], not enough events had been recorded to estimate the 99% quantile. The lower quantiles indicated a nearly constant scaling above 3000 m a.s.l. .

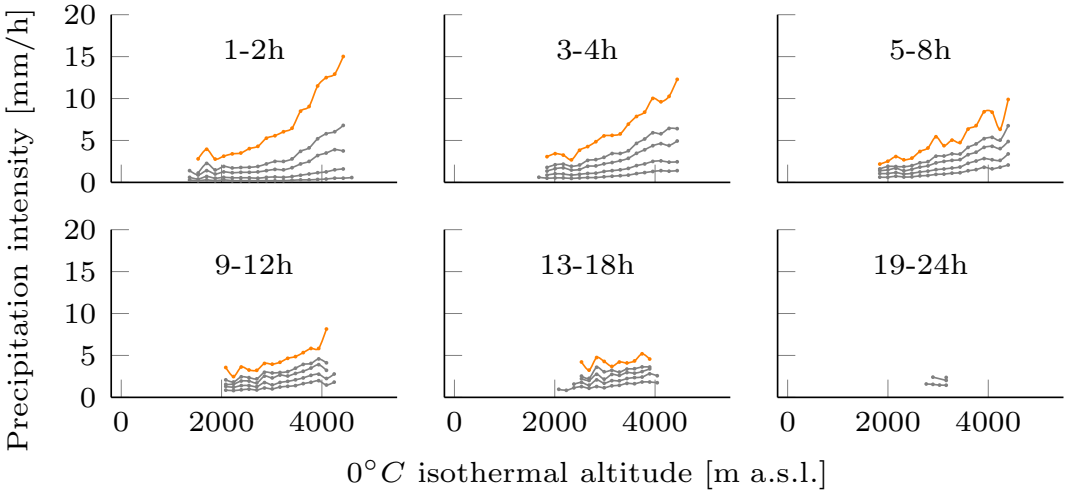

Figure 4.5: 0.5, 0.75, 0.90, 0.95 and 0.99 quantiles of the different considered precipitation duration classes north of the Alps (Payerne meteorological soundings) and for the summer period (June-August) for $\lambda = 0$.

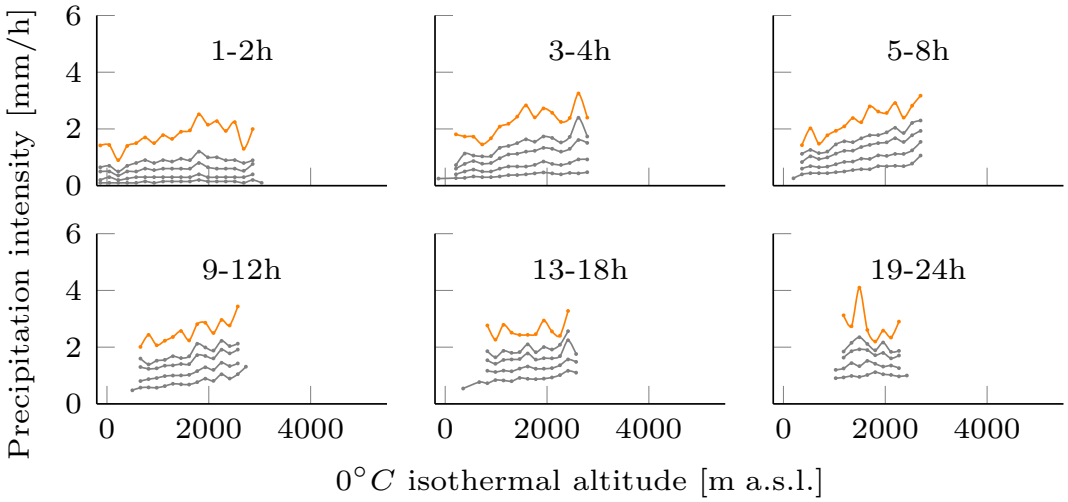

Figure 4.6: 0.5, 0.75, 0.90, 0.95 and 0.99 quantiles of the different considered precipitation duration classes north of the Alps (Payerne meteorological soundings) and for the winter period (December-February) for $\lambda = 0$.

For winter, the Payerne soundings (Figure 4.6) suggested the existence of moisture availability limitations for the duration classes [1,2] and [3,4] for high 0°C isothermal altitudes. The scalings of the classes [5,8] and [9,12] showed an increasing trend without any signs of moisture limitations. The 99% quantile line of the duration class [13,18] showed a nearly constant scaling, that could also have been a sign of moisture availability limitations. The scaling for the duration class [19,24] had a decreasing trend for high 0°C isothermal altitudes when considering the 99%

quantile. Concerning the soundings from Milan (Figure B.6), the duration class [1,2] showed that an upper limit for the precipitation intensity could have been reached for a certain isothermal altitude. The negative scaling of the 99% quantile line appeared rather abruptly; however, the quantile points that led to this negative scaling were calculated based on more than 500 data points. The lower 95% quantile also indicated a negative scaling for the same 0°C isothermal altitude. The other duration classes suggested that moisture availability limitations could have led to the decrease in scaling rates for the 99% quantiles.

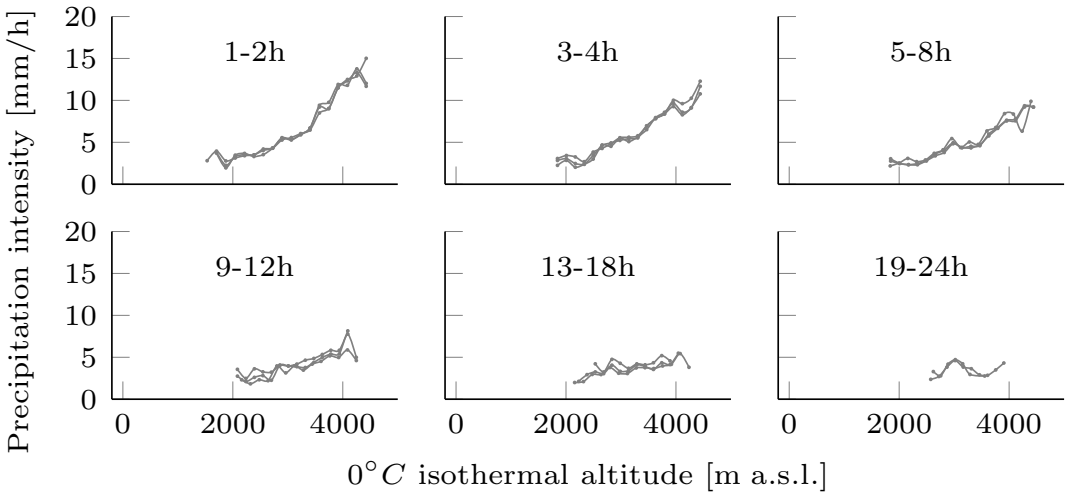

Figure 4.7: Superposition of the results based on the three definitions (λ =0,1,2) for the precipitation events. Represented are the results for the soundings from Payerne during the summer period for the **0.99** quantile.

For spring, the scaling rates were clearly decreasing for high 0°C isothermal altitudes for the duration classes [1,2] as well as [3,4] when the Payerne soundings (Figure B.3) have been considered. However, for the duration classes [5,8] and [13,18], the scaling remained positive over the entire 0°C isothermal altitude range. On the other hand, the duration class [9,12] seemed to lead to reduced scaling rates at high 0°C isothermal altitudes, but the tendency was not clear. For the [19,24] class, the same reduced scaling was noticeable. Regarding the soundings from Milan (Figure B.7), a clear reduction of the scaling rates was recognizable for the classes [1,2] and [3,4]. The scaling of the events of class [9,12] was even negative for high 0°C isothermal altitudes when looking at 95% quantiles or lower. Concerning the 99% quantile, not enough values have been measured for the very high 0°C isothermal altitudes, thus the positive scaling was not representative. A less pronounced decrease for high 0°C isothermal altitudes was visible for the duration class [13,18]. Unfortunately, the class [19,24] did not allow to conclude on the 99% quantile.

For fall, a decreasing scaling rate was perceivable for the Payerne soundings (Figure B.2) for the duration classes [1,2], [3,4], [5,8] and [9,12]. The two other classes showed a constant increase of the scaling rate. Concerning the soundings from Milan (Figure B.5), only the class [9,12]

showed a decreasing scaling rate for the 99% quantile. When looking at the 95% quantile, also the classes [1,2] and [13,18] showed a decreasing trend for high 0°C isothermal altitudes.

The above discussion shows that the scaling plots do not lead to a clear and unique conclusion of an upper precipitation limit for a certain 0°C isothermal altitude. The nature of the $P - H_{ms}$ scaling is different for different duration classes and the low amount of "extreme" data leads to low confidence for the points with high isothermal altitude. Therefore a reliable conclusion on a maximum precipitation associated to a certain isothermal altitude (beyond which the intensity would decrease again) cannot be drawn. Nevertheless, signs of limitations of moisture availability can be detected for short and longer events throughout the four analyzed seasons, but are not clearly related to the precipitation duration. Furthermore, the maximum 0°C isothermal altitude observed within each precipitation duration class showed a clear continuous decreasing trend with precipitation duration (Figure 4.8). This observation holds for all seasons and all regions and does not depend on the event definition (see results for λ =0, λ =1 and λ =2 in Figure 4.8). The winter shows the lowest maximum isothermal altitudes for a given duration class, followed by spring, fall and summer (for Payerne and Milan). Except for winter, the maximum isothermal altitudes were slightly higher for Milan than for Payerne.

An analysis of the temperature gradient, deduced directly from the soundings (slope of regression line in Figure 4.2) could lead to an explanation of the behaviour of this decreasing isothermal altitude with precipitation duration. Figure 4.9 showed, in fact, that the mean value of the gradients for the three event definitions was decreasing with duration (the negative value was increasing). The decrease of the gradient values before a long rainfall event could be due to the air mass flux acceleration. This could induce the air mass to lift and consequently to cool down, leading to the homogenization of the air mass, inducing smaller gradients. Long rainfall events often occur on generalized degradations of the weather, and thus in colder situations (lower 0°C isothermal altitude) than short heavy rainfall episodes. This generalized alteration of the weather tends to produce effects far in advance. Gradient decrease could be one of them.

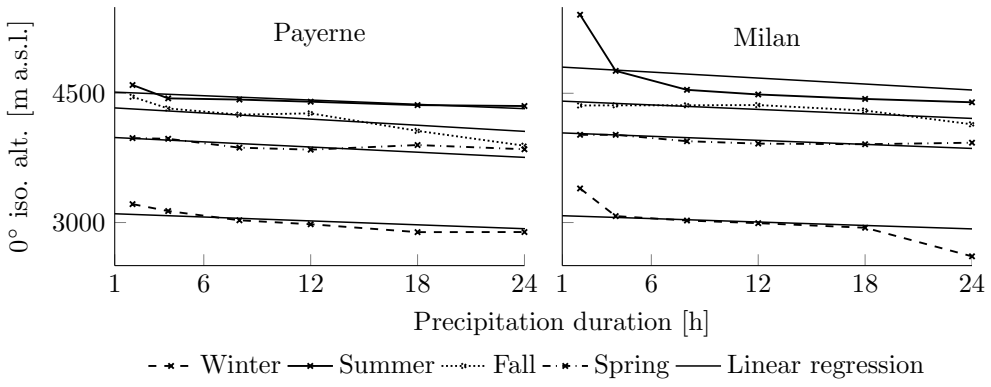

Figure 4.8: Maximum 0°C isothermal altitude plotted against the precipitation duration. The altitude values are the mean values of the three considered event durations.

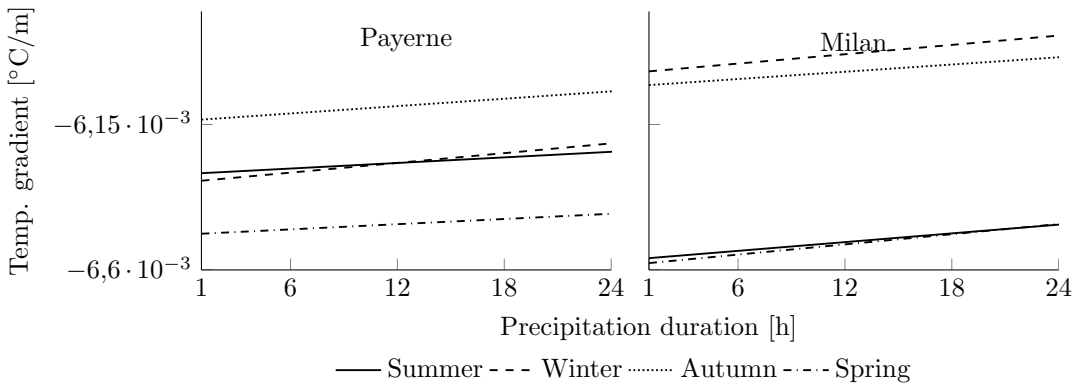

Figure 4.9: Temperature gradients plotted against the precipitation duration.

4.5 Relevance of the results for extreme flood estimation

4.5.1 Discussion of the 0°C isothermal altitude in a hydrological context

The presented scaling analysis and in particular the absence of a scale-break (decreasing scaling beyond a certain isothermal altitude) seems to suggest that in the Swiss Alps, even the highest precipitation intensities can occur with very high isothermal altitudes, up to 4800 m a.s.l. in summer for Milan. Comparing this value to the hypsometric curve of Switzerland (Figure B.12), showed that this would cause the majority of the Swiss Alpine catchments to contribute entirely to the discharge generation (no solid precipitation) and and that, in presence of a pre-existing snowpack or in presence of glaciers, melt processes would play a crucial role. In the context of PMP-PMF, this result would a priori require to consider the maximum measured isothermal altitude in relation with the PMP. This assumption is conservative because it could lead to an overestimation of the snow or/and glacier melt. As PMP-PMF is used for the estimation of the safety flood for dam design, a conservative assumption is justifiable.

Analyzing the precipitation-duration-0°C isothermal altitude scaling on a seasonal basis shows, however, two important facts that are not directly visible from a simple precipitation-temperature scaling analysis: i) the maximum 0°C isothermal altitude per duration class strongly depend on the season and ii) the maximum 0°C isothermal altitude decrease with precipitation duration.

The above points imply that in certain seasons (winter, spring), high intensity precipitation cannot occur as rainfall at all elevations but will partly fall as snow. The maximum isothermal altitude was as low as 2550 m a.s.l. for a 72h winter event in Payerne. This might have practical implications for flood estimation in catchments for which the critical situations tend to occur in winter and spring. For high Alpine hydropower reservoirs, critical situations are known to occur only in late summer and early fall when the reservoirs are full. The results presented here suggest that for this time of the year, very high 0°C isothermal altitudes (implying a high percentage of rainfall and melt contribution) should be assumed for all precipitation durations when safety

flood estimations are undertaken.

The identified decreasing trend of maximum isothermal altitude as a function of precipitation duration was 230 m/24 h (average for the 4 seasons and the two sounding stations). For small catchments where the relevant precipitation duration for PMP estimation will be short, this low gradient suggests that the choice of an 0°C isothermal altitude should essentially depend on seasonal considerations. For larger catchments with higher relevant durations for the PMP, the 0°C isothermal altitude decrease might become relevant. The lowering of the 0°C isothermal altitude of up to 500 m for summer for events of 72h might play a crucial role regarding the simulation of discharge in Alpine catchments. In the following case study, it has been assumed that PMP events occur under high temperature. Summer conditions are therefore considered for the hydrological application.

4.5.2 Application: the case study of the Mattmark dam catchment

The relevance of the relationship between air temperature and precipitation event duration for extreme flood event simulations under summer conditions is illustrated in this paper with the GSM-Socont hydrological model (Schaefli et al., 2005; Jordan et al., 2012; Schaefli and Zehe, 2009) used for precipitation-runoff simulation . This model is a semi-distributed conceptual hydrological model developed for mountainous catchments.

We applied the model to the catchment of the Mattmark dam in the Southern Swiss Alps (Figure 4.1). Around 28% (10 km^2) of the entire catchment surface, 36 km^2, is covered by glaciers . The basin goes from 2197 m a.s.l. to around 3898 m a.s.l. Given the size of the study catchment, this model does not take into account river routing.

The considered precipitation event was a 6h-PMP derived from the Swiss PMP maps (Hertig et al., 2005) with a mean intensity of 56 mm/h. An example of a hyetograph of this 6h-PMP is shown in Figure B.13 for a selected point of the catchment. This temporal structure resulted from rainfall mass curves (WMO, 2009) and has been kept constant over the entire catchment. The spatial structure was given by the Swiss PMP maps (Hertig et al., 2005) with a resolution of 2×2 km^2. 0°C isothermal altitude intervals starting at 3000 m a.s.l. (low 0°C isothermal altitude for summer) and going up to 4500 m a.s.l. (high 0°C isothermal altitude for summer) in a 500 m step, have been considered in order to assess the sensitivity of the PMF to the 0°C isothermal altitude.

Hydrological model set up

The snow accumulation has been simulated with a linear transition from snowfall to rainfall at temperatures between 0°C and 2°C (which fits well with observed snow and rainfall data (Rohrer et al., 1994). The snowmelt has been computed with a degree-day approach (Hock, 2003). Melt water leaves the snowpack only if a certain liquid-to-solid threshold (set to $\theta_{cr} = 0.1$) is reached and can refreeze during periods of negative temperatures. The melt and rainwater (in

case of rain-on-snow events) that leaves the snowpack is assumed to infiltrate into the subsoil. The catchment-scale runoff resulting either from snowpack outflow or from direct rainfall on snow-free areas is computed via a two reservoir approach (fast and slow component). Runoff from glacier-covered areas is computed with a separate ice-melt module that uses also a degree-day approach and two linear reservoirs to transform melt water into runoff.

The initialization of the hydrological model is done for summer conditions as the PMP maps are admitted to represent summer PMP values. The model has been initialized with the median summer snow height (3 mm equivalent water height) and the median aestival soil moisture (0.1 m equivalent water height corresponding to 40 % of the infiltration capacity). The snow pack is considered to be saturated.

4.5.3 The role of the 0°C isothermal altitude for summer PMF

To illustrate the effect of the choice of a 0°C isothermal altitude on the probable maximum flood (PMF) estimation of a typical high Alpine Swiss catchment, Figure 4.10 shows the results of the hydrological simulation for Mattmark (see section 4.5.2) under several assumptions of the 0°C isothermal altitude. Given the high elevation range of this catchment and the glacier cover, the increase of the simulated flood discharge as a function of isothermal altitude was very strong, which emphasized the importance of a detailed analysis of the 0°C isothermal altitude for flood estimation in similar catchments. The simulation results illustrate that, under summer conditions, the influence of the isothermal altitude on the flood peak is important. Thus, in the context of safety flood estimations, the possibility of very high 0°C isothermal altitudes should not be neglected.

The simulations showed that the main difference between the flood discharges for the different 0°C isothermal altitudes came from the precipitation aggregation state. Solid precipitations for areas higher than the 0°C isothermal altitudes reduced significantly the flood discharge if the 0°C isothermal altitude was low. For the warmest scenario (0°C isothermal at 4500 m a.s.l.), the initial snow cover melted down during the first 40 minutes of the event. The glacier discharge of this worst case does not contribute significantly to the flood discharge. In fact, only 1.75% of the total discharge are generated by the glacier. The rather low difference between the simulations that considered 4000 m a.s.l. and 4500 m a.s.l. as 0°C isothermal altitude can be explained by the fact that the catchment area above 4000 m a.s.l. . is very small. In general, the sensitivity of the PMF discharge is less pronounced for catchments with less topographical variability. For catchments that are too low to experience snowfall during summer, the PMF sensitivity to the 0°C isothermal altitude would only depend on the spatial distribution of the pre-existing snowpack. The limiting case are lowland areas with zero probability of showing a pre-existing snowpack during summer.

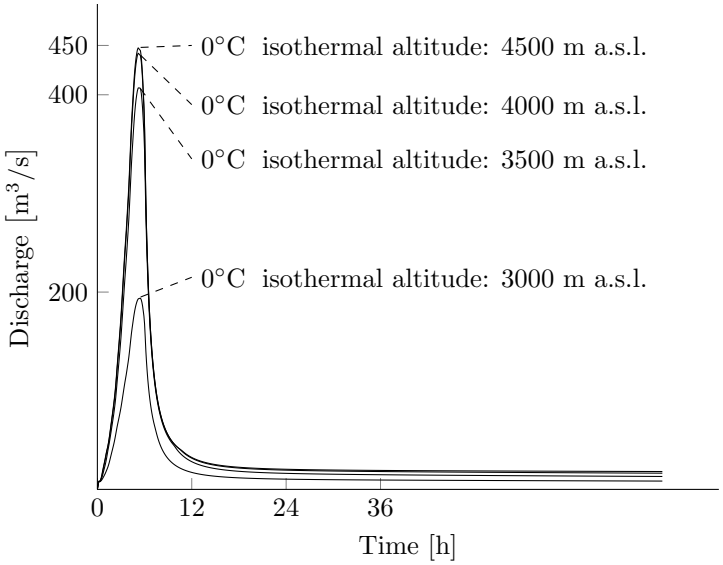

Figure 4.10: A ratio of 4.3 can be observed between the peak discharges of the PMF hydrographs for an 0°C isothermal altitude varying from 3000 m a.s.l. to 4500 m a.s.l. .

4.6 Conclusions

This chapter presented an analysis of the scaling of precipitation intensity as a function of the 0°C isothermal altitude and of precipitation duration for Switzerland. In the context of potentially snow-influenced extreme flood estimation, the 0°C isothermal altitude has been shown to be very closely related to air temperature, whose link to precipitation intensity is more classically analyzed in the literature.

Three conclusions can be drawn. The first one is that the observed precipitation data did not show any clear upper limit for the increase of precipitation intensity with the 0°C isothermal altitude (or, equivalently, with air temperature). However, in agreement with earlier findings, moisture availability limitations were noticeable. Concerning these limitations, we found that the southern and northern part of Switzerland had a different behaviour and that they could not be clearly related to the precipitation duration or the season. For all the duration classes, positive and negative (or constant) scaling could be found. The largest number of classes without moisture availability limitations were detected during the warmest period.

The second conclusion element is that the maximum isothermal altitude per precipitation duration class strongly depended on the season. The maximum 0° isothermal altitudes for the winter season were similar for the south and the north of Switzerland. On the other hand, the maximum 0° isothermal altitudes for the spring, summer and autumn period were higher in the southern part of Switzerland.

The third outcome is that the maximum isothermal altitude is approximately linear with precipi-

tation duration. It has been shown that this relation can approximately be described by a linear regression. The analysis of the temperature gradient helped to explain this relation. In particular, the homogenization of the air mass temperature due to more pronounced fluxes before longer rainfall events could lower the 0°C isothermal altitude before long duration events.

These findings should be considered for event-based rainfall-runoff simulation of rare events with the help of PMPs in settings where snowfall and snow and ice melt processes might play a role. As illustrated for the high Alpine Mattmark catchment (36km^2), even an increase of a couple of hundred meters of the 0°C isothermal altitude for a short duration precipitation event in summer might have a significant impact on flood estimation in a comparable high elevation catchment.

The presented results suggest that seasonal considerations might play a crucial role for the choice of 0°C isothermal altitudes in PMP-based flood estimation studies. These seasonal considerations might reduce the estimated flood peak for settings where critical events are known to occur during winter and spring when 0°C isothermal altitudes are lower than during summer and fall. It is noteworthy, however, that available PMP maps often only apply to summer precipitation conditions (as is the case for Switzerland, where the maps have been derived for warm conditions).

Future research should focus on the evolution of the air temperature during precipitation events. Furthermore, a precipitation event type distinction (frontal or convective) could be performed to quantify the influence on the presented scaling results and namely on the relationship between precipitation duration and the maximum 0°C isothermal altitude.

5 State variable analysis for the derivation of the initial conditions for extreme flood simulations

5.1 Introduction and objectives

A state variable is, as the name says, a variable describing the state of the model at a specific moment in time. The state variables do thus evolve during the simulations and depend on the model inputs as well as on the parameters of the model. The model output (discharge) at a certain moment directly depends on the state variables one time step before and, of course, on the meteorological model inputs. The initialization of the model becomes negligible after a certain simulation period (some days to some months). This period is often called "warming period". This means that the state variable values simulated after the warming period can be considered as correct in the context of the model.

The initial conditions considered for a hydrological simulation can have a high impact on the simulated discharge (Hingray et al. (2009); Chen et al. (2016), as has been underlined in the state of the art in Section 2.6.9). The initialization of a hydrological model is the process of attributing a certain initial value to the state variables of the model.

The warming period of a hydrological model is in general longer than the design event that is introduced in the model for event based flood estimation approaches. For this reason, the state initial variables are crucial inputs for an event based simulation, as it is the case for a PMP-PMF simulation for instance.

The semi-continuous approach described by Beauchamp et al. (2013) was determined as the most realistic in Section 2.6.9. Thus this approach will be considered for the following analysis. Besides this semi-continuous approach, that proposes to derive the initial conditions from a continuous simulation by injecting a design storm event at a certain moment of the simulation. This approach has been used in the present study in a stochastic manner. Additionally, a deterministic approach has been considered. The state variable time series that have been simulated during the continuous simulation have been subjected to a quantile analysis to derive the state variable values corresponding to a certain quantile under the assumption of independent variables. The

variation interval of the simulated PMF discharges based on different initial conditions have been investigated based on the state variables for the two approaches. The goal was to analyze the importance of the initial conditions influence on the PMF estimate and to compare the results of the stochastic and deterministic approaches.

In order to assess the importance of the initial conditions and to compare the two approaches, a case study on the Mattmark dam catchment has been performed. The fact that the analysis is based on a case study induces that the results are not generalizable. Nevertheless, they illustrate the role the different state variables can play in the generation of floods. The influence of the dependence between the state variables can be better understood through this analysis. Therefore, the necessity of the stochastic approach, respectively the sufficiency of the deterministic approach could be discussed.

5.2 Data

The state variable values used for the present study has been extracted from simulations on the Mattmark dam catchment (described in Section 5.4) using the GSM-Socont hydrological model (Schaefli et al., 2005; Schaefli and Zehe, 2009; Jordan et al., 2012). The hydrological model is briefly described below (5.3).

The present study is based on the state variables of the GSM-Socont hydrological model. The model has been explained in the literature review in Section 2.7.1. This model uses 8 state variables, i.e. snow height, snow saturation, soil saturation, runoff height (for the non glacial components) and snow height, snow saturation, glacier discharge as well as snow melt (for the glacial component). As mentioned, the values of the state variables have been extracted from the calibrated model by simulating the longest possible period with an hourly time step. For the Mattmark case study (further explained in Section 5.5), this period reaches from October 1995 to November 2009.

5.3 Hydrological model set up

The Mattmark catchment has been modelled with a semi-distributed hydrological model. Therefore, a subdivision in altitude bands has been performed. A vertical resolution of 300m has been admitted to be sufficient. The determination of the altitude bands has been based on a digital elevation model with an horizontal resolution of 25m. The resultant altitude bands are shown on Figure E.6 for the main catchment and on Figure E.7 for the lateral catchments. A topographic map with the catchment is shown on Figure 9.18 included in Section 9.5 destined for the application of the flood estimation methodology developed during this research project.

The snow accumulation has been simulated with a linear transition from snowfall to rainfall at temperatures between 0°C and 2°C (which fits well with observed snow and rainfall data (Rohrer

et al., 1994). The snowmelt has been computed with a degree-day approach (Hock, 2003). Melt water leaves the snowpack only if a certain liquid-to-solid threshold (set to $\theta_{cr} = 0.1$) is reached and can refreeze during periods of negative temperatures. The melt and rainwater (in case of rain-on-snow events) that leaves the snowpack is assumed to infiltrate into the subsoil. The catchment-scale runoff resulting either from snowpack outflow or from direct rainfall on snow-free areas is computed via two reservoirs (fast and slow component). Runoff from glacier-covered areas is computed with a separate ice-melt module that uses also a degree-day approach and two linear reservoirs to transform melt water into runoff.

5.4 The case study of the Mattmark dam catchment

The hydrological application has been used to quantify the variation interval of the inflow discharge and the lake level due to various initial conditions. Thus the case study allowed to clarify if the initially known quantiles of the initial conditions contain information about the quantile of the simulated discharge and lake level or if this information is lost. Such a loose could occur due to an eventual important dependence between the different state variables.

The Mattmark dam is situated in the Southern Swiss Alps (Figure 4.1). Around 28% (10 km^2) of the entire catchment surface, 36 km^2, is covered by glaciers . The basin goes from 2197 m a.s.l. to around 3898 m a.s.l. Given the small size of the study catchment, the hydrological model used for this study does not take into account river routing.

For the PMP-PMF simulations, a 3h-PMP, derived from the PMP-maps with wind sector south, has been chosen. The mean intensity of this precipitation event is 94 mm/h for the examined region. The temporal rainfall structure has been derived from the reference rainfall mass curves, determined in Section 3 and shown on Figure 3.13. The height of the 0°C isothermal altitude has been fixed at H=4780 m a.s.l., according to the isothermal analysis exposed in Chapter 4. The linear relation derived in the latter chapter valid for summer in the southern part of the Alps is expressed by $H = -11.554 \cdot d + 4815.2$, where d is the duration of the precipitation event in hours. The temperature conditions are thus high enough to avoid snowfall during the PMP event.

5.5 Methodology: The stochastic and deterministic approaches

Two different approaches to obtain the initial conditions have been tested and compared in order to assess the issue of the influence of the initial conditions and the related variation interval of the simulated discharge. Both approaches are explained in the following paragraphs. They refer both to the state variable values simulated during the longest possible period, corresponding to the entire period of available meteorological data. The state variables are then averaged weighting them by the surface of the corresponding elevation band of the hydrological model. In the next step, the simulated set of state variables have been divided into seasonal sets. The seasons are defined as follows: winter goes from December to February, spring from March to May, summer

from June to August and Autumn from September to November.

The stochastic approach was based on a random selection of a moment in time for which the simulated state variables are selected as initial conditions for the PMP-PMF simulation after having chosen a season. A set of 5000 initial conditions has been generated with this approach. The corresponding model response (PMF) was determined for each initialization. After the PMP-PMF simulations have been performed, a quantile analysis was undertaken on the simulated PMF hydrograph ensemble. This approach made it possible to respect a realistic dependency of the different variables.

For the deterministic approach, a quantile for each state variable has been chosen and the corresponding state variable values have been determined. The chosen quantile is the same for each variable. The number of simulations is corresponding to the chosen number of state variable quantiles. The PMP-PMF simulations were performed fixing the initial conditions to the previously determined quantile values. For this study, the 0.25, 0.5 and 0.95 quantiles have been chosen.

Finally, the comparison of the results returned from the two approaches has been undertaken. The influence of the initial conditions on the inflow discharge and the lake level has been discussed.

5.6 Determination of initial conditions

In this section, the values for the initial conditions, on which the PMF estimates have been based, are explained and are represented for the four seasons of the year for exhaustivity reasons. However, for the initialization of the PMP-PMF simulation, it has been assumed that the PMF could only occur during summer (Hertig and Fallot, 2009).

5.6.1 Stochastic approach

The first approach is based on a generator to randomly engender initial conditions sets. As it is not possible to represent the 5000 generated initial conditions sets, the representation of the evolution of the state variables has been admitted to be a good indication to illustrate the data set the generator is based on. The state variable evolutions are exposed on Figure 5.1 showing the variation quantiles derived from the superposition of the mean simulated state variable values for the considered years. The mean value has been calculated by weighting the values of each altitude band by the surface of the latter.

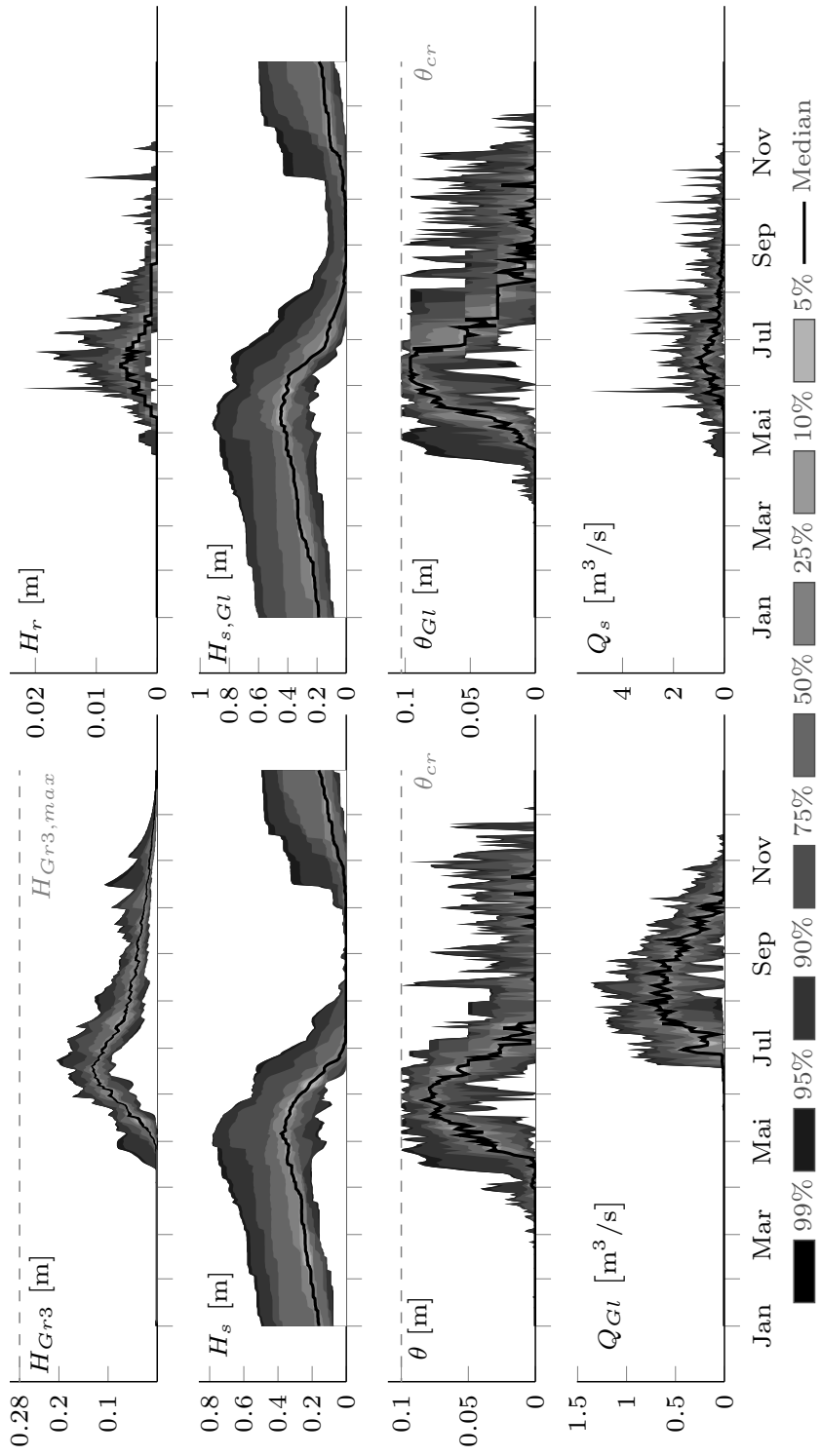

Figure 5.1: Evolution over time with variation interval of the 8 state variables of the GSM-SOCONT model, i.e. soil saturation H_{GR3}, runoff height H_r, snow height H_s, snow height on glacier $H_{s,GL}$, snow saturation θ, snow on glacier saturation θ_{Gl}, glacier melt Q_{Gl}, snow melt on glacier Q_s.

5.6.2 Deterministic approach

The values of the state variables retained as initial conditions for the PMP-PMF simulations are derived from the empirical cumulative density functions shown on Figure 5.2. Table 5.1 reports the values for the 25%, 50% and 95% quantiles for summer.

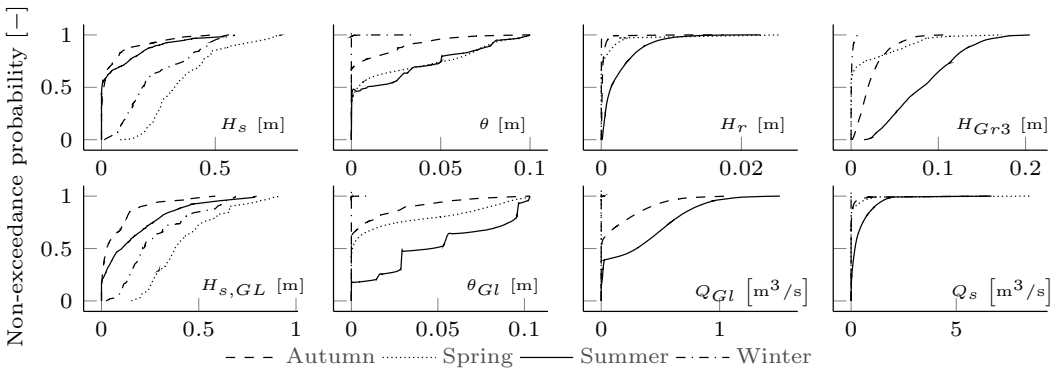

Figure 5.2: Seasonal cumulative density functions of the state variables of the GSM-SOCONT model, i.e. soil saturation H_{GR3}, runoff height H_r, snow height H_s, snow height on glacier $H_{s,GL}$, snow saturation θ, snow on glacier saturation θ_{Gl}, glacier melt Q_{Gl}, snow melt on glacier Q_s.

Table 5.1: Summer state variable values for the 25%, 50% and 95% quantiles considered for the hydrological model initialization.

Region	State variable	Symbol	25%	50%	95%	Unit
Non glacial	Snow height	H_s	0	0.002	0.364	[m]
	Snow saturation	θ	0	0.009	0.083	[m]
	Runoff height	H_r	0.0006	0.0014	0.008	[m]
	Soil saturation	H_{Gr3}	0.050	0.081	0.154	[m]
Glacial	Snow height	$H_{s,Gl}$	0.018	0.104	0.570	[m]
	Snow saturation	θ_{Gl}	0.015	0.046	0.101	[m]
	Glacier melt	Q_{Gl}	0.012	0.299	0.932	[m^3/s]
	Snow melt	Q_s	0.036	0.182	1.441	[m^3/s]

5.7 Results and discussion

In order to compare the results of the two approaches (stochastic and deterministic) the results of the stochastic approach have not only been represented as prediction intervals. Furthermore, the 25%, 50% as well as 95% quantiles have derived from the discharge ensemble. These quantile hydrographs have then been compared to the simulation results of the deterministic approach. For the comparison, the results of the two approaches have been superposed. Figure 5.3 shows the hydrographs and Figure 5.4 reports the water level of the lake of Mattmark.

The results indicate a high sensitivity of the hydrograph to the initial terrain conditions. The pronounced sensitivity confirms the importance of the choice of the initial conditions when extreme flood estimations are performed.

It is interesting to notice that the deterministic approach returned result quantiles that, when compared to the quantiles derived from the stochastic approach, are nearly identical. This result can be explained through the sensitivity analysis, showing the influence of every initial state variable value on the peak discharges.

5.7.1 Sensitivity analysis: Determination of the effect of each state variable

A sensitivity analysis has been performed in order to evaluate the influence of the different state variables. This analysis allowed to identify the most important state variables for the initialization of extreme flood estimations. Knowing the predominant state variables also leads to better comprehension of the simulation results and allows a more detailed analysis of the latter.

The sensitivity analysis has been designed according to Box et al. (1978). They described a method to design experiments in order to determine the effects of variables. The so-called *two-level factorial design* was utilized. This means that for every analysed variable, a maximum and a minimum value had to be admitted. Consequently, for N variables, the number of possible combinations is 2^N. In the context of this study, this means that with 8 state variables, $2^8 = 256$ simulations have been performed in order to determine the main state variables (main effects in the vocabulary of Box et al. (1978)) . The sensitivity has been undertaken for the peak discharges.

The sensitivity analysis was performed distinguishing between three different quantile ranges. This is necessary to discrete the analysis and to overcome the limitation of the two-level approach accounting only for two values per variable. This discretization leads indirectly to an analysis with more than two levels. This allowed to analyze if the sensitivity was changing in a certain range of values. The quantiles that have been considered as minimum and maximum values for the two-level design are $\{0.05, 0.25\}$, $\{0.40, 0.60\}$ and $\{0.75, 0.95\}$, derived from the summer time series. Hence the number of simulations increases to $3 \cdot 2^8 = 768$. The estimated quantiles are reported in Table 5.2.

Once the 2^N (here $2^8 = 256$) simulations have been performed for each quantile range, the influence of the different variables can be determined. The effects of the different considered state variables have been estimated, according to Box et al. (1978), by using Equation 5.1.

$$E_j = \frac{A_j^T R}{N \sum_{i=1}^{N} R_i} \tag{5.1}$$

where A is the design matrix with size $2^N \times (N + \frac{N^2 - N}{2})$ containing 1 (to indicate the high level

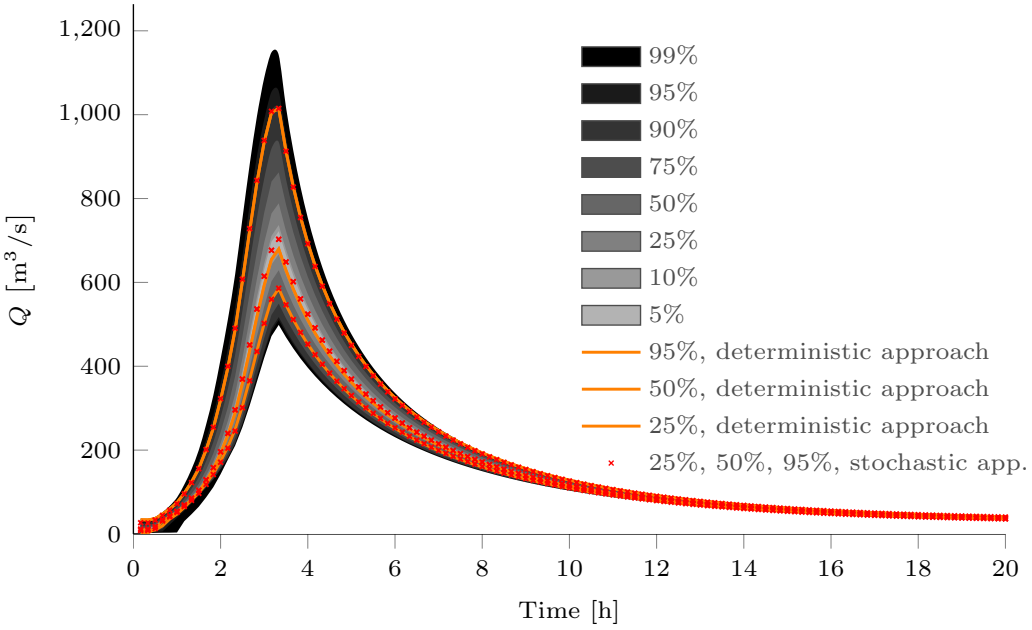

Figure 5.3: Superposition of the hydrographs derived from the stochastic and deterministic approach as well as the prediction intervals (shaded in gray) derived from the stochastic approach.

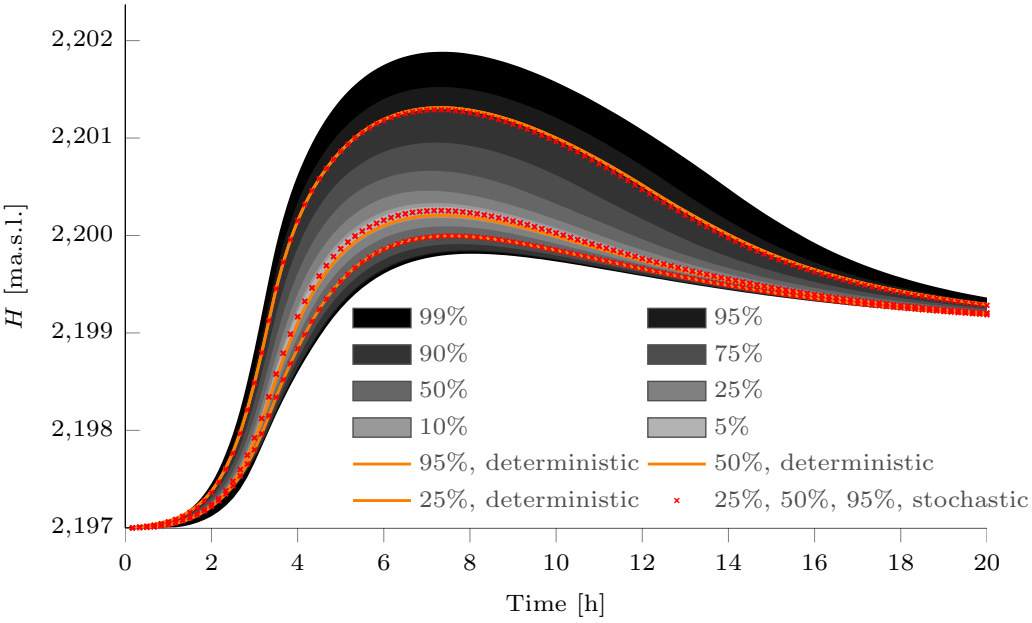

Figure 5.4: Superposition of the reservoir water levels derived from the stochastic and deterministic approach as well as the variation interval derived from the stochastic approach.

value) and -1 (to indicate the low level value), N is the number of considered state variables, j indicates the index of the state variable and R is a column vector containing the model outputs per run and has thus the dimensions $2^N \times 1$, i indicates the index of the run.

The approach considered for this analysis also accounts for two-factor interactions. This means that, for example, the combined effect of the soil saturation and the snow height could be analysed. The presence of the two-factor interactions in this analysis explains the number of columns of the design matrix. The columns corresponding to the interactions are derived by multiplying the columns of the design matrix (containing 1 and -1) corresponding to the state variables for which the interactions are considered to be interesting. In this study, all two-factor interactions have been considered. This leads to $\frac{N^2-N}{2}$ supplementary columns in the design matrix. The generated matrix (with dimensions 256×36) is too large to be represented in this report. The construction is described in detail in literature by Box et al. (1978).

The estimated effects have then been plotted on a bar plot in order to visualize the effect for reach variable (Figure 5.5). The most significant interactions have been plotted as well.

5.7.2 Results of the sensitivity analysis

As explained earlier, the sensitivity analysis is based on a two-level factorial design. The values arranged according to the design matrix are shown in Table 5.2 for the three ranges of chosen quantiles.

Table 5.2: Summer state variable values for the quantiles considered for the hydrological model initialization in the context of the sensitivity analysis.

			Range 1		Range 2		Range 3		
Region	State variable	Symbol	5%	25%	40%	60%	75%	95%	Unit
Non glacial	Snow height	H_s	0	0	0	0.022	0.120	0.360	[m]
	Snow sat.	θ	0	0	0	0.026	0.05	0.083	[m]
	Runoff height	H_r	0.0002	0.0006	0.001	0.002	0.004	0.008	[m]
	Soil sat.	H_{Gr3}	0.027	0.050	0.066	0.094	0.115	0.154	[m]
Glacial	Snow height	$H_{s,Gl}$	0	0.018	0.0.056	0.16	0.260	0.570	[m]
	Snow sat.	θ_{Gl}	0	0.015	0.029	0.054	0.091	0.100	[m]
	Glacier melt	Q_{Gl}	0	0.012	0.055	0.423	0.586	0.932	[m^3/s]
	Snow melt	Q_s	0	0.036	0.115	0.279	0.559	1.440	[m^3/s]

Results of the sensitivity analysis

The bar plot of Figure 5.5 shows that, under the assumed summer conditions, the soil saturation is the most important for low and high quantile values. The influence of snow height is also important when median values are chosen. However, the small snow height (cf Table 5.1) makes the absolute influence rather negligible in the case of Mattmark. The fact that the 25% and

95% quantile hydrographs were mainly guided by a single state variable explains the good correspondence between the results of the deterministic and stochastic approaches. The estimates of the median hydrograph from the two approaches correspond less well. The sensitivity analysis indicates an important influence of two state variables, i.e. soil saturation and snow height. The fact that these state variables are dependent together with the negligence of their dependency within the deterministic approach, leads to the differences that can be observed on Figure 5.3.

An interesting result is that the snow effects are negative for high quantile values. This means that the snow is actually attenuating the peak discharge. This is done by retaining a part of the precipitation in the snow that remains after the precipitation event and that was not initially saturated. It should be remembered here, that the water holding capacity of the snow is reached for $\theta = 0.1$.

An important remark that has to be made here is that the effect analysis shows that the initial conditions of the glacial bands do not have much influence on the peak discharge. However, the glacier cover is not negligible. In this case, the glacier cover corresponds to 28% of the total surface. The simulations have shown that the median glacial discharge portion is 46% for the low quantiles and decreases down 29% for the high quantiles. The maximum glacial discharge portion goes from 49% for the low quantiles down to 32% for the high quantiles and the minimum glacial discharge portion reaches from 42% to 26%. The discharge generated by the glacial bands is thus not negligible either. The question arises, why the influence of the initial conditions is not important.

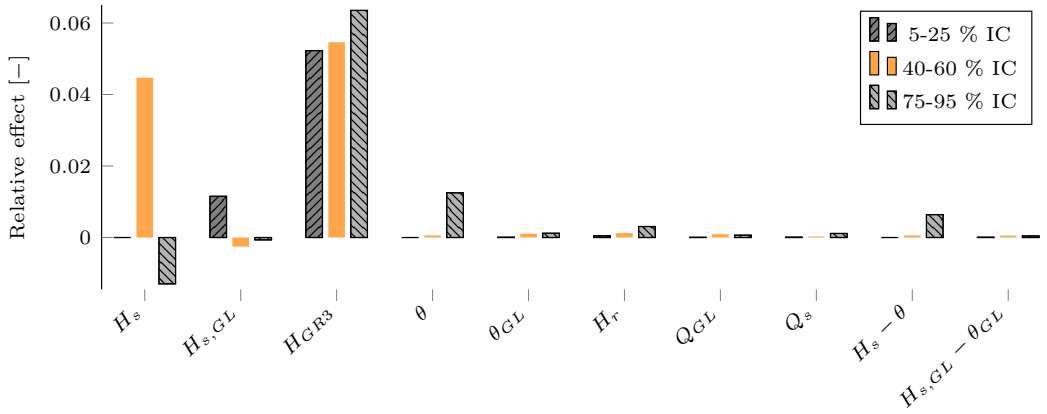

Figure 5.5: Relative effects on the PMF peak discharge of the initial state variables of the GSM-SOCONT model, i.e. soil saturation H_{GR3}, runoff height H_r, snow height H_s, snow height on glacier $H_{s,GL}$, snow saturation θ, snow on glacier saturation θ_{Gl}, glacier melt Q_{Gl}, snow melt on glacier Q_s as well as the effect of the interaction between the snow height and the saturation for glacial and non-glacial zones.

A reflection on the origin of the glacial discharge can clarify this issue. In fact, the glacial discharge is generated by a snow and glacier melt model. The initial conditions of the glacier melt

model only concern its initial melt outflow. The melting of the glacier and the snow is modelled by a degree-day approach and depends only on temperature. The routing of the precipitation falling on the glacier is thus not influenced by the initial conditions of the glacial bands. Whereas in the case of non glacial bands, the routing of the precipitation is influenced by the initial infiltration capacity of the soil. The soil has the ability to retain a part of the water and release it slowly as base flow what leads to an attenuating of the discharge. The initial snow cover on the glacial and non-glacial bands can be seen as a water volume added to the water coming from the precipitation. Under the assumption that the snow is saturated or completely melts during the precipitation event, this initial condition has no capacity of storing the precipitated water and thus of reducing the routed water amount. The case of a non saturated snow has already been discussed. The sensitivity analysis shows that the reduction of the discharge due to the snow is rather small and occurs only if the initial snow cover is high. For these reasons, the influence on the peak discharge of non-glacial bands is higher than the influence of the glacial bands.

Regarding the interactions, this case study did not allow to satisfactorily address this issue. In catchments, where the snow pack is remaining longer than it is the case for this analysis, the interaction between the snow and the soil saturation cannot be neglected. In the present study, the snow cover was too small to generated significant interaction effects. If interactions have a non negligible influence on the model output, the dependence between the variables should be taken into account. Thus, the deterministic approach would certainly not be a reliable approach for extreme flood estimate, as it cannot account for the variable dependence. The stochastic initial generator would be a better solution in that case. In order to determine which approach is best, a sensitivity analysis should be performed if the predominance of a single state variable cannot be proven a priori.

5.8 Conclusions

The analysis on the sensitivity of the PMF peak discharge to the initial conditions showed that the choice of the initial conditions has a high impact on the simulated flood discharge. A stochastic and a deterministic approach have been exposed and applied to the catchment of the Mattmark dam. The results of the sensitivity showed that in the present case study, the main factor within the initial conditions was the soil saturation followed by the snow height. The influence of the glacial initial conditions was small.

The approach of Box et al. (1978) could be applied successfully and valuable information could be extracted from the sensitivity analysis. The results of the deterministic and stochastic approaches could be analysed with full knowledge of the facts. It could be explained why the results of the two approaches are very close. The reason is because the number of factors that mainly effect the PMF is limited. In general, it can not be stated that the results would always depend on mainly one factor as it was the case for Mattmark. The main hydrological processes and their influence on the discharge guide the importance of the different state variables. Therefore, the here presented sensitivity analysis on the Mattmark dam catchment allowed to better understand

the important influence of the initial conditions, but could not lead to a generalization of the results.

For the flood estimation methodology developed during the CRUEX++ project, the choice of the initial conditions should always be subjected to a detailed analysis that is case oriented. A sensitivity analysis, like the one performed here, can add precious information. If the main state variables are interacting or have a non negligible dependence, the stochastic approach should be preferred. If the main driving factors can be reduced to one single state variable, as it has been the case for Mattmark, the deterministic approach can give very satisfactory results.

6 Swiss PMP map application limits

6.1 Introduction

The application limits of the Swiss PMP maps (Hertig et al., 2005; Hertig and Fallot, 2009) is addressed in this chapter. As explained in the state of the art (Section 2.6.5), the decrease of the intensity of the precipitation with the distance from the centre of the precipitation event can be neglected when the basin is sufficiently small. What sufficiently small means in the context of Swiss PMP maps has been determined in this research project and is described in this chapter.

Through multiple PMP-PMF simulations for basins with different catchment areas, the upper surface limit above which the raw PMP map data should not be considered for PMF estimations could be determined. The reasoning was based on the knowledge of realistic discharge-catchment area relations, described in Section 2.8. The basic assumption of this analysis is that realistic PMF discharges follow a law similar to the observed discharge-catchment area relations. This means that the PMF estimates have been used to determine an unreasonable expansion for a PMP event deduced from Swiss PMP maps.

It is shown in this chapter, that, for small basins, the PMF-catchment area relation is indeed similar to observed discharge-catchment area relations that can be found in literature (Marchi et al., 2010, e.g.). From a certain catchment area on, the PMF estimates increased much faster with the catchment area as expected compared to realistic discharge-catchment area relations. It should rather be spoken about a transition zone that is considered to define the aimed upper surface limit.

This transition zone defines the application limit of the CRUEX++ methodology. Furthermore, it has been determined how many Swiss dams can be verified regarding the spillway capacity in order to judge the degree of practicality of the methodology.

The usage of precipitation depth-area curves would be a different but interesting approach. The analysis would be conducted on the precipitation and not on the generated discharge. Two types of these curves are existing, i.e. storm-centred and geographically fixed relationships (Durrans et al.,

2002). These relationships are normally applied on point measurements under the assumption that the known measurement is at the center of the event. The determination of a storm center in the context of PMP maps is however not straight forward and may be even impossible. The application of depth area-curves in the context of this research project is thus not realizable due to the usage of PMP maps. This approach would, however, be very attractive if catchment related PMP estimations would be undertaken.

6.2 Study catchments and available data

The current study requires an important amount of meteorological and discharge data. A total of 13 catchments, with areas reaching from 3 km^2 to 443 km^2 have been modelled and PMP-PMF simulations have been undertaken.

The map of Figure 6.1 illustrates the situation of the catchments. A zoom on every catchment on a topographic map is shown in appendix C.1. Figure 6.2 shows a bar plot of the surfaces of the considered catchments. It can be seen on this figure that the choice of the basins covers well a continuous range of surfaces between 3 km^2 and 443 km^2. Table C.1 summarizes the exact catchment surface in appendix C.2.

The calibration of the hydrological model requires meteorological data (precipitation and temperature) as well as discharge data. The period of the available data for the 13 considered basins have been summarized on the graph of Figure C.20. The meteorological data acquisition is performed with a daily time step for the stations measuring only precipitation amounts and with a ten minutes time step for the automatic meteorological stations measuring precipitation and temperature. For computational reasons, hourly data have been considered for these stations. A data set with a temporal resolution of 10 minutes would be to voluminous due to the required length of the time series. Indeed, the latter should be as long as possible. The daily data have been disaggregated in hourly data sets. To do so, two nearby stations, for which hourly data have been available, had to be chosen. The data of these two stations were then interpolated, using the inverse squared distance weighting, to get an estimate of hourly precipitation at the location of the station to be disaggregated. Finally, the daily measured precipitation volume of the station to be disaggregated has been used to adjust the volume of the generated hourly time series. The meteorological stations taken into account for every catchment as well as the period of available data are shown in Appendix C.3.

The discharge data has been provided by the department of *Hydrological data and forecasts* of the *Federal Office for the Environment*. The data sets have an hourly temporal resolution. The situation of the measurement stations is shown on Figure 6.1.

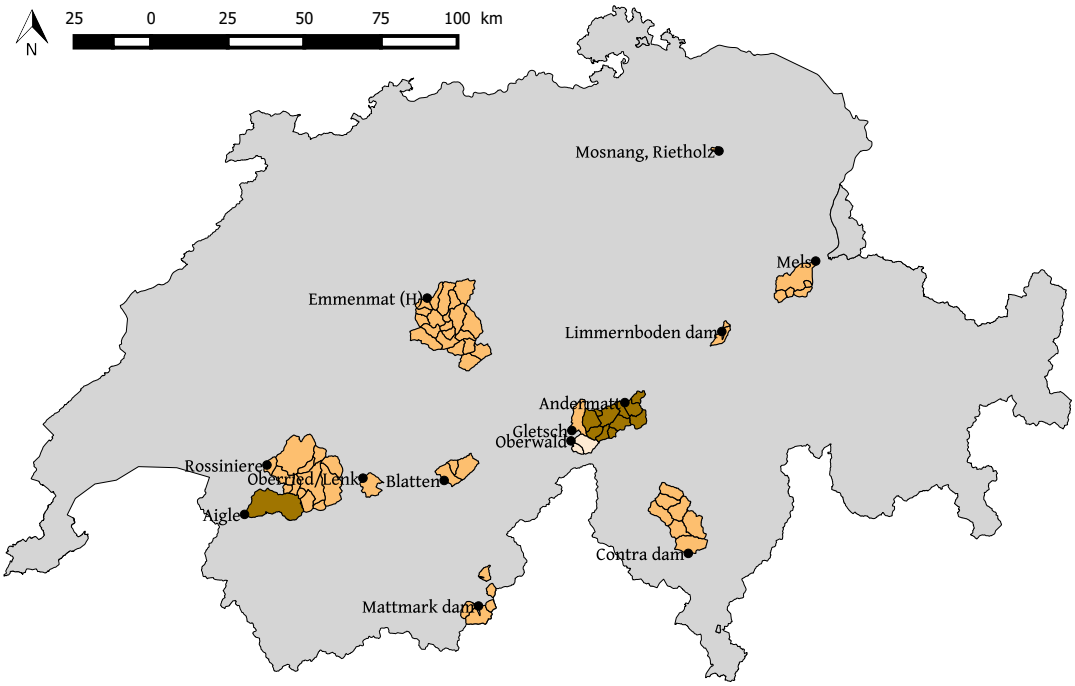

Figure 6.1: Situation of the considered catchments and of the discharge measurement stations (black dots), i.e Aigle, Andermatt, Blatten, Contra dam, Emmenmatt, Gletsch, Limmernboden dam, Mattmark dam, Mels, Mosnang/Rietholz, Oberried/Lenk, Oberwald, Rossiniere.

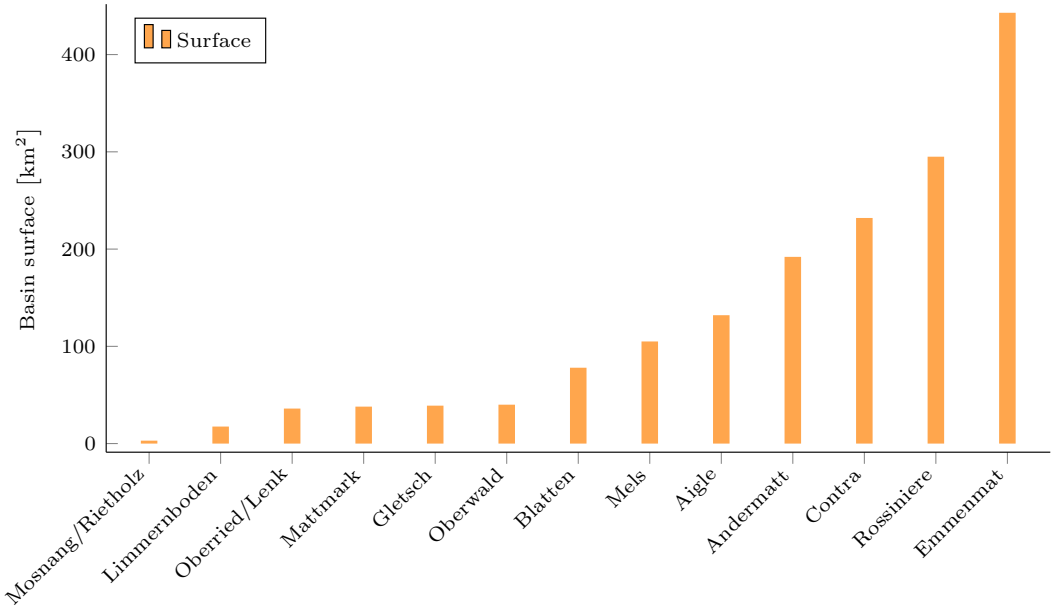

Figure 6.2: Bar plot of the surfaces of the catchments used for the determination of the upper surface limit for the application of the Swiss PMP maps.

6.3 Methodology

The different steps for the determination of the upper surface limit beyond which the Swiss PMP maps lead to overestimated spatial PMP expansion are explained in this section and illustrated on Figure 6.3. The reasoning has been performed on the generated PMF and the PMF-catchment area relation was used to conclude on the issue.

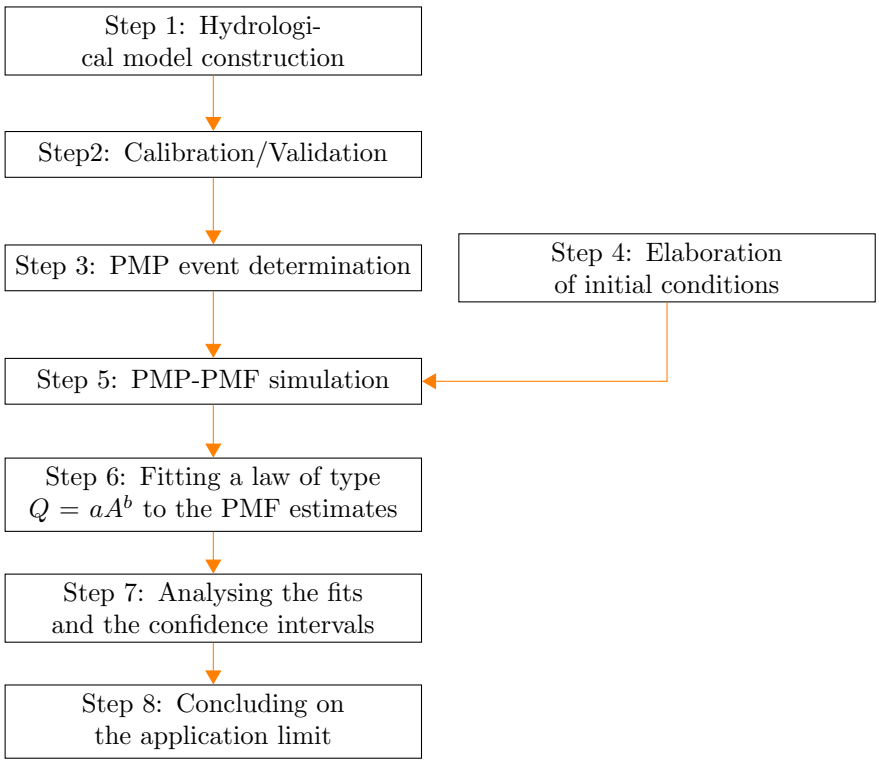

Figure 6.3: Flowchart of the 8 steps followed to determine the application limit of the Swiss PMP maps.

6.3.1 Hydrological model construction

The first step is to construct the hydrological model for each studied catchment. The model that is used here is the semi-distributed GSM-Socont hydrological model (Schaefli et al., 2005; Jordan et al., 2012; Schaefli and Zehe, 2009). The subdivision of the catchments into sub-basins is shown on Figure 6.1. The sub-basins have then been discretized in altitude bands with a vertical resolution of 300 m based on numerical terrain models with a horizontal resolution of 25 m.

The second step is to calibrate these models in order to guarantee that they reproduce the hydrological processes taking place in the modelled basins. The model performance has been evaluated using Nash-Sutcliffe efficiency and the volume ratio. The calibration and validation periods depend on the catchment and are illustrated on Figure C.20. The equations to estimate the performance coefficients can be found in Appendix E.2.

6.3.2 Determination of the PMP events

In a third step, the PMP events have been determined. The Swiss PMP maps have been used to extract the PMP data over the considered catchments. Then, the temporal rainfall distribution was determined according to the Swiss rainfall mass curve derived in Section 3. The conservative 5% quantile rainfall mass curve has been admitted to structure the PMP event in time. The spatial variability was affirmed to be the one reported on the PMP maps. This means that stationary PMP events have been assumed. The temperature data are derived according to the duration of the precipitation event. The relations combining the temperature and the duration of the PMP event have been developed in Chapter 4.

6.3.3 Elaboration of the initial conditions

As initial conditions, the median and 99% quantile state variables values were derived during the fourth step from the longest possible simulation period. These two initial condition scenarios have been considered to address the robustness of the determined upper surface limit compared to the initial conditions. The deterministic approach described in Chapter 5 (Section 5.5) has been admitted to be sufficient for the determination of the initial conditions considered for the PMP-PMF simulations.

6.3.4 PMP-PMF simulations and treatment of the results

In step (5), the PMP-PMF simulations were performed. Different event durations have been considered. As the PMP maps were developed for three different wind sectors, the PMF estimates per event duration have been repeated for every sector. The most critical PMP has been considered to be the one leading to the largest PMF discharge peak. Only the critical events were retained and exposed here. The critical PMF peak discharge was then plotted against the corresponding catchment surface in a log-log plot for both initial condition scenarios, the median and the 99% quantile state variables.

Then, in step (6), a law of type $Q = aA^b$ is fitted to the PMF estimates and 95% confidence intervals are estimated. Such a law is frequently used in literature to characterize the evolution of the maximum measured discharge with the catchment are (Francou and Rodier, 1967; Herschy, 2001; IAHS, 2003; Gaume et al., 2009; Marchi et al., 2010). This fit allows to separate the PMF estimates into two main groups, the valid and invalid PMF estimates. The invalid estimates are characterized by an overestimation of the PMF illustrated by the difference between the simulated PMF-catchment area relation and the observed discharge-catchment relation. The valid estimates are considered to be comparably important for the different basins, meaning that their discharge-area relation has a behaviour comparable the the observation derived relations. The magnitude of the PMF estimates compared to the catchment surfaces was quantified by the Francou coefficient estimated by Equation 2.8. The theoretical discharges corresponding to a constant Francou coefficient derived for different catchment surfaces are represented by a straight

line in a log-log space. This line is compared to the regression of type $Q = aA^b$, also linear in a log-log space. When the two lines are parallel, the regression line can be considered to represent similarly important floods. The distinction between valid and invalid floods is undertaken by determining by trial-and-error the biggest flood below which the regression line is parallel to the constant Francou coefficient line. The remaining floods are, though, in the group of invalid floods. This group is also fitted by a law of type $Q = aA^b$. The confidence intervals allow to account for the variability of the PMF estimates for the two groups.

Step (7) consists in analyzing the regression lines and the confidence intervals. This analysis led to the determination of the upper surface limit above which the PMP data from the PMP maps should not be considered to precipitate simultaneously over the entire catchment. Due to the consideration of confidence intervals, the surface limit would rather be a transition zone than a single value.

In step (8), the final analysis aimed at judging on the general applicability of the extreme flood estimation methodology. A comparison of the determined upper surface limit with the catchment areas of the major Swiss dams (200 dams that are under direct federal supervision [1]) let conclude on this point.

6.4 Hydrological simulations

The studied catchments have been modelled with the GSM-Socont hydrological model. A brief description of the model is given in the following. The snow accumulation (solid/liquid precipitation) has been simulated with a linear transition from snowfall to rainfall at temperatures between 0°C and 2°C (which fits well with observed snow and rainfall data (Rohrer et al., 1994). The snowmelt has been computed with a degree-day approach (Hock, 2003). Melt water leaves the snowpack only if a certain liquid-to-solid threshold (set to $\theta_{cr} = 0.1$) is reached and can refreeze during periods of negative temperatures. The melt and rainwater (in case of rain-on-snow events) that leaves the snowpack is assumed to infiltrate into the subsoil. The catchment-scale runoff resulting either from snowpack outflow or from direct rainfall on snow-free areas is computed via two reservoirs (fast and slow component). Runoff from glacier-covered areas is computed with a separate ice-melt module that uses also a degree-day approach and two linear reservoirs to transform melt water into runoff, one for snow and one for ice.

The models have been calibrated based on the available meteorological and discharge data. The periods of available data and the subdivision of these periods into calibration and validation periods are shown on Figure C.20. The performance coefficients Nash-Sutcliffe as well as the volume ratio are reported on Figures 6.4 and 6.5 respectively. Moriasi et al. (2007) qualified a Nash-Sutcliffe efficiency between 0.5 and 0.65 as satisfactory, between 0.65 and 0.75 as good and between 0.75 and 1 as very good. According to the Nash-Sutcliffe efficiencies for the models considered for this study, all models could reproduce the measured discharges in a way that they

[1] For confidential reasons, details about these dams and their catchments could not be included in this report.

can be assumed to be reliable. For the calibration, 5 models could be qualified to be good and 8 to be very good. For the validation period, one model was qualified as satisfactory, 3 as good and 9 as very good.

6.5 Results and discussion

PMP-PMF simulations have been performed with two different scenarios for the initial conditions have been considered. The peak discharges have been plotted on Figures 6.6 and 6.7 against the surface of the corresponding catchment.

The comparison between the European envelope curve (Marchi et al., 2010) and the PMF estimates show that the PMFs are below the European envelope curve for the scenario with median initial conditions and mainly below for the 99% quantile state variable values considered as initial conditions. It should be mentioned that the determination of this curve was mainly driven by Mediterranean floods. However, the Swiss PMF estimates are far more important than the discharges returned by the approximated European Alpine envelope curve (cf Section 2.8).

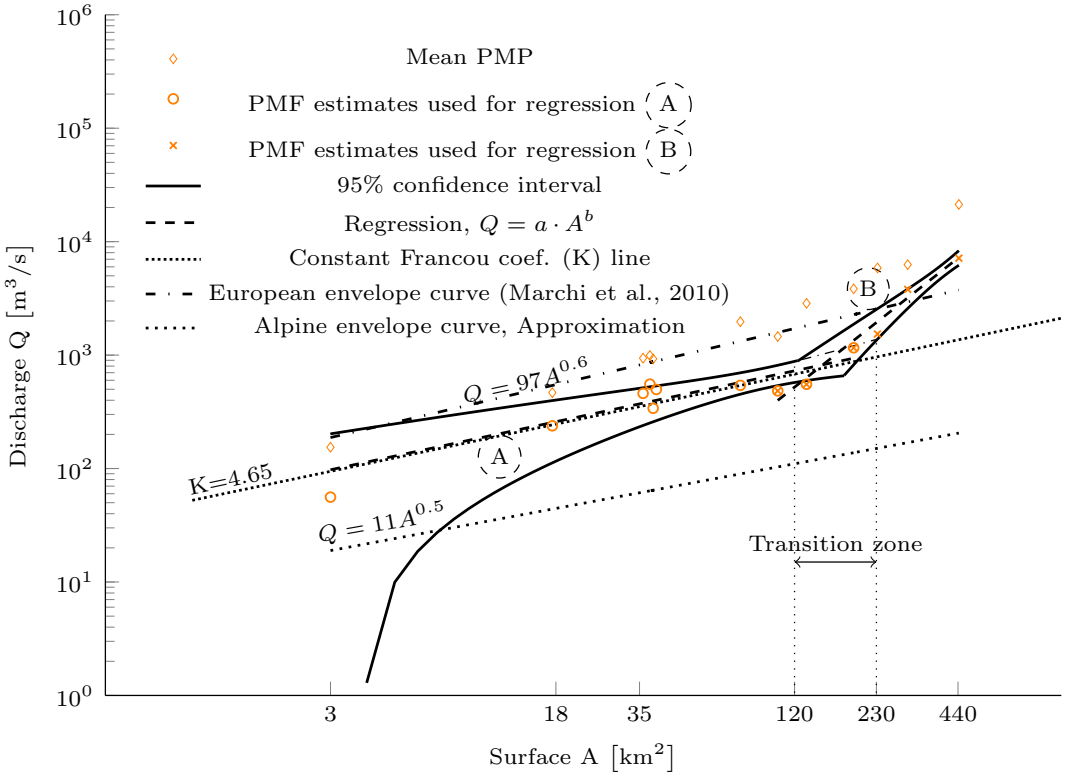

Figure 6.6: Discharge-surface plot for the PMF estimates of the considered basins for the initial conditions corresponding to the median values of the state variables of the GSM-SOCONT model, i.e. soil saturation, runoff height, snow height, snow height on glacier, snow saturation, snow on glacier saturation, glacier melt, snow melt on glacier.

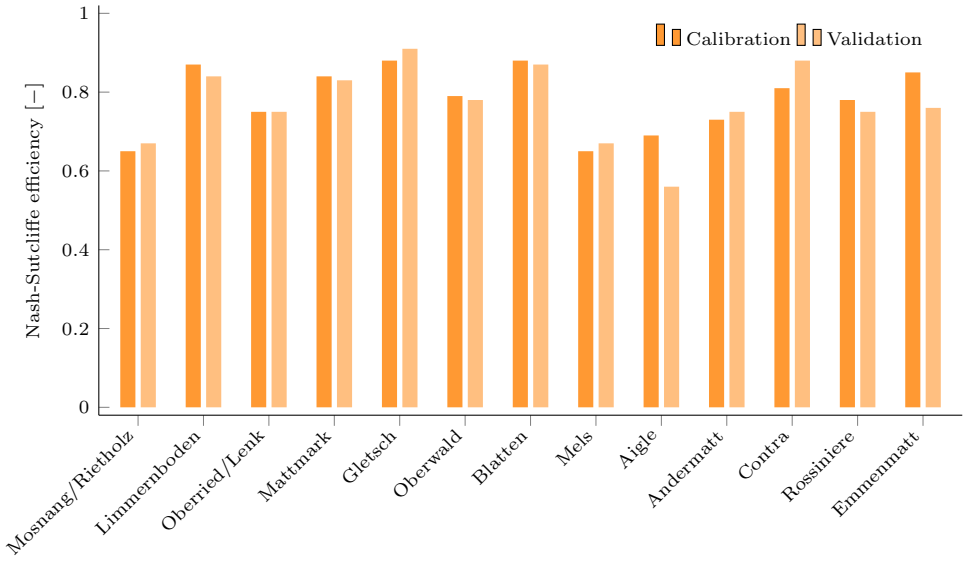

Figure 6.4: Nash-Sutcliffe efficiencies for the considered catchments for the calibration and the validation periods illustrated on Figure C.20.

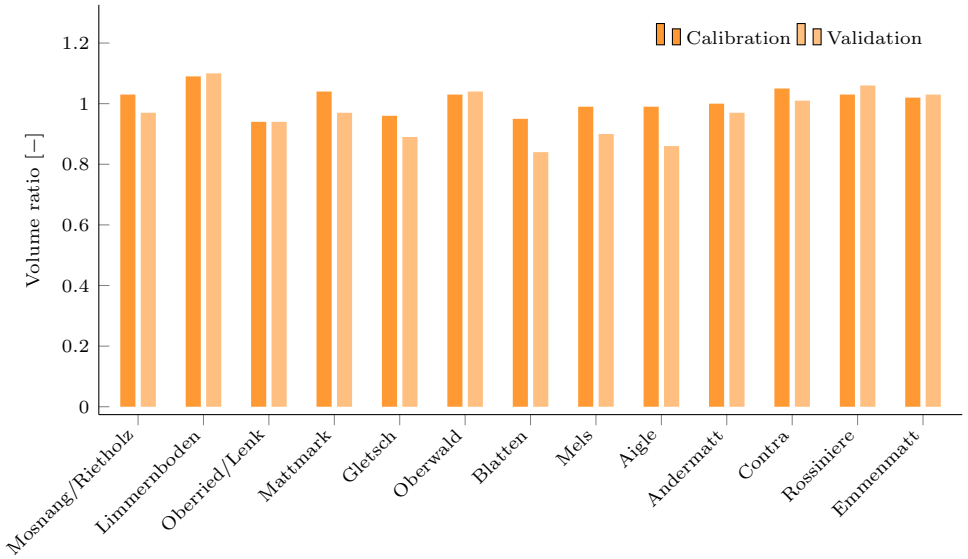

Figure 6.5: Volume ratios for the considered catchments for the calibration and the validation period illustrated on Figure C.20.

Considering the scenario with median state variables as initial conditions, the estimated PMFs (represented on Figure 6.6) have Francou coefficients with a mean value of $K = 4.65$. The linear regression line (named (A) on the graph of Figure 6.6, ($Q = 53.62 \cdot A^{0.54}$) of the estimated PMFs (ignoring the three largest catchments) shows that the discharge increase with the surface is comparable to the increase of the envelope curves and the curves derived for a constant Francou coefficient. This underlines the reliability of the estimated PMF discharges.

The regression line (B) (regression of the PMFs from the six largest analysed catchments,($Q = 0.034 \cdot A^{2.02}$) is much steeper than the regression line (A), the constant Francou line and the envelope curves. Compared to the latter, the increase of the discharge with the surface is unrealistically fast regarding the regression (B).

A very important element of the analysis are the confidence intervals of the two regression lines. These intervals, intersecting each other, lead to a transition zone between the valid and invalid PMF estimates. The beginning of the zone is defined by the intersection point of the upper confidence limits from the two regressions. This points defines the smallest catchment area above which an invalid estimation can occur. The lines are intersecting for $A = 120\,\text{km}^2$. In fact, from this surface on, overestimations can occur as illustrated by the upper confidence limit of regression (B). However, the simulation results show that realistic floods have indeed been simulated. Their intensity is lower than the upper confidence limit. Actually, the two floods below the 95% lower confidence limit are even likely to be underestimated.

If the lower confidence level of regression (B) is above the upper confidence limit of regression (A) lets conclude that there is quasi no chance of not overestimating the PMF. This is the case for a surface of $A = 230\,\text{km}^2$. The end of the zone is thus defined by the intersection point of the upper confidence limit of regression (A) and the lower confidence level of regression (B). In fact, all simulations are above the upper confidence limit from regression (A).

This zone from 120 to 230 km^2 is very important for the aimed methodology because the beginning and the end of the zone define the catchment surfaces for which valid and invalid PMFs can be found. Thus, the estimates in this zone should be treated carefully. The end of the transition zone defines the absolute upper surface limit above which the PMP data from the PMP maps should not be considered to precipitate simultaneously over the entire catchment.

For the second initial conditions scenario (99% quantile of the state variable values), the determined transition zone (70-210 km^2) is very similar to the zone determined above. The results for this initial conditions scenario are shown on Figure 6.7. The equation for the regressions (A) and (B) are respectively $Q = 114.7 \cdot A^{0.47}$ and $Q = 0.96 \cdot A^{1.5}$.

An interesting appraisal is that the European envelope curve is still above most of the valid PMF estimates. The only exception is probably due to an overestimation, the point being above the upper confidence limit. Furthermore, for the catchments in the transition zone and above, the points being above the European envelope curve are all considered as being invalid. It can

be observed that the upper confidence limit extension from regression (A) is nearly identical and appears to be parallel to the European envelope curve. This lets assume that the analysis performed here is well in line with the upper limit for floods compared to the catchment surface, as it has been presented in literature by different authors (Francou and Rodier, 1967; Herschy, 2001; IAHS, 2003; Gaume et al., 2009; Marchi et al., 2010).

It should be mentioned, that it would have been interesting to consider a larger number of catchments. In fact, the regression and the related confidence intervals would be more reliable. This could effect the final conclusion on the transition zone and thus on the upper surface limit for the applicability of the PMP maps. However, the goodness of the regression lets being confident about the results. The values of R^2 are reported in Table 6.1. They show that the regression is reliable for both initial conditions scenarios and both regressions (A) and (B).

Interesting is also the comparison of the mean PMP intensities (converted to discharge units m^3/s) with the simulated PMF peak discharges. It is apparent in Figures 6.6 and 6.7 that the mean ratio between the mean PMP intensity and the PMF peak discharges (runoff coefficient) is 0.38 for the PMF estimates based on the 50% quantile initial conditions and 0.62 for the PMF estimates based on the 99% quantile initial conditions. One should be aware that this comparison does neglect the contribution of snow and glacier melt, therefore the runoff coefficient may be smaller than the mentioned ratios.

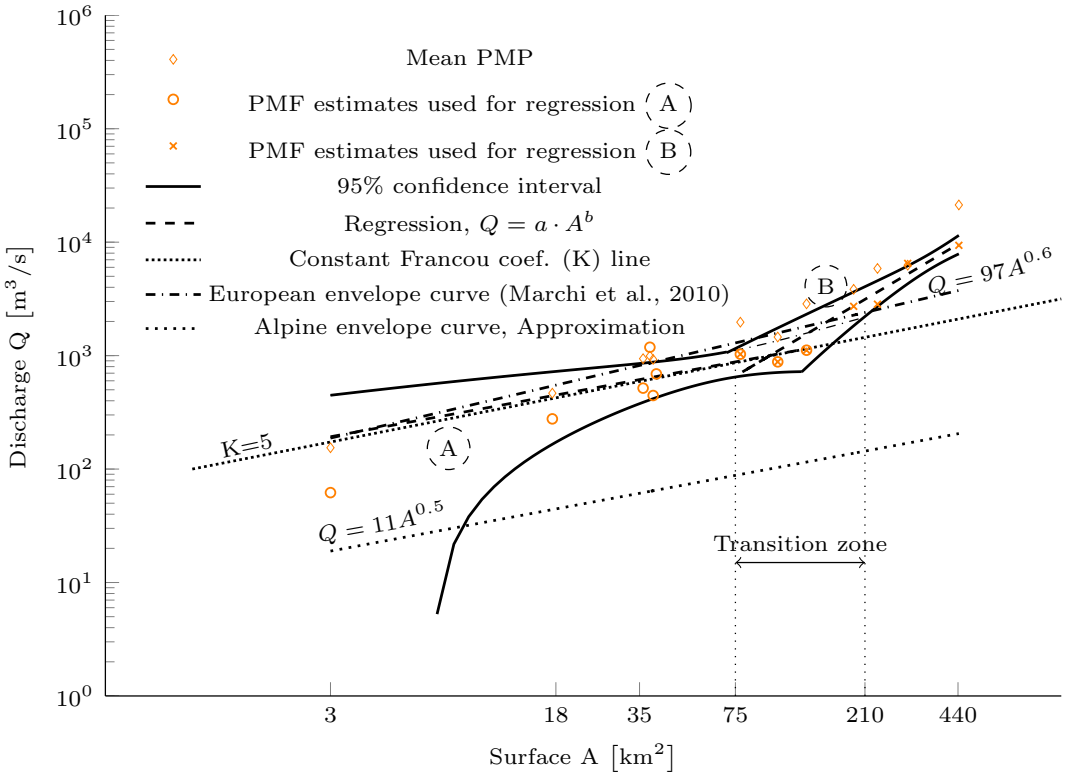

Figure 6.7: Discharge-surface plot for the PMF estimates of the considered basins for the initial conditions corresponding to the 99% quantile values of the state variables of the GSM-SOCONT model, i.e. soil saturation, runoff height, snow height, snow height on glacier, snow saturation, snow on glacier saturation, glacier melt, snow melt on glacier.

Table 6.1: Values of R^2 for the evaluation of the goodness of fit of the regressions under the two initial conditions (IC) scenarios.

	50 % IC	99% IC
A	0.75	0.65
B	0.98	0.96

The widest transition zone can derived from the combination of the two above derived transition zones. It results a zone that reaches from 75 to 230 km^2. At this point, the question of how many dams in Switzerland have a smaller catchment than this upper limit surface arises, because the percentage of smaller dam catchments quantifies the applicability of the PMP maps in the Swiss context. Figure 6.8 shows the histogram of the dam catchments that are under direct supervision of the Swiss federal Office of Energy (SFOE). Roughly 200 reservoirs enter these statistics. The cumulative percentage (Figure 6.8) indicates that about 69-85% of the Swiss dams can be verified regarding flood safety with the Swiss PMP maps (for the widest tranistion zone from 75-230 km^2). This corresponds in the most optimistic case to 170 dams. Switzerland has about 1200 registered dams of which approximately 200 are under SFOE supervision and 100 under cantonal supervision. Under the assumption that all of the catchments of the 100 dams, being under cantonal supervision, are smaller than 230 km^2, it can be assumed that the CRUEX++ methodology can be applied to approximately 90% of these 300 dams. Of course, there are another 900 very small dams which are neither under direct SFOE supervision nor under cantonal supervision. It has been assumed that these 900 dams do not need to be verified for PMFs.

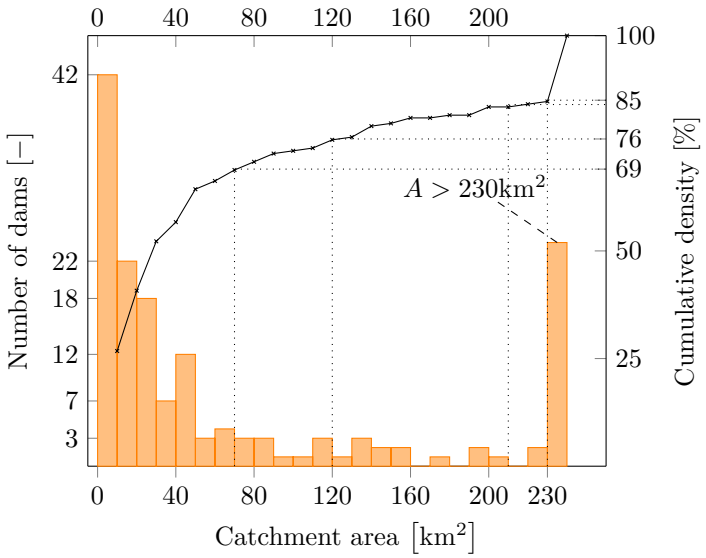

Figure 6.8: Histogram of the catchment areas of roughly 200 dams under direct SFOE supervision with cumulative percentage indications.

6.6 Conclusions

In this chapter, 13 catchments have been modelled with GSM-Socont hydrological model and PMP-PMF simulations have been undertaken. Two different initial conditions scenarios have been considered for the simulations in order to analyse if the initial conditions influence the conclusion significantly or not. A difference in the determined transition zone could be found. The consequences for the applicability of the methodology was, however, only slightly influenced because the majority of the dams have a catchment with an area smaller than the most restrictive limit of 75 km^2. The resulting PMFs have been plotted against the surface of the corresponding catchment and regression lines with 95% confidence intervals have been determined.

The comparison of the simulation result with Alpine and European maximum flood envelope curves from literature allowed to conclude that the order of magnitude of the estimated discharges is realistic. Furthermore, the comparison to the theoretical discharges for a certain Francou coefficient proves that the PMF estimates, considered as valid, are all having the same magnitude. This comparison can be considered as an homogeneity test. All valid PMFs can be assumed to be similarly large.

The regression of the valid and invalid PMF estimates let to the determination of the upper surface limit above which the PMP data from the PMP maps could not be considered to represent simultaneously precipitating water volumes over the entire concerned surface. The confidence intervals of the regression lines allowed to determine a transition zone between the valid and invalid PMFs. The consequences of this transition zone for the extreme flood estimation methodology is that the flood estimates for catchments fitting the transition zone should be discussed and judged in order to make sure that the discharges are not overestimated.

The determined transition zones for the two initial conditions scenarios are very similar. For the median initial state variable values, the transition zone reaches from 120 to 230 km^2. For the 99% quantile values, the zone goes from 70 to 210 km^2. These differences do not effect the applicability of the methodology in a strong way, because the majority (69%) of the Swiss dam catchments (for the dams under direct SFOE supervision) are smaller than 70 km^2. Counting also the dams under cantonal supervision, this percentage would probably increase in favour of the CRUEX++ methodology. The fact, that only about 24 dams (of the 200 dams under direct SFOE supervision) are directly excluded from the application of the CRUEX++ methodology shows that the PMP maps have a wide applicability range in the Swiss context. Most of these 24 dams are weirs of run-of-the-river power plants which have very large catchments that can reach up to 35 000 km^2 for Switzerland.

For the analysis, only 13 catchments have been studied. A larger number of simulated PMFs may have let to a better description of the regression, the confidence intervals and thus the transition zones. However, the comparison of the results with the envelope curves and the constant Francou coefficient line allowed to prove the coherence of the results with observations regarding the order of magnitude and the evolution of the simulated discharges compared to the catchment

surfaces. The results are thus in line with the literature and can be assumed to be sufficiently reliable for a significant conclusion, as it has been drawn above.

6.7 Remarks on volume overestimation

An aspect that could not be treated with the here presented approach, is the question of the PMF volume overestimation. The reasoning had to be based in a first time on the PMF peak discharges because flood volume - catchment area relations could not be found in literature. A comparison taking into account the PMF volume with measured volumes, analogue to the peak comparison as it has been performed in this Chapter, was not possible due to limited time. A flood volume - catchment area relation could be derived from measurements and used for the verification of the applicability limits focusing on the flood volume.

7 Upper bounded statistical distributions in the context of extreme flood estimations

7.1 Introduction and objectives

This chapter aims at analyzing the usefulness and advantages of upper bounded statistical distributions for extreme flood estimations. A comparison between bounded and unbounded distributions is made to address their sensitivity to the extrapolated sample. Furthermore, the sensitivity of the upper bounded distributions to the deterministically estimated upper bound is carried out.

For this analysis, the existence of an upper maximum discharge bound has been assumed. This assumption, discussed and justified by Enzel et al. (1993), is the basis of one of the most used extreme flood estimation approaches for the estimation of safety floods for dam design, i.e. the PMP-PMF method. In Switzerland, the design flood that has to be considered for dam design is the 1000 year flood. If it is derived by simulation from a design storm, it is often assumed, that the return period of the simulated flood is the same as the one from the rainfall event. But this is not necessarily true. If the simulation is undertaken under the assumption of severe terrain conditions the return period can be larger than 1000 years. The other way round, if attenuation effects (like for example snowfall or water retention in an initially non saturated snow pack) occur during the simulation, the return period of the estimated flood could be lower than the return period of the underlying rainfall event. If the 1000 year flood is estimated with commonly used unbounded statistical distributions, contradictions with the PMP-PMF approach can occur. As the information of the PMF is missing in the extrapolated time series, an over or underestimation of rare to extreme floods can occur. For example, if the GEV is used, the skewness of the sample has a high impact on the distribution fit. A high sample skewness may lead to severe overestimations. The 1000 year flood may even be higher than the PMF if the skewness of the sample is high enough. In the case where major floods have not been observed, the extrapolation using the GEV can induce underestimations due to a smaller skewness coefficient. The flexibility of the GEV may thus be problematic for extreme flood estimations. A less flexible two-parameter distribution can cause similar problems, but for different reasons. It may not be able to sufficiently account for high observed floods and can thus lead to underestimations even if important flood events have

been in the sample. Analogously, an overestimation can be imagined if the sample tail flattens significantly compared to a rather highly skewed main sample body.

This clearly shows that the two approaches (statistical and simulation) can lead to different conclusions. Combining the advantages of both approaches should enhance the quality of the flood estimates. In the literature review, two different upper bounded statistical distributions have been retained as applicable to discharge time series, i.e. the EV4 and LN4 distributions (cf Section 2.5). These distributions allow to account for an a priori deterministically estimated PMF peak discharge for the extrapolation. The information expansion of systematic data (as accounting for non systematic data is frequently referred to in literature) is, according to Merz and Blöschl (2008a), increasing the quality of the statistical extrapolation and is therefore of very high importance for extreme flood estimations. In fact, when using conventional statistical approaches without information expansion, the uncertainty on the estimate increases considerably with increasing return periods. Therefore an approach reducing this uncertainty is of high value in the context of this research project.

In this analysis, the upper bounded distributions EV4 and LN4 are compared to the unbounded GEV and log-normal distributions. The extrapolations from the upper bounded distributions are compared to their unbounded parent distributions (GEV and log-normal), that, among others, are frequently used in hydrology (Vogel and Wilson, 1996; Merz and Thieken, 2005; Apel et al., 2006; Stedinger and Griffis, 2008; Apel et al., 2009; Aronica et al., 2012; Sarhadi et al., 2012; DWA, 2012; Kiczko et al., 2013; Candela et al., 2014; Dung et al., 2015; Romanowicz and Kiczko, 2016).

An analysis is carried out in order to analyze the sensitivity of the extrapolations to the sample size. This analysis gives important information as the hydrologists are mostly concerned about too short samples as well as the high uncertainty on the estimation of rare events. Furthermore, the sensitivity of the extrapolations to the deterministically determined upper bound is addressed.

7.2 Synthetic data samples for the distribution fits

For the analysis presented in this chapter, a synthetic data sample has been considered. In order to respect the findings of Takara and Tosa (1999), who found that the EV4 distributions gives best results when the sample skewness is larger than 2 and the LN4 distribution should be preferred when the sample skewness is smaller than 1.5, two synthetically generated data samples have been generated, one for the analysis of each distribution. The samples are generated in order to control the skewness of the sample, what would not be possible for a sample with observed values.

The generation of the samples was based on the LN4 and EV4 distributions. The randomly sampled data have been modified by adding white Gaussian noise, with a signal to noise ratio of 25 dB, in order to simulate the imperfections of realistic samples. As upper bound, a value of 3500

m^3/s has been admitted. The lower bound has been assumed to be 0, what is consistent with the works of Kanda (1981), Takara and Tosa (1999), Botero and Francés (2010) and Fernandes et al. (2010). For the EV4 distribution, the scale parameter has been chosen to be $\nu = 15$ and the shape parameter $k = 2$. For the LN4 distribution the following values have been admitted: $\mu_y = -1.8$ and $\sigma_y = 0.5$. These parameters have been determined by trial and error in order to generate a sample close the realistic values. For this application, a comparison with the measured data and the PMF estimate of the Contra dam can be made. For a realistic analysis, the generated sample of flood peak discharges and the assumed upper limit of $g = 3500\,m^3/s$ have to be coherent. The measured discharge data are indeed of the same order of magnitude than the samples generated for this analysis as can be seen by comparing Figure E.16 (Appendix D), showing the annual maximum values sample of the Contra dam catchment, with the generated samples shown on Figure 7.1 and 7.2. The PMF estimate for the Contra dam catchment, detailed in Chapter 9, is of the same order of magnitude than the assumed upper bound ($g = 3500\,m^3/s$). The generated sample and the considered upper limit can thus be assumed to be realistic and coherent.

The generated sample size corresponds to 43 values. The sample size has been chosen for an aesthetic reason. As explained in Section 7.3, a bootstrap re-sampling has been performed. Disposing of 43 values allows to generate a large number of samples with 40 values, a round number for the graphs. The generated samples are shown on Figure 7.1 and 7.2. The skewness of the generated samples (Equation 2.1) is $\gamma = 2.87$ and $\gamma = 0.97$ for the EV4 and LN4 distributions respectively.

7.3 Methodology for assessing the distribution sensitivities

First, the bounded (EV4, LN4) and unbounded (GEV, log-normal) distributions were fitted to the complete generated sample of 43 values. The mathematical expression of the GEV and log-normal distributions are provided in Appendix D.2. The distributions were fitted using the Maximum Likelihood Method (ML), explained in detail by Coles (2001). Different criteria were used for the evaluation of the suitability for the different distribution fits. The Komogorov-Smirnov statistic was used, assuming a rejection if the p-value $p < 0.05$. This statistic has been well exposed by Meylan et al. (2008). Furthermore, the Akaike and Baysian information criteria (AIC and BIC, also explained by Meylan et al. (2008)) were used for model comparison. Due to the rather small size of the sample, the corrected AIC (AICc) has also been considered. It has been presented by Burnham and Anderson (2002). In addition, the root mean squared error was considered. The recommendation of Takara and Tosa (1999) concerning the sample skewness and the related distribution choice has also been considered for the discussion of the results.

Second, the sensitivity of the different distributions to the sample was analysed. In order to give an example of the sensitivity, the distributions were fitted to the dataset with a length varying from 30 to 43 values. This allowed to visualize the sensitivity of the distributions to the sample sizes. It illustrates the effect 13 years of additional data would have in a real world application. This step allows to get a first impression of the sample sensitivity and to illustrate the necessity of

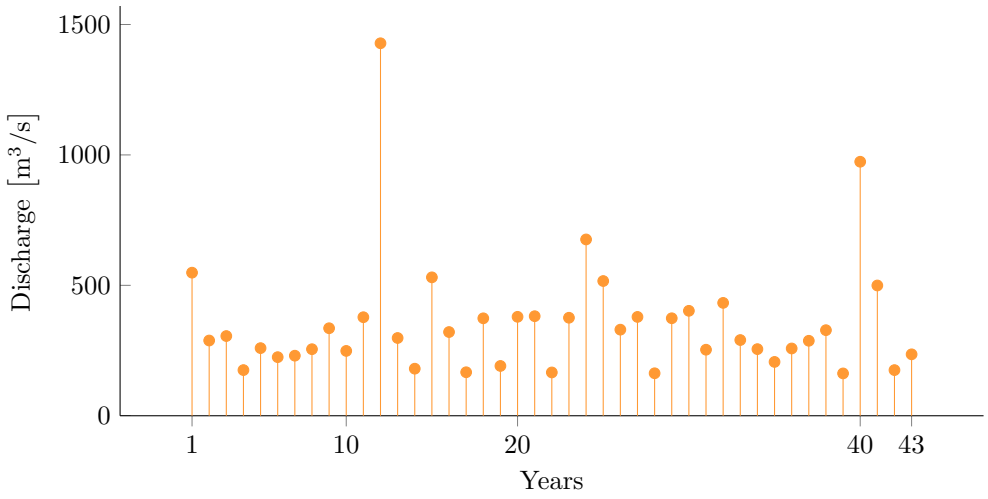

Figure 7.1: Sample generated by an EV4 distribution. Parameters: $\nu = 15$, $k = 2$, $a = 0$, $g = 3500$.

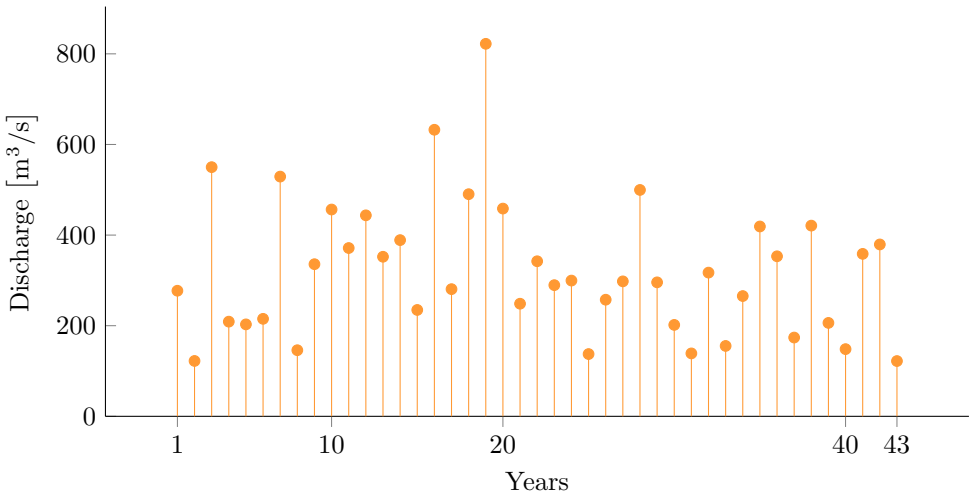

Figure 7.2: Sample generated by an LN4 distribution. Parameters: $\mu_y = -1.8$, $\sigma_y = 0.5$, $a = 0$, $g = 3500$.

the bootstrap approach.

Then, a more deepened analysis has been performed using a bootstrap approach. This approach allowed to quantify the variability of the discharge estimates for a given return period for every considered sample size. The minimum sample size was fixed to 30 values and the maximum number to 40 values. For every sample size, 1000 samples were generated by randomly sampling the aimed number of events in the complete sample containing 43 maximum annual values. The size of 43 values would actually allow to generate 12341 different samples of 40 values. A sample of 42 values would only allow to generate 861 different samples of 40 values. Therefore, 43 values are the necessary minimum to generate 1000 different samples. For every generated sample, 10 samples with a length from 30 to 40 values have been determined by ignoring the last 0 to 10 values. The statistical distributions were fitted with the ML method to every sample (11 000 in total). The mean estimate, the 5% and 95% quantiles for the 1000 and 10 000 year floods were estimated and plotted against the sample size. This plot allowed to analyze the robustness of a distribution compared to the sample size.

The third aspect of the analysis treats the sensitivity of the 1000 and 10 000 year return period flood to the estimate of the upper bound. An over and underestimation up to 30% of the upper bound has been considered in order to assess the sensitivity of the extrapolation to the latter. The sample size had to be fixed for this analysis. A constant sample size of 40 values has been considered. Bootstrap re-sampling has been used for the estimation of the confidence intervals of the flood estimates.

7.4 Goodness of fit analysis

The goal of the discussion concerning the goodness of fit, was to select for each fitted sample two distributions, one with and one without upper bound that was retained as adapted for the sensitivity analysis exposed in Section 7.5.1.

An important part of the analysis was to select the best fitting unbounded distribution under the consideration of conventional approaches as decision criteria. The consideration of the bounded distributions for the goodness of fit evaluation was done in order to prove that the added white Gaussian noise would not induce the underlying bounded distributions to be unsuited for the fit.

Sample with small skewness ($\gamma < 1.5$)

The EV4, LN4, GEV and log-normal distributions have been fitted to the complete generated sample of 43 values with skewness $\gamma = 0.97$. The fit, as well as the assumption of the PMF are plotted on Figure 7.3. This figure shows clearly that the two unbounded distributions are returning estimates that are larger than the PMF from a return period of approximately 10^7 years. The tail of the distribution is clearly incoherent with the PMP-PMF approach. Concerning the upper bounded distributions, Figure 7.3 shows that the EV4 distribution is approaching the upper

limit faster than the LN4 distribution.

The sample. on which the fit of the distribution has been based, has been generated using an LN4 distribution. Therefore, the fit of the LN4 distribution should be the most appropriate. The performance coefficients shown in Table 7.1 do lead to mixed conclusions. The Kolmogorov-Smirnov test does not allow to reject any of the four distributions. The AIC, AICc and BIC indicate that the log-normal distribution is the most appropriate, followed by the LN4 distribution. The difference between the two models is, however, very small. Due to the origin of the samples, it could have been awaited that the underlying bounded distribution for the generation of the samples would clearly be the best adapted. The discussion above showed that this is not necessarily the case. The introduction of non systematic data (in this case causal information expansion according to Merz and Blöschl (2008a)) may lead to a more holistic model, but could induce the fit to respect less well the structure of the systematic data set.

It can be noticed, that the smallest RMSE estimates have been found for the two other distributions, i.e. GEV and EV4. The difference between the four RMSE estimates are very small. The criterion is very basic and only describes the goodness of the fit for the sample points. The reason could be the flexibility of the distributions to join the structure of the sample. For the following sensitivity analysis (for the sample with $\gamma = 0.97$), the log-normal and the LN4 distributions have been retained. The conclusion has been drawn based on the AIC, AICc and BIC criterion. They express the quality of a model compared to other models that are considered to be suitable. These criteria express how close the model is to the true model. Thus, they also contain information about the goodness of the extrapolation, what is not the case for the other criteria.

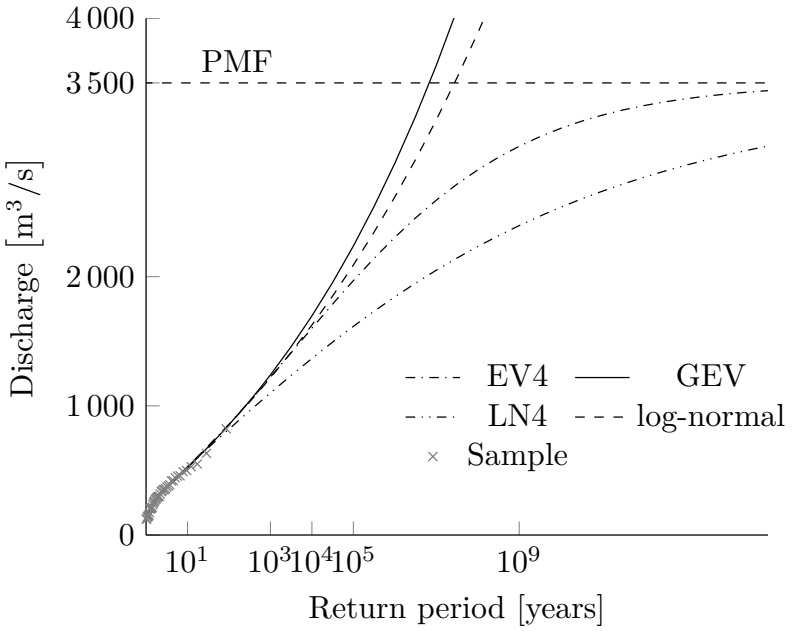

Figure 7.3: Comparison of the four distributions fitted to the sample generated using the LN4 distribution ($\gamma = 0.97$) and assuming an upper limit of PMF=3500 m^3/s.

Table 7.1: Statistical quantities for judging the distribution fits for the sample generated using the LN4 distribution ($\gamma = 0.97$) and assuming an upper limit of PMF=3500 m^3/s.

Distribution	Kolmogorov	p-value	Reject	AIC	AICc	BIC	RMSE
LN4	0.0698	0.999	no	548.8	549.4	554.06	15.2
EV4	0.0698	0.999	no	549.7	550.4	555.03	14.5
GEV	0.0667	0.999	no	549.8	550.4	555.1	14.3
Log-normal	0.0667	0.999	no	547.2	547.5	550.7	16.8

Sample with large skewness ($\gamma > 2$)

The EV4, LN4, GEV and log-normal distributions have been fitted to the generated sample with skewness $\gamma = 2.87$. The fit, as well as the assumption of the PMF are plotted on Figure 7.4. This figure shows that the log-normal distributions clearly misses the two largest data points. In addition it surpasses the assumed PMF values between return periods of 10^6 and 10^7 years. The GEV distribution increases much faster than the log-normal distribution and leads to higher flood estimates from a return period of approximately 10^3 years on. As for the sample with a small skewness coefficient ($\gamma = 0.97$), the EV4 distribution approaches the upper bound faster than the LN4 distribution.

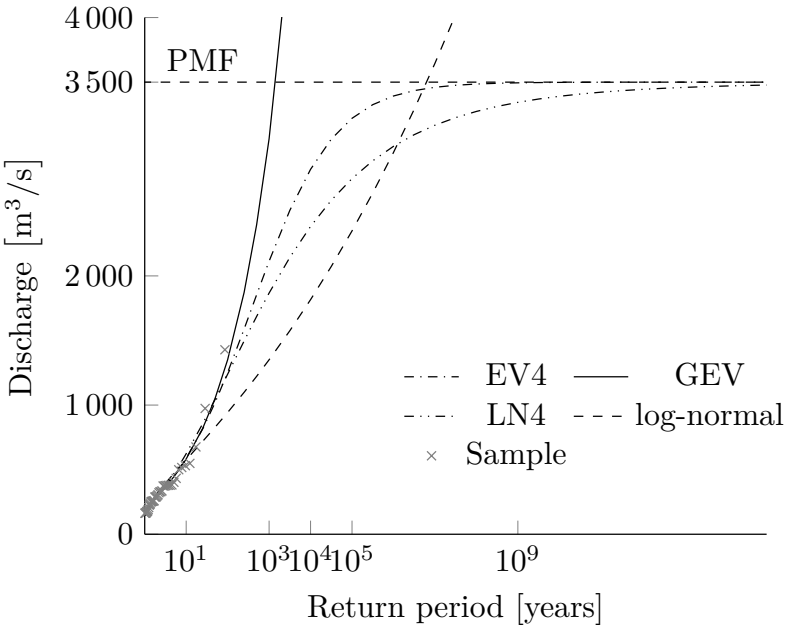

Figure 7.4: Comparison of the four distributions fitted to the sample generated using the EV4 distribution ($\gamma = 2.87$) and assuming an upper limit of PMF=3500 m^3/s.

The performance coefficients shown in Table 7.2 allowed to evaluate the goodness of the models. The Kolmogorov-Smirnov criterion did not lead to the rejection of any of the fitted distributions.

According to AIC, AICc and BIC, LN4 and EV4 would be the most appropriate models. The goodness of the LN4 model is, however, partly due to the high estimate of the lower bound. The lower bound has been estimated to be $a = 145.5\,\mathrm{m}^3/\mathrm{s}$. However, for the generation of the sample the lower bound was assumed to be zero. Hence, the LN4 fit does not well represent the behaviour of the sample. Constraining the lower bound to zero would lead to bad performance criterion for the LN4 distribution (AIC=559.5, AICc=560.1, BIC=564.7) and still very good criteria for the EV4 distribution (AIC=549.8, AICc=550.4, BIC=555.1). The difference between the performance criteria for a constrained lower bound and an unconstrained lower bound induces the conclusion that the EV4 distribution is rather insensitive to the lower bound. The unconstrained fit of the EV4 distribution leads to an acceptable lower bound estimation of $a = 43.5\,\mathrm{m}^3/\mathrm{s}$. This value is tolerable because it corresponds to the order of magnitude of the deviation that the generated sample with gaussian noise can have compared to the sample without added noise for the assumed signal to noise ratio of 25dB. The difference between the GEV end EV4 distributions is hardly noticeable when only considering the criteria AIC, AICc and BIC. The GEV is even better when the RMSE criterion is examined. Again, the reason may be the flexibility of this distribution. The log-normal distribution is clearly not adapted regarding the criteria AIC, AICc, BIC and RMSE.

This discussion leads to the conclusion that the underlying sample ($\gamma = 2.87$) could be well fitted by the GEV and EV4. These two distributions have therefore been considered for sensitivity analysis exposed in Section 7.5.1.

Table 7.2: Statistical quantities for judging the distribution fits forthe sample generated using the EV4 distribution ($\gamma = 2.87$) and assuming an upper limit of PMF=3500 m^3/s.

Distribution	Kolmogorov	p-value	Reject	AIC	AICc	BIC	RMSE
LN4	0.116	0.917	no	548.2	548.9	553.5	48.5
EV4	0.0698	0.999	no	549.6	550.2	554.9	47.2
GEV	0.0667	0.999	no	549.8	550.4	555.1	32.3
Log-normal	0.116	0.917	no	554.1	554.4	557.6	91.2

7.5 Results and discussion

7.5.1 Sample sensitivity

Example of the sample sensitivity for the EV4 and GEV distributions

To get a first impression of an eventual sensitivity of the distribution to the sample, it has been chosen to illustrate the sample sensitivity focussing on the GEV and EV4 for one sample as well as one random permutation of the latter. The GEV is known for its large uncertainty due the huge sensitivity to large sample values. For this reason it has been chosen as example for this analysis making the issue very clear. The analysis presented below illustrates why the bootstrap approach

is important.

The sample size would varies from 30 to 43 values. The up to 13 added values changes the fit according to their occurrence order. Figure 7.5 shows an example of the influence of the occurrence order of the floods in the case of the GEV and EV4 distributions. It can be seen that for the considered sample, the variation of the fitted curves is rather small. However, the steep slope of the curves, especially for the GEV distribution, induces a large variability of the flood estimate for a certain return period.

Changing the order of the sample values would generate different samples (because the order of occurrence does play a role in this analysis). In order to illustrate the important influence of a rearranged sample, a random permutation of the sample shown on Figure 7.1 has been generated, the values did thus not change. The corresponding permuted sample values are plotted on Figure D.1 in appendix D. It can be seen on Figure 7.6 that the rearranged sample can considerably change the extrapolation. From a certain sample size on (here: 35 values), the extrapolation stabilizes somehow. The fact that the sample arrangement plays an important role made it a necessity to re-sample a large number of data sets (1000 re-samplings for each sample size) to be fitted for the different sample sizes in order to quantify the variability of the estimates.

This analysis made it possible to illustrate how the extrapolation can change when additional values are added to the sample. For flood observations, this means that a small data set does not necessarily contain all information necessary to characterize the extreme flood observations in terms of their statistical behaviour. In order to analyse the global variability induced by the sample size, and, hence, the robustness of a distribution, the results returned from the fits of the bootstrapped samples are exposed hereafter.

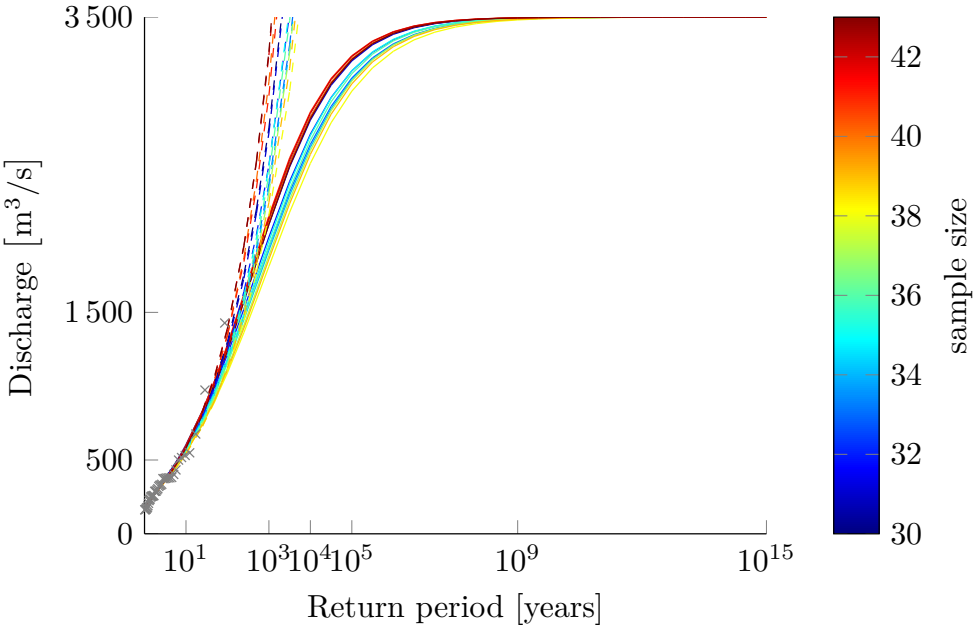

Figure 7.5: EV4 (continuous line) and GEV (dashed line) fitted to the sample shown on Figure 7.1.

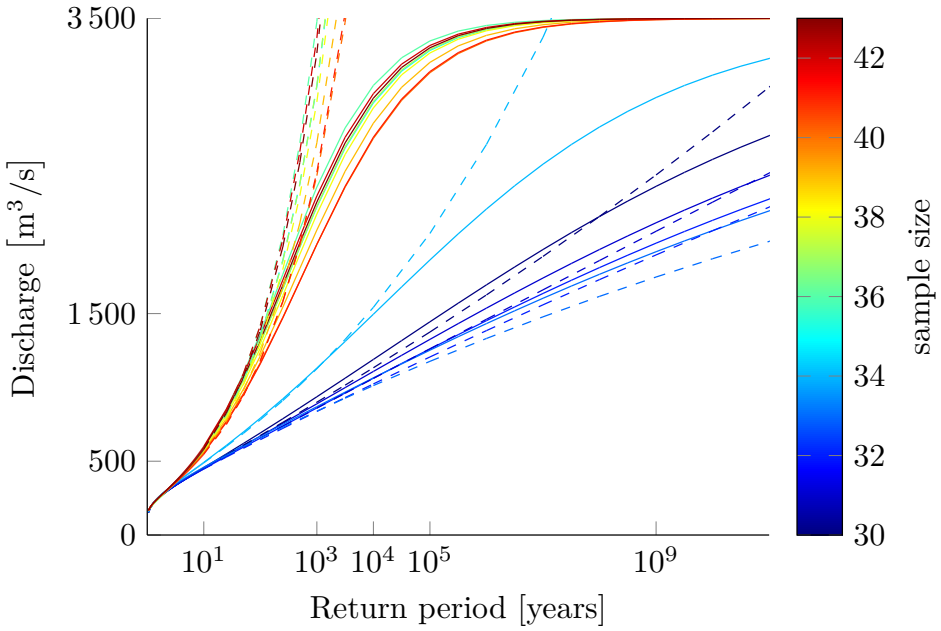

Figure 7.6: EV4 (continuous line) and GEV (dashed line) fitted to permuted discharge time series, represented on Figure D.1.

Sample size sensitivity using a bootstrap approach

For every sample size, 1000 data sets have been generated using bootstrap re-sampling. The variability of the extrapolations has been quantified by estimating the 5% and 95% quantiles to represent a prediction interval. The sample size sensitivity is illustrated on Figures 7.7 and 7.8 for the estimates of the thousand and ten thousand year flood estimations.

Concerning the LN4 distribution compared to the log-normal distribution, it can seen on Figure 7.7 that the median estimates of the LN4 distribution are below the median estimates of the log-normal distribution for both the $Q_{1\,000}$ and the $Q_{10\,000}$. The confidence intervals of the log-normal distribution are slightly larger than those of the LN4 distribution. As expected, the confidence intervals get smaller with an increasing sample size but even for the largest sample of 40 values, the LN4 distribution leads to a smaller uncertainty than the log-normal distribution. These observations are even more pronounced for the $Q_{10\,000}$ estimates than for the $Q_{1\,000}$ estimates. The causal information expansion of the systematic data set could thus reduce the uncertainty of the flood estimates for large return periods compared to the unbounded parent distribution.

Regarding the EV4 and GEV distributions, this behaviour is even more pronounced. The largest variability for small sample sizes could be observed for the GEV distribution. This is due to the fact that this distribution has three parameters and is thus more flexible to fit the sample, but with flexibility comes sensitivity to large sample values. Figure 7.8 clearly shows that the GEV distribution induces a huge uncertainty on the $Q_{1\,000}$ estimate. Furthermore, that median estimate is close to the assumed PMF, illustrating that the distribution is probably overestimating the thousand year flood. A look at the 95% quantile curve shows that this distribution can lead to absurd estimates for small samples. But even for the sample with 40 values, the 1000 year estimate can be larger than the assumed PMF. This gets even more obvious when looking at the estimates of the $Q_{10\,000}$ (Figure 7.8b). It can be seen that the $Q_{10\,000}$ flood estimate is over two times the assumed PMF. The 95% quantile curve can even go up to approximately 10 times the PMF value. The EV4 has a much better performance. The prediction interval is much smaller. It is a bit larger than the prediction interval of the LN4 distribution. It is interesting to mention that the EV4 estimates for $Q_{1\,000}$ are completely contained in the prediction interval of the GEV estimates. This means that the GEV does agree in some cases with the EV4 distribution. For the $Q_{10\,000}$ estimates, the EV4 distribution leads to estimates below the 5% quantile curve of the GEV from a sample size of approximately 36 values on.

This analysis showed that unbounded distributions can lead to unrealistically high estimates, even for large samples. In fact, the often used thumb rule not to extrapolate beyond two to three times the sample size would not allow to estimate a thousand or even a ten thousand year flood. However, extrapolating beyond three times the samples length is common practice because extreme flood estimates with an associated return period are necessary in some cases, especially for risk analysis. This analysis allowed to show the advantage of upper bounded distributions in terms of uncertainty of the estimation but also in terms of high return period estimates making sense and being realistic throughout the range of tested sample sizes. In the context of dam safety

verification in terms of extreme floods, a sample size of 40 years is a fairly large sample, but even for this amount of data the unbounded distributions have been outperformed by their bounded derivatives in terms of uncertainty and trustfulness of the estimates.

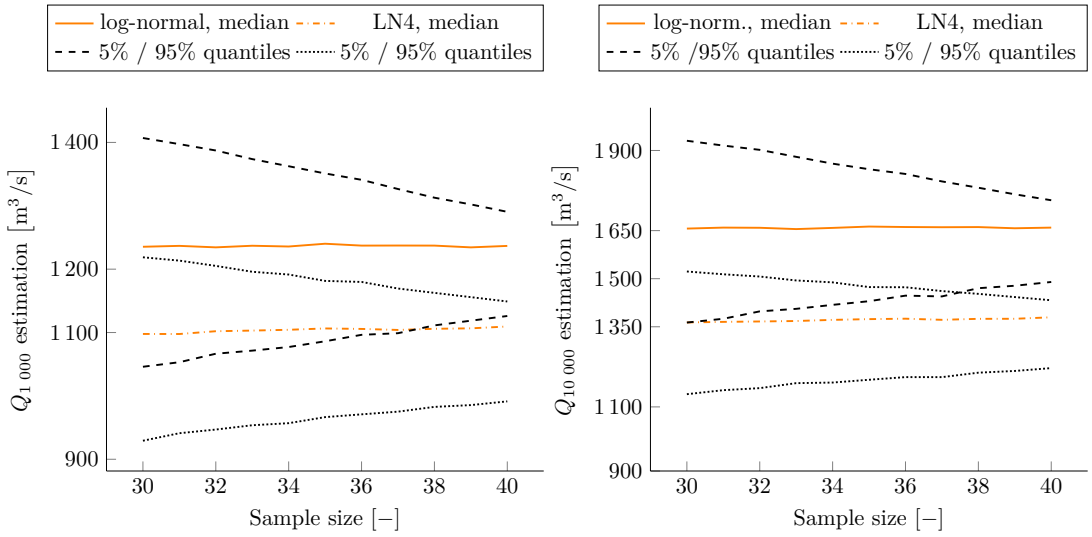

(a) Q_{1000} versus sample size.

(b) Q_{10000} versus sample size.

Figure 7.7: Discharge estimate plotted against the sample size qith indication of the 5% and 95% quantiles derived by bootstrap resampling.The sample skewness is $\gamma = 0.97$.

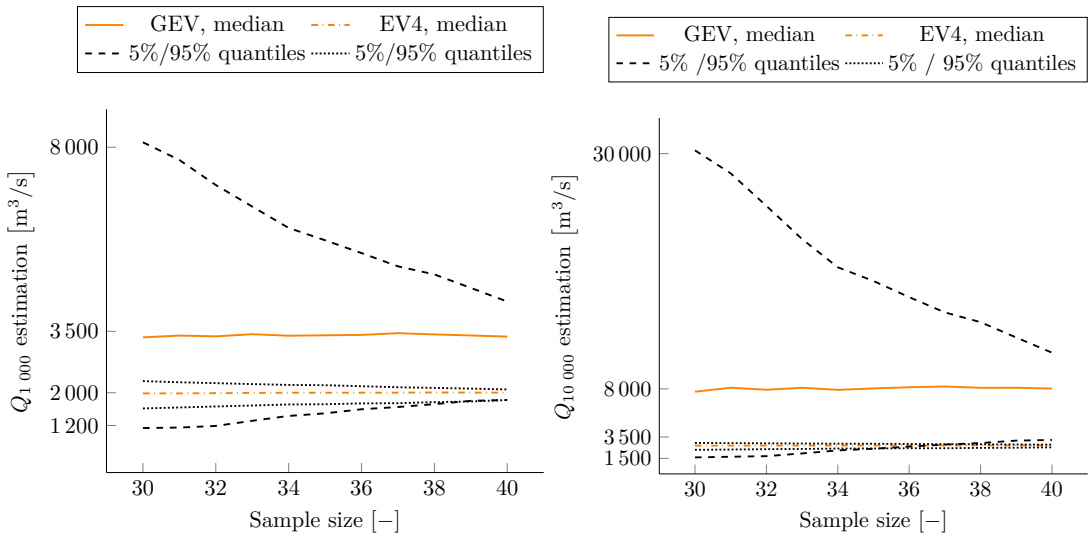

(a) Q_{1000} versus sample size.

(b) Q_{10000} versus sample size.

Figure 7.8: Discharge estimate plotted against the sample size with indication of the 5% and 95% quantiles derived by bootstrap resampling. The sample skewness is $\gamma = 2.87$.

Sensitivity to the upper bound

After the analysis of sensitivity of the distributions to the sample size, the influence of the PMF on the estimates of $Q_{1\,000}$ and $Q_{10\,000}$ has been investigated. The unbounded distributions did naturally not enter this part of the analysis, the extrapolation being independent from the PMF. The faster approach to the upper limit of the EV4 distribution compared to the LN4 distribution makes the EV4 distribution more sensitive to the upper limit estimate concerning the thousand and ten thousand year flood estimates, as it can be detected by considering Figure 7.9.

Regarding the LN4 distribution, the variation of the upper bound from 2500 to roughly 4500 (increase of 80%) induced an increase of only 10% of the $Q_{1\,000}$ estimate and 15% of the $Q_{10\,000}$ estimate. As shown on Figure 7.9, the variation of the extrapolations is much more pronounced when using the EV4 distribution. It can be seen that the $Q_{1\,000}$ increases by roughly 30% and the $Q_{10\,000}$ by 45% for an 80% increase of the upper bound. This variation from 1700 m^3/s to 2200 m^3/s for the $Q_{1\,000}$ estimate, induced by the variation of the upper bound of the EV4 distribution, is still smaller than the variation given by the uncertainty interval of the GEV distribution for a sample size of 40 values (1800 m^3/s to 4200 m^3/s). The same statement can be made for the estimate of $Q_{10\,000}$; the upper bound induces an estimation variation from 2100 m^3/s to 3100 m^3/s for the EV4 distribution whereas the prediction interval of the GEV varies from 3200 m^3/s to 11 400 m^3/s. This means that, despite an eventually high uncertainty on the upper bound, the bounded statistical distributions can outperform the unbounded distributions when extrapolations to high return periods are carried out.

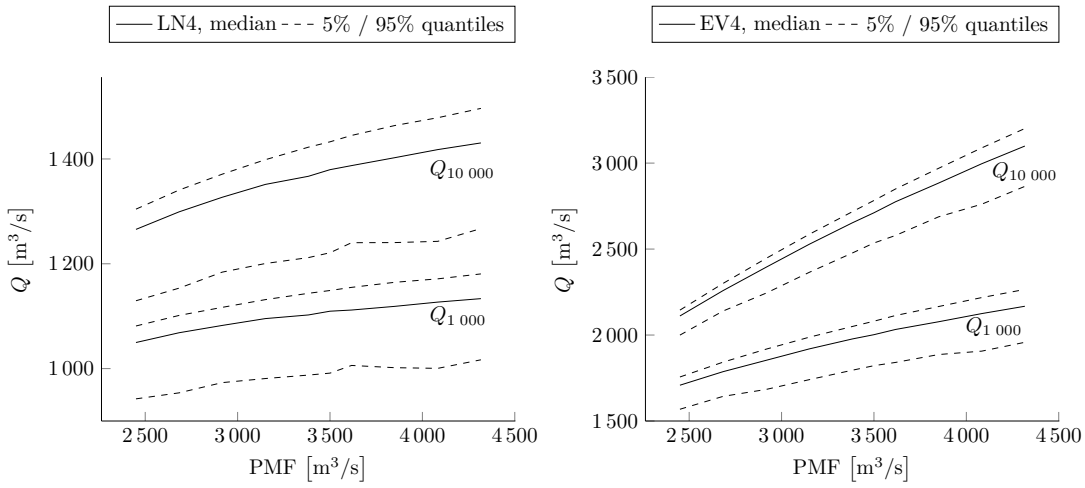

(a) LN4, sample skewness $\gamma = 0.97$

(b) EV4, sample skewness $\gamma = 2.87$

Figure 7.9: Estimates of $Q_{1\,000}$ and $Q_{10\,000}$ versus the upper bound (PMF.)

7.6 Conclusion

The analysis conducted in this chapter addressed the sensitivity of flood estimates to the sample size in the case of bounded and unbounded distributions. The sensitivity of upper bounded distributions to the estimation of the upper bound has also been addressed. Synthetic samples have been generated with different sample skewness coefficients in order to join the findings of Takara and Tosa (1999). They stated that the LN4 distribution better fits samples with a smaller skewness and that the EV4 distribution is better adapted to samples with larger skewness coefficients. The bounded distributions EV4 and LN4 have been considered and compared to their parent unbounded distribution, i.e. the GEV and the log-normal distribution. It has been confirmed, that the LN4 and log-normal distribution are both adapted to fit the sample with a small skewness coefficient. The GEV and EV4 distributions could be shown to be best adapted to fit the sample with a larger sample skewness.

The analysis allowed to increase the understanding of the behaviour of upper bounded distributions compared to unbounded distributions. It could be shown that the bounded distributions lead to considerably lower variability and thus lower uncertainty than the unbounded distributions, especially regarding the EV4 and GEV. The large uncertainty of the GEV is due to the fact that it is a three parameter distribution that is more flexible and thus more sensitive than the two parameter log-normal distribution considered for this analysis. The three parameter log-normal distribution has not been considered for this analysis, but the comparison between the LN4 and the three parameter distribution would probably have led to similar improvements than those that could be observed for the EV4 distribution compared to the GEV.

The findings of the low sensitivity to the sample size is however only valuable if the uncertainty induced by the upper bound estimate does not induce a larger sensitivity to the flood estimates than the sample itself. The analysis of sensitivity to the upper bound could show that for the LN4 distribution, the sensitivity is very small. The prediction interval shows a larger range of possible estimates related to the sample than the range returned by the variation of the upper bound. For the EV4 distribution, the variability is larger than for the LN4. The increase of 80% of the upper bound induces an 35% increase of the thousand year flood and a 45% increase of the ten thousand year flood. This variation is however still smaller than the variation range given by the prediction interval of the GEV. Therefore the uncertainty induced by the upper bound estimate cannot be considered to disadvantage the upper bounded EV4 distribution compared to the GEV.

Finally, it can be retained that the bounded distributions do indeed increase the reliability of the extrapolations. They are a valuable tool for the combination of the PMP-PMF method and the statistical flood estimation approach in a holistic model. The causal information expansion of the systematic data set led to reduced uncertainty and to a coherent flood estimation model returning realistic estimates compared to the unbounded distributions.

7.7 Remarks

Among the distributions considered in this study, only the use of GEV can be mathematically justified in the context of block maxima extrapolations through the extremal types theorem. As the EV4 distribution has been deduced from the GEV, it can be assumed to be solidly funded.

However, neither the log-normal nor the LN4 distributions can be justified in a similar manner. Nevertheless, the use of the log-normal distribution in hydrology is frequently performed (Vogel and Wilson, 1996; Merz and Thieken, 2005; Apel et al., 2006; Stedinger and Griffis, 2008; Apel et al., 2009; Aronica et al., 2012; Sarhadi et al., 2012; DWA, 2012; Kiczko et al., 2013; Candela et al., 2014; Dung et al., 2015; Romanowicz and Kiczko, 2016). The acceptance of this distribution in hydrology may result from the experience of hydrologists. The appropriateness of the LN4 distribution can thus only be related to the argument that it has been derived from a distribution whose usage has been accepted by hydrologists, i.e. the log-normal distribution.

8 Integrated methodology for extreme flood estimation in alpine catchments

8.1 Introduction

In the previous chapters, different research questions, identified during the literature review, have been treated. The conclusions that were drawn allowed to formulate an extreme flood estimation methodology for alpine catchments applicable under current climate conditions. The methodology combines extreme flood simulations and statistics coherently through upper bounded statistical distributions. In this chapter, the methodology is presented in detail.

8.2 The CRUEX++ methodology

The final outcome of the CRUEX++ methodology is a safety flood hydrograph whose peak flow return period can be estimated by a maximum annual peak discharge extrapolation causally expanded by an upper bound derived from the PMP-PMF approach. The safety flood hydrograph is derived using hydrological simulations based on a design storm. For the PMP-PMF simulation, the Swiss PMP maps can be used to determine the PMP depth. Due to the application limits of these maps, determined and discussed in Chapter 6, the catchment of interest should be smaller than 230 km^2. Caution should be taken when areas are between 75-230 km^2, as this range corresponds to the transition zone from valid to invalid results. This is due to the overestimation of spatial coverage of the PMP event as derived from the Swiss PMP maps.

The methodology is separated into two different approaches: one deterministic (Figure 8.1) and the other stochastic (Figure 8.2). Both are developed in detail in this chapter. The main difference between the two approaches is the way in which initial conditions are considered.

8.2.1 Model construction

The first step is the construction of a hydrological model of the catchment of interest. The model should be able to reproduce the hydrological processes as well as the hydraulic characteristics

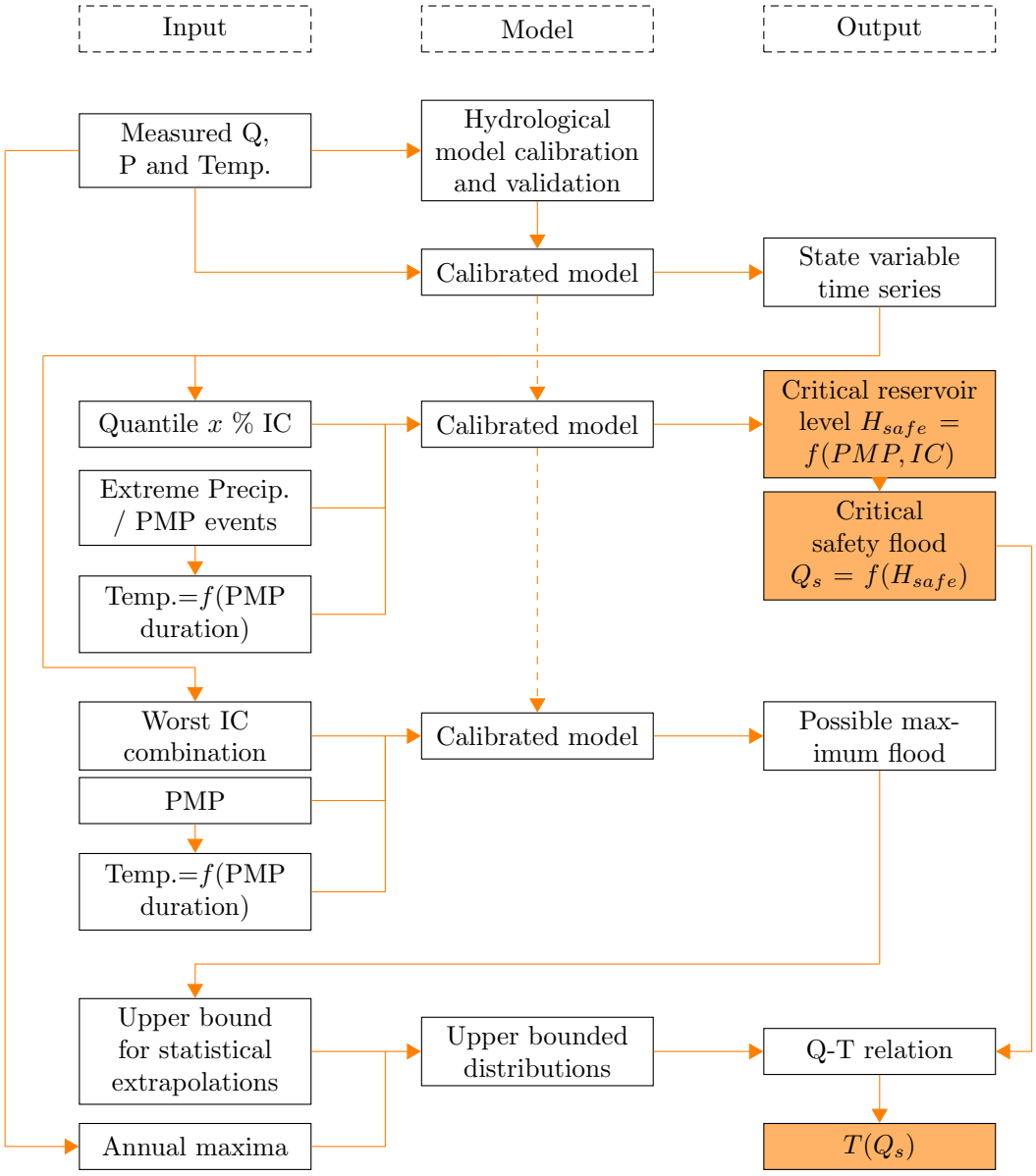

Figure 8.1: Flowchart of the methodology proposed for the deterministic estimation of extreme floods. IC = initial conditions, PMP = probable maximum precipitation, Q = discharge, T= return period, Temp. = temperature, Precip.=precipitation., H_{safe} = safety level, Q_s = safety discharge.

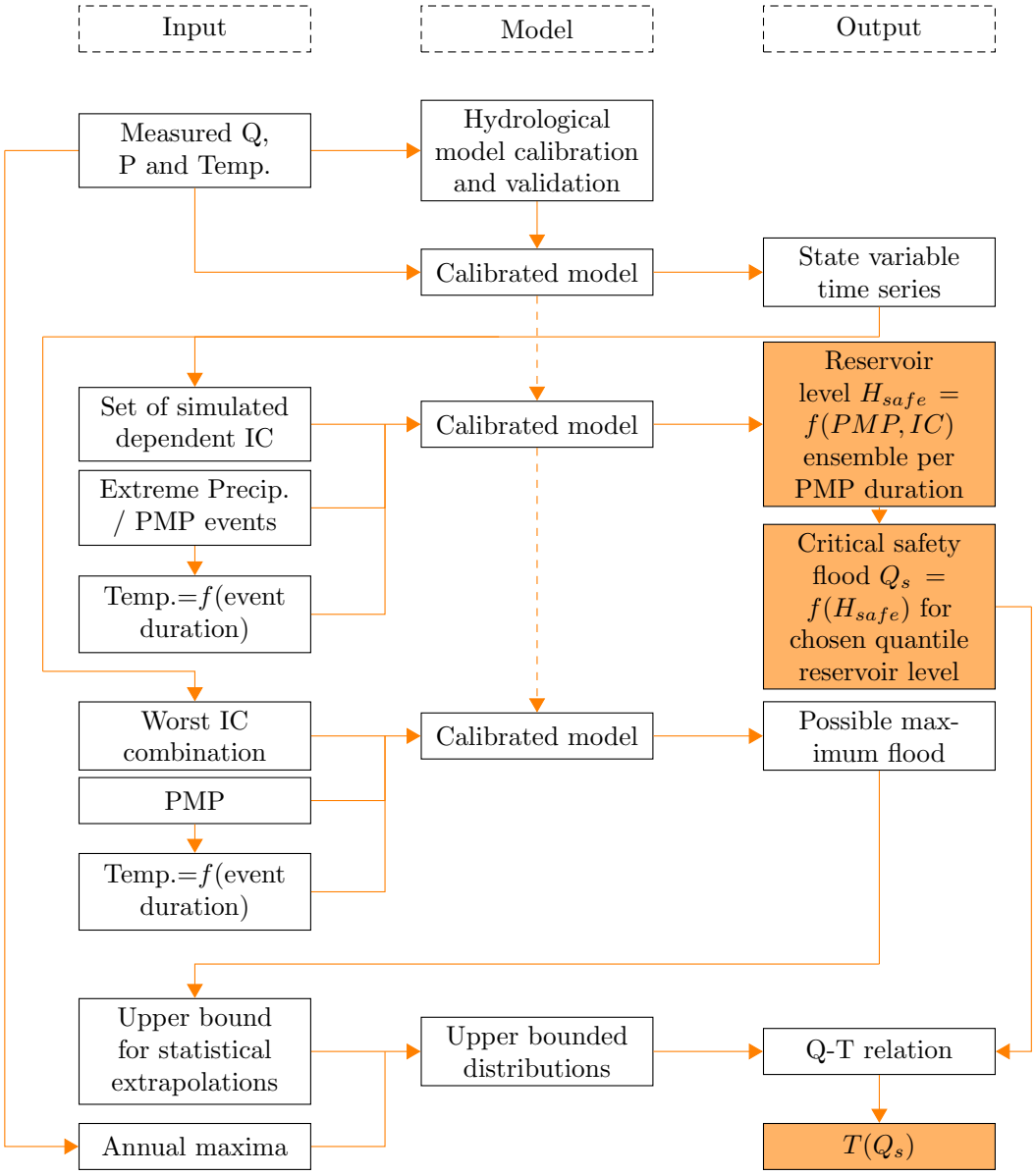

Figure 8.2: Flowchart of the methodology proposed for the stochastic estimation of extreme floods. IC = initial conditions, PMP = probable maximum precipitation, Q = discharge, T= return period, Temp. = temperature, Precip.=precipitation., H_{safe} = safety level, Q_s = safety discharge.

of the basin and the dam, in order to simulate the flood attenuation effect of the lake. In mountainous catchments, the hydrological model should account for snow fall and snow melt at different altitudes of the basin. These requirements can be easily achieved by using a semi-distributed conceptual hydrological model. For the development of the present methodology, the GSM-SOCONT model (Schaefli et al., 2005; Schaefli and Zehe, 2009; Jordan et al., 2012; Garcia Hernandez et al., 2016) has been applied. Other semi-distributed conceptual models, for example HBV (Bergström, 1992) , SAC (Burnash, 1995), GR4J (Perrin et al., 2003), could also be used. The main steps of the construction of a semi-distributed conceptual model, i.e. the delimitation of the basin, the determination of altitude bands and the attribution of model elements to the altitude bands, are illustrated in Figure 8.3. The model should be calibrated and validated based on measured discharge data that are compared to the simulated discharges derived from measured precipitation and temperature data.

8.2.2 Determination of the precipitation for synthetic extreme meteorological events

Two possibilities for the determination of the precipitation depth are worth considering: the Swiss PMP maps and intensity duration frequency curves (IDF). The choice depends on the aimed result, i.e. the safety flood ($T(Q_s) >> 1000$ years) or the maximum employed in the extrapolation with upper bounded statistical distributions.

In fact, for the determination of the maximum considered for the bounded statistical distributions, the probable maximum precipitation (PMP) has to be used. In Switzerland, this information can be extracted from the Swiss PMP maps (Pérez and Hertig, 1998; Hertig et al., 2005; Audouard et al., 2006; Hertig et al., 2008; Hertig and Fallot, 2009). In the case of extreme precipitations, for example PMPs, it has been shown in the CRUEX++ project that high precipitation depths are likely to occur concurrently with high temperatures. The summer season is therefore the most coherent with the PMP data. Seasonality plays an important role for the temperature determination and the assumptions concerning the initialisation of the hydrological model. As such, summer conditions have been assumed for the elaboration of the Swiss PMP maps (Hertig and Fallot, 2009). Furthermore, the development of the Swiss PMP maps accounted for three different wind sectors (North, South and West-North-West). The critical sector depends on the region of application and can be determined by hydrological simulation in order to determine which sectors leads to the highest discharges. Moving towards flows, a PMP event has to be combined with severe initial model conditions in order for the upper bound for the statistical extrapolation to be prepared. Some may call this upper bound the **possible maximum flood (PoMF)**.

For the determination of the **safety flood** (not suitable for the upper bound estimation considered for the bounded statistical extrapolations), the precipitation depth may correspond directly to the PMP or alternatively be derived from intensity duration frequency (IDF) curves. The latter option can be chosen if the flood generation from extreme precipitation, less intense than the PMP, is aimed for (e.g. for the determination of P_{1000}). Combined with less severe initial conditions, the

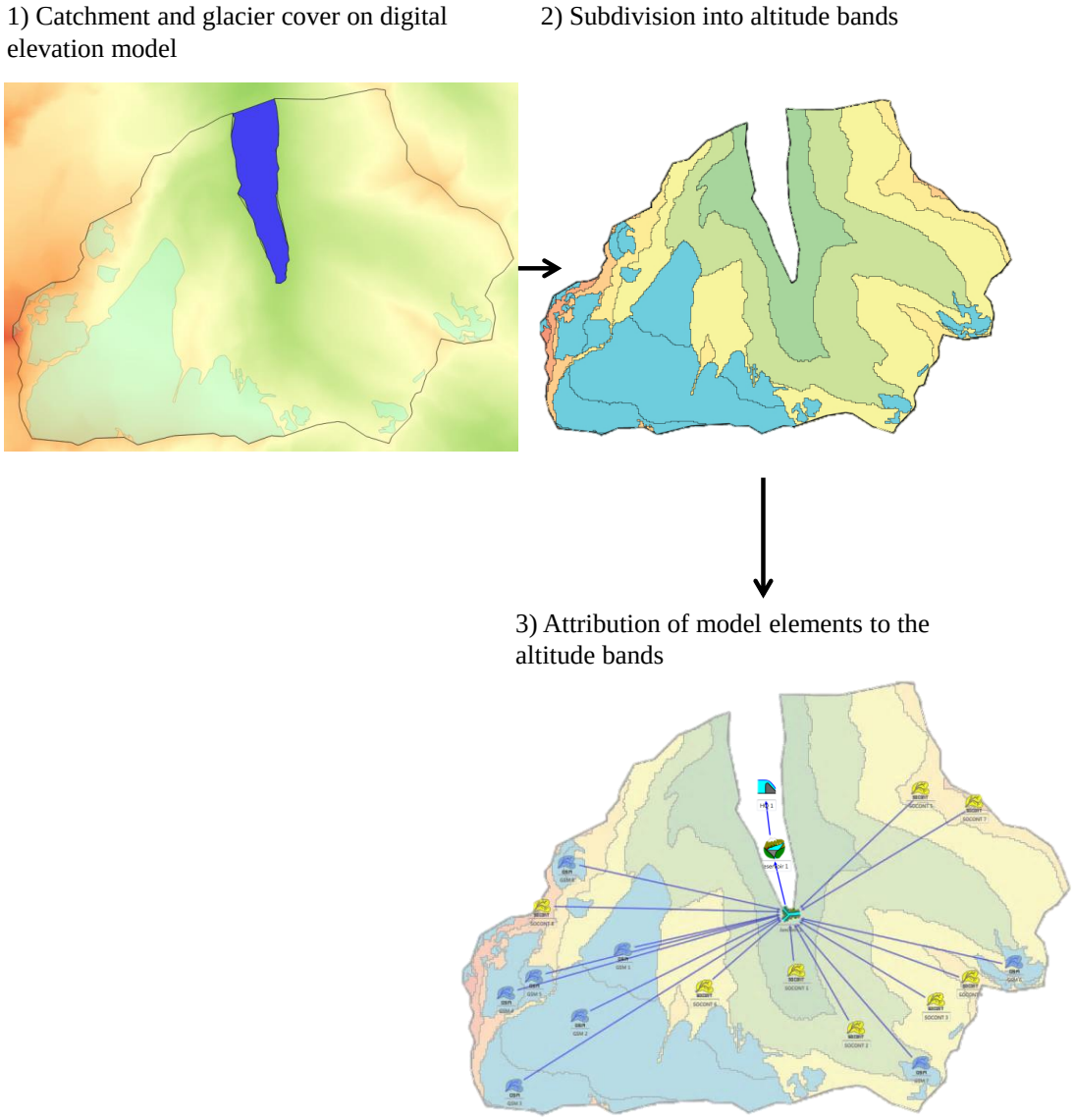

Figure 8.3: Three main steps of the semi-distributed hydrological model construction: 1)Delimitation of the catchment and glacier cover, 2) subdivision into altitude bands, 3)Attribution of model elements to the altitude bands.

routing of the PMP translates to a flood that is less severe than the PoMF and may be considered as safety flood. The routing of a design storm derived from IDF curves follows the same steps as for the PMP. The spatial distribution of the PMP is provided by mapped PMP data (Pérez and Hertig, 1998; Hertig et al., 2005; Audouard et al., 2006; Hertig and Fallot, 2009);. A stationary event is assumed. On the contrast, the spatial distribution is not necessarily known in the case of IDF curves. To determine it, observed events can be considered. Once chosen, an observed event can then be scaled to equal the precipitation intensity derived from the IDF curves. An advantage of the IDF curves is that a return period is associated to the precipitation depth.

Concerning the Swiss PMP maps, they have been elaborated for precipitation durations of 1h, 3h, 6h, 9h, 12h and 24h as well as for different wind directions, i.e. north, south and west-north-west winds. For the determination of PMP-durations in between the duration for which the PMP maps have been developed, the findings of Bérod et al. (1992b) can be considered. Bérod et al. (1992b) showed that the PMP data displayed on a IDF plot in a log-log space, produce a line that is parallel to IDF curves (Figure 8.4). The PMP durations not originally mapped can thus be easily deduced by interpolation for every map pixel.

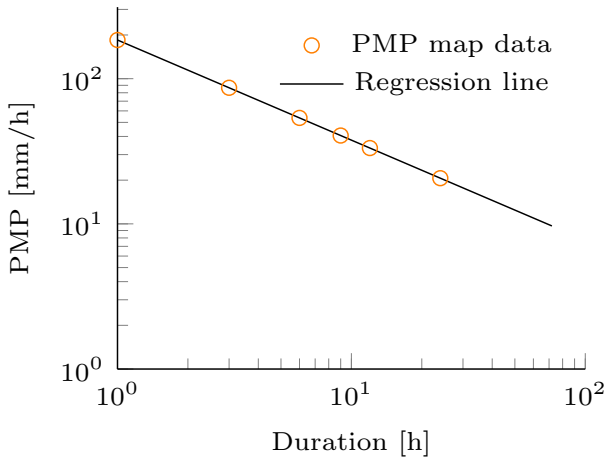

Figure 8.4: Example of PMP data plotted on an IDF like plot.

The temporal structure of the precipitation event is deduced from a rainfall mass curve. Rainfall mass curves reduce the precipitation events to a dimensionless curve by adimensionalizing the total duration of the event and the cumulative rainfall depth. They allow the derivation of a hyetograph from any given precipitation height and duration. Figure 8.5 schematically shows the procedure of temporal structuring. According to Bonta and Rao (1992) and Bonta (2004), it can be assumed that the temporal structure is independent of the precipitation duration. The rainfall mass curve considered for the CRUEX++ methodology has been derived from precipitation events observed in Switzerland. Following the superposition of the curves of several thousand events, the 5% quantile curve has been deduced. It is represented in Figure 8.6, whose plotted values are provided in Table 8.1. The 5% quantile curve is more conservative than the rainfall mass curve proposed by the World Meteorological Organization (WMO, 2009) for a PMP distribution. Their

curve is comparable to the Swiss median rainfall mass curve.

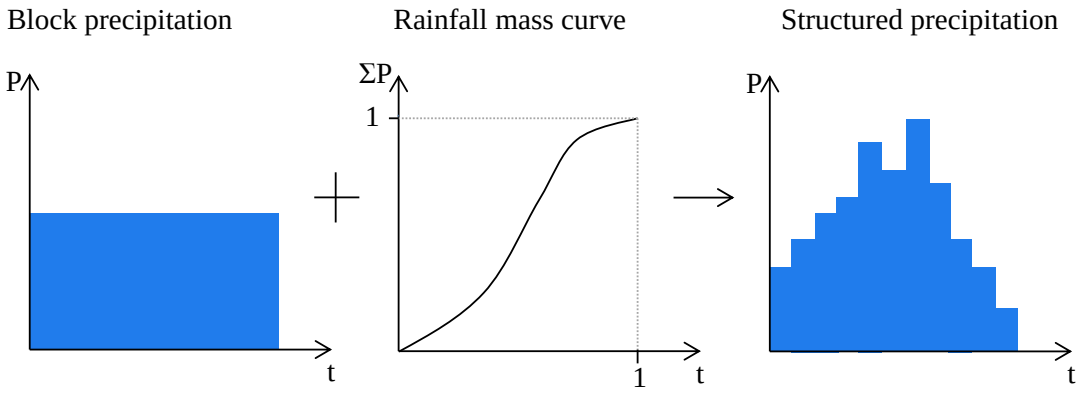

Figure 8.5: A block precipitation (left) and a rainfall mass curve (middle) allow to derive the temporally structured hyetograph (right).

8.2.3 Determination of the temperature for synthetic extreme meteorological events

The temperature that can be considered in combination with extreme precipitations has been shown to be related to the duration of the precipitation event during the CRUEX++ research project. The methodology uses the 0°C isothermal altitude as a means to define the temperature. The relations between the precipitation duration and the isothermal altitude to be combined with extreme precipitations are depicted in Figure 8.8. The two relations have been derived under summer conditions, distinguishing between regions north and south of the Alps. The geographical separation is shown in Figure 8.7.

These relations allow to introduce into the model a single value, i.e. the 0°C isothermal altitude, that is assumed to be valid for the entire catchment. This implies that the used model adopts a temperature-altitude gradient to derive the temperature at the surface from the 0°C isothermal altitude. The temperature gradient to adapt should be part of the calibration procedure of the hydrological model. According to Rolland (2003) and Damm and Felderer (2013), gradients from -0.4 to -0.7 °C/100 m are common in the Alps. During summer a gradient between -0.55 and 0.7 °C/100 m is likely to occur (Rolland, 2003).

Table 8.1: Detailed values of the 5% quantile rainfall mass curve.

Duration [%]	0	4	8	13	17	21	25	29	33	38	42	46	50
Precipitation [%]	0	1	2	4	6	8	11	13	17	20	24	28	33
Duration [%]	54	58	63	67	71	75	79	83	88	92	96	100	-
Precipitation [%]	37	42	48	53	58	65	71	77	84	90	96	100	-

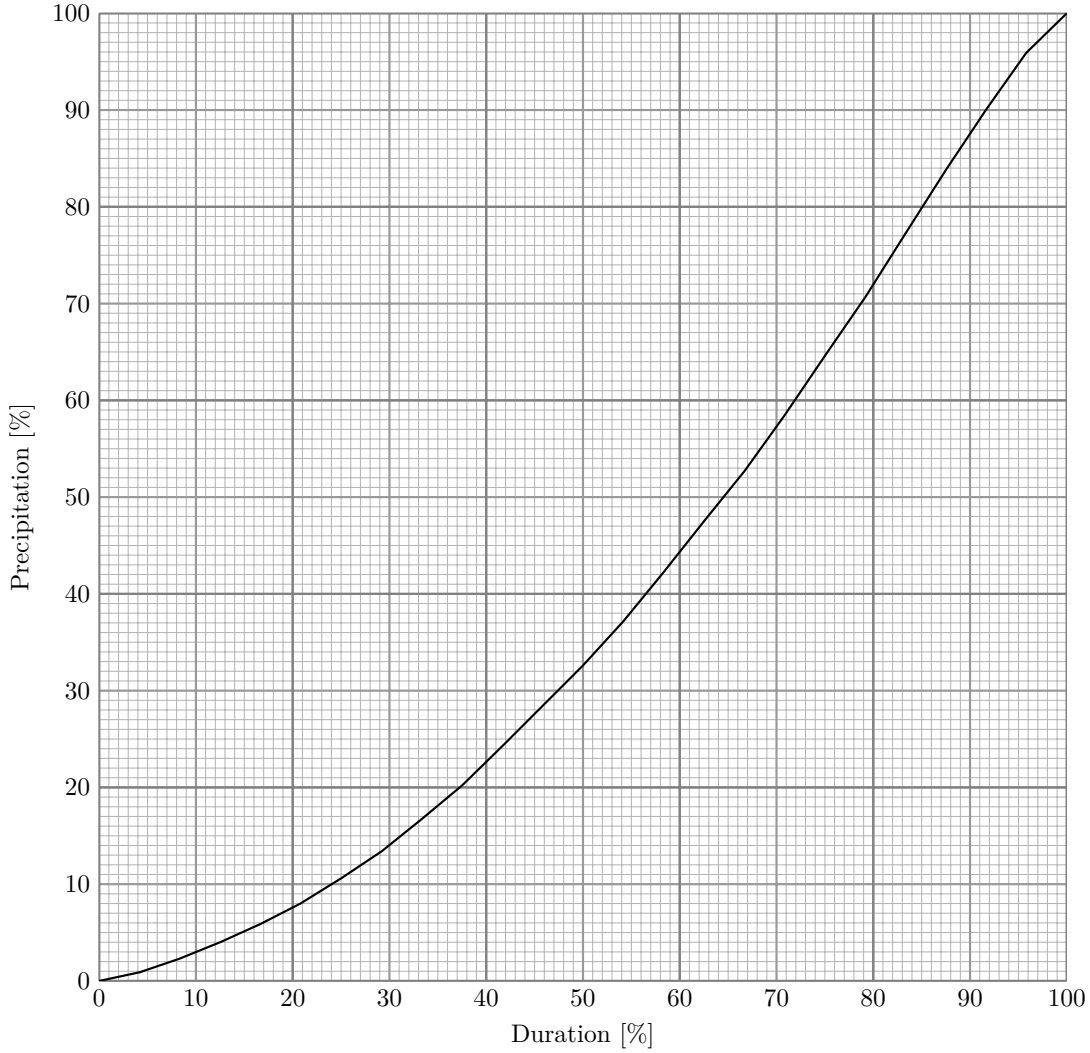

Figure 8.6: Swiss 5% quantile rainfall mass curve for the temporal distribution of extreme precipitation data determined during the CRUEX++ project.

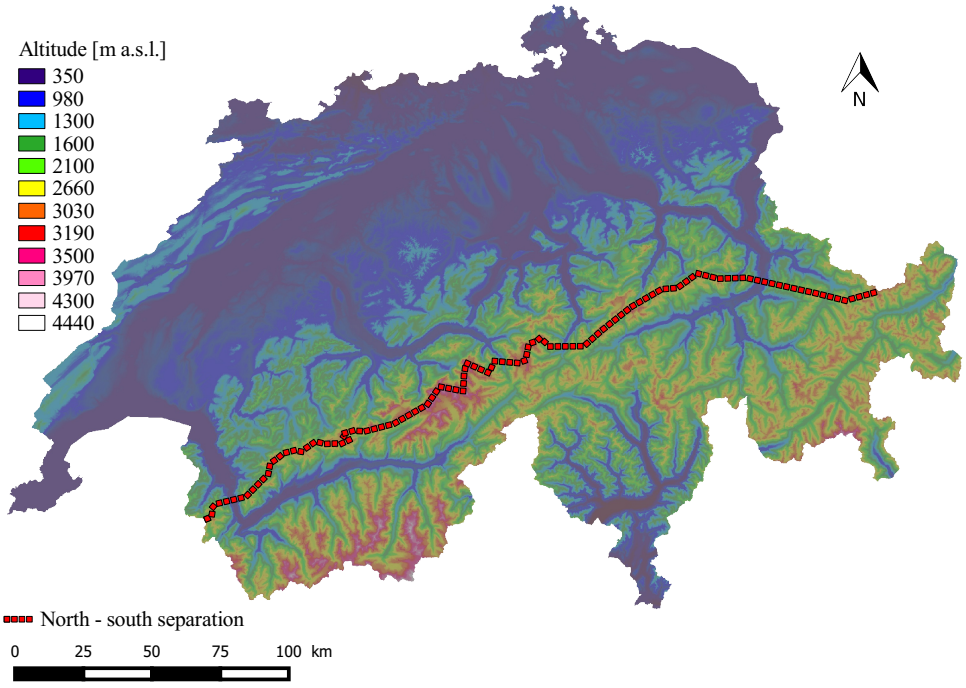

Figure 8.7: Separation line between north and south as considered for the determination of the relations between the precipitation duration and the 0°C isothermal altitude.

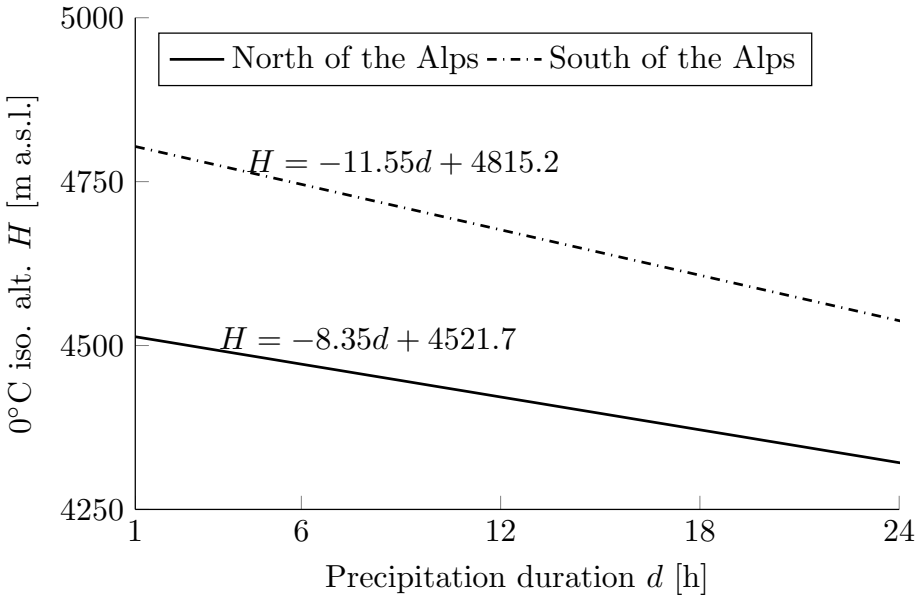

Figure 8.8: Relations between the precipitation duration and the 0°C isothermal altitude for the summer season distinguishing between north and south of the Alps.

8.2.4 Determination of the initial conditions for deterministic event based flood simulations

The event based simulations can be highly influenced by initial conditions. The number and values of the initial conditions depend on the hydrological model that is adopted. In general, the state variables of a hydrological model need to be fixed at the beginning of the event based simulation in order to describe the initial state of the model. Consequently, in order to promote the use of coherent initial conditions, the initial values of the state variables should be derived from a continuous simulation. Accordingly, they can be drawn from the generated state variable time series considering the period after the warming period of the model. As the retained initial conditions should be coherent with the meteorological event, it is well advised to take seasonality into account when the initial conditions are determined.

For the determination of the initial conditions, a deterministic and a stochastic approach have been presented (see Chapter 5). The stochastic approach uses an initial condition set generator, illustrated on Figure 8.9. This generator chooses random instants in the time interval corresponding to the period of the simulated state variable time series. The values of the state variables at that precise moment correspond to one possible initial condition set. The advantage of this approach is that the dependence of the initial conditions is respected. If the number of initial conditions sets is large enough, the generated hydrograph ensemble can be used to derive quantile hydrographs. The quantiles are a useful tool to describe the prediction interval of the discharges derived from a certain design storm. The disadvantage of this approach lies in its computational cost; it may demand substantial computation capacity and the simulations take several hours (much longer than the computational time of the deterministic approach).

Regarding the deterministic approach, the initial values are chosen independently in the range of possible values determined for the season of interest. In the context of the CRUEX++ project, the initial state variable values were determined according to a certain probability of non-exceedance from the cumulative distribution of each state variable, as illustrated in Figure 8.10. The quantile is proposed to be the same for all state variables. When the main influence on the variation of the peak discharge stems from one single state variable, the quantile of the estimated discharge corresponds to the quantile of the initial condition. In the context of the GSM-Socont model, used for this research project, this would be typically the case if, for the considered season, there is no snow or ice present being soil saturation the main driver. The advantage of this approach, if applicable, is that the computational effort is small. The disadvantage is that the detection of the main driving state variable may not always be straightforward. Sensitivity analyses can be used to determine the main driving state variable. If the dependency between the state variables was mistakenly neglected, the simulated flood can be under or overestimated. The degree of under or overestimation varies from case to case.

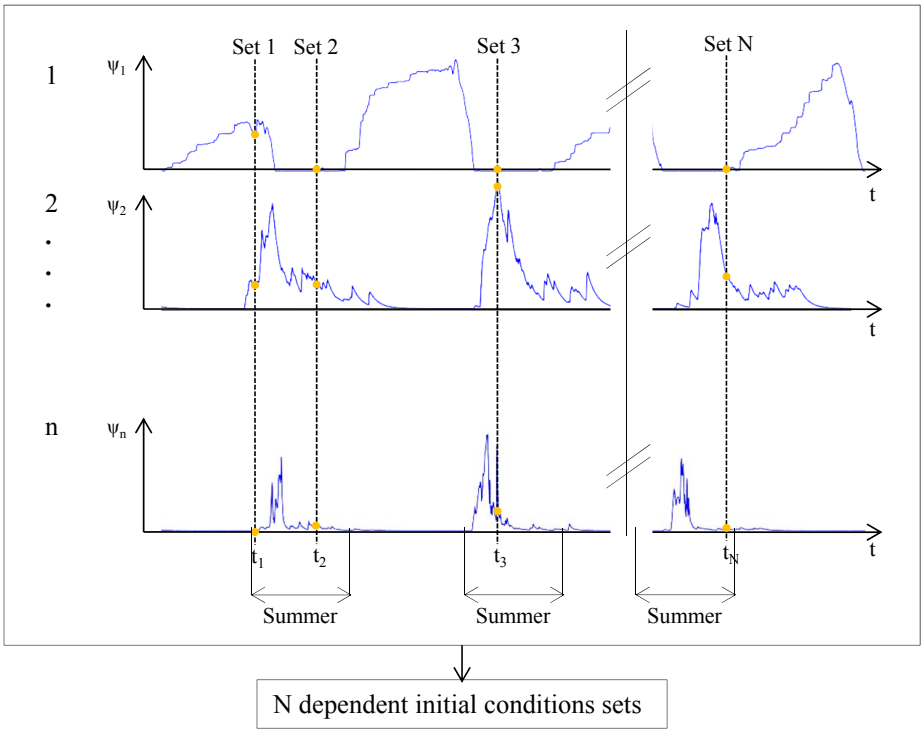

Figure 8.9: Schema of the stochastic initial conditions generator. Randomly, N moments in time in the season of interest, here the summer, are chosen to derive dependent initial state variable values from the state variable time series. The state variable are denoted ψ_i, where i goes from 1 to n, n being the number of different state variables.

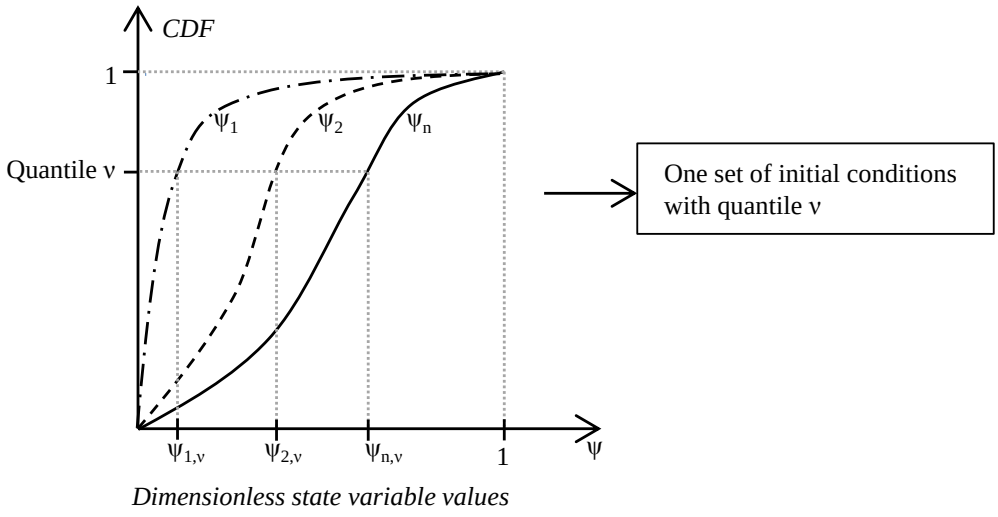

Figure 8.10: Schema of the determination of the initial conditions from the cumulative distribution functions (CDF) of the different state variables ψ_i, where i goes from 1 to n, n being the number of different state variables.

8.2.5 Simulation of the safety flood and the possible maximum flood

Once the initial conditions have been determined, the synthetic meteorological event can be transformed into a runoff hydrograph. The simulation of the safety flood and the possible maximum flood (PoMF) only differ due to the chosen inputs. An extreme precipitation smaller than a PMP (for example P_{1000}) in combination with the chosen initial conditions leads to a safety flood. The PMP in combination with initial conditions less severe than the worst initial condition combination also leads to a safety flood, which one could name as probable maximum flood (PMF). The appropriate way of generating the PoMF (to be considered as upper bound for the bounded statistical extrapolations) is to consider the worst possible initial conditions in combination with a PMP.

The number of simulations required to estimate the critical safety flood and the PoMF depends on the approach chosen to determine the initial conditions. The decision criterion for a flood to be considered as a critical safety flood is the maximum reservoir level it induces. For the determination of the PoMF, the decision criterion is the maximum discharge. This is because it is used to extend the data set of annual maximum inflow observations for the upper bounded statistical extrapolation. Consequently, the critical safety flood and the possible maximum flood may be generated by a precipitation event with a different duration.

The deterministic approach, for which the quantile of the initial conditions has already been chosen, the number of simulations per PMP duration corresponds to the number of initial condition sets that are explored. The procedure of the stochastic approach is illustrated in Figure 8.11. The critical lake level is derived by routing PMP events with different durations under the assumed non-exceedance probability of the initial conditions through the basin and the reservoir. The safety flood is derived from the most critical PMP event. The PoMF is derived by considering the initial conditions to be the 99% quantile values of the state variables. Theoretically it should be the 100% quantile, but assuming the absolute maximum can coincide for all variables simultaneously is not realistic from a physical point of view. For instances, the maximum snow height cannot concur with the maximum saturation.

For the stochastic approach, the simulation of reservoir level ensembles for each PMP duration combined with each set of initial conditions allows the derivation critical lake level under the assumption of a certain residual risk that is linked to the chosen conditional probability of non-exceedance of the lake level under the considered precipitation event. For the chosen probability (for example 50%), the corresponding quantiles are estimated from the simulated ensembles for each PMP duration. The PMP duration leading to the highest lake level (under the assumed conditional probability of non-exceedance) is considered to be the critical PMP event. The safety flood corresponds to the flood event generated by the critical PMP event. The procedure of the stochastic approach to determine the critical safety flood is illustrated in Figure 8.12. The PoMF corresponds simply to the highest simulated discharge (without quantile estimation). For the stochastic approach, the number of simulated hydrographs should be large enough in order not to miss rare combinations of state variable values used to initialize the model.

Once the critical PMP event has been determined, the hydrological model, incorporating the hydraulic characteristics of the reservoir (level-volume relation) and the spillway (level-outflow relation), allow simulating the attenuation effect of the safety flood due to the reservoir, as shown on Figures 8.12 and 8.11. After the determination of the possible maximum flood and the safety flood, the return period of the safety flood can be determined resorting to the aforementioned upper bounded statistical distributions.

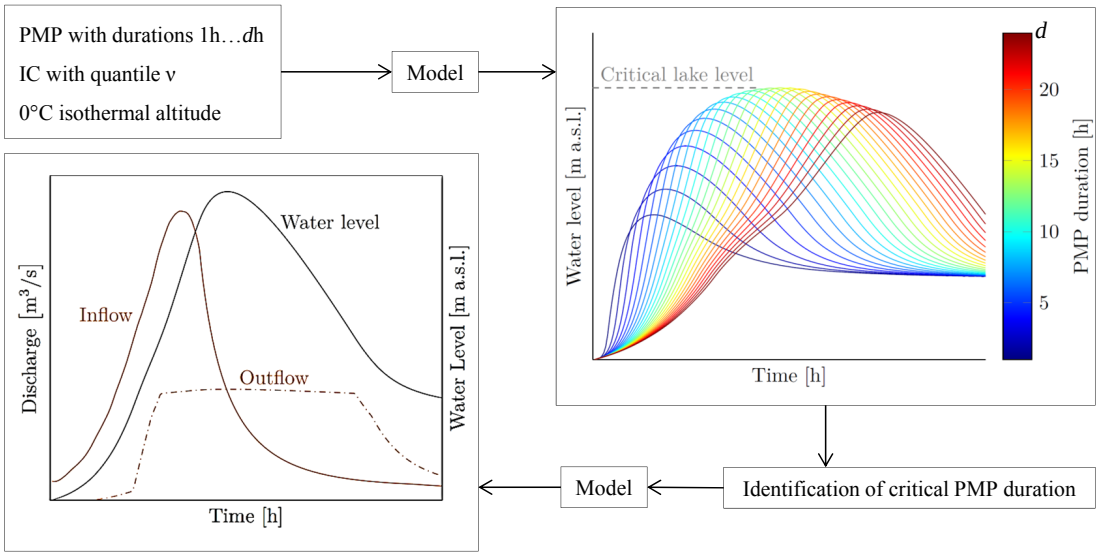

Figure 8.11: Procedure of the deterministic approach to determine the critical safety flood, the reservoir level and the outflow discharge, for a single quantile ν chosen for the determination of the initial conditions (IC).

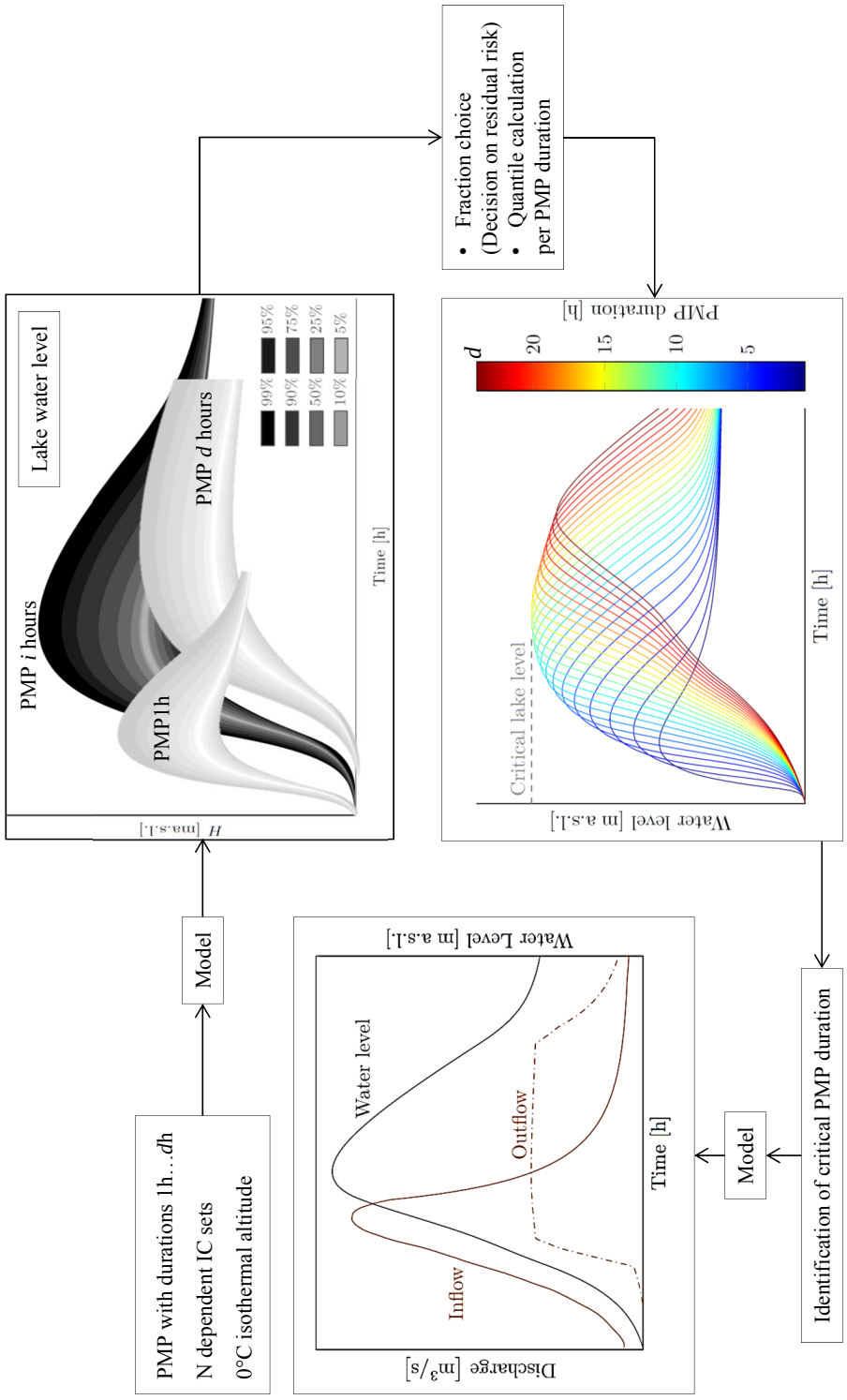

Figure 8.12: Procedure of the stochastic approach to determine the critical safety flood, the reservoir level and the outflow discharge based on N randomly sampled dependent initial conditions (IC) sets.

8.2.6 Estimation of the return period of the safety flood

The upper bounded distributions (EV4, LN4) allow taking into account an upper limit for the discharge value determined a priori . The PoMF is considered as the upper limit for the extrapolations using these distributions. In order to fit the distributions, annual maximum discharge data are needed. For coherence, the temporal resolutions (daily, hourly...) of the annual maximum data and the possible maximum flood should be the same. Once an adapted distribution has been determined it can be used to derive the return period of the peak discharge of the critical safety flood. Figure 8.13 illustrates the determination of the return period of a safety flood discharge from a fitted upper bounded distribution.

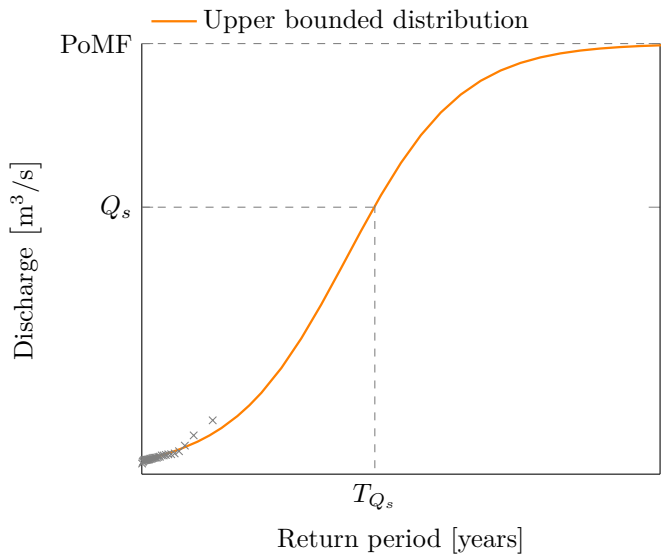

Figure 8.13: Schema of an upper bounded distribution fitted to annual maximum discharge data. The PoMF (possible maximum flood) is taken as the upper bound. The return period T_{Q_s} of the safety flood discharge Q_s can be derived from the fitted distribution.

8.3 Application limits of the methodology

The methodology presented in this chapter has been developed based on different analyses focussing on temporal rainfall distribution, the correlation between temperature and precipitation, initial conditions for extreme flood simulations and on the application limits of the Swiss PMP maps. Each part of the analysis has been undertaken for current climatic conditions. Climate change has not been accounted for because at the current state of the art, the effect of climate change is smaller than other methodological uncertainties. The methodology's main objective is assumed to be the verification of the spillway capacities of existing and new dams. Due to the constant evolution of technology and to climate change, the methodology should evolve in the future. Besides this general consideration, different parts of the methodology can be discussed as follows.

Analysing the correlation between the precipitation and the temperature, it has been found that it was reasonable to consider the maximum 0°C isothermal altitude observed before a rainfall event. The precipitation could be shown to increase with increasing isothermal altitude. Some cases have been observed, however, where the maximum temperature did not concur with the maximum observed precipitation (see Chapter 4). This means that the consideration of the temperature for PMP-PMF simulations as it is proposed in this work can lead to an overestimation of the 0°C isothermal altitude. Consequently, snowfall in high altitudes could be underestimated, snow melt overestimated and, therefore, the estimated PMF could also be overestimated. This shortcoming is hard to address as precipitation temperature scalings cannot be extrapolated beyond the measured values. Eventually, the assumption to consider such a high 0°C isothermal altitude may be confirmed in the future when further observations in the range of high temperatures are available due to observations in a warming climate.

It is also assumed that the isothermal altitude is constant during a precipitation event. This is not the case in reality where the isothermal altitude usually decreases during an event. Unfortunately, the meteorological soundings that have been used for the analysis that derived the relation between the precipitation duration and the 0°C isothermal altitude are only performed every 12h. This temporal resolution is not sufficient for a reliable characterisation of the evolution of the isothermal altitude during a rainfall event. Fortunately, the assumption of a constant 0°C isothermal altitude during a precipitation event is safe because snowfall tends to be underestimated.

Regarding initial conditions, the determination of the initial model state for PMP-PMF simulations is based on simulated values derived from the longest possible simulation over a period where meteorological observations are available. In case the observed meteorological data set does not contain any major event, the initial conditions derived from the simulations may not be severe enough. Therefore, attention should be paid on the presence of major events in the data set used for the derivation of the initial conditions. The presence of a major observed event is indeed important, not only for the initial conditions but also for the calibration of the model itself. In fact the calibration should contain those, so that the model can reproduce rare flood events.

The choice of the initial conditions according to the 99% quantile for the deterministic approach to estimate the PoMF can be discussed. The argument not to take the 100% quantile because maximizing all the state variables for the initialization of the model may be correct, but the choice of a 99% quantile is not easily justifiable. In qualitative terms, the dependence of the state variables is neglected in this approach. If dependence does play a role in some catchments, it could be dangerous to opt for using lower quantiles. Also, the case of one variable to be dominating the flood's characteristics is common, which provides a further argument for the choice of a high quantile such as 99%.

About the application limits of the Swiss PMP maps, regarding the size of the catchments, it can be stated that the analysis was carried out on a limited number of basins. More basins would have increased the power of the determined upper spatial coverage of PMP events from the Swiss PMP maps, especially if it would have been possible to simulate a large number of glacial and

non-glacial basins. This distinction could be of interest since the glacial regime differs from the non-glacial one. However, it can be assumed that the upper surface limit derived from only glacial catchments would have been less severe because the glacier acts as a discharge buffer: Ice starts melting only once the snow cover on the glacier has gone. Thus an attenuation of the peak discharge can be induced by the glacier. This effect may have led to an overestimation of the application limit (maximum catchment surface) for non-glacial catchments. At the same time, an underestimation of the application limit for glacial catchments can be imagined.

In regard to the PMP-PMF simulations, it can be underlined that the hydrological model has to be assumed valid for the simulations of meteorological events that are rarer than those the model has been calibrated on. There is unfortunately no possibility to verify this assumed validity because events that would be comparable to a PMP event have seldom been observed. Furthermore, the methodology assumes that the hydrological processes do not change during a PMP event. Nevertheless, it may be concluded that the application is reasonable as it can be assumed that a sufficiently long time series for the calibration and validation of the hydrological model allows mobilising almost all hydrological processes in the model. For example, Hortonian overland flow is not taken into account by the used model. It occurs when rainfall and snowmelt rates exceed the infiltration rate (Kirkby, 1988), what can occur in extreme cases. The model should thus be well trained for all situations including large floods. It follows that the simulation of floods generated by unobserved meteorological events can be assumed trustful, given the assumption that the hydrological processes do not change during the simulations.

Part III

Application procedure of the methodology and conclusions

9 Application of the CRUEX++ methodology

9.1 Introduction

In the preceding chapters, five research questions could be identified and treated. Satisfying conclusions could be reached, leading to the formulation of a holistic methodology for extreme flood estimation. In this chapter, the application of the developed methodology is demonstrated as an example. In order to cover different catchment characteristics, three basins have been identified according to their geographical situation, glacier cover and area.

9.2 Choice of the case study catchments

The geographical situation has a high impact on the meteorological conditions. That is the reason why the Swiss PMP maps have been developed for three different wind sectors, i.e. north, south and west-north-west. The selection of the catchments should allow to consider PMP maps from different sectors.

In addition, in a country like Switzerland, where topography has a major influence on the hydrological processes, the presence of glaciers highly impacts on the discharge generation. The choice of the study catchments should therefore also account for the glacier cover.

Regarding the area of the catchment, it plays an important role because the magnitude of floods do not increase linearly with the size of the catchments. The discharge of floods of the same order of magnitude logarithmically increase with the surface. In Chapter 6, this aspect has been considered to determine the upper catchment surface beyond which the Swiss PMP maps should not be used in order to avoid unrealistic overestimations of the PMF.

The choice of three basins is certainly a compromise and does not represent an exhaustive list of catchments covering all possible combinations of the three above mentioned factors, but it has been assumed to be reasonably representative to prove the applicability of the methodology to different alpine catchments with different characteristics.

The chosen catchments are the basins of the Limmernboden dam (17.8 km^2), the Mattmark dam (38 km^2) and the Contra dam (233 km^2). Their geographical situation is shown on the map of Figure 9.1. The safety flood estimation is undertaken by applying the CRUEX++ methodology explained in Chapter 8. The procedure adopted here for the methodology application has been detailed in section 9.3. It should be mentioned that the area of the Contra dam catchment is slightly outside of the application limits of the methodology. Nevertheless, the methodology has been applied in order to further exploit the limits of the methodology applied close to the transition zone, to which a great uncertainty could be attributed.

Finally, the results are presented and discussed for each catchment. The estimation of the return period of the safety flood using upper bounded statistical distributions has been compared to conventional statistical approaches, like AM (annual maxima) and POT (peak over threshold).

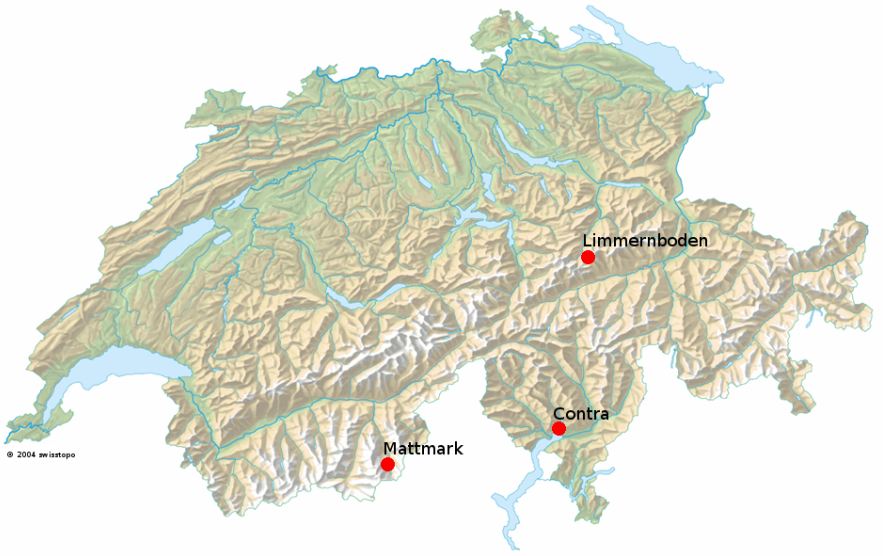

Figure 9.1: Situation of the three chosen case study dams in Switzerland.

9.3 Procedure for the application of the CRUEX++ methodology

The approach adopted for the application is exposed hereafter. For each of the three catchments, the following steps have been carried out.

9.3.1 Step 1: Catchment characteristics

First the catchment is characterised. The description of the catchments and the available data are important elements of the case study. It allows to expose the technical context of the study.

9.3.2 Step 2: The hydrological model

The second step is the hydrological model construction. The semi-distributed conceptual GSM-Socont model (Schaefli et al., 2005; Jordan et al., 2012; Schaefli and Zehe, 2009) has been used. The model takes into account the elevation of the catchment through altitude bands, in this case, with a vertical resolution of 300 m. The altitude bands have been determined based on a numerical terrain model with a horizontal resolution of 25 m. If lateral intakes are existing, the capacity of the collector has been estimated and considered in the model.

9.3.3 Step 3: Meteorological and discharge data

The model has then been calibrated and validated on observed data. The different considered meteorological stations have been exposed for each case study and the period of available data has been highlighted. The calibration and validation of the model has been done by comparing the simulated time series with the observed discharge time series made accessible by the dam operator. In the case of the Contra dam, two additional stations of the Federal Office for the Environment (FOEN) could be taken into account. The discharge data from the dam operators have been obtained by converting the level measurements into daily inflow volumes. Consequently, the discharge data are daily averaged values. Therefore, the model has to be assumed valid for smaller time steps when it is applied for flood estimations with intra-daily time resolution.

9.3.4 Step 4: Level-volume and level-outflow relations

The level-volume as well as the level-outflow relations of the reservoirs and spillways have been supplied by the dam operators for the Limmernboden and Mattmark dams. For the Contra dam, the level-outflow relation has been estimated. These relations have been implemented in the model to account for the flood attenuation and to evaluate the maximum level that occurred during the critical PMP event. The simulated maximum reservoir level and the corresponding outflow has than been used to verify if the existing spillway has been designed in order to make the dam withstand the safety flood event.

9.3.5 Step 5: PMP data

The PMP has been extracted from the Swiss PMP maps and interpolated as explained in Section 2.6.3 in order to derive PMP volumes for different event durations with an hourly time step. The PMP data have been temporally distributed using the 5% quantile rainfall mass curve shown in Figure 3.13. The temperature attributed to each PMP event has been derived from the linear relations between the precipitation duration and the maximum measured 0°C isothermal altitude determined in Chapter 4.

9.3.6 Step 6: PMP-PMF simulation

The generation of the PMF event has been based on two different approaches. The first approach accounts deterministically for the initial conditions set for the PMP-PMF simulation. The longest possible simulation has been performed to generate state variable time series to derive the 99% quantile values for a severe initialization of the model. The second approach uses a stochastic initial conditions scenario generator in order to account for the dependence between the different state variables. The two approaches have been compared in order to judge if the state variable dependences are representative or can be neglected. This analysis has already been conducted in section 5 for the Mattmark dam catchment and has thus not been repeated for this application. The here performed PMF estimation is used to determine the upper bound for the bounded statistical extrapolation carried out in a later step.

In Chapter 5, it has been shown that the initial conditions have a high impact on the simulated discharge. Therefore, a large number of different extreme floods can be obtained from a PMP event. For this study, median values for the initial state variable values have been admitted as terrain conditions for the estimation of the safety flood. If significant state variable dependences would lead to a big difference between the stochastically determined median safety flood discharge and the discharge derived under median initial conditions, the stochastic approach should be preferred. The PMP duration leading to the highest reservoir water level has been considered to generate the critical safety flood.

9.3.7 Step 7: Statistical distribution fit and estimation of the return period

The observed discharge data are daily averaged inflows. Daily flood estimates are, however, not valuable for the flood estimation in the context of dam safety verifications. Therefore, the calibrated hydrological model has been used to determine the maximum hourly inflow discharge data. This approach can extend the discharge time series when the meteorological time series is longer than the observed discharge series. The flood simulations (PMF and safety flood) have been performed with a 10 minutes time step. This short time step allowed to properly estimate the flood damping effect of the reservoir. However, this does not correspond to the time step of the extrapolated data set (hourly values derived by simulation). Therefore, a moving average approach has been used to determine the maximum hourly averaged discharge peak. The maximum hourly averaged PMF value has been retained as upper bound for the extrapolations. The upper bounded statistical distributions have been used to attribute a return period to the maximum hourly averaged safety flood.

Finally, a comparison of the extrapolations using upper bounded statistic distributions with the extrapolation from conventional distributions has been performed and discussed. The distributions that have been considered besides the EV4 and LN4, are the GEV (General Extreme Value distribution) and the Log-Normal distribution, as they are the parent distributions of the used bounded distributions. Furthermore, the POT method has been applied. It should be remembered

that the application of the POT method refers to the fit of a two parameter GP (General Pareto) distribution. Its mathematical expression is provided in Appendix E.1. These three distributions (GEV, log-normal and GP) are commonly used in hydrology and are thus interesting to compare to the bounded distributions. The comparison allows to evaluate the benefits of the CRUEX++ methodology compared to the more traditional approaches.

9.4 Application to the Limmernboden dam catchment

9.4.1 Description of the Limmernboden dam catchment

The Limmernboden concrete dam (Figure 9.2) is located in the northern part of the Swiss Alps in the canton of Glarus (Figure 9.1).

Figure 9.2: Photo of the Limmernboden dam (SwissCOD, 2011).

A detailed representation of the main catchment, the glacier cover, the reservoir and the lateral intakes are shown in Figure 9.3. The altitude range of the main catchment varies from 1 857 m.a.s.l. at reservoir level up to 3 419 m.a.s.l. and from 1 927 m.a.s.l. up to 3 614 m.a.s.l. for the lateral catchments. The total capacity of the lateral intakes is limited to 10.5 m^3/s. The main characteristics of the Limmernboden dam catchment, the reservoir and the lateral catchments are presented in Table 9.1.

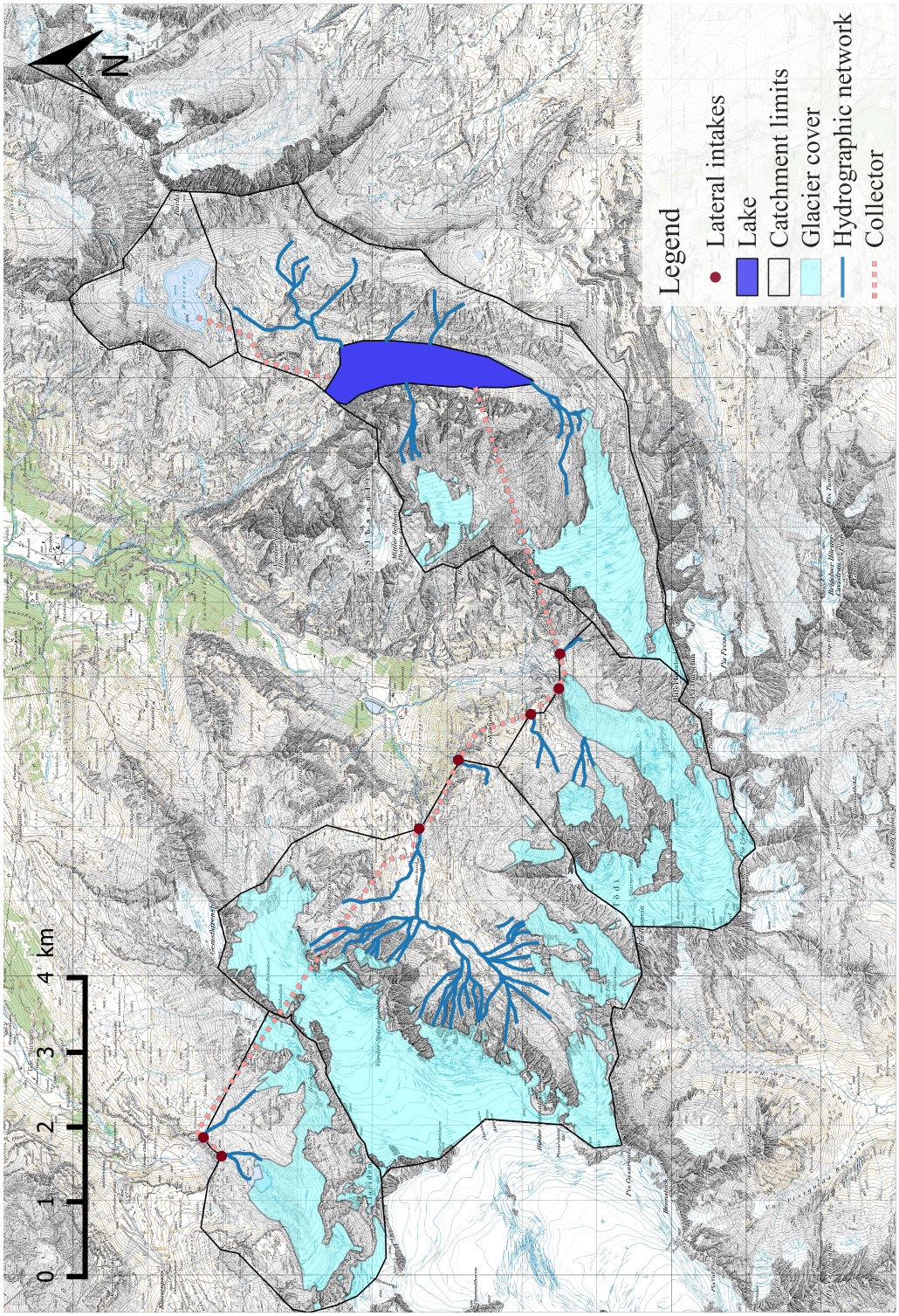

Figure 9.3: Limmernboden catchment with lateral catchments, glacier covered zones and the location of the intakes. Map source: Swisstopo

Table 9.1: Main characteristics of the Limmernboden catchment and the reservoir (SwissCOD, 2011)

Reservoir	
Name	Limmernboden
Canton	Glarus
Reservoir surface [km^2]	1.36
Volume [mio m^3]	92
Max spillway discharge [m^3/s]	89
Max discharge of ground outlet [m^3/s]	98
Spillway crest [m a.s.l.]	1857
Dam crest [m a.s.l.]	1858.5
Catchments	
Area [km^2]	17.8
Glacier cover [km^2]	2.2
Primary Inflows	Muttenbach
Primary Outflows	Limmernbach
External catchments	
Number of additional catchments	4
Additional area [km^2]	31.8
Additional glacier cover [km^2]	14.6
Collector capacity [m^3/s]	10.5

9.4.2 Description of the spillway of the Limmernboden dam

The spillway of the Limmernboden dam has been designed as lateral weir, situated on the left bank of the dam. The evacuated flow is then led into a gallery. According to the report on the hydraulic design of the spillway (KLL, 1988), this gallery could be damaged if it gets pressurized. Therefore its capacity should be high enough in order to evacuate the safety flood without pressurization. The spillway capacity is limited due to the latter criterion and has been estimated to be $Q = 90\,\mathrm{m}^3/\mathrm{s}$ (KLL, 1988). Figure 9.4, taken from the report on the hydraulic design of the spillway (KLL, 1988), shows the situation of the Limmernboden dam with the lateral spillway and the gallery. In the same report, a profile of the spillway crest could be found. It is illustrated in Figure 9.5.

The level-outflow relation given in the report on the hydraulic design of the spillway (KLL, 1988) is plotted together with the level-volume relation in Figure 9.6.

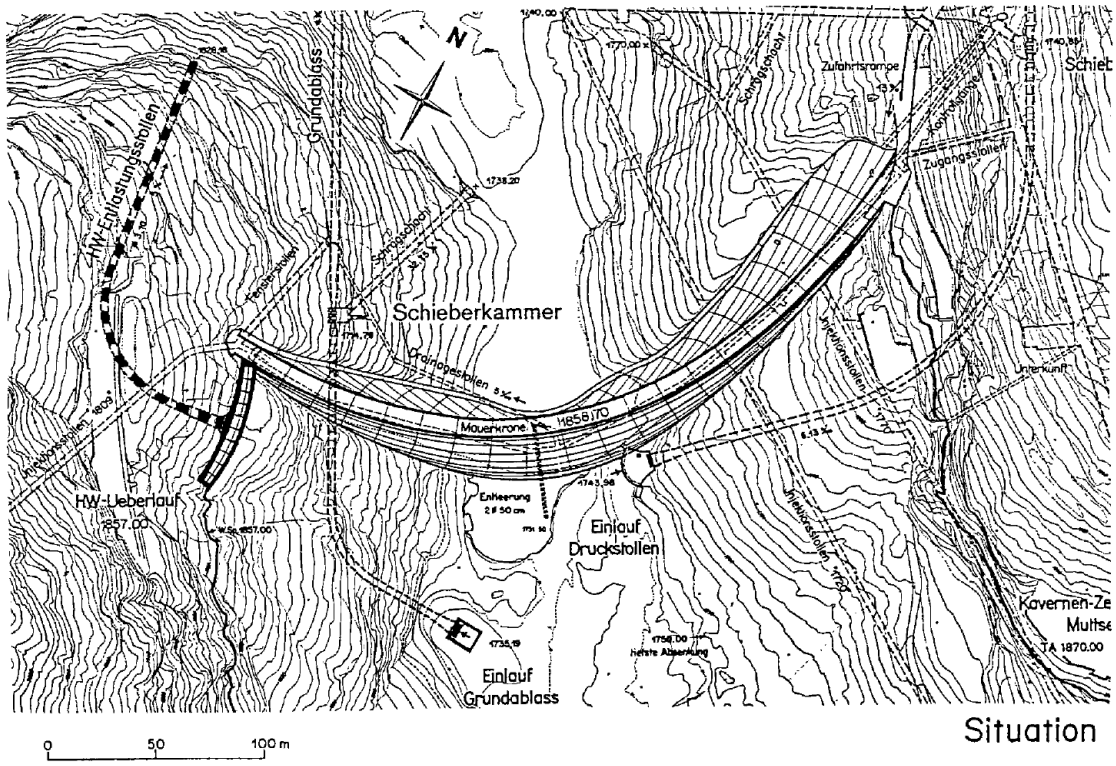

Figure 9.4: Limmernboden dam situation plan. Taken from the report on the hydraulic design of the spillway (KLL, 1988).

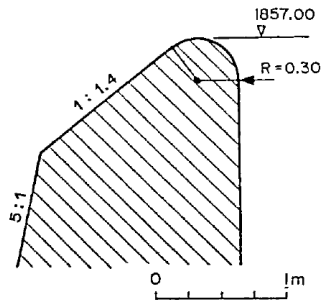

Figure 9.5: Limmernboden dam spillway crest profile. Taken from the report on the hydraulic design of the spillway (KLL, 1988).

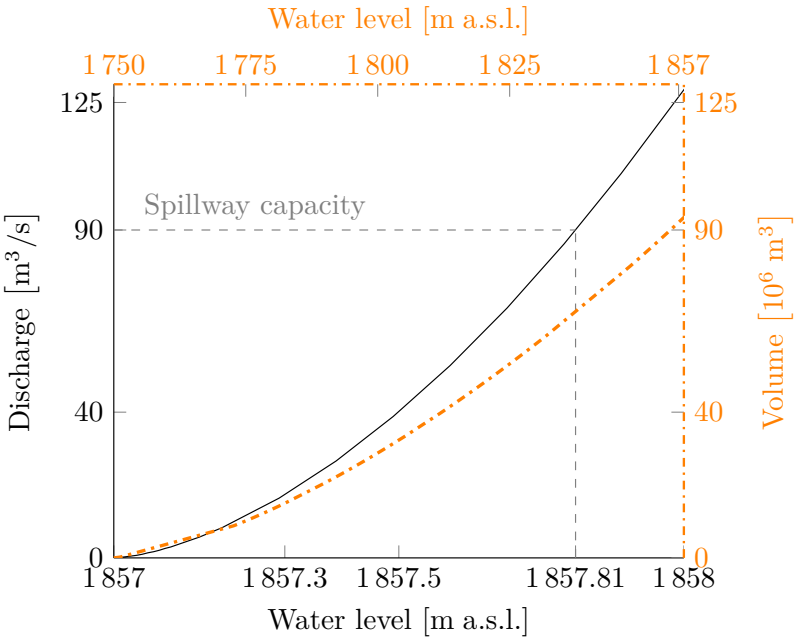

Figure 9.6: Spillway routing curve of the Limmernboden dam and level-volume relation of the reservoir.

9.4.3 Meteorological and discharge data

The available meteorological (precipitation and temperature) and discharge time series are briefly described in the following.

The situation of the meteorological stations around the Limmernboden dam catchment is illustrated in Figure 9.7. The meteorological data has been provided by MeteoSwiss. For the present analysis, 10 meteorological stations have been taken into account. At all stations precipitation data have been available but only at 4 stations temperature was measured for the period from 01/01/1981 to 31/12/2009.

Regarding the temporal resolution of the meteorological data sets, values at a daily time step have been available at the stations measuring only precipitation (cf Figure 9.7). For the stations measuring precipitation and temperature, data at an hourly time step was accessible. The daily data have been disaggregated in hourly data sets. To do so, two nearby stations, for which hourly data were available, had to be chosen. The data of these two stations were then interpolated, using the inverse squared distance weighting, to get an estimate of hourly precipitation at the location of the station to be disaggregated. Finally, the daily measured precipitation volume of the station to be disaggregated was used to adjust the volume of the generated hourly time series.

Figure C.14 illustrates the periods covered by the meteorological time series. The detailed dates of the begin and end of the time series are shown in Table C.8.

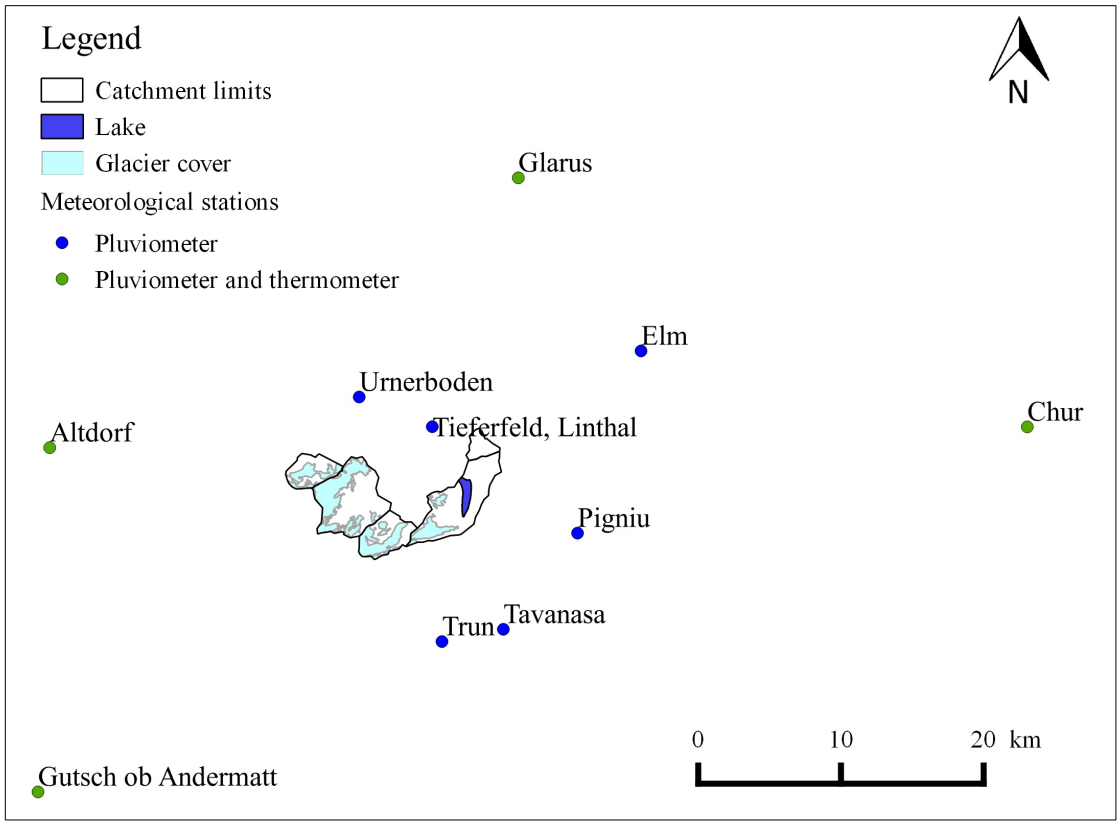

Figure 9.7: Situation of the meteorological stations in the vicinity Limmernboden catchment.

The discharge data was provided by the dam operator Kraftwerke Linth-Limmern AG (KLL) with a daily temporal resolution. The data are based on water level measurements in the reservoir and have been converted by the operator into mean daily discharge values. The covered period goes from 01/10/1997 to 31/03/2013. Figure 9.8 illustrates the discharge observation period and allows to compare it to the meteorological time series period.

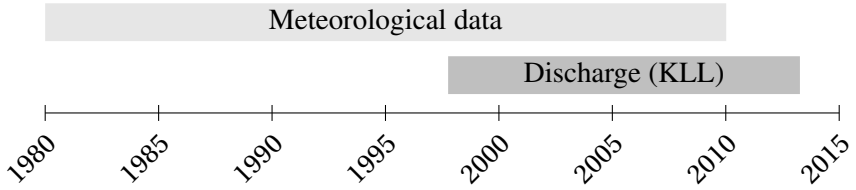

Figure 9.8: Diagram showing the periods of available meteorological and discharge data.

9.4.4 Hydrological model design

The catchment has been subdivided into altitude bands with a vertical resolution of 300 m based on a numerical terrain model with a 25 m horizontal resolution. The subdivision into altitude

bands is shown in appendix in Figure E.1.

Due to the small size of the steep basin, river routing has been ignored for this model. The discharges generated by the different altitude bands are considered to sum at the outlet of the corresponding sub-basin. The inflow discharge into the Limmernboden reservoir is the sum of the different outlet discharges (from the sub-basins or the collector).

The level-volume and the level-outflow relations of the Limmernboden dam used for the simulation of the flood attenuation are shown in Figure 9.6. The initial height of the water level has been assumed to be 1857 m a.s.l. . This corresponds to full water condition and should be assumed for dam safety verifications according to SFOE (2008a).

9.4.5 Model calibration and validation

The hydrological model has been calibrated and validated based on the available meteorological data as well as the discharge time series exposed in section 9.4.3. The periods considered for the calibration and the validation are respectively from 01/01/1997 to 01/10/2003 and from 01/10/2003 to 31/12/2009.

The performance coefficients (Nash-Sutcliffe efficiency, Volume ratio, Kling-Gupta efficiency) of the calibration and validation results are represented by the bar plot of Figure 9.9. The equations to estimate these coefficients are shown in appendix E.2. The optimum values of 1 is well approached by each coefficient. According to the performance coefficient qualification of Moriasi et al. (2007), the model can be qualified as very good regarding the Nash-Sutcliffe efficiency if this coefficient is larger than 0.75. In this case, the latter coefficient is larger than 0.85. The final simulation results, compared to the observations, are shown in Figure 9.10. This figure shows that the flood events are well represented, with the exception of the flood from 2001. The reason of the lack of reproduction of this flood by the model is the lack of important precipitation observations. If intense precipitation events would have been observed for the concerned period, the flood would probably have been reproduced by the model.

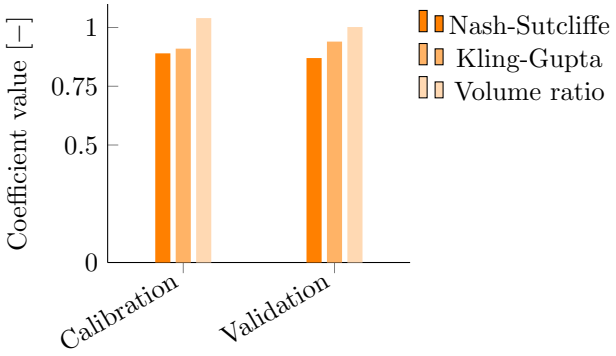

Figure 9.9: Performance coefficients proving the goodness of the hydrological model of the Limmernboden dam catchment.

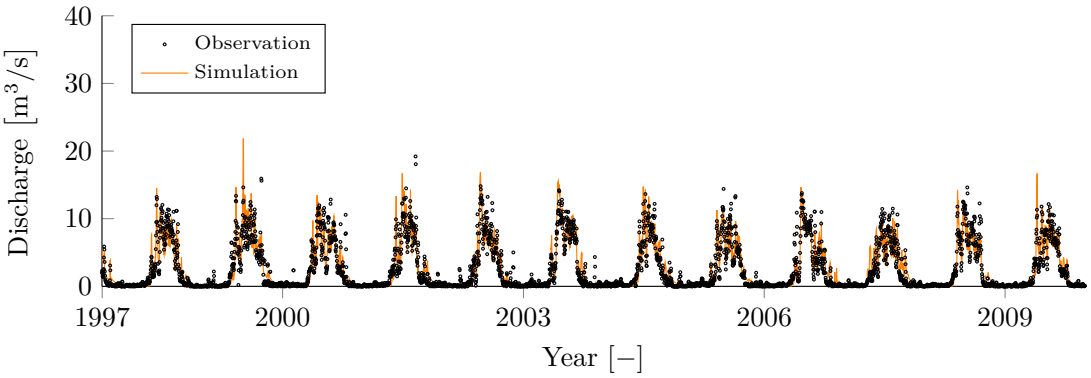

Figure 9.10: Comparison between the mean daily observed discharge and the simulation with a daily time step from 1980 to 2009 for the Limmernboden dam catchment.

9.4.6 PMP-PMF simulation

Initial conditions

The initial conditions have been deduced from a continuous simulation of the period going from 01/10/1997 to 31/12/2009. The deterministic and stochastic approach have been considered in order to compare the results.

The determined values for the deterministic approach are reported in Table 9.2. The values correspond to the 50% and 99% quantile of the simulated state variables. Under the assumption that summer conditions are necessary to generate a PMP, the estimation of the 50% and 99% quantile values has been based on the summer period (June-August). The contemplation of the initial saturation values should be made in awareness of the calibrated soil infiltration capacity $H_{GR3,max} = 0.47$ m.

For the stochastic approach, the data set has also been separated into seasonal sets. The summer

time series has been retained for the determination of the initial conditions scenarios. Randomly determined moments in time have been generated and the simulated state variable values for these moments have been retained as dependent initial conditions for the simulations. A total of 5000 scenarios were generated.

Table 9.2: Summer state variable values for the 50% and 99% quantiles considered for the deterministic initialization of the hydrological model of the Limmernboden dam catchment.

Region	State variable	Symbol	50%	99%	Unit
Non glacial	Snow height	H_s	0.009	0.78	[m]
	Snow saturation	θ	0.03	0.1	[m]
	Runoff	H_r	0.004	0.021	[m]
	Soil saturation	H_{Gr3}	0.198	0.34	[m]
Glacial	Snow height	$H_{s,Gl}$	0.006	0.985	[m]
	Snow saturation	θ_{Gl}	0.01	0.1	[m]
	Glacier melt	Q_{Gl}	0.16	0.75	[m^3/s]
	Snow melt	Q_s	0.04	0.95	[m^3/s]

Temperature assumption for PMP events

The temperature attributed to the PMP events, in terms of 0°C isothermal altitude, depends on the duration of the considered event. The justification for this consideration has been elaborated in Chapter 4. The Limmernboden dam is situated in the northern part of Switzerland (according to the subdivision in northern and southern part illustrated in Chapter 4). Beside the geographical situation of the Limmernboden dam, the PMP is supposed to occur under summer conditions. The relation considered to derive the 0°C isothermal altitude for each PMP event has been derived using Equation 9.1.

$$H = ad + b \tag{9.1}$$

where H is the altitude of the 0°C isothermal altitude in [m a.s.l.], d the duration of the PMP event in [h], $a = -8.352$ [m a.s.l. / h] and $b = 4521.7$ [m a.s.l.] are the parameters determined in Chapter 4 for the northern part of Switzerland under summer conditions.

Critical wind direction

The PMP data has been elaborated by Hertig et al. (2005) for different wind directions, i.e. North, South and West-North-West. For the determination of the critical wind sector, a 3h-PMP has been randomly chosen and the corresponding PMP data was introduced in the calibrated hydrological

model (initialized with the 50% quantile state variable values) in order to determine which sector generates a higher discharge than the two others.

The simulation results are shown in Figure 9.11. It can be seen that the North and the West-North-West sectors give very close estimations. The North is however slightly higher. This sector has thus been retained as the critical wind direction.

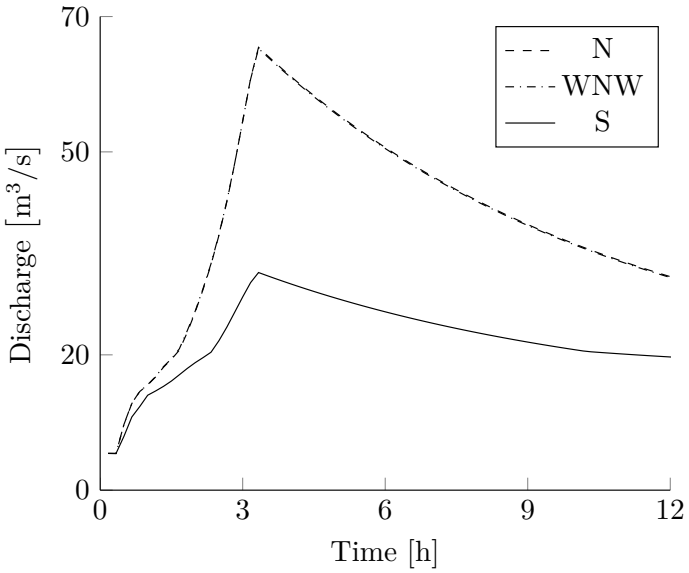

Figure 9.11: Hydrographs derived from 3h-PMPs for the three different wind sectors north (N), south (S) and west-north-west (WNW) for the Limmernboden dam catchment.

PMF estimates

In a first step, the PoMF used as upper bound for the statistical extrapolations has been estimated. The initial conditions derived from the 99% quantile values of the state variables have been used for the simulations. These values have been reported in Table 9.2. PMP events from 1h to 24h have been considered for the simulations. The maximum hourly averaged peak discharge has been derived with the moving average approach, as explained earlier. Figure 9.12 shows the maximum hourly peak discharges for the different PMP durations. The 3h PMP generated the highest hourly averaged discharge. The detailed hydrographs for the 99% quantile initial conditions are shown in Figure E.2. A comparison with the results derived from a 3h-PMP event with the stochastic approach (Figure 9.13) shows that the deterministic approach overestimates the PMF if rare initial conditions are considered, and slightly underestimates the median discharge value. This shows that the simultaneous occurrence of the 99% quantile state variable values is not accurate in this case. Due to the respect of the dependence between the state variables of the stochastic approach, the latter has been considered to estimate the upper limit for the bounded statistical extrapolation. The retained hourly averaged discharge is $Q = 275\,\mathrm{m}^3/\mathrm{s}$.

The next step is the determination of the safety flood. It has been retained in Section 9.3.6 that a flood generated under the assumption of median initial state variable values would be used for the safety verification. Figure 9.14 shows the reservoir water level estimates for different PMP durations. It can be seen that the critical PMP duration under the considered initial conditions is 23h. The corresponding inflow and outflow hydrographs as well as the reservoir level evolution are shown in Figure 9.15. It can be concluded that the safety flood generated by a 23h-PMP and median initial condition could be withstood without over-topping. The spillway capacity has not been exceeded during the simulations.

The probability of the peak discharge of the considered safety event can be derived once the statistical distribution has been fitted. For this purpose, the corresponding hourly averaged discharge has to be derived. The hourly peak discharge corresponding to the 23h-PMP event has been estimated to be $Q = 55\,\mathrm{m}^3/\mathrm{s}$ (under median initial conditions).

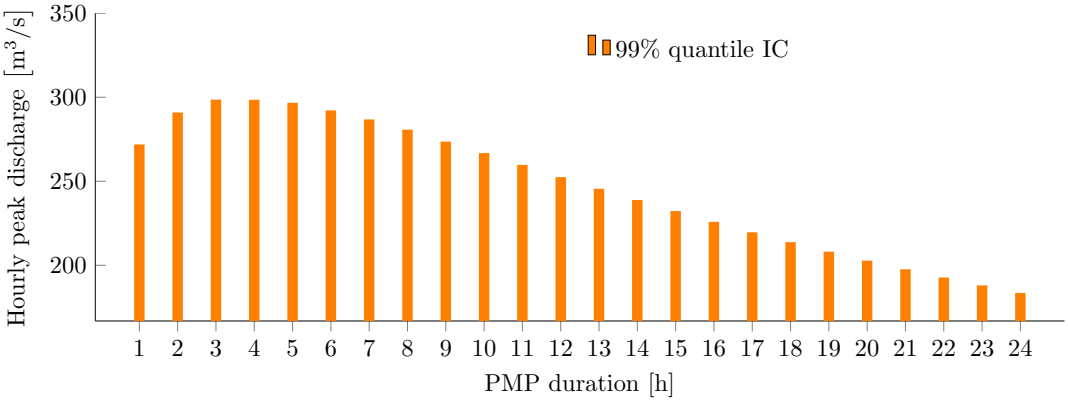

Figure 9.12: Hourly inflow peak discharges derived from different PMP events with wind sector "north" for the Limmernboden dam. "IC" stands for initial conditions.

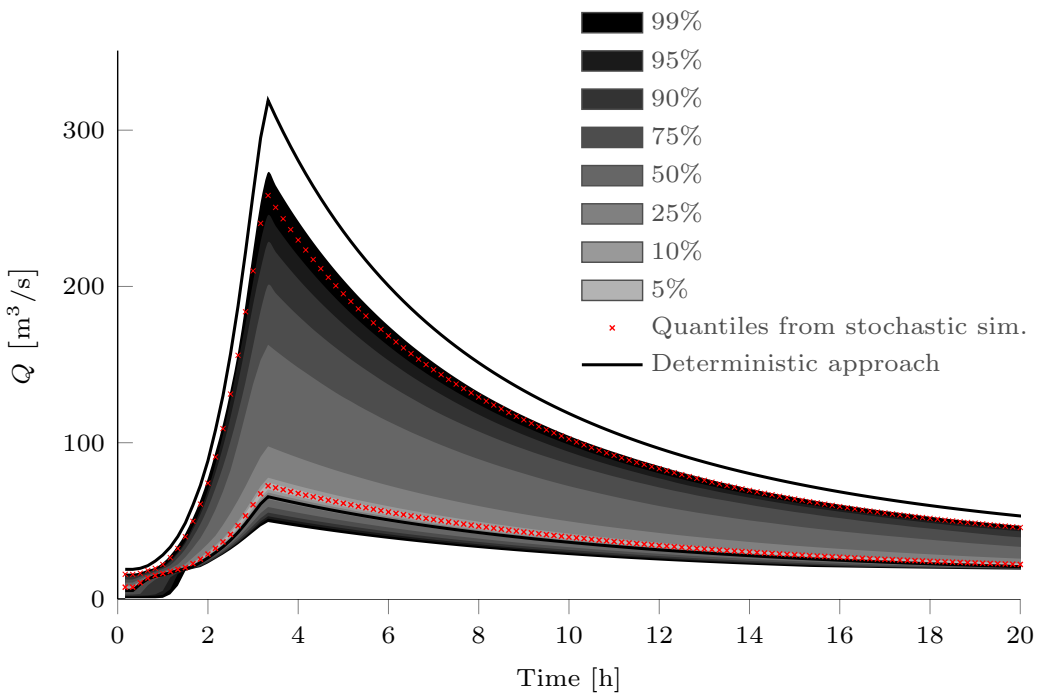

Figure 9.13: PMF estimates derived from a 3h-PMP based on 5000 initial conditions scenarios. The 50% and 99% quantile discharges are shown by the red crosses. The continuous black lines show the discharge generated when 50% and 99% quantiles for the initial state variable values were used.

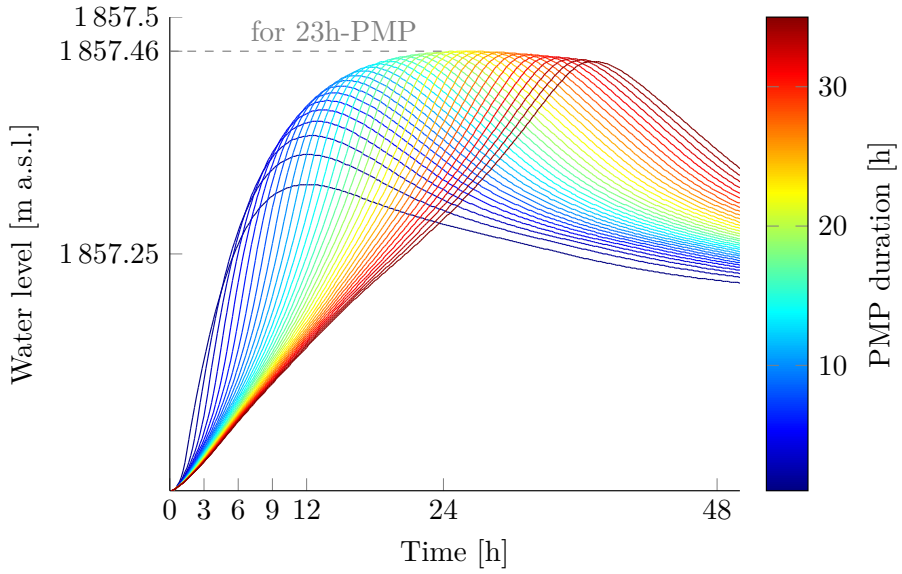

Figure 9.14: Reservoir water level estimates for the Limmernboden dam for different PMP events (wind sector "North") for 50% quantile initial values. The maximum reservoir level is reached for a 23h-PMP event.

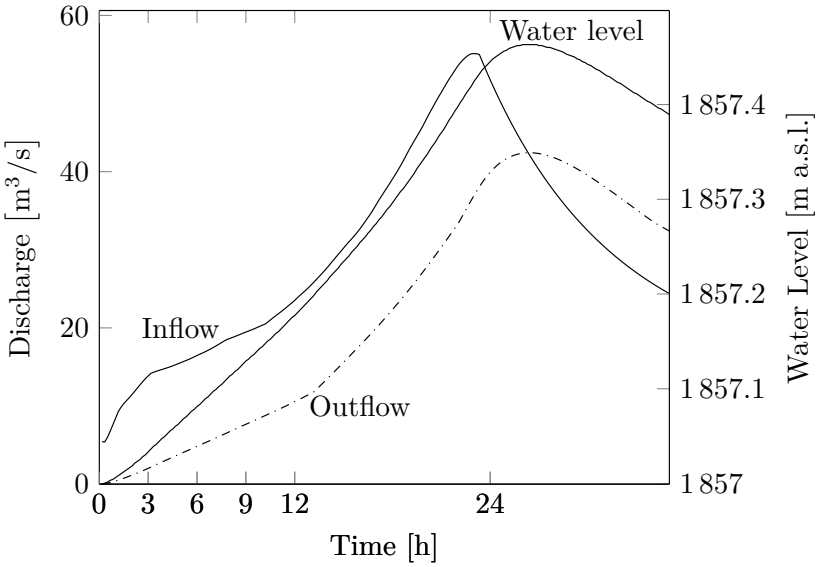

Figure 9.15: Inflow and outflow hydrographs with corresponding reservoir water level for a 23h-PMP event and median initial conditions.

9.4.7 Statistical extrapolations

The hydrological model has been used to generate the hourly maximum discharge peaks for each year. The simulation covers the period from 1980 to 2009. The resulting annual maximum values considered for the distribution fit are shown in Figure E.4. They have been fitted with a bounded distribution as well as the Log-Normal distribution and the GEV. For the POT method, a threshold of $u = 11.5\text{m}^3/\text{s}$ has been determined. This threshold was fixed in order to have at least one value per year. Furthermore, a minimum of 14 days between two peaks has been admitted to be the minimum period to guarantee independence between the events. A total of 72 peak discharges have been determined. They are highlighted in Figure E.5. This means that, on average, 2.4 values have been considered per year. According to Tavares and Da Silva (1983), the average number of events per year should be around 2, in order to get the best performance of the POT method.

The largest discharge generated by the critical PMP event has been determined to be $Q = 275\ \text{m}^3/\text{s}$. This value has been admitted as upper bound for the statistical fit. The sample skewness, estimated with Equation 2.1, is $\gamma = 0.85$. The LN4 distribution should be used in this case according to Takara and Tosa (1999). The estimated parameters for the different distribution are shown in appendix in Table E.1.

Figure 9.16 shows the statistical extrapolations. It can be seen on this figure that the hourly peak discharge of the 23h-PMP has a return period of more than 10^{11} years according to the LN4 distribution. The other approaches (GEV, Log-normal, POT) underestimate the flood discharges compared to the LN4 distribution. The log-normal distribution is the closest to the

LN4 distribution. The GEV and the POT distributions start to deviate from the LN4 distribution from a return period of 10^4 years on. This means that, up to this deviation point, the four distributions lead to very similar estimations.

According to the Swiss guidelines for dam safety (SFOE, 2008a), quantity $Q_s = 1.5Q_{1000}$ can be considered as safety flood. In this case, $Q_s = 41.5\ \mathrm{m}^3/\mathrm{s}$. The estimated discharge can be attributed a return period of approximately 10^7 according to the LN4 distribution. The safety flood derived under median initial conditions from the 23h PMP has a peak discharge that is roughly 30% higher.

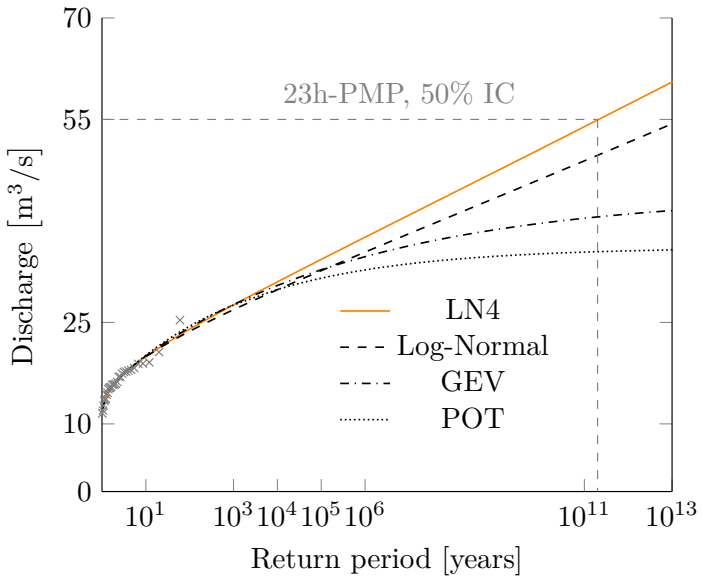

Figure 9.16: Annual maximum hourly discharge data fitted with the LN4 distribution considering an upper bound of PMF=275 m^3/s.

9.4.8 Intermediate conclusions

The case study of the Limmernboden dam could show that the upper bounded statistical distribution LN4 gave more conservative estimates than the conventional methods. Nevertheless, the spillway capacity has not been exceeded by the safety flood, that could be attributed a return period of roughly 10^{11} years. The return period of the quantity $Q_s = 1.5Q_{1000}$ has been estimated to be 10^7 years.

9.5 Application to the Mattmark dam catchment

9.5.1 Description of the Mattmark dam catchment

In this chapter, the Mattmark embankment dam (Figure 9.17) and its catchment are presented. The Mattmark dam is situated in the southern part of Switzerland in the Canton of Valais (Figure 9.1) upstream the village of *Saas Almagell* on the river *Saaser Vispa*. The limits of the catchment as well the the glacier cover and the lateral intakes are shown in Figure 9.18. The main catchment of the Mattmark reservoir, with an area of 35.6 km^2, is completed by four surrounding catchments augmenting the catchment area to 83.2 km^2. In Table 9.3, the main charatceristics of the Mattmark catchment and its reservoir are listed.

Figure 9.17: Photo of the Mattmark dam (SwissCOD, 2011).

Table 9.3: Main characteristics of the catchments and the reservoirs (SwissCOD, 2011)

Reservoirs	
Name	Mattmark
Canton	Wallis / Valais
Reservoir surface [km^2]	1.76
Volume [mio m^3]	100
Max spillway discharge [m^3/s]	230
Max discharge of ground outlet [m^3/s]	57
Spillway crest [m a.s.l.]	2197
Dam crest [m a.s.l.]	2204
Main catchment	
Area [km^2]	35.6
Glacier cover [km^2]	9.2
Primary Inflows	Stafelbach
Primary Outflows	Saaser Vispa
External catchments	
Number of additional catchments	4
Additional area [km^2]	47.6
Additional glacier cover [km^2]	20.5
Collector capacity [m^3/s]	16

9.5.2 Meteorological and discharge data

The precipitation and temperature data have been provided by MeteoSwiss. The periods covered by the meteorological time series per station are shown in Figure C.15. The detailed dates are given in Table C.9. The overlapping period of the meteorological time series is shown in Figure 9.19. The situation of the meteorological stations around the Mattmark dam are shown in Figure 9.20.

Regarding the temporal resolution of the meteorological data sets, values at a daily time step have been available at the stations measuring only precipitation (cf Figure 9.20). For the stations measuring precipitation and temperature, data at an hourly time step was accessible. The daily data has been disaggregated in hourly data sets. To do so, two nearby stations with hourly data were chosen. The data of these two stations were then interpolated using the inverse squared distance weighting, to get an estimate of hourly precipitation at the location of the station to be disaggregated. Then, the daily measured precipitation volume of the station to be disaggregated has been used to adjust the volume of the generated hourly time series.

The discharge data has been provided by the dam operator Kraftwerke Mattmark AG (KWM) with a daily time resolution. The data have been based on water level measurements in the

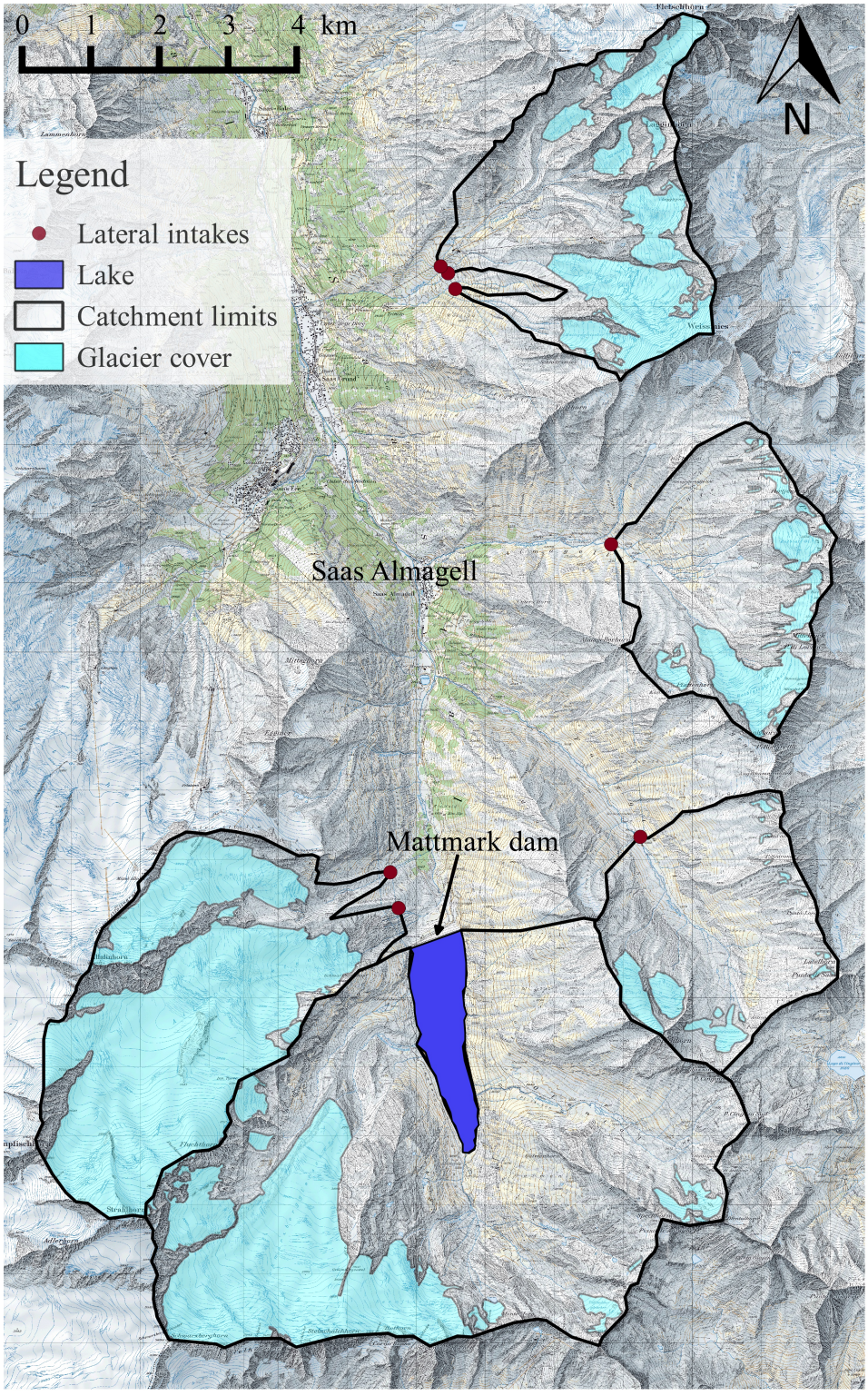

Figure 9.18: Mattmark catchment with lateral catchments, glacier covered zones and the location of the intakes.

reservoir and have been converted into mean daily discharge values. The covered period goes from 01/10/1971 to 31/05/2013. Figure 9.19 illustrates the discharge observation period and allows to compare it to the meteorological time series period.

9.5.3 Description of the spillway of the Mattmark dam

The spillway of the Mattmark dam is situated on its right bank. A sketch of the spillway is shown in Figure 9.21. The study of Boillat and Schleiss (2002) was aimed at re-evaluating and adapting the spillway capacity of the Mattmark dam. The adaptation of the original spillway is represented on the sketch of Figure 9.21. Three orifices have been introduced and the spillway crest has been elevated by 2 m. The level-outflow curve, as it has been described by Boillat and Schleiss (2002) , is shown in Figure 9.22 together with the level-volume relation of the reservoir.

9.5.4 Hydrological model

The catchment has been subdivided into altitude bands with a vertical resolution of 300 m based on a numerical terrain model with a horizontal resolution of 25m . The subdivision into altitude bands is shown in Figure E.6 and E.7.

The capacity of the collector, used to derive the water coming from the lateral catchments to the Mattmark dam has been estimated to $16 m^3/s$.

Due to the small size of the basin, river routing has been ignored for this model. The discharges generated by the different altitude bands are considered to sum at the outlet of the corresponding sub-basin. The inflow discharge into the Mattmark reservoir is the sum of the different outlet discharges (from the sub-basins or the collector).

Model calibration and validation

The capability of the hydrological model to reproduce the observed discharge data is exposed in this section. As shown in Figure 9.19, the meteorological data set changed during the observation period. Therefore the performance of the model has been evaluated for the two main periods, each with invariable meteorological time series, i.e. from 1980 to 1994 (period P1) and from 1995 to 2009 (period P2). The two periods have been separated into a calibration and a validation period. For the period P1 the calibration period goes from 1987 to 1994 and the validation period goes from 1980 to 1987. For the period P2 the calibration has been made for the period from 2002 to 2009 and the model has been validated from 1995 to 2002. Figure 9.23 illustrates the performance coefficients Nash-Sutcliffe and Kling-Gupta as well as the volume ratio for the two mentioned periods P1 and P2. The equations to estimate these performance coefficients are shown in appendix E.2. The final simulation results (with the calibrated model) over the complete period and the observations are shown in Figure 9.24. It can be seen that the two major floods from

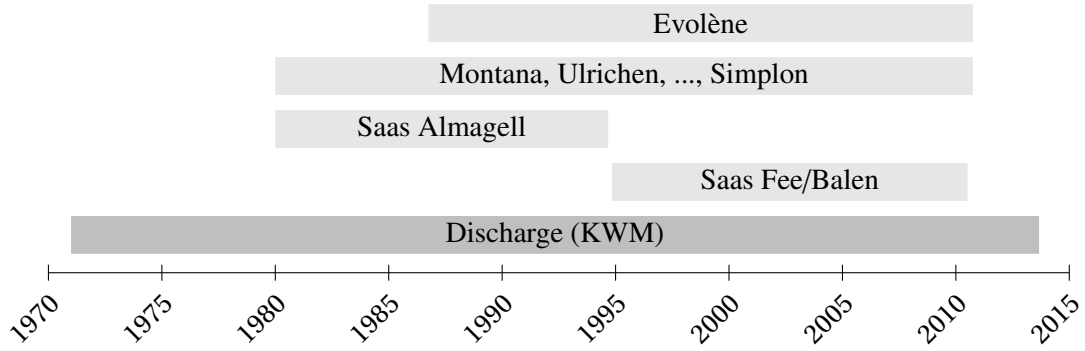

Figure 9.19: Diagram showing the periods of available meteorological discharge data.

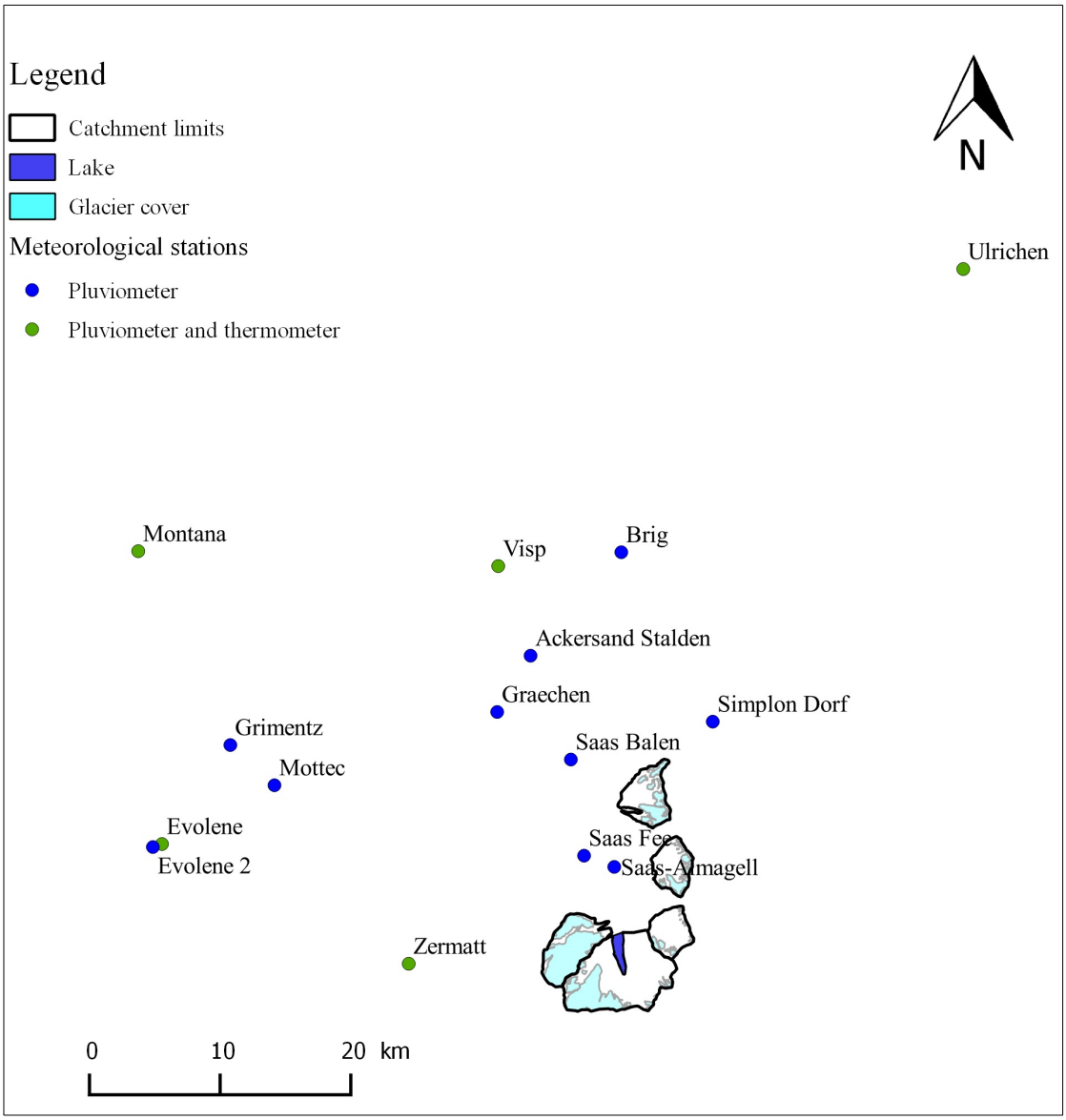

Figure 9.20: Situation of the meteorological stations in the vicinity of the Mattmark catchment.

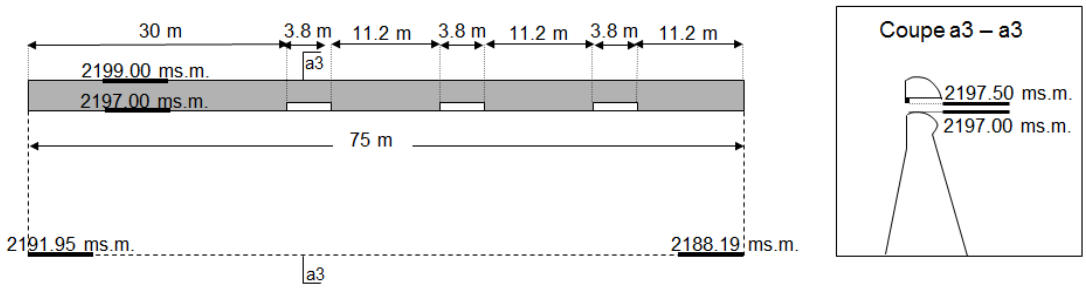

Figure 9.21: Sketch of the Mattmark spillway with lateral profile. The sketch is taken from Boillat and Schleiss (2000)

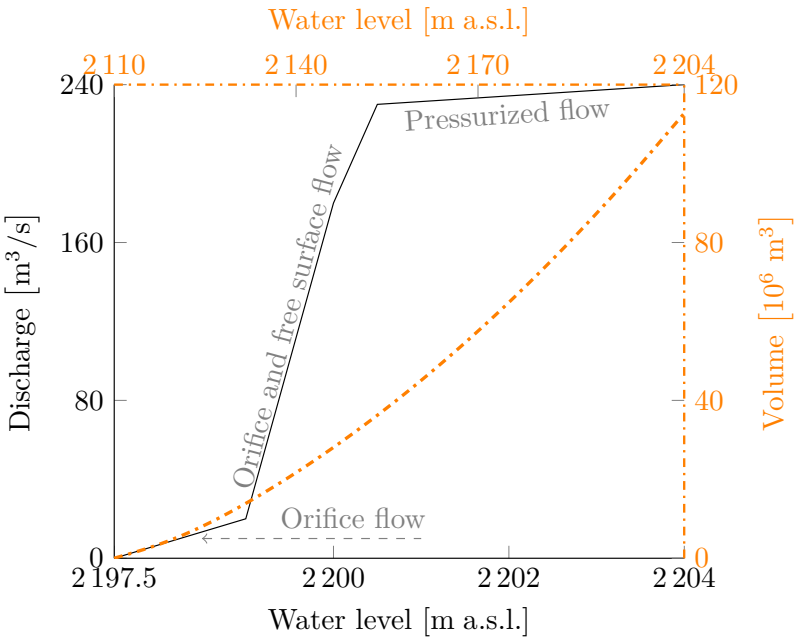

Figure 9.22: Spillway routing curve of the Mattmark dam and level-volume relation of the reservoir.

1993 and 1994 are not well represented. A comparison with the meteorological observations led to the conclusion that the measured rainfall intensities were too small to generate such high discharges. The precipitation events that caused these major flood events were probably too local to be registered by the pluviometers. However, the flood of 1993 is still represented by 70% of the observed discharge. For the flood of 1994 the model reproduced the peak discharge by 40% of the observed value.

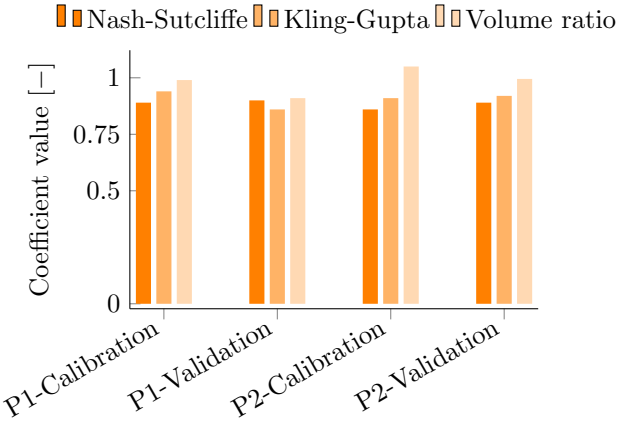

Figure 9.23: Performance coefficients proving the goodness of the hydrological model of the Mattmark dam catchment.

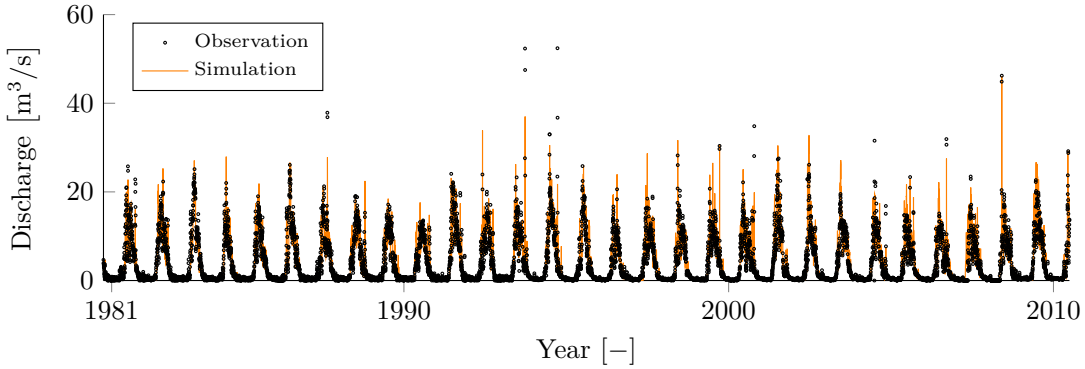

Figure 9.24: Comparison between the mean daily observed discharge and the simulation with a daily time step from 1981 to 2010.

9.5.5 PMP-PMF simulation

Initial conditions

The initial conditions for the PMP-PMF simulations have been derive by quantile analysis from the state variable values simulated during summer (June-August). The retained values are reported in Table 9.4. These values have been used to initialize the model when the deterministic approach

is used. The contemplation of the initial saturation should be made being aware of the calibrated soil infiltration capacity $H_{GR3,max} = 0.28$ m.

In Chapter 5, it could be shown that the results from the deterministic and stochastic approaches are equivalent for the Mattmark dam. Therefore only the deterministic approach has been considered for this case study.

Table 9.4: Summer state variable values for the 50% and 99% quantiles considered for the hydrological model initialization.

Region	State variable	Symbol	50%	99%	Unit
Non glacial	Snow height	H_s	0.002	0.54	[m]
	Snow saturation	θ	0.009	0.097	[m]
	Runoff	H_r	0.0014	0.013	[m]
	Soil saturation	H_{Gr3}	0.081	0.18	[m]
Glacial	Snow height	$H_{s,Gl}$	0.104	0.78	[m]
	Snow saturation	θ_{Gl}	0.046	0.10	[m]
	Glacier melt	Q_{Gl}	0.299	1.19	[m^3/s]
	Snow melt	Q_s	0.182	2.02	[m^3/s]

Temperature for PMP events

The temperature attributed to the PMP events, in terms of 0°C isothermal altitude, has been derived using Equation 9.2.

$$H = ad + b \tag{9.2}$$

where H is the altitude of the 0°C isothermal altitude in [m a.s.l.], d the duration of the PMP event in [h], $a = -11.554$ [m a.s.l. / h] and $b = 4815.2$ [m a.s.l.] are the parameters determined in Chapter 4 for the southern part of Switzerland under summer conditions.

Critical wind direction

The most critical wind sector of the PMP maps had to be determined. For this purpose, a 3h-PMP event has been extracted from the PMP maps for the three available wind directions. The three events have been used to derive the PMF with the calibrated hydrological model. The PMP data have been temporally distributed using the 5% quantile rainfall mass curve shown in Figure 3.13. This curve has been proven to be valid for the entire territory of Switzerland in Chapter 3. The simulations were performed with a time step of 10 minutes. The PMP event that led to the highest PMF discharge has been considered to determine the most critical wind direction and thus the

PMP maps that have been retained for the following simulations. The hydrographs derived from the three 3h-PMP events are represented in Figure 9.25. It can be seen that the most critical wind sector is "south".

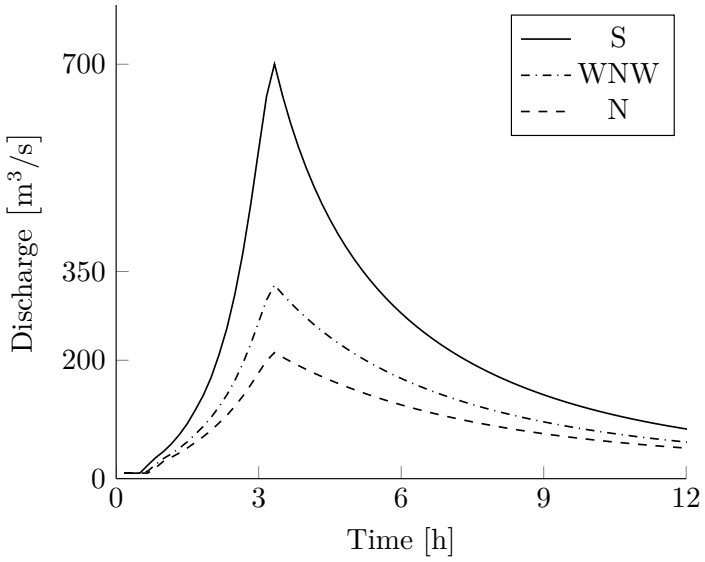

Figure 9.25: Hydrographs derived from 3h-PMPs for three different wind sectors: north (N), south (S) and west-north-west (WNW).

PMF estimates

The PMP maps used for the following simulations are the maps generated for the wind sector "south". The deterministic approach has been used to determine the critical PMP duration. The PMP-PMF simulations were performed with a 10 minutes time step. As mentioned before, the stochastic approach has not been applied here because the analysis of Chapter 5 showed that the results for the Mattmark dam catchment are very similar.

First, the PoMF, used as upper bound for the statistical extrapolations, has been determined. The initial conditions have been derived from the 99% quantile values of the state variables. They are reported in Table 9.4. The hourly maximum peak discharges have than been derived calculating the hourly average with gliding window of a one hour width. Figure 9.26 shows the maximum hourly peak discharges for the different PMP durations. The detailed hydrographs for the different PMP durations are shown in Figure E.8. The 3h-PMP generated the highest hourly peak discharge when considering the 99% quantile for the initial value determination. The value of $Q = 1000\ \mathrm{m^3/s}$ has been retained as upper bound for the statistical fit, performed below in section 9.5.6.

The next step is to determine the safety flood. It has been retained that the median state variable values would be admitted for the estimation of the safety flood. The PMP duration leading to the highest peak discharge is not necessarily the most critical for the dam and the spillway when the

initial conditions change. The simulations of the reservoir level showed that the critical PMP for the dam has a duration of 16h (time step: 10 minutes, 50% quantile initial conditions). Figure 9.27 shows the simulation results. The corresponding inflow and outflow hydrographs as well as the water level evolution are shown in Figure 9.28. The hourly averaged discharge peak value has been estimated to be $Q = 450\,\mathrm{m}^3/\mathrm{s}$.

From the shape of the outflow hydrograph and the level-outflow curve (Figure 9.22), it can be deduced that the spillway conduit was pressurized at a certain moment. For the 50% quantile initial values, the critical event was a 16h-PMP. From Figure 9.28, it could be deduced that the outflow conduit was also pressurized for this event.

Finally, it can be retained that the safety flood generated by a 16h-PMP and median initial condition would not lead to overtopping. It would not even occur for the 99% quantile initial values, for which a PMP duration of 13h is critical for the reservoir water level. The water level evolution estimates for different PMP durations are shown in Figure 9.27. The inflow and outflow hydrographs of the scenario with 99% quantile initial conditions are shown in Figure E.11. The hourly averaged peak discharge (for a 13h-PMP and the 99% quantile initial conditions) has been estimated to be $Q = 620\,\mathrm{m}^3/\mathrm{s}$.

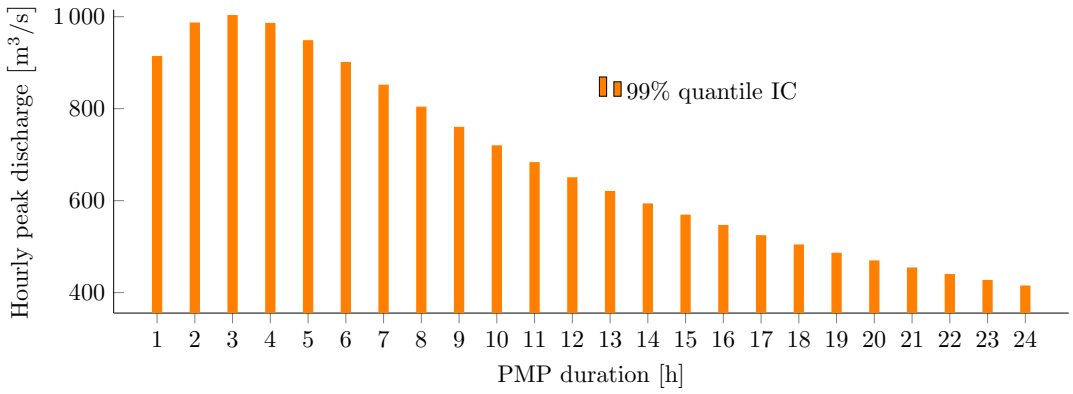

Figure 9.26: Hourly inflow peak discharges derived from different PMP events with wind sector "south". "IC" stands for initial conditions.

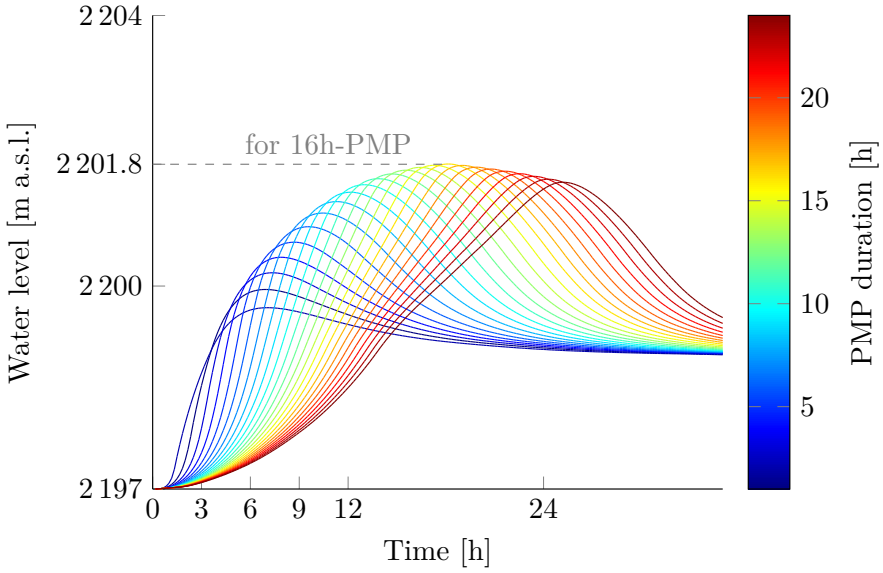

Figure 9.27: Reservoir water level for different PMP events (wind sector "south") for 50% quantile initial values. The maximum level is reached for a 16h-PMP event.

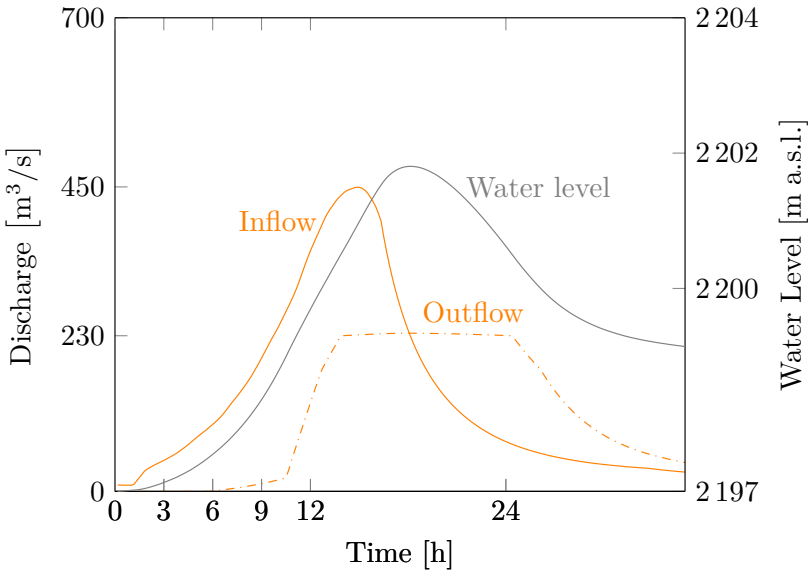

Figure 9.28: Reservoir water level for different PMP events (wind sector "south") for 50% quantile initial values. The maximum level is reached for a 16h-PMP event.

9.5.6 Statistical extrapolation acounting for the estimated PMF

The hydrological model has been used to generate the annual maximum values with an hourly temporal resolution. Figure 9.24 showed, however, that the two major floods from 1993 and 1994 have not been well represented by the model. The flood estimations underestimate these

observations. Boillat and Schleiss (2002) presented reconstructed hydrographs of the two mentioned floods with an hourly time step. The reconstruction was based on data sets of the turbined water volumes and the reservoir level measurements. The peak discharges of these two reconstructed floods have been used to replace the simulated values under the assumption that the detailed analysis of the two mentioned floods, performed by Boillat and Schleiss (2002), better represents the real hourly discharge. The generated data set, used for the fit of the statistical distributions, is shown in Figure E.12. These data have been fitted with the log-normal distribution as well as the GEV and a bounded distribution. For the POT method, a threshold of $u = 26\text{m}^3/\text{s}$ has been determined. This threshold was fixed in order to have at least one value per year. Furthermore, a minimum of 10 days between two peaks has been admitted to be the minimum period to guarantee independence between the events. A total of 87 peak discharges have been determined like this. They are highlighted in Figure E.13. This means that, on average, 2.8 values have been considered per year. According to Tavares and Da Silva (1983), the average number of events per year should be around 2, in order to get the best performance of the POT method. Madsen (1996) concluded that good performances of the POT method can be awaited when the threshold definition results in 2 to 5 values per year.

In Section 9.5.5, the PMF has been estimated to be 1000 m^3/s. This quantity is considered as upper limit for the statistical extrapolation. The sample skewness of the yearly maximum discharge values has been estimated with Equation 2.1. The results, $\gamma = 2.75$, led to the conclusion that, according to Takara and Tosa (1999), the EV4 distribution is most appropriate for the extrapolations. The fitted values using the EV4 distribution is shown in Figure 7.3. The estimated parameters for the different distribution are shown in appendix in Table E.2.

The two above exposed scenarios, i.e. 50% and 99% initial values, with critical PMP durations of 16h and 13h led to maximum hourly average discharge of 450 m^3/s and 620 m^3/s. The statistical extrapolation shown in Figure 7.3 could be used to attribute return periods to the hourly averaged maximum discharges. The 16h-PMP combined with initial conditions being the median values of the state variable values, led to a discharge of 450 m^3/s. The attributed return period is $0.7 \cdot 10^5$ years, according to the EV4 distribution. For the scenario with 99% quantile initial conditions, the derived discharge for a 13h-PMP was 620 m^3/s. The return period of this discharge was estimated to be $0.7 \cdot 10^6$ years, according to the EV4 distribution.

The extrapolation using conventional statistical approaches show significant differences compared to the EV4 distribution. The log-normal distribution is clearly not adapted to fit the data. The extrapolations using GEV and POT show similar shapes. The latter reach the upper bound for return periods of roughly 10^5 to 10^8 years. Due to the slope of the extrapolation curves, a small increase of the return period would induce to highly increase the discharge estimation. Estimation way above the estimated upper bound would thus be possible even for return periods smaller than 10^6 years (considering the GEV distribution), what is clearly a contradiction to the PMP-PMF approach. The GEV and POT can therefore be assumed to unrealistically approach the deterministically determined upper bound. Furthermore, the GEV is returning considerably higher discharge values than the POT method for the same return periods. The EV4 is situated in

between the GEV and POT estimations. Around return periods of 10^7, the EV4 starts to flatten in order to approach the upper bound.

According to the Swiss guidelines for dam safety (SFOE, 2008a), quantity $Q_s = 1.5Q_{1000}$ can be considered as safety flood. In this case, $Q_s = 283.5\,\mathrm{m}^3/\mathrm{s}$. The estimated discharge can be attributed a return period of slightly than 10^4 years according to the EV4 distribution. The safety flood derived under median initial conditions from the 16h PMP has a peak discharge that is roughly 60% higher.

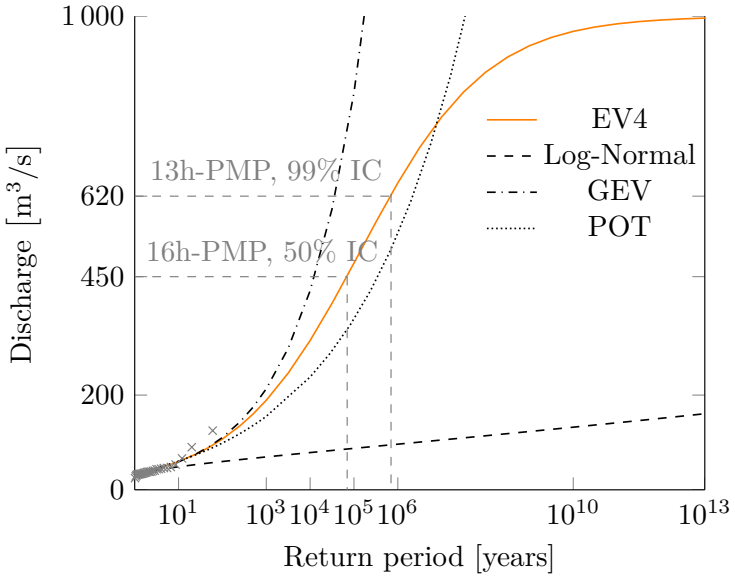

Figure 9.29: Annual maximum hourly discharge data fitted with the EV4 distribution considering an upper bound of PMF=1000 m^3/s.

9.5.7 Intermediate conclusions

It can be concluded that the CRUEX++ methodology led to plausible flood estimates compared to the GEV and POT. As such, it could be successfully applied to the medium size catchment of the Mattmark dam. The simulations allowed to derive the critical combination between assumed initial conditions and the PMP duration after the critical wind sector had been determined. The maximum generated discharge value under very severe initial conditions (99% quantile) has been retained as upper bound for the application of the upper bounded statistical distribution. The extrapolation with the EV4 distribution allowed to attribute return periods to the to simulated scenarios. The return periods of the critical event discharges could be estimated to vary from roughly 10^5 to 10^6 when the initial conditions vary 50% quantile to 99% quantile.

9.6 Application to the Contra dam catchment

The Contra dam catchment has an area of 233 km^2, which it is theoretically outside of the application bounds of the CRUEX++ methodology, as it has been exposed in Chapter 6. The application is nevertheless performed. Therefore, the results have to be contemplated under reserve and do not allow to definitely conclude on an insufficient spillway capacity if the latter would result from the calculations. It can be expected that the precipitation is overestimated since the spatial PMP coverage is slightly to high. The analysis illustrates what could be the observations when the methodology is applied on a catchment with a surface being in the transition zone described in Chapter 6. This is why the analysis is interesting to be conducted.

9.6.1 Description of the catchment of the Contra dam

In this section, the Contra concrete dam (Figure 9.30) and its catchment are presented. The Contra dam is located in the Souther Alps in the canton of Ticino (Figure 9.1). A detailed representation of the main catchment, with an area of 233 km^2, and the discharge measurement stations is presented in Figure 9.31.

Figure 9.30: Photo of the Contra dam (SwissCOD, 2011).

The Contra dam is not connected to lateral intakes and no glacier cover is present or has been present since the beginning of the discharge measurements in the basin. The altitude range of the catchment reaches from around 470 m a.s.l. at reservoir level up to 2864 m a.s.l., the summit

called Pizzo Barone. The spillway capacity of the Contra arc dam is 2150 m^3/s according to SwissCOD (2011). The main characteristics of the Contra dam and its catchment are summarized in Table 9.30.

Table 9.5: Main characteristics of the Contra dam catchment and the reservoir (SwissCOD, 2011)

Reservoirs	
Name	Contra
Canton	Tessin / Ticino
Reservoir surface [km^2]	1.68
Volume (without the volume reserved for sediments) [mio m^3]	94.1
Max spillway discharge [m^3/s]	2150
Max discharge of ground outlet [m^3/s]	340
Spillway crest [m a.s.l.]	470
Dam crest [m a.s.l.]	473.5
Main catchment	
Area [km^2]	233
Glacier cover [km^2]	0
Primary Inflows	Verzasca
Primary Outflows	Verzasca

9.6.2 Meteorological and discharge data

The meteorological data has been provided by MeteoSwiss. For the present study, 11 meteorological stations have been taken into account. At all stations precipitation has been measured, but only at 5 stations temperature measurements have been performed. The overlapping measurement period of the different stations goes from 01/01/1981 to 30/11/2014. Figure C.11 illustrates the periods covered by the meteorological time series for each station. The detailed dates of the begin and end of the time series are given in Table C.5.

Regarding the temporal resolution of the meteorological data sets, values at a daily time step have been available at the stations measuring only precipitation (cf Figure 9.33). For the stations measuring precipitation and temperature, data at an hourly time step was accessible. The daily data has been disaggregated in hourly data sets. To do so, two nearby stations, for which hourly data have been available, had to be chosen. The data of these two stations were then interpolated, using the inverse squared distance weighting, to get an estimate of hourly precipitation at the location of the station to be disaggregated. Finally, the daily measured precipitation volume of the station to be disaggregated has been used to adjust the volume of the generated hourly time series.

The discharge data have been provided by the dam operator Verzasca SA with a daily time step. The covered period reaches from 01/01/1968 to 31/12/2014. Furthermore, hourly measurements have been obtained at two discharge measurement stations handled by the Federal Office for the

Environment (FOEN). These two stations, named Campioi-Lavertezzo and Riale di Pinascia, are situated on the map of Figure 9.31. The periods that have been available from these stations go from 01/09/1989 to 01/11/2014 for Campioi-Lavertezzo and from 01/07/1992 to 01/11/2014 for Riale di Pinascia. Figure 9.32 illustrates the discharge observation periods and allows to compare it to the overlapping period of the considered meteorological stations.

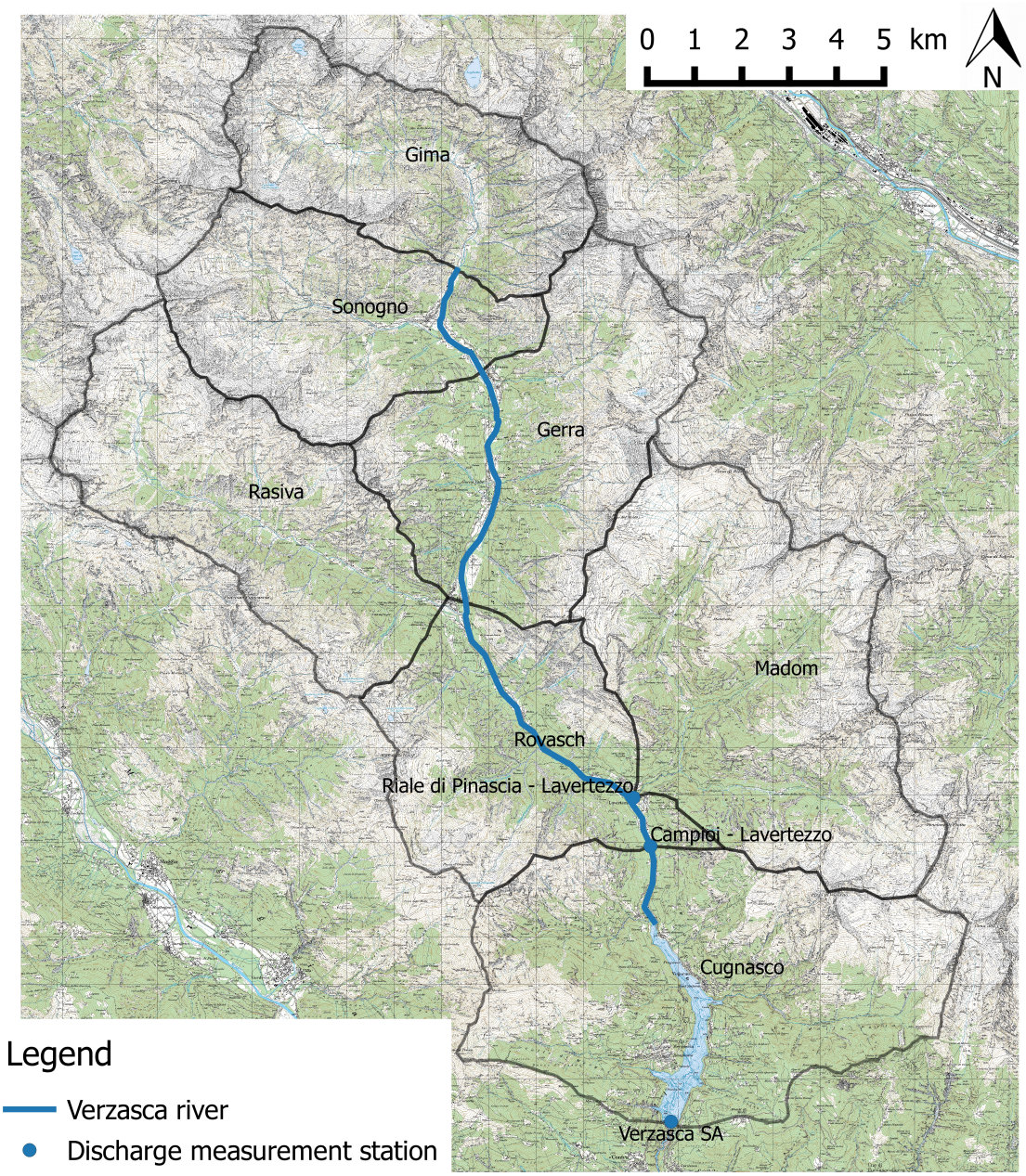

Figure 9.31: Contra dam catchment with discharge measurement stations.

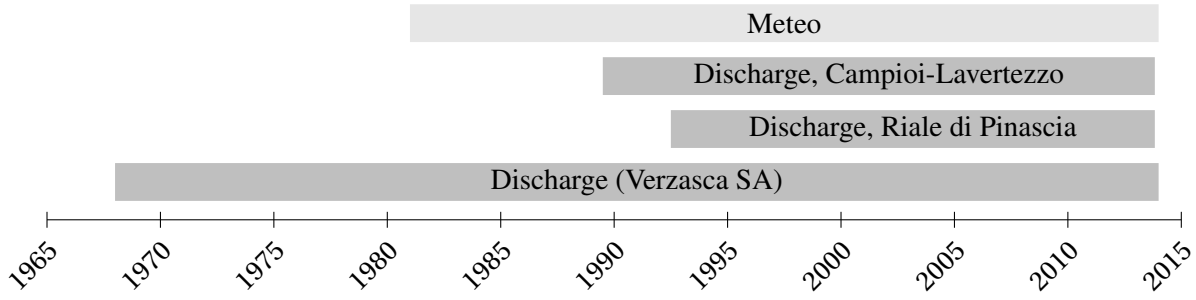

Figure 9.32: Diagram showing the periods of available meteorological and discharge data for the Contra dam modelisation.

9.6.3 Description of the spillway

The spillway of the Contra dam is integrated in the concrete structure. It is composed of 12 standard spillways, 6 on the right and 6 on the left side of the dam. The spillway has been adapted in 1994. The works have been described by Bremen and Bertola (1994). Figure 9.34, taken from the ICOLD publication of Bremen and Bertola (1994), shows that the spillway crest is at 470 m a.s.l. . Three meters higher, the road passing above the spillway limits the free surface flow of the spillway to a water level of 474.5 m a.s.l ($= 470 + \frac{3}{2} h_{cr}$; $h_{cr} = 3$ m being the admissible critical height). Pressurized orifice flow has been admitted for water levels between 474.5 to 474.93 m a.s.l. Above 474.93 m a.s.l., overtopping occurs parallel to pressurized orifice flow. The level outflow relation is plotted together with the level-volume relation in Figure 9.35.

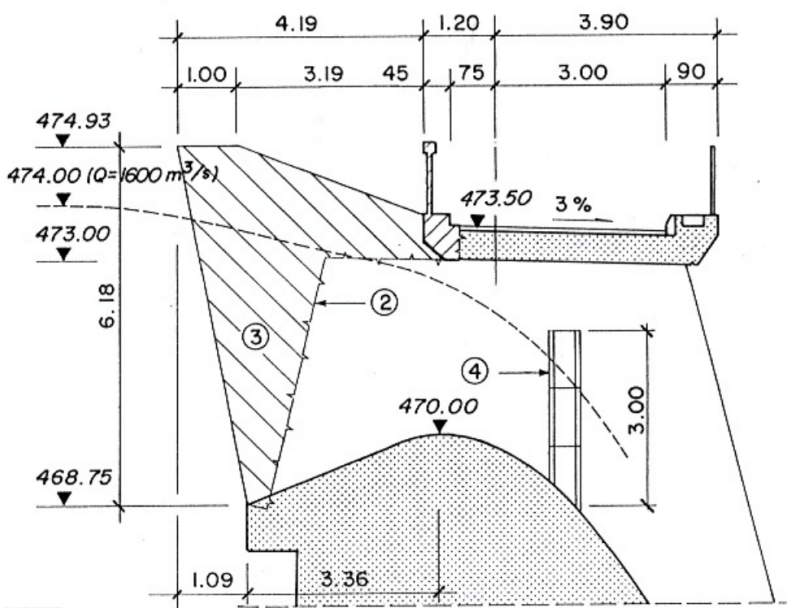

Figure 9.34: Profile of the spillway crest of the Contra dam. The illustration has been published by Bremen and Bertola (1994).

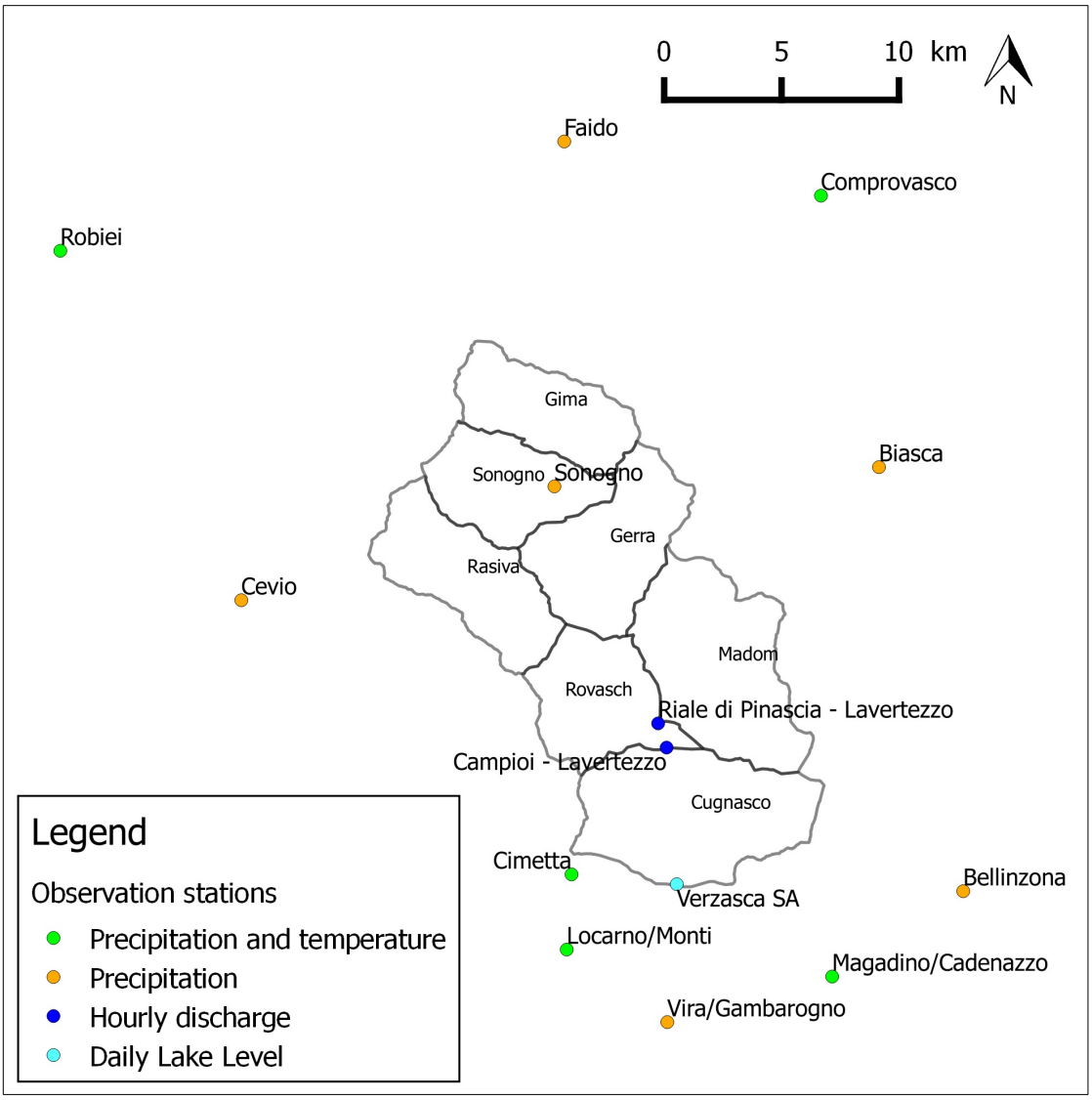

Figure 9.33: Contra dam catchment with discharge and meteorological observation stations.

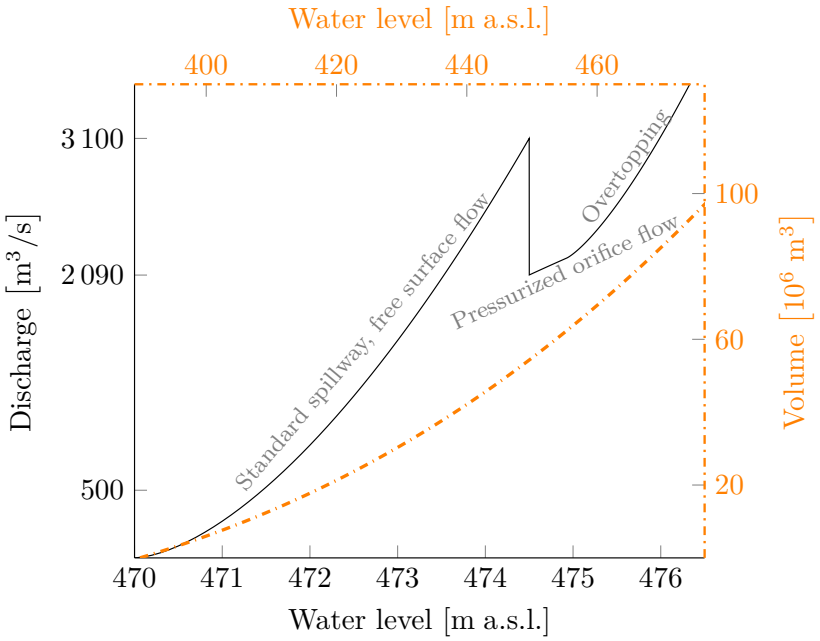

Figure 9.35: Spillway routing curve of the Contra dam and level-volume relation of the reservoir.

9.6.4 Hydrological model design

Due to the considerable size of the catchment, sub-basins have been determined based on topographic maps. Then each sub-basin has been subdivided into altitude bands with a vertical resolution of 300m based on numerical terrain model with a horizontal resolution of 25m. The subdivision in sub-basins is shown in Figure 9.31, the altitude bands are illustrated in Figure E.14. The discharges generated by the different altitude bands are considered to sum at the outlet of the corresponding sub-basin. The outflow of each sub-basin is routed towards the reservoir using the kinematic wave approach.

The level-volume and the level-outflow relation of the Contra dam used for the simulation of the flood attenuation are shown in Figure 9.35. The initial height of the water level has been assumed to be 470 m a.s.l. . This corresponds to full water condition and should be assumed for dam safety verifications according to SFOE (2008a).

9.6.5 Model calibration and validation

The hydrological model has been calibrated and validated based on the available meteorological data as well as the discharge time series presented earlier. Due to the availability of discharge measurements at three different locations, it was possible to subdivide the catchment into three zones. Each zone has been calibrated and validated based on the discharge observations from the closest downstream measurement station.

The calibration period for the three zones goes from 01/10/2003 to 30/09/2014. The validation periods depend on the measurement station. For Campioi-Lavertezzo, the validation period goes from 09/01/1989 to 01/10/2003. The calibrated zone has a surface of 142km^2. For the Riale di Pinascia, the calibration has been validated for the period going from 01/07/1992 to 01/10/2003. The concerned zone has a surface of 44km^2. The validation of the calibration of the zone downstream of the two above mentioned stations has been performed on the daily data set provided by Verzasca SA and covers the period going from 01/01/1981 to 01/10/2003. The surface of the calibrated zone is 47km^2.

The performance coefficients (Nash-Sutcliffe efficiency, Volume ratio, Kling-Gupta efficiency) of the calibration and validation results represented in Figure 9.36 prove that the optimum values of 1 is well approached by each coefficient for each of the three zones. According to the performance coefficient qualification of Moriasi et al. (2007), the model can be qualified as very good regarding the Nash-Sutcliffe efficiency if this coefficient is larger than 0.75. For the observation station Riale di Pinascia, the Nash-Sutcliffe efficiency is less good than for the two other zones. However, this zone has still a good Kling-Gupta efficiency and the volume ratio is as good as for the other two zones. All in all, the performance coefficients let conclude that the model has been well calibrated. The final simulation results compared to the observations are shown in Figure 9.37. It can be seen that the flood events are well represented, with the exception of the flood from 2001. The reason of the lack of reproduction of this flood by the model is the lack of important precipitation observations. If intense precipitation events would have been observed for the concerned period, the flood would probably have been reproduced by the model.

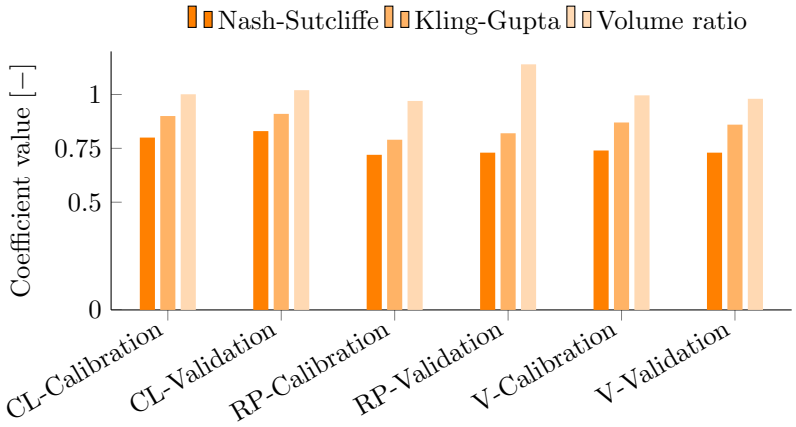

Figure 9.36: Performance coefficients proving the goodness of the hydrological model of the Contra dam catchment. "CL" stands for the station Campioi-Lavertezzo, "RP" for the station Riale di Pinascia and "V" stands for Verzasca SA (inflow discharge deduced from reservoir level measurements).

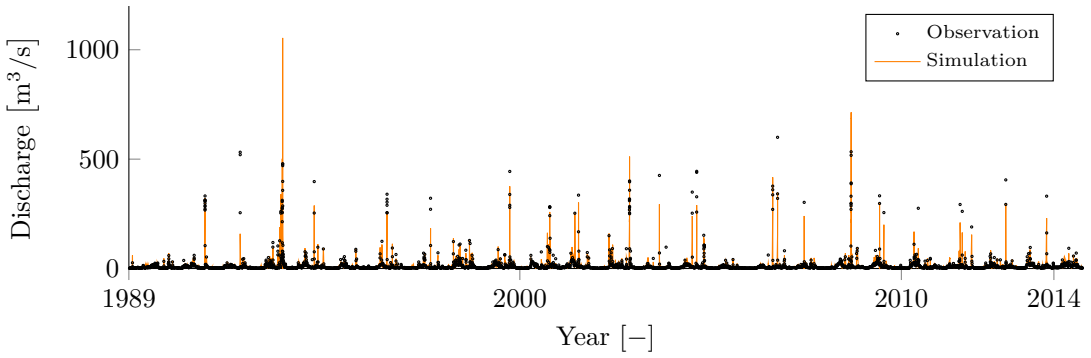

(a) Observations and simulation results with an hourly time step at the discharge measurement station Campioi -Lavertezzo.

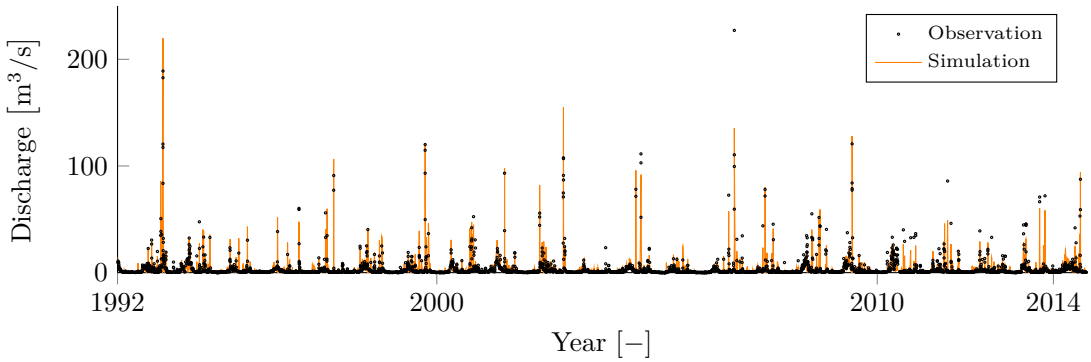

(b) Observations and simulation results with an hourly time step at the discharge measurement station Riale di Pinascia.

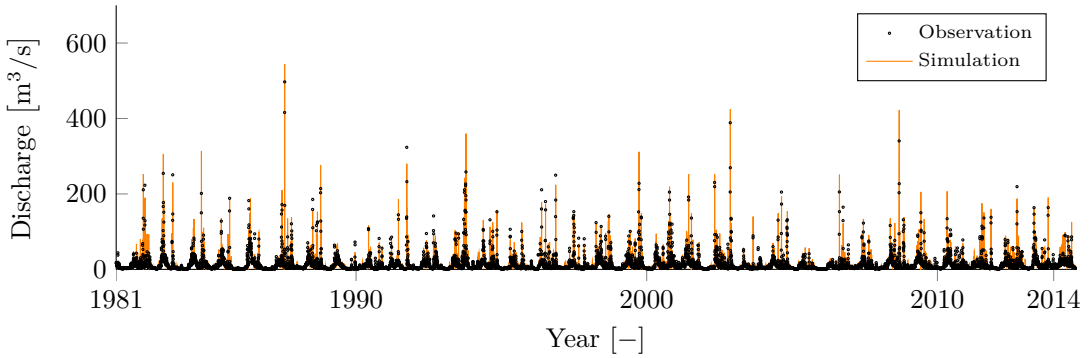

(c) Observations and simulation results with daily time step at the for the inflow discharge into the Contra dam reservoir (Verzasca SA measurements).

Figure 9.37: Comparison between observed discharges and the simulation for the three discharge observation stations, i.e. Campioi-Lavertezzo, Riale di Pinascia and Verzasca SA data.

9.6.6 PMP-PMF simulation

Initial conditions

The initial conditions for the PMP-PMF simulations have been derived by quantile analysis from the state variable values simulated during summer (June - August). The retained values are reported in Table 9.6. It has been distinguished between the different sub-basins due to the important size of the basin. The contemplation of the initial saturation should be made being aware of the calibrated soil infiltration capacity $H_{GR3,max}$ = 0.4 m for the sub-basin Madom, $H_{GR3,max}$ = 0.26 m for the sub-basin called Cugnasco and $H_{GR3,max}$ = 0.26 m for the remaining sub-basins. The values in Table 9.6 indicate very small to non-existent initial snow cover. Therefore, the soil saturation can be considered as main driver among the initial state variables. Consequently, the stochastic approach has not been considered; it can be assumed to return very similar results compared to the deterministic approach.

Temperature for PMP events

The 0°C isothermal altitudes attributed to the PMP events have been derived using Equation 9.3.

$$H = ad + b \tag{9.3}$$

where H is the altitude of the 0°C isothermal altitude in [m a.s.l.], d the duration of the PMP event in [h], $a = -11.554$ [m a.s.l. / h] and $b = 4815.2$ [m a.s.l.] are the parameters for the southern part of Switzerland under summer conditions.

Critical wind direction

The PMP maps have been derived for three different wind sectors. One of these sectors should lead to the most severe PMP event. Figure 9.38 shows the hydrographs derived from a 3h PMP, median initial conditions and temperature conditions corresponding to an isothermal altitude of 4780 m a.s.l.. It can be seen, that in the case of the Contra dam catchment, the highest discharge and volume has been generated by the maps corresponding to the sector "south". The sectors "west-north-west" and "north" return nearly the same results that are considerable lower than the estimates based on the sector "south".

Table 9.6: Summer state variable values (equivalent water height) for the 50% and 99% quantiles considered for the deterministic initialization of the hydrological model of the Contra dam catchment.

Region	State variable	Symbol	50%	99%	Unit
Madom	Snow height	H_s	0	0	[m]
	Snow saturation	θ	0	0	[m]
	Runoff	H_r	0.005	0.06	[m]
	Soil saturation	H_{Gr3}	0.3	0.36	[m]
Cugnasco	Snow height	H_s	0	0.05	[m]
	Snow saturation	θ	0	0.1	[m]
	Runoff	H_r	0.004	0.05	[m]
	Soil saturation	H_{Gr3}	0.148	0.22	[m]
Sonogno	Snow height	H_s	0	0.05	[m]
	Snow saturation	θ	0	0.033	[m]
	Runoff	H_r	0.007	0.07	[m]
	Soil saturation	H_{Gr3}	0.17	0.24	[m]
Gima	Snow height	H_s	0	0.05	[m]
	Snow saturation	θ	0	0.017	[m]
	Runoff	H_r	0.007	0.07	[m]
	Soil saturation	H_{Gr3}	0.17	0.24	[m]
Rasiva	Snow height	H_s	0	0.05	[m]
	Snow saturation	θ	0	0.04	[m]
	Runoff	H_r	0.007	0.06	[m]
	Soil saturation	H_{Gr3}	0.17	0.23	[m]
Gerra	Snow height	H_s	0	0.03	[m]
	Snow saturation	θ	0	0.02	[m]
	Runoff	H_r	0.007	0.07	[m]
	Soil saturation	H_{Gr3}	0.17	0.24	[m]
Rovasch	Snow height	H_s	0	0.05	[m]
	Snow saturation	θ	0	0.03	[m]
	Runoff	H_r	0.006	0.06	[m]
	Soil saturation	H_{Gr3}	0.16	0.23	[m]

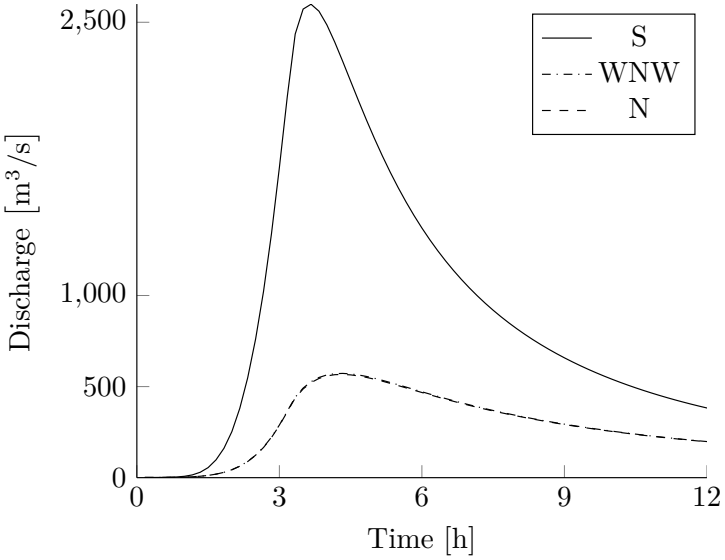

Figure 9.38: Hydrographs derived from 3h-PMPs for three different wind sectors: North (N), South (S) and West-North-West (WNW).

PMF estimates

After the determination of the most critical wind sector, the precipitation duration, generating the highest peak discharge has been determined. PMP durations from 1h to 10h have been simulated. The model has been initialized with the state variable values corresponding to the 99% quantile. The hourly averaged peak discharges are represented in Figure 9.39. It can be seen that the maximum hourly discharge of 4100 m^3/s has been generated by a 3h-PMP. The complete hydrographs, calculated with a time step of 10 minutes, are shown in Figure E.15. Comparing the peak discharge ($Q \approx 4200\,m^3/s$ for a 10 minutes time step) to the envelope curve of Marchi et al. (2010), described by the formula $Q_E = 97A^{0.6} = 2550\,m^3/s$, it can be stated that the ratio $\frac{Q}{Q_E} = 1.65$ would not lead to the conclusion of a significant overestimation of the PoMF. Such a verification is useful as the catchment is outside of the transition zone of the application limits of the Swiss PMP maps.

It has been retained that median initial conditions would be considered for the estimation of a safety flood. The critical PMP duration for the safety flood corresponds to the duration of the precipitation event that leads to the highest reservoir level. Figure 9.40 illustrates that the maximum reservoir level is reached for a PMP duration of 8h. The corresponding inflow and outflow hydrographs as well as the reservoir level evolution is shown in Figure 9.41. Thanks to the works undertaken to increase the spillway capacity of the Contra dam, described by Bremen and Bertola (1994), the 8h-PMP event combined with median initial conditions does not lead to overtopping. The hourly peak discharge corresponding to the safety flood has been estimated to be 2568 m^3/s. The return period of such a discharge has been estimated in section 9.6.7.

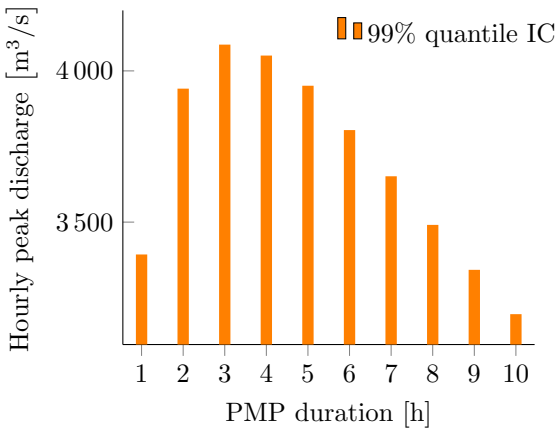

Figure 9.39: Hourly inflow peak discharges derived from different PMP events with wind sector "south" for the Contra dam catchment. "IC" stands for initial conditions.

9.6.7 Statistical extrapolation accounting for the estimated PMF

For this case study, hourly discharge data have been available. The discharge observation station Campioi-Lavertezzo (Figure 9.33) is situated inside the basin and measures the discharge generated by a catchment of $186 km^2$. This corresponds to 80% of the total catchment surface (A=$233 km^2$). It has been assumed that the flood discharges are proportional to the square root of the catchment area. The peak discharges observed at Campioi-Lavertezzo have been multiplied by $\sqrt{\frac{A_{tot}}{A_{CL}}} = 1.12$ ($A_{tot} = 233\ km^2$ is the total catchment area and $A_{CL} = 186\ km^2$ is the catchment area upstream of the Campioi-Lavertezzo observation station) to estimate the peak discharges at the outlet of the entire catchment.

The data set, used for the fit of the statistical distributions, is shown in Figure E.16. In the previous section, the hourly averaged PMF has been estimated to be 4100 m^3/s. This quantity has been considered as upper limit for the statistical extrapolation. The sample skewness of the yearly maximum discharge values has been estimated with Equation 2.1 to be $\gamma = 0.03$. This leads to the conclusion that, according to Takara and Tosa (1999), the LN4 distribution is most appropriate for the extrapolations. The fitted values using the LN4 distribution is shown in Figure 7.3. Furthermore, the more conventional GEV and log-normal distributions have been fitted. The POT method has been applied as well. A threshold of $u = 180\ m^3/s$ has been considered. This induces a data set, illustrated in Figure E.17, with 2.3 values per year. According to Tavares and Da Silva (1983), the average number of events per year should be around 2, in order to get the best performance of the POT method. Madsen (1996) concluded that good performances of the POT method can be awaited when the threshold definition results in 2 to 5 values per year. Figure 7.3 also shows the results of the three latter extrapolations. The estimated parameters for the different distribution are shown in appendix in Table E.3.

The statistical extrapolation using LN4, shown in Figure 7.3, has been used to attribute a return

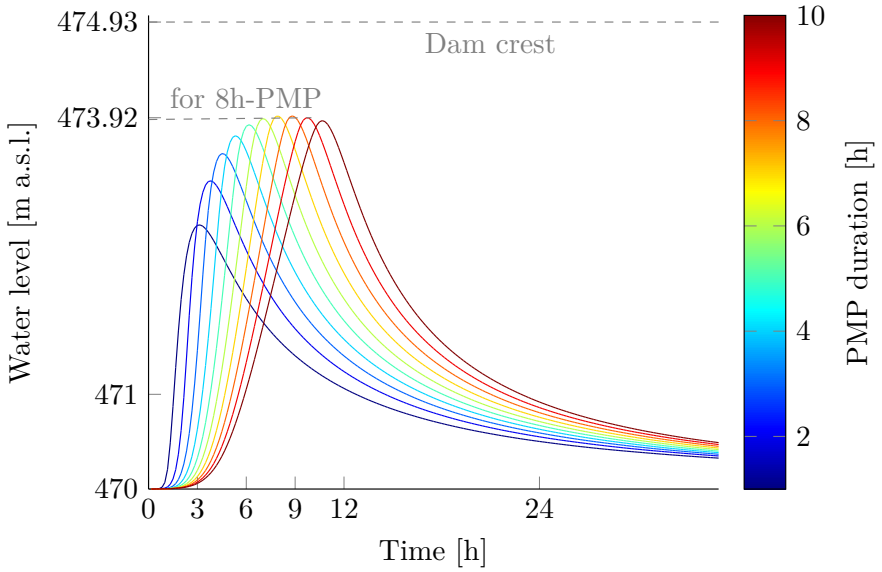

Figure 9.40: Contra dam reservoir level for different PMP events (wind sector "south") for 50% quantile initial values. The maximum level is reached for a 8h-PMP event.

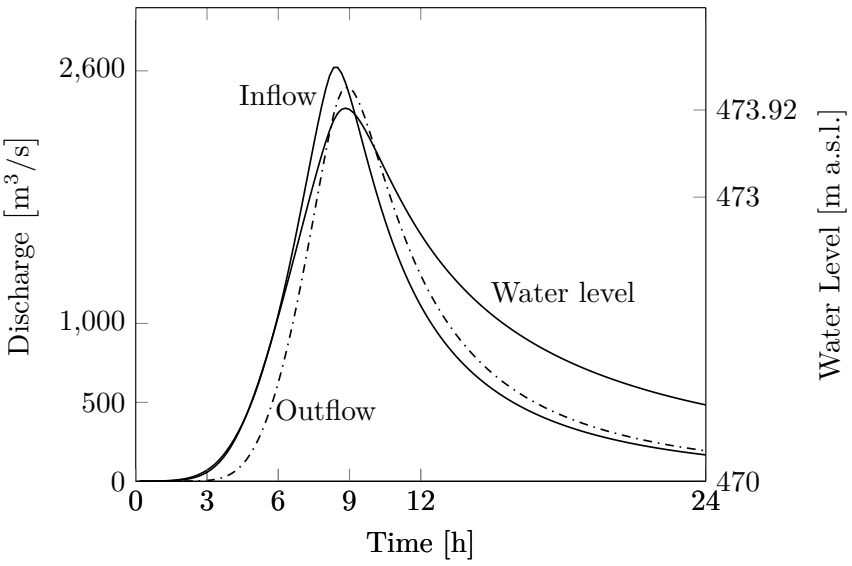

Figure 9.41: Inflow and outflow hydrographs with corresponding reservoir water level for a 8h-PMP event and median initial conditions.

period to the hourly averaged maximum discharge of the safety flood. The 8h-PMP combined with initial conditions being the median values of the state variable values, led to a discharge of 2568 m^3/s. The attributed return period is $1.7 \cdot 10^7$ years.

The LN4 distribution and POT method return the most similar extrapolations. The LN4 estimates are higher than the POT estimates for a certain return period. The log-normal distributions tends to overestimate the discharge for a certain return period compared to the LN4 distribution. The fact that the log-normal distribution reaches the PMF, assumed as upper limit, already for a return period of approximately 10^6 does not lead to much confidence in this extrapolation. In fact, the log-normal distribution overestimated the floods probably due to the fact that it only has two parameters. The fit of a two parameter distribution to a sample is only little influenced by larger values (DWA, 2012). The distribution is less flexible than a three parameter distribution and can thus in some cases not be fitted satisfactorily to the sample (DWA, 2012).

Regarding the GEV, the low skewness of the sample leads to a weibullian behaviour of the GEV ($\xi < 0$), meaning that it tends to a limit value. Therefore, compared to LN4 and POT, the GEV can be considered to underestimate the discharge estimates for high return periods.

According to the Swiss guidelines for dam safety (SFOE, 2008a), the quantity $Q_s = 1.5Q_{1000}$ can be considered as safety flood. In this case, $Q_s = 2100\ m^3/s$. The estimated discharge can be attributed a return period of slightly than $3 \cdot 10^5$ years according to the LN4 distribution. The safety flood derived under median initial conditions from the 8h-PMP has a peak discharge that is roughly 20% higher. Both estimations are close and coherent.

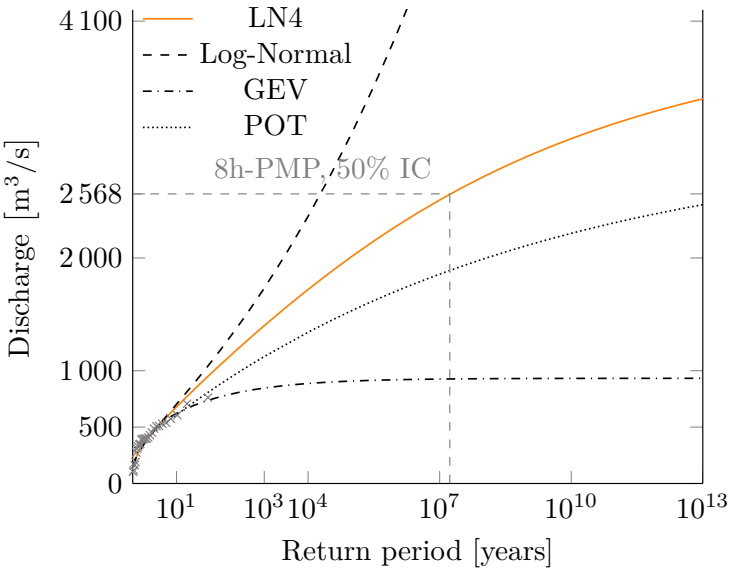

Figure 9.42: Annual maximum hourly discharge data fitted with the LN4 distribution considering an upper bound of PMF=4100m^3/s.

9.6.8 Intermediate conclusions

The case study of the Contra dam could show that the upper bounded statistical distribution LN4 gave more conservative estimates than the GEV and POT approach. The LN4 gave, however, smaller flood estimates than the log-normal distribution. The latter seems indeed not adapted for this case, as it has been mentioned earlier. The same conclusion can be drawn for the GEV, but for a different reason. The shape of the fitted distribution would simply not allow to attribute a reasonable return period to the PMF. thus the GEV does not seem adapted for the present case study, under the assumption that the PMF approach is valid.

The Contra dam catchment is slightly outside of the application limits for the CRUEX++ methodology that has been determined in Chapter 6. Therefore, an overestimation of the precipitation volume could have been occurring. Nevertheless, overtopping was not simulated for the considered safety flood. The outflow discharge, however, is larger than the spillway capacity given by SwissCOD (2011) (cf Table 9.5).

The return period estimated for the considered safety flood is $1.7 \cdot 10^7$ years. The return period of the quantity $Q_s = 1.5Q_{1000}$ has also been estimated. It can be retained that the return period of $3 \cdot 10^7$ years would also fulfil the requirements of the Swiss dams safety guidelines (SFOE, 2008a) that demand that the safety flood has to be much higher than the 1000 years.

9.7 Conclusions

In this chapter, the CRUEX++ methodology has been applied to three different dams. The catchments are differing in size, geographical situation and glacier cover. This allowed to apply the methodology to basins with different characteristics.

Comparing the results of the three case studies, i.e. Limmernboden, Mattmark and Contra, it can be concluded that the **return periods** estimated for the safety floods are **corresponding to the order of magnitude of the return periods associated to the PMF in literature**, i.e. 10^4 - 10^9 years (Cluckie and Pessoa, 1990; Resendiz-Carrillo and Lave, 1990; Shalaby, 1994; Smith, 1998; Hogg et al., 2004; Harris and Brunner, 2011; McClenathan, 2013). The range of these return periods is, however, very large. The uncertainty on its estimation is thus considerable. Generally, these return periods are estimated for PMF estimates that are assumed reasonable. It is normally not considered to be the possible maximum flood, but the probable maximum flood. The assumption of reasonable initial conditions (median state variable values) made for the applications performed in this chapter led to return periods from 10^5 to 10^{11} years.

The largest return period has been determined for the case study of the Limmernboden dam. Different aspects let assume that the estimation of the safety flood having this return period is not exaggerated. A ratio of 1.3 between the simulated safety flood and $Q_s = 1.5Q_{1000}$ is reasonable. The uncertainty of Q_{1000}, in the case of Limmernboden, should be small in this case as all applied statistical distributions agreed on its estimation. Furthermore, the rather small slope of

the extrapolation curve induces a considerable uncertainty on the estimate of the return period. Indeed, a small change of the discharge value leads to a large change of the related return period.

The advantage of the CRUEX++ methodology is that the combination of statistics and simulation form a holistic model that allows the estimation of the **discharge return periods and the hydrographs**. The eventual lack of extreme discharges in the observed time series induce conventional statistical approaches to over or underestimate the floods with a high return period. The **causal information expansion** performed in the CRUEX++ methodology allows to overcome this disadvantage. An example of this benefit can be illustrated by considering the extrapolation using the GEV and the log-normal distribution in the case of the Contra dam, discussed earlier. In this application, the GEV could be identified to underestimate the flood discharges and the log-normal distribution was discussed to overestimate the latter. The CRUEX++ methodology allowed in this case to generate flood estimates in between the two doubtful extrapolations. Consequently, the credibility of the result could be significantly increased. It is perhaps not very dexterous to speak about credibility in the context of the Contra dam as it is situated outside of the application limits of the methodology. However, two things should be remembered. The catchment size is only slightly outside of the maximum admissible size and the determination of the upper area has been based on only 13 catchments, what induces a certain uncertainty on the estimated upper admissible catchment area. In the context of the argumentation on the extrapolation performed on the data of Contra, the sensitivity of the bounded extrapolation to the upper bound should not turn this conclusion in its contrary as the sensitivity of LN4 extrapolations to the estimation of the upper bound, discussed in Chapter 7, are rather small.

Similar advantages could be found for the Limmernboden and Mattmark case study. In the case of the Limmernboden dam, the LN4 distribution could avoid underestimations from a return period of 10^3 years on. Especially the classical extreme value theory, postulating the usage of GEV and POT, was underestimating the flood discharges. The attribution of a return period to the safety flood was not even possible with these methods. The extrapolation to the simulated safety flood discharge would induce extremely high and unrealistic return periods, whereas the LN4 and log-normal distribution could show a similar behaviour and led to satisfactory results. For the case study of Mattmark, the extrapolation using the EV4 distribution could avoid to approach the deterministically estimated upper bound in an unrealistic manner as it could be observed and described for the GEV and POT method in section 9.5.6.

Finally, it can be concluded that the CRUEX++ methodology led to the most satisfactory results since unrealistic over and underestimations obtained by conventional statistical approaches could be overcome. **The combination of the statistics and the simulation based approach has the advantage to increase the plausibility of the results.**

10 Conclusions and perspectives

10.1 Main conclusions

The CRUEX++ methodology had to compromise about scientific feasibility and pragmatic practicality as it is destined to be utilized by engineers engaging reasonable investment of time and effort yet guaranteeing the reliability of the results. In the present context, a compromise unavoidably leads to the disregard of some scientific details in favour of the practicality. Consequently the methodology embodies uncertainties and limitations, but was ultimately advantageous compared to the conventional approaches.

After an extensive literature review, relevant methods for extreme flood estimations could be identified. However, what could be found in literature was not sufficient to satisfy the demand of clarification in the context of extreme flood estimations for Swiss dam safety verifications. The literature review rather brought up some research questions whose answers could contribute to the closure of the lack of knowledge. There was a strong need to:

1. enhance the comprehension of temporal rainfall structures and its regional, seasonal and precipitation duration related variability (the spatial structure has not been treated in this research project, it is discussed in Section 10.2 as future work);

2. determine temperature conditions that can be assumed coherent with event based PMP-PMF simulations;

3. address the possibility of a systematic choice of initial terrain conditions for PMP-PMF simulations and to better understand their influence on the PMF estimates;

4. investigate the robustness of upper bounded statistical distributions in terms of sensitivity to both the upper bound and the sample;

5. formulate an integrated holistic methodology for extreme flood estimation in Alpine catchments.

All mentioned issues could be addressed through the different analyses conducted in this research project. A holistic methodology for extreme flood estimation could be formulated taking into account the following findings:

1. The temporal distribution of the PMP can be performed using a rainfall mass curve standardized for Switzerland.
2. The linear relation function between the precipitation duration and the related maximum observed 0°C isothermal altitude can be considered to attribute temperature conditions to the PMP event.
3. Moving towards hydrological simulation, if a single state variable is dominating the hydrological processes, the initial conditions for the hydrological PMP-PMF simulation can be estimated by the 99% quantile values of the state variable time series from continuous simulations to derive the PoMF (possible maximum flood). Smaller quantiles can be used to simulate a safety flood (PMF). If more state variables are effecting the simulated discharge, the a stochastic approach taking into account the dependence of the state variables has to be used. The decision on which approach to consider can be made based on a sensitivity analysis to quantify the influence of the state variables on the simulated discharge and thus the number of dominating variables.
4. The maximum admissible spatial coverage of 230 km^2 for the PMP events derived from the Swiss PMP maps has been determined.
5. The combination of statistical approaches with the PMP-PMF concept through upper bounded statistical distributions can enhance the plausibility of the estimation of the return period of extreme floods.

In fact, the PMP-PMF approach and the upper bounded statistical distributions are both based on the hypothesis of a physical upper discharge limit. Their combination is thus leading to a holistic and coherent methodology.

10.1.1 Temporal precipitation structures using rainfall mass curves

The determined 5% quantile rainfall mass curve is used to temporally distribute the PMP data. The curve is applicable for the entire territory of Switzerland.

The hydrological application performed to analyse the influence of the rainfall mass curves on the hydrographe and the reservoir water level could show that the rainfall mass curve seasonal, geographical and event duration related variations do not have a significant effect. The influence on the reservoir level could be shown to be even smaller than on the hydrograph. The estimated

peak discharge ratios between the hydrographs generated based on the different rainfall mass curves ranged from 3% to 16%. In regard to the peak level ratios, they were smaller than 1.8%. These ratios have been considered to be sufficiently small to justify the simplification of the temporal rainfall structuring by using the same quantile rainfall mass curves for the entire territory of Switzerland.

The determined 5% quantile rainfall mass curve, derived from an ensemble of rainfall mass curves, leads to late bursting precipitation events . In this way, the soil is wetted considerably before the arrival of the peak of the hyetograph. When the precipitation reaches the intensity peak, the wetted soil leads to higher discharge compared to an earlier burst. This effect can of course be intensified when using rainfall mass curves that are even more severe than the 5% quantile curve. Furthermore, the distribution of the precipitation using rainfall mass curves assumes a stationary event. This assumption is conservative but coherent with intense precipitation events, according observations reported by the World Meteorological Organization (WMO, 2009).

10.1.2 Temperature conditions in terms of 0°C isothermal altitude depending on the precipitation duration

The linear relation $H = ad + b$ between the 0°C isothermal altitude H and the precipitation duration d is used to attribute temperature conditions to an extreme precipitation event. The parameters a and b depend on the season (summer, autumn, winter, spring) and on the geographical situation (north or south of the Alps).

Regarding the temperature conditions for PMP-PMF simulations, the scaling of precipitation intensity as a function of the 0°C isothermal altitude and of precipitation duration let to the three following conclusions:

1. An upper limit for precipitation intensity due to negative scaling above a certain 0°C isothermal altitude (or, equivalently, temperature) could not be clearly identified.
2. The maximum measured 0°C isothermal altitude showed a strong seasonal dependence. Slight differences between the northern and southern part of Switzerland could be noted as well.
3. A linear relation between the maximum measured isothermal altitude and the precipitation duration could be observed for the four seasons.

It could be retained that seasonal considerations might play a crucial role for the choice of the 0°C isothermal altitude for extreme flood simulations. The peak of the simulated flood may be attenuated when critical events are simulated during seasons with a lower isothermal altitude,

especially in mountainous regions, where snowfall could occur. It should be remembered that the Swiss PMP maps apply to summer conditions. It can thus be expected that, for most catchments, no snowfall is occurring during a PMP-PMF simulation. In high alpine catchments and for longer PMP events, snowfall can, however, not be excluded in summer.

10.1.3 Initial conditions for PMP-PMF simulations

Th initial conditions can be determined by a deterministic (not accounting for state variables dependences) and a stochastic (accounting for variable dependences) approach. If one state variable is dominating the hydrological routing, the deterministic approach can be used. If more than one state variables guide the flood generation the stochastic approach should be preferred.

A stochastic and a deterministic approach have been considered for the determination of the initial conditions. Two dominant state variables could be identified for the GSM-SOCONT model. The initial saturation and snow height could be shown to be the principal drivers among the state variables, at least for flood simulations. If the considered season has no snow, saturation mainly guides the peak discharge of the simulated flood. In this case the deterministic and stochastic approach lead to equivalent results, presupposed that eventual initial conditions of the glacier are not significant. Due to the overall high impact of the initial conditions on the simulated flood hydrograph, a detailed analysis of the simulated state variable time series should always be performed. In case of doubt, concerning the interaction between state variables, the stochastic approach should be preferred.

10.1.4 Upper catchment surface limit

The maximum spatial expansion of PMP events derived from the Swiss PMP maps is 230 km^2*. The catchment surface should therefore be smaller than 230* km^2 *to apply the CRUEX++ methodology.*

It could be shown that the PMP-PMF simulation results were in agreement with discharge-catchment surface relationships found in literature up to a certain catchment size. Above this catchment size, the simulation results showed a significantly different behaviour from what has been reported in literature. The reason is that the assumed expansion over the entire catchment of the PMP event, derived from the Swiss PMP maps, is not realistic any more. The surface limit, above which a reduction factor derived from area-depth curves should be taken into account, is reached. The application of such a factor is however not straight forward in the context of the PMP maps. This issue is further discussed in Section 10.2.

The detected upper surface limit has been considered to mark the applicability limit of the Swiss PMP maps. The assumption of a PMP event precipitating simultaneously over the entire catchment cannot be justified over a larger area.

The analysis let to the conclusion that the surface limit is represented by a transition zone rather than a single value. Due to the chosen approach to argue on the generated discharge, depending on the initial conditions of the simulations, the invariance of the determined zone to the chosen initial conditions had to be proven. Therefore, two initial condition scenarios have been considered, i.e. 50% and 95% quantile state variable values. For the two scenarios, the transition zone has been determined. The two resulting zones showed slight differences. The determined zone reaches from 75 to 210 km^2 for the 99% quantile initial conditions and from 120 to 230 km^2 for the 50% quantile initial conditions. These differences are assumed to be related to model uncertainty.

Comparing the catchment sizes defining the transition zone to the catchments of Swiss dams, it could be retained that the PMP maps should applicable to roughly 90% of the 300 Swiss dams being under direct federal and cantonal supervision.

10.1.5 Towards a holistic model through upper bounded statistical distributions

The combination of simulated floods and statistical approaches could be reached through the usage of upper bounded statistical distributions. The PoMF is used as upper bound. In this way, the plausability of the estimation of high return periods is increased.

Upper bounded distributions have been identified in literature as very interesting in the context of this research project as they allow to construct a holistic model combining the estimation of return periods with the simulation of flood hydrographs. The benefit of these distributions can, however, only be guaranteed if they increase the robustness of statistical extrapolations compared to the conventional statistical approaches.

The sensitivity analysis conducted on the extrapolated sample through a bootstrapping approach and on the estimation of the upper bound could illustrate the benefits of the causal information expansion performed through the deterministic estimation of the upper bound. It could be confirmed that the causal information expansion due to the consideration of the PoMF for statistical extrapolations using upper bounded distributions enhances the robustness of the extrapolations. Furthermore, unrealistic over and under estimations can be avoided using upper bounded statistical distributions with an a priori determined upper bound.

10.1.6 Formulation of the CRUEX++ methodology

The CRUEX++ methodology is applicable to Swiss alpine catchments and allows to combine the PoMF estimates with a statistical approach in order to attribute return periods to the simulated

safety flood peak discharge. Case studies could show application examples for three basins with different catchment sizes. The CRUEX++ methodology could be successfully applied to the catchments of the Limmernboden, Mattmark and Contra dams. The return periods attributed to the peak discharges of the floods (10^5-10^{11} years), simulated in this research project, taking into account PMP map data and 50% initial conditions are in line with the order of magnitude of the return periods attributed in literature to PMF values.

Discussion of the methodology

Despite the advantages of the CRUEX++ methodology some drawbacks have to be mentioned. It has been discussed that climate change has not been taken into account. This induces that the CRUEX++ methodology is only valid for current climatic conditions. However, effects of climate change on the simulated floods can be assumed smaller than methodological uncertainties. Climate change is thus secondary at the current state. Besides this general limitation, more focussed limitations have been discussed.

The temporal rainfall distribution, using quantile rainfall mass curves, can lead to severe temporal structures when considering, for example, the 5% quantile rainfall mass curve. This is the quantile curve that has been considered for the case studies. However, it may not represent the most severe distribution that can be imagined. Therefore, the possible maximum flood estimate can be larger when smaller quantiles would be considered.

Concerning the relation linking the precipitation duration to the 0°C isothermal altitude (or equivalently the temperature), it could be discussed that the resulting temperature may be overestimated and consequently the flood may be as well, the melting processes being intensified. In regard to the initial conditions, the chosen values depend on the simulation and thus on the observed meteorological events. Consequently, in absence of rare observed events, the determined initial conditions can be mistakenly thought to be severer as they are in reality.

Concerning the extreme flood simulations, the model is assumed to be valid for events that are more severe than those the model has been calibrated on. This assumption is necessary and can not be bypassed. However, if long time series are available for the calibration and validation phases, it can be assumed that extreme events do not lead to unseen hydrological processes. Furthermore, the methodology assumes that the configuration of the basin is not changing during an extreme event, what may not be the case in reality.

10.2 Perspectives on future work

Regarding the **temporal rainfall distribution**, the CRUEX++ methodology is based on rainfall mass curves assuming stationary events. The spatial distribution is admitted to be provided by the PMP maps. In the context of IDF use, observed events can be scaled, keeping the spatial distribution of the measured event. Normally, rainfall events are not perfectly stationary,

but change in time and space simultaneously. This spatio-temporal event distribution may be further analysed in the future. Enhancement of the understanding of the spatio-temporal distributions of extreme precipitation events may be reached if radar driven analyses would be performed. Analyses of this type would be valuable for the utilization of spatio-temporal rainfall distribution models such as the MPF model developed by Receanu (2013). Once the spatio-temporal precipitation distribution is better understood, the possibility of extending the applicability limits of the CRUEX++ methodology can be addressed. Furthermore, the spatial distribution of precipitation events deduced from the PMP maps and the IDF curves can be harmonized.

If radar data are not accessible for the analysis of the **spatio-temporality of precipitation events**, the spatial distribution of precipitation events should be analysed nonetheless. Spatial structuring methods like for example the Thierssen polygon, Kriging or the inverse distance approaches should be analysed for their performances in the context of extreme flood estimates. Depth-area curves, taking into account the duration of the precipitation events, would also be valuable elements for the spatial precipitation distribution.

Concerning the temperature-precipitation relations, future work could account for the **evolution of the temperature** during a precipitation event to refine the melt process simulations and enhance the precision of the quantity of melt water. Due to the rather sparse executions of meteorological soundings (only two per day), used for the determination of the temperature-precipitation relations in this study, this issue could not be addressed in this research project. In addition, the distinction of different precipitation types could be accounted for in order to analyse its influence on the scaling results, in particular on the relationship between the precipitation duration and the 0°C isothermal altitude. An interesting approach for the distinction of precipitation types by considering the presence of lighting (identification of convective events) has been used in Switzerland by Molnar et al. (2015) and Molnar et al. (2016).

The last step of the CRUEX++ methodology is the attribution of a return period to the simulated discharge peak by means of upper bounded statistical distributions. However, this step is in a few aspects limiting. First, the flood event is not only characterized by its peak discharge but more importantly by its volume. Statistics on flood volume or even copula models for the **bivariate peak-volume analysis** could be used to better describe the probability of the simulated event. Second, the estimation of the flood peak return period is straightforward, whereas the determination of an event with a certain return period may be iterative and lead to multiple simulations. The issue would be to determine the initial conditions that lead to the aimed peak under the assumption of a certain precipitation event, or the other way around, to determine the precipitation event that leads to the targeted discharge under the assumption of a certain initial conditions set. This reflection leads to the concept of stochastic event-based flood simulations with multiple precipitation events crossed with numerous initial conditions in order to determine the event leading to the critical lake level. Together with the concept of bivariate copula laws that can model the probability of a discharge-volume couple (Genest and Favre, 2007; Gaál et al., 2015; Brunner et al., 2016), this approach could be interesting for the attribution of a return

period to the event and not only to one dimension of the event. A two-dimensional frequency analysis could be particularly interesting for risk analysis related to dam safety.

When dwelling on risk, uncertainty should be mentioned. Approaches like GLUE (Generalised Likelihood Uncertainty Estimation) allow to account for **model parameter uncertainty** (Beven and Binley, 1992, 2014). This approach was applied by Blazkova and Beven (2004) in the context of dam safety assessments with a stochastic rainfall generator taking PMP estimates into account. The issue of model uncertainty has not been addressed in this research project. However, when simulating flood events that are way beyond the observed events the model has been calibrate and validated on, model parameter uncertainty may be very important for assessing the reliability of the simulation results. At the current state of the CRUEX++ methodology, the hydrological model is assumed to be valid for events larger than those the model has been trained on. Estimating model uncertainty could be a beneficial extension of the methodology because the quantification of uncertainty is an indication of reliability. Other sources of uncertainty are of course existing. Besides the uncertainty linked to the observation measurements used to calibrate the hydrological model, uncertainty can come from the design storm estimation and from the eventually too short time series used for statistical extrapolations. Furthermore, uncertainty linked to the change of hydrological processes during an extreme flood event and other unmodelled processes is an issue for extreme flood estimations. For instances, events like landslides, creating natural dams that can alter the course of the river or even break and lead to a tsunami-like wave entering the dam reservoir, could be one of them. Such events could additionally lead to driftwood clogging the spillway of the dam. Together with an extreme flood inflowing into the lake this may lead to over-topping. Other aspects like the sudden emptying of water pockets trapped in glaciers has not been taken into account in this research project. The integration of different uncertainty types and sources may be a constructive completion of the CRUEX++ methodology.

Climate change has not been taken into account for this research project because the effect of climate change has been assumed smaller than other methodological uncertainties and had thus only a secondary importance. Furthermore, present uncertainty and contradictions in climate projections make the formulation of a pragmatic methodology for practitioners impossible. However, if future research in the domain of climate change and its consequences on meteorological phenomena start to converge, the methodology should be updated according to the new findings. For instances, in the context of climate projections using GCMs (General Circulation Model), Giorgi et al. (2016) could contradict earlier results by showing that the global GCMs are not well representing the consequences of climate change for precipitation in Alpine regions. The spatial resolution has to be finer for topographically complex zones. Together with the findings concerning climate change influences on PMP estimates, GCMs with a sufficiently fine spatial and temporal resolution could be used to re-evaluate the Swiss PMP data under a changing climate. For example, Kunkel et al. (2013) and Stratz and Hossain (2014) found that climate change may lead to higher PMP estimates. Complete PMP events, simultaneously taking into account precipitation-temperature relations and spatio-temporal characteristics due to different wind directions as well as topographic influence could be generated. The comparison of these completely coherent simulated PMP events could be used for comparison with the PMP events

and the related temperatures as proposed in the CRUEX++ methodology.

Bibliography

Apel, H., Merz, B., and Thieken, A. H. (2009). Influence of dike breaches on flood frequency estimation. *Computers & Geosciences*, 35(5):907–923.

Apel, H., Thieken, A. H., Merz, B., and Blöschl, G. (2006). A Probabilistic Modelling System for Assessing Flood Risks. *Natural Hazards*, 38(1):79–100.

Arnaud, P. and Lavabre, J. (2000). La modélisation stochastique des pluies horaires et leur transformation en débits pour la prédétermination des crues. *Revue des Sciences de l'Eau / Journal of Water Science*, 13(4):441–462.

Arnaud, P., Lavabre, J., and Masson, J.-M. (1999). Amélioration des performances d'un modèle stochastique de génération de hyétogrammes horaires: application au pourtour méditerranéen français. *Revue des Sciences de l'Eau / Journal of Water Science*, 12(2):251–271.

Aronica, G. T., Candela, A., Fabio, P., and Santoro, M. (2012). Estimation of flood inundation probabilities using global hazard indexes based on hydrodynamic variables. *Physics and Chemistry of the Earth, Parts A/B/C*, 42–44:119–129.

Aubert, Y. (2012). *Estimation des valeurs extrêmes de débit par la méthode Shyreg: réflexions sur l'équifinalité dans la modélisation de la transformation pluie en débit*. PhD thesis. Université Pierre et Marie Curie.

Audouard, A., Hertig, J.-A., and Fallot, J.-M. (2006). Modélisation des précipitations extrêmes en Suisse. *Actes du 19e colloque de l'Association Internationale de Climatologie*, pages 83–88.

Azli, M. and Rao, A. R. (2010). Development of Huff curves for Peninsular Malaysia. *Journal of Hydrology*, 388(1–2):77–84.

Back, A. J. (2011). Time distribution of heavy rainfall events in Urussanga, Santa Catarina State, Brazil. *Acta Scientiarum. Agronomy*, 33(4):583–588.

Barben, M. (2003). *Beurteilung von Verfahren zur Abschätzung seltener Hochwasser in mesoskaligen Einzugsgebieten.* PhD thesis, G 71, CD-Rom. Geographisches Institut der Universität Bern.

Beauchamp, J., Leconte, R., Trudel, M., and Brissette, F. (2013). Estimation of the summer-fall PMP and PMF of a northern watershed under a changed climate. *Water Resources Research*, 49(6):3852–3862.

Beniston, M. and Stoffel, M. (2016). Rain-on-snow events, floods and climate change in the Alps: Events may increase with warming up to 4 °C and decrease thereafter. *Science of The Total Environment*, 571:228–236.

Benito, G., Brázdil, R., Herget, J., and Machado, M. J. (2015). Quantitative historical hydrology in Europe. *Hydrol. Earth Syst. Sci.*, 19(8):3517–3539. HESS.

Berg, P. and Haerter, J. O. (2011). Unexpected increase in precipitation intensity with temperature - A result of mixing of precipitation types? *Atmospheric Research*, 119(2013):56–61.

Berg, P., Haerter, J. O., Thejll, P., Piani, C., Hagemann, S., and Christensen, J. H. (2009). Seasonal characteristics of the relationship between daily precipitation intensity and surface temperature. *Journal of Geophysical Research: Atmospheres*, 114(D18102):1–9.

Bergström, S. (1992). The HBV model - its structure and applications. *SMHI Report Hydrol.*, RH No. 4.

Beven, K. (2012). *Rainfall-Runoff Modelling: The Primer, second Edition*. Wiley Blackwell.

Beven, K. and Binley, A. (1992). The future of distributed models - model calibration and uncertainty prediction. *Hydrological Processes*, 6(3):279–298.

Beven, K. and Binley, A. (2014). GLUE: 20 years on. *Hydrological Processes*, 28(24):5897–5918.

Beven, K. and Freer, J. (2001). A dynamic TOPMODEL. *Hydrological Processes*, 15(10):1993–2011.

Beven, K., Quinn, P., Romanowicz, R., Fisher, J., and Lamb, R. (1994). TOPMODEL and GRIDATB, A users guide to the distribution versions (94.01). *Tech. Report*, TR110/94.

Beven, K. J. and Kirkby, M. (1979). A physically based, variable contributing area model of basin hydrology. *Logical Sciences Bulletin*, 24(1):43–49.

Bezak, N., Brilly, M., and Šraj, M. (2014). Comparison between the peaks-over-threshold method and the annual maximum method for flood frequency analysis. *Hydrological Sciences Journal*, 59(5):959–977.

Bhunya, P., Singh, R., Berndtsson, R., and Panda, S. (2012). Flood analysis using generalized logistic models in partial duration series. *Journal of Hydrology*, 420:59–71.

Blazkova, S. and Beven, K. (2004). Flood frequency estimation by continuous simulation of subcatchment rainfalls and discharges with the aim of improving dam safety assessment in a large basin in the Czech Republic. *Journal of Hydrology*, 292(1–4):153–172.

Bodoque, J., Díez-Herrero, A., Eguibar, M., Benito, G., Ruiz-Villanueva, V., and Ballesteros-Cánovas, J. (2014). Challenges in paleoflood hydrology applied to risk analysis in mountainous watersheds–A review. *Journal of Hydrology*, 529:449–467.

Boillat, J. L. and Schleiss, A. (2000). *Création d'un volume de rétention supplémentaire dans la retenue de Mattmark pour la protection contre les crues*. Rapport N°4/00, Laboratoire de Constructions Hydrauliques (LCH). EPFL, Lausanne.

Boillat, J. L. and Schleiss, A. (2002). Détermination de la crue extrême pour les retenues alpines par une approche PMP-PMF. *Wasser Energie Luft*, 94(3/4):107–116.

Bonta, J. (2004). Development and utility of huff curves for disaggregating precipitation amounts. *Applied Engineering in Agriculture*, 20(5):641.

Bonta, J. V. and Rao, A. R. (1992). Estimating Peak Flows from Small Agricultural Watersheds. *Journal of Irrigation and Drainage Engineering*, 118(1):122–137.

Botero, B. A. and Francés, F. (2010). Estimation of high return period flood quantiles using additional non-systematic information with upper bounded statistical models. *Hydrol. Earth Syst. Sci.*, 14(12):2617–2628. HESS.

Box, G., Hunter, W., and Hunter, J. (1978). *Statistics for experimenters: an introduction to design, data analysis, and model building*. John Wiley & Sons, Inc. United States of America.

Box, G. and Jenkins, G. (1970). *TimeSeries Analysis, Forecasting and Control*. Holden-Day series in time series analysis and digital processing. Holden-Day, San Francisco.

Brandsma, T. and Buishand, T. A. (1997). Statistical linkage of daily precipitation in Switzerland to atmospheric circulation and temperature. *Journal of Hydrology*, 198(1–4):98–123.

Bremen, R. and Bertola, P. (1994). Increasing the spillway capacity of the Contra dam. *ICOLD Proceedings, XVIII Congress*, Q.68(R.27).

Bremicker, M. (2000). Das Wasserhaushaltsmodell LARSIM, Modellgrundlagen und Anwendungsbeispiele. *Freiburger Schriften zur Hydrologie*, Vol. 11.

Brigode, P., Mićović, Z., Bernardara, P., Paquet, E., Gailhard, J., Garavaglia, F., Garçon, R., and Ribstein, P. (2015). Probabilistic and deterministic extreme flood estimation methods: Estimation comparison on two British Columbia catchments (Canada). *Houille Blanche*, 2015(3):72–78. EDP Sciences.

Brunner, M. I., Seibert, J., and Favre, A.-C. (2016). Bivariate return periods and their importance for flood peak and volume estimation. *Wiley Interdisciplinary Reviews: Water*, 3(6):819–833.

Brázdil, R., Benito, G., Demarée, G., Macdonald, N., and Roald, L. (2012). *Historical Floods in Europe in the Past Millennium*, pages 121–166. CRC Press. doi:10.1201/b12348-9.

Bureau of Reclamation, USBR (1974). *Design of Small Dams*. U.S. Government Printing Office.

Burnash, R. (1995). *The NWS River Forecast System - catchment modeling*. Chapter 10, in Computer models of watershed hydrology, Vijay P. Singh, editor. Water Resources Publications, Highlands Ranch.

Burnham, K. and Anderson, D. (2002). *Model Selection and Multimodel Inference: A Practical Information-Theoretic Approach*. Springer-Verlag New York.

Busuioc, A., Birsan, M.-V., Carbunaru, D., Baciu, M., and Orzan, A. (2016). Changes in the large-scale thermodynamic instability and connection with rain shower frequency over Romania: verification of the Clausius–Clapeyron scaling. *International Journal of Climatology*, 36(4):2015–2034.

Bérod, D., Devred, D., and Laglaine, V. (1992a). La problématique PMP/PMF: une méthode déterministe pour l'estimation de la crue extrême, avantages, inconvénients et possibilités d'amélioration. *Internationales Symposium INTERPRAEVENT 1992 - Bern, Tagungspublikation*, 4.

Bérod, D., Devred, D., Laglaine, V., Chaix, O., Altinakar, M., and Delley, P. (1992b). *Calcul des crues extrêmes par des méthodes déterministes du type pluie maximale probable (PMP) / crue maximual probable (PMF), Application au cas de la Suisse*. Institut d'aménagement des terres et des eaux, Ecole Polytechnique Fédérale de Lausanne (EPFL); Bonnard et Gardel, Ingénieurs Conseils SA (BG); SA Ufficio d'ingegneria Maggia, Locarno (IM), Lausanne.

Caballero, W. and Rahman, A. (2013). Variability in Rainfall Temporal Patterns: A Case Study for New South Wales, Australia. *Journal of Hydrology and Environment Research*, 1(1):41–48.

Candela, A., Brigandì, G., and Aronica, G. (2014). Estimation of synthetic flood design hydrographs using a distributed rainfall–runoff model coupled with a copula-based single storm rainfall generator. *Natural Hazards and Earth System Sciences*, 14(7):1819–1833.

Casas, M. C., Rodríguez, R., Prohom, M., Gázquez, A., and Redaño, A. (2011). Estimation of the probable maximum precipitation in Barcelona (Spain). *International Journal of Climatology*, 31(9):1322–1327.

CDA (1999). *Dam safety guidelines*. Canadian Dam Association / Association Canadienne des Barrages, Edmonton.

Cernesson, F., Lavabre, J., and Masson, J.-M. (1996). Stochastic model for generating hourly hyetographs. *Atmospheric Research*, 42(1–4):149–161.

Chen, J., Kavvas, M. L., Ishida, K., Trinh, T., Ohara, N., Anderson, M. L., and Chen, Z. Q. R. (2016). Role of snowmelt in determining whether the maximum precipitation always results in the maximum flood. *Journal of Hydrologic Engineering*, 0(0):04016032.

Cluckie, I. D. and Pessoa, M. L. (1990). Dam safety: an evaluation of some procedures for design flood estimation. *Hydrological Sciences Journal*, 35(5):547–569.

Cohen, T., García Hernández, J., Dubois, J., and Boillat, J. L. (2009). Influence of hydrological Model Complexity on the Estimation of Floods in an Alpine Catchement for PMP Conditions. *Proceedings of 33rd IAHR Congress, 2009, Vancouver*, pages 1763–1770.

Coles, S. (2001). *An Introduction to Statistical Modeling of Extreme Values*. Springer Series in Statistics. Springer-Verlag London.

Cowpertwait, P. S. P. (1991). Further developments of the neyman-scott clustered point process for modeling rainfall. *Water Resources Research*, 27(7):1431–1438.

Croke, B. F. W. and Jakeman, A. J. (2004). A catchment moisture deficit module for the IHACRES rainfall-runoff model. *Environmental Modelling & Software*, 19(1):1–5.

Cudworth, A. (1992). *Flood Hydrology Manual*. Bureau of Reclamation, U.S. Department of the Interior, Denver CO.

Cunnane, C. (1973). A particular comparison of annual maxima and partial duration series methods of flood frequency prediction. *Journal of Hydrology*, 18(3):257–271.

Damm, B. and Felderer, A. (2013). Impact of atmospheric warming on permafrost degradation and debris flow initiation - a case study from the eastern European Alps. *Quaternary Science Journal*, 62(2):136–149.

Davison, A. C. and Smith, R. L. (1990). Models for exceedances over high thresholds. *Journal of the Royal Statistical Society. Series B (Methodological)*, 52(3):393–442.

DHI (1993). *MIKE SHE*. Technical Reference Manual. Danish Hydraulic Institute.

Drobinski, P., Alonzo, B., Bastin, S., Silva, N. D., and Muller, C. (2016). Scaling of precipitation extremes with temperature in the French Mediterranean region: What explains the hook shape? *Journal of Geophysical Research: Atmospheres*, 121(7):3100–3119.

Dubois, J. and Boillat, J. L. (2000). *Routing System, Modélisation du routage de crues dans les systèmes hydrauliques à surface libre*. Communication 9. Laboratoire de constructions hydrauliques, Ecole polytechnique fédérale de Lausanne, EPFL.

Dubois, J. and Pirotton, M. (2002). *Génération et transfert des crues extrêmes. Le logiciel Faitou.* Communication 10. Laboratoire de constructions hydrauliques, Ecole polytechnique fédérale de Lausanne.

Dung, N. V., Merz, B., Bárdossy, A., and Apel, H. (2015). Handling uncertainty in bivariate quantile estimation – An application to flood hazard analysis in the Mekong Delta. *Journal of Hydrology*, 527:704–717.

Durrans, S. R., Julian, L. T., and Yekta, M. (2002). Estimation of depth-area relationships using radar-rainfall data. *Journal of Hydrologic Engineering*, 7(5):356.

DWA (2012). *Merkblatt DWA-M 552. Ermittlung von Hochwasserwahrscheinlichkeiten*. DWA, Dt. Vereinigung für Wasserwirtschaft, Abwasser u. Abfall.

Elíasson, J. (1994). Statistical estimates of pmp values. *Hydrology Research*, 25(4):301–312.

Elíasson, J. (1997). A statistical model for extreme precipitation. *Water Resources Research*, 33(3):449–455.

Enzel, Y., Ely, L. L., House, P. K., Baker, V. R., and Webb, R. H. (1993). Paleoflood evidence for a natural upper bound to flood magnitudes in the Colorado River Basin. *Water Resources Research*, 29(7):2287–2297.

FERC (2001). *Determination of the Probable Maximum Flood, Chapter 8 in : Engineering Guidelines for the Evaluation of Hydropower Projects*. Federal Energy Regulatory Commission, Washington D.C.

Fernandes, W., Naghettini, M., and Loschi, R. (2010). A Bayesian approach for estimating extreme flood probabilities with upper-bounded distribution functions. *Stochastic Environmental Research and Risk Assessment*, 24(8):1127–1143.

FOEN (2001). *Die biogeographischen Regionen der Schweiz*. Umwelt-Materialien UM. Federal Office for the Environment FOEN, Bern.

Fourmigué, P. and Lavabre, J. (2005). Prévision de crues avec le modèle conceptuel pluie-débit GR3H. Adaptabilité aux incertitudes sur la pluie. *Revue des sciences de l'eau, Journal of Water Sciences*, 18(1):87–102.

FOWG (2003). *Evaluation des crues dans les bassins versants de Suisse. Guide pratique*. Rapport de l'OFEG, Série Eaux N°4. Federal Office for Water and Geology, Bern.

Francou, J. and Rodier, J.-A. (1967). Essai de classification des crues maximales observées dans le monde. *Cah. O.R.S.T.M. sér. Hydrol.*, 4(3).

Froidevaux, P. (2014). *Meteorological characterisation of floods in Switzerland*. PhD thesis. Geographisches Institut der Universität Bern.

Garavaglia, F. (2011). *Méthode SCHADEX de prédétermination des crues extrêmes: Méthodologie, applications, étude de sensibilité*. PhD thesis, HAL Id: tel-00579507. Université de Grenoble, Unité de Recherche Hydrologie-Hydraulique, Cemagref Lyon.

Garcia-Guzman, A. and Aranda-Oliver, E. (1993). A stochastic model of dimensionless hyetograph. *Water Resources Research*, 29(7):2363–2370.

Garcia Hernandez, J., Paredes Arquiola, J., Foehn, A., and Roquier, B. (2016). RS Minerve - Technical manual v1.7.

Garçon, R. (1996). Prévision opérationnelle des apports de la Durance à Serre-Ponçon à l'aide du modèle MORDOR. Bilan de l'année 1994-1995. *La Houille Blanche*, 1996(5):71–76.

Gaume, E., Bain, V., Bernardara, P., Newinger, O., Barbuc, M., Bateman, A., Blaškovičová, L., Blöschl, G., Borga, M., Dumitrescu, A., Daliakopoulos, I., Garcia, J., Irimescu, A., Kohnova, S., Koutroulis, A., Marchi, L., Matreata, S., Medina, V., Preciso, E., Sempere-Torres, D., Stancalie, G., Szolgay, J., Tsanis, I., Velasco, D., and Viglione, A. (2009). A compilation of data on European flash floods. *Journal of Hydrology*, 367(1–2):70–78.

Gaál, L., Szolgay, J., Kohnová, S., Hlavčová, K., Parajka, J., Viglione, A., Merz, R., and Blöschl, G. (2015). Dependence between flood peaks and volumes: a case study on climate and hydrological controls. *Hydrological Sciences Journal*, 60(6):968–984.

Genest, C. and Favre, A.-C. (2007). Everything you always wanted to know about copula modeling but were afraid to ask. *Journal of Hydrologic Engineering*, 12(4):347–368.

Ghassabi, Z., kamali, G. A., Meshkatee, A.-H., Hajam, S., and Javaheri, N. (2016). Time distribution of heavy rainfall events in south west of Iran. *Journal of Atmospheric and Solar-Terrestrial Physics*, 145:53–60.

Giorgi, F., Torma, C., Coppola, E., Ban, N., Schar, C., and Somot, S. (2016). Enhanced summer convective rainfall at Alpine high elevations in response to climate warming. *Nature Geosci*, Advance Online Publication.

Gironás, J., Roesner, L. A., Rossman, L. A., and Davis, J. (2010). A new applications manual for the Storm Water Management Model (SWMM). *Environmental Modelling & Software*, 25(6):813–814.

Guo, J. C. and Hargadin, K. (2009). Conservative design rainfall distribution. *Journal of Hydrologic Engineering*, 14(5):528–530.

Haddad, K. and Rahman, A. (2016). *Estimation of Large to Extreme Floods Using a Regionalization Model*. Chapter 14, Part III, in Landscape Dynamics, Soils and Hydrological Processes in Varied Climates. Melesse, M. Assefa, Abtew, Wossenu, editors. Springer International Publishing, Cham.

Haiden, T. (1991). A deterministic approach to the determination of orographic PMP. *Institute of Meteoroloy and Geophysics, University of Vienna, Austria*.

Haiden, T., Kerschbaum, M., Kahlig, P., and Nobilis, F. (1992). A refined model of the influence of orography on the mesoscale distribution of extreme precipitation. *Hydrology Sciences Journal*, 37(5):417–427.

Hardwick Jones, R., Westra, S., and Sharma, A. (2010). Observed relationships between extreme sub-daily precipitation, surface temperature, and relative humidity. *Geophysical Research Letters*, 37(22):L22805.

Harris, J. and Brunner, G. (2011). Approximating the probability of the probable maximum flood. *World Environmental and Water Resources Congress 2011, Proceedings*, pages 3695–3702.

Herschy, R. (2001). The world's maximum observed floods. *The Extremes of the extremes: Extraodinary Floods*, 271.

Hershfield, D. M. (1961). Technical paper no. 40: Rainfall frequency atlas of the united states, department of commerce. *Weather Bureau, Washington, DC*.

Hertig, J., Fallot, J., and Brena, A. (2008). *Projet CRUEX. Directive Crues de l'OFEN. Etablissement des cartes des précipitations extrêmes pour la Suisse. Méthode d'utilisation des cartes PMP pour l'obtention de la PMF.* Swiss Federal Office of Energy SFOE.

Hertig, J.-A., Audouard, A., and Plancherel, A. (2005). Cartes des précipitations extrêmes pour la Suisse (PMP 2005). *Rapport EFLUM-EPFL*.

Hertig, J.-A. and Fallot, J.-M. (2009). Validation et utilisation des cartes de PMP pour l'obtention de la PMF. Projet CRUEX: Directives Crues de l'OFEN. *unpublished report*.

Hingray, B., Mezghani, A., Schaefli, M., Niggli, M., Faivre, G., Guex, F., Hamdi, Y., and Musy, A. (2006). Rapport final réalisé dans le cadre du projet CONSECRU 2. Estimation des débits de crue du Rhône à Porte du Scex et autres points amont caractéristiques. Technical report, HYDRAM - EPFL.

Hingray, B., Picouet, C., and Musy, A. (2009). *Hydrologie 2 - Une science pour l'ingénieur*. Presses polytechniques et universitaires romandes, Lausanne.

Hock, R. (2003). Temperature index melt modelling in mountain areas. *Journal of Hydrology*, 282(1–4):104–115.

Hogg, W., Leytham, K., Neill, C., Sellars, C., and Watt, W. (2004). *Guidelines on extreme Flood Analysis*. Alberta Transportation, Transportation & Civil Engineering Division, Civil Projects Branch, Canada.

Huff, F. A. (1967). Time distribution of rainfall in heavy storms. *Water Resources Research*, 3(4):1007–1019.

IAHS (2003). *World catalogue of maximum observed floods: Répertoire mondial des crues maximales observées*. International Association of Hydrological Sciences, Wallingford, UK.

ICOLD (2016). Flood Evaluation and Dam Safety. *ICOLD Bulletin*, not yet published.

Jakeman, A. J., Littlewood, I. G., and Whitehead, P. G. (1990). Computation of the instantaneous unit hydrograph and identifiable component flows with application to two small upland catchments. *Journal of Hydrology*, 117(1–4):275–300.

Jasper, K., Gurtz, J., and Lang, H. (2002). Advanced flood forecasting in alpine watersheds by coupling meteorological observations and forecasts with a distributed hydrological model. *Journal of Hydrology*, 267(1–2):40–52.

Jenkinson, A. F. (1955). The frequency distribution of the annual maximum (or minimum) values of meteorological elements. *Quarterly Journal of the Royal Meteorological Society*, 81(348):158–171.

Jongman, B., Hochrainer-Stigler, S., Feyen, L., Aerts, J. C. J. H., Mechler, R., Botzen, W. J. W., Bouwer, L. M., Pflug, G., Rojas, R., and Ward, P. J. (2014). Increasing stress on disaster-risk finance due to large floods. *Nature Clim. Change*, 4(4):264–268.

Jordan, F., Brauchli, T., Garcia Hernandez, J., Bieri, M., and Boillat, J. L. (2012). *RS 2012, Rainfall-Runoff Modelling. User guide*. unpublished manual. e-dric.ch, Lausanne.

Jothityangkoon, C., Hirunteeyakul, C., Boonrawd, K., and Sivapalan, M. (2013). Assessing the impact of climate and land use changes on extreme floods in a large tropical catchment. *Journal of Hydrology*, 490:88–105.

Kan, C. (1995). *Die höchsten in der Schweiz beobachteten Abflussmengen bis 1990*. Diplomarbeit in der Gruppe für Hydrologie des Geographischen Instituts der Universität Bern. Publikation Gewässerkunde Nr.169. Geographisches Institut der Universität Bern, Bern.

Kanda, J. (1981). A New Extreme Value Distribution with Lower and Upper Limits for Earthquake Motions and Wind Speeds. *Theoretical and Applied Mechanics, Tokyo University Press*, 31:351–360.

Keifer, C. and Chu, H. (1957). Synthetic storm pattern for drainage design. *ASCE Journal of the Hydraulics Division*, 83(HY4):1–25.

Kessler, E. (1969). On the distribution and continuity of water substance in atmospheric circulation. *American Meteorological Society*, 10(32):84.

Kiczko, A., Romanowicz, R. J., Osuch, M., and Karamuz, E. (2013). Maximising the usefulness of flood risk assessment for the River Vistula in Warsaw. *Nat. Hazards Earth Syst. Sci.*, 13(12):3443–3455. NHESS.

Kimoto, A., Canfield, H. E., and Stewart, D. (2011). Comparison of Synthetic Design Storms with Observed Storms in Southern Arizona. *Journal of Hydrologic Engineering*, 16(11):935–941.

Kirkby, M. (1988). Hillslope runoff processes and models. *Journal of Hydrology*, 100(1):315–339.

Kite, G. W. (1995). Scaling of input data for macroscale hydrologic modeling. *Water Resources Research*, 31(11):2769–2781.

KLL (1988). Kraftwerke Linth-Limmern AG, Stauanlage Limmernboden. Hochwasser Entlastung: Hydraulische Berechnung. Unpublished report. KLL Nr. 10988.

Koutsoyiannis, D. (2004). Statistics of extremes and estimation of extreme rainfall: I. theoretical investigation / statistiques de valeurs extrêmes et estimation de précipitations extrêmes: I. recherche théorique. *Hydrological Sciences Journal*, 49(4):575–590.

Krysanova, V., Bronstert, A., and Müller-Wohlfeil, D. I. (1999). Modelling river discharge for large drainage basins: from lumped to distributed approach. *Hydrological Sciences Journal*, 44(2):313–331.

Kunkel, K. E., Karl, T. R., Easterling, D. R., Redmond, K., Young, J., Yin, X., and Hennon, P. (2013). Probable maximum precipitation and climate change. *Geophysical Research Letters*, 40(7):1402–1408.

Kölla, E. (1987). Estimating flood peaks from small rural catchments in Switzerland. *Journal of Hydrology*, 95:203–225.

Kürsteiner, L. (1917). Das neue Elektrizitätswerk der Stadt Chur an der Plessur bei Lüen. *Schweizerische Bauzeitung*, 69/70(4).

Lagos-Zúñiga, M. A. and Vargas M, X. (2014). PMP and PMF estimations in sparsely-gauged Andean basins and climate change projections. *Hydrological Sciences Journal*, 59(11):2027–2042.

Lenderink, G., Mok, H. Y., Lee, T. C., and van Oldenborgh, G. J. (2011). Scaling and trends of hourly precipitation extremes in two different climate zones – Hong Kong and the Netherlands. *Hydrol. Earth Syst. Sci.*, 15(9):3033–3041. HESS.

Lenderink, G. and Van Meijgaard, E. (2008). Increase in hourly precipitation extremes beyond expectations from temperature changes. *Nature Geosci*, 1(8):511–514. 10.1038/ngeo262.

Lenderink, G. and Van Meijgaard, E. (2010). Linking increases in hourly precipitation extremes to atmospheric temperature and moisture changes. *Environmental Research Letters*, 5(2):025208.

Lima, C. H. R., Lall, U., Troy, T., and Devineni, N. (2016). A hierarchical Bayesian GEV model for improving local and regional flood quantile estimates. *Journal of Hydrology*, 541, Part B:816–823.

Machado, M. J., Botero, B. A., López, J., Francés, F., Díez-Herrero, A., and Benito, G. (2015). Flood frequency analysis of historical flood data under stationary and non-stationary modelling. *Hydrol. Earth Syst. Sci.*, 19(6):2561–2576. HESS.

Madsen, H. (1996). *At-site and regional modelling of extreme hydrologic events*. PhD Thesis. Technical University of Denmark, Department of Hydrodynamics and Water Resources.

Madsen, H., Pearson, C. P., and Rosbjerg, D. (1997). Comparison of annual maximum series and partial duration series methods for modeling extreme hydrologic events: 2. regional modeling. *Water Resources Research*, 33(4):759–769.

Marchi, L., Borga, M., Preciso, E., and Gaume, E. (2010). Characterisation of selected extreme flash floods in Europe and implications for flood risk management. *Journal of Hydrology*, 394(1–2):118–133.

Marco, J., Harboe, R., and Salas, J. (1989). *Stochastic Hydrology and its Use in Water Resources Systems Simulation and Optimization*. Springer Netherlands.

McClenathan, J. T. (2013). We Can, But Should We? PMF Frequency Estimates. *World Environmental and Water Resources Congress 2013, Proceedings*, pages 1923–1928.

Melli, E. (1924). Die Dimensionierung städtischer Kanäle. *Schweizerische Bauzeitung*, 83/84(12):137–141.

Merz, B. and Thieken, A. H. (2005). Separating natural and epistemic uncertainty in flood frequency analysis. *Journal of Hydrology*, 309(1–4):114–132.

Merz, R. and Blöschl, G. (2008a). Flood frequency hydrology: 1. temporal, spatial, and causal expansion of information. *Water Resources Research*, 44(W08432):1–17.

Merz, R. and Blöschl, G. (2008b). Flood frequency hydrology: 2. combining data evidence. *Water Resources Research*, 44(W08433):1–16.

Meylan, P., Favre, A.-C., and Musy, A. (2008). *Hydrologie fréquentielle : une science prédictive*. Presses polytechniques et universitaires romandes, Lausanne.

Molnar, P., Fatichi, S., Gaál, L., Szolgay, J., and Burlando, P. (2015). Storm type effects on super Clausius–Clapeyron scaling of intense rainstorm properties with air temperature. *Hydrol. Earth Syst. Sci.*, 19(4):1753–1766. HESS.

Molnar, P., Fatichi, S., Paschalis, A., Gaal, L., Szolgay, J., and Burlando, P. (2016). On extreme rainfall intensity increases with air temperature. *Geophysical Research Abstracts*, 18(EGU2016-8128-1).

Moriasi, D. N., Arnold, J. G., Van Liew, M. W., Bingner, R. L., Harmel, R. D., and Veith, T. L. (2007). Model Evaluation Guidelines for Systematic Quantification of Accuracy in Watershed Simulations. *Transaction of ASABE*, 50(3):885–900.

Müller, R. (1943). Theoretische Grundlagen der Fluss- und Wildbachverbauung. *Mitteilung der Versuchsanstalt für Wasserbau der ETH Zürich*, Nr. 4.

Nathan, R., Hill, P., and Griffith, H. (2001). Risk Implications of the PMF and the PMP Design Flood. *NZSOLD / ANCOLD Conference on Dams*.

NERC (1975). *Flood Studies Report*, volume 2 of *Meteorological studies*. Whitefriars Press Ltd., London.

Niemi, T. J., Guillaume, J. H. A., Kokkonen, T., Hoang, T. M. T., and Seed, A. W. (2015). Role of spatial anisotropy in design storm generation: Experiment and interpretation. *Water Resources Research*, 52.

Niggli, M., Consuegra, D., and Bérod, D. (1997). Etude CONSECRU. Modélisation des crues du Rhône en Valais. Rapport final. Technical report, IATE/HYDRAM-EPFL.

Nobilis, F., Haiden, T., and Kerschbaum, M. (1991). Statistical Considerations Concerning Probable maximum Precipitation (PMP) in the Alpine Country of Austria. *Theoretical and Applied Climatology*, 44:89–94.

NRCS (1986). *Technical Release 55 (TR-55)*. Urban hydrology for small watersheds. Natural Resources Conservation Service, Engineering Division, Washington, D.C.

Ohmura, A. (2001). Physical basis for the temperature-based melt-index method. *Journal of Applied Meteorology*, 40(4):753–761.

Pall, P., Allen, M. R., and Stone, D. A. (2006). Testing the Clausius–Clapeyron constraint on changes in extreme precipitation under CO_2 warming. *Climate Dynamics*, 28(4):351–363.

Panthou, G., Mailhot, A., Laurence, E., and Talbot, G. (2014). Relationship between surface temperature and extreme rainfalls: A multi-time-scale and event-based analysis. *Journal of Hydrometeorology*, 15(5):1999–2011.

Papalexiou, S. M. and Koutsoyiannis, D. (2006). A probabilistic approach to the concept of probable maximum precipitation. *Adv. Geosci.*, 7(-):51–54. ADGEO.

Paquet, E. (2004). Evolution du modèle hydrologique mordor: modélisation du stock nival à différentes altitudes. *La Houille Blanche*, 2004(2):75–82.

Paquet, E., Gailhard, J., and Garçon, R. (2006). Evolution de la méthode du Gradex: approche par type de temps et modélisation hydrologique. *La Houille Blanche*, 2006(5):80–90.

Paquet, E., Garavaglia, F., Garçon, R., and Gailhard, J. (2013). The SCHADEX method: A semi-continuous rainfall–runoff simulation for extreme flood estimation. *Journal of Hydrology*, 495:23–37.

Perrin, C., Michel, C., and Andréassian, V. (2003). Improvement of a parsimonious model for streamflow simulation. *Journal of Hydrology*, 279(1):275–289.

Pfahl, S. and Niedermann, N. (2011). Daily covariations in near-surface relative humidity and temperature over the ocean. *Journal of Geophysical Research: Atmospheres*, 116(D19104):1–12.

Pickands, J. (1975). Statistical inference using extreme order statistics. *The Annals of Statistics*, 3(1):119–131.

Pilgrim, D. H. and Cordery, I. (1993). *Flood runoff*. in Handbook of Hydrology. Maidment, D.R., editor. McGraw-Hill, New York.

Plate, E., Ihringer, J., and Lutz, W. (1988). Operational models for flood calculations. *Journal of Hydrology*, 100(1-3):489–506.

Prodanovic, P. and Simonovic, S. P. (2004). Generation of Synthetic Design Storms for the Upper Thames River Basin. CFCAS Project: Assessment of Water Resources Risk and Vulnerability to Changing Climatic Conditions. Technical report, The University of Western Ontario, Department of Civil and Environmental Engineering.

Pérez, R. and Hertig, J.-A. (1998). Projet CRUEX. Détermination d'une carte PMP orographique pour la région de l'Oberalpass. *Unpublished report*.

Receanu, R. (2013). *Simulation fine des précipitations et des crues extrêmes. Application aux petits bassins versants alpins non glaciaires*. PhD thesis. Faculté des géosciences et de l'environnement, Université de Lausanne UNIL.

Receanu, R., Hertig, J.-A., and Fallot, J.-M. (2013). Modélisation hydrologique des précipitations et des crues extrêmes dans les bassins versants alpins. *Mémoires de la Société Vaudoise des Sciences Naturelles*, 25:35–54.

Resendiz-Carrillo, D. and Lave, L. B. (1990). Evaluating Dam Safety Retrofits with Uncertain Benefits: The case study of Mohawk Dam (Walhonding River, Ohio). *Water Resources Research*, 26(5):1093–1098.

Roche, P., Miquel, J., and Gaume, E. (2012). *Hydrologie quantitative: Processus, modèles et aide à la décision*. Springer.

Rohrer, M. B., Braun, L. N., and Lang, H. (1994). Long-term records of snow cover water equivalent in the Swiss Alps. 1. Analysis. *Nordic Hydrology*, 25(1-2):53–64.

Rolland, C. (2003). Spatial and seasonal variations of air temperature lapse rates in alpine regions. *Journal of Climate*, 16(7):1032–1046.

Romanowicz, R. J. and Kiczko, A. (2016). An event simulation approach to the assessment of flood level frequencies: risk maps for the warsaw reach of the river vistula. *Hydrological Processes*, 30(14):2451–2462.

Rothe, B. and Wolf-Schumann, U. (2013). Nasim 4.2, Speicherformeln, Stofftransport, Radar-Niederschlagsdaten. *Hydrothemen*, 24:8.

Rössler, O., Froidevaux, P., Börst, U., Rickli, R., Martius, O., and Weingartner, R. (2014). Retrospective analysis of a nonforecasted rain-on-snow flood in the alps – a matter of model limitations or unpredictable nature? *Hydrol. Earth Syst. Sci.*, 18(6):2265–2285. HESS.

Salas, D. J., Gavilán, G., R. Salas, F., Y. Julien, P., and Abdullah, J. (2014). *Uncertainty of the PMP and PMF*, volume Modeling Climate Change and Variability of *Handbook of Engineering Hydrology*. Taylor & Francis Group, LLC.

Sarhadi, A., Soltani, S., and Modarres, R. (2012). Probabilistic flood inundation mapping of ungauged rivers: Linking GIS techniques and frequency analysis. *Journal of Hydrology*, 458–459:68–86.

Schaefli, B. (2016). Snow hydrology signatures for model identification within a limits-of-acceptability approach. *Hydrological Processes*, doi: 10.1002/hyp.10972.

Schaefli, B., Hingray, B., Niggli, M., and Musy, A. (2005). A conceptual glacio-hydrological model for high mountainous catchments. *Hydrol. Earth Syst. Sci.*, 9(1/2):95–109.

Schaefli, B. and Huss, M. (2011). Integrating point glacier mass balance observations into hydrologic model identification. *Hydrology and Earth System Sciences*, 15:1227–1241.

Schaefli, B. and Zehe, E. (2009). Hydrological model performance and parameter estimation in the wavelet-domain. *Hydrol. Earth Syst. Sci.*, 13(10):1921–1936. HESS.

Schiemann, R. and Frei, C. (2010). *Hydrological Atlas of Switzerland, Weather Types and Distribution of Precipitation troughout the European Alps, Plate 2.8*. Office fédéral de l'environnement OFEV.

Schleiss, A. and Pougatsch, H. (2011). *Les barrages: Du projet à la mise en service*. TGC 17. Presses polytechniques et universitaires romandes, Lausanne.

Schulla, J. (2012). *Model description. WASIM (Water balance simulation model)*. Hydrology Software Consulting J. Schulla. Hydrology Software Consulting J. Schulla, Zürich.

SFOE (2008a). Sécurité des ouvrages d'accumulation. documentation de base relative à la véréfication de al sécurité en cas de crue. *Directives de l'OFEN*, Juin.

SFOE, S. F. O. o. E. (2008b). Documentation de base relative à l'élaboration de la sécurité en cas de crue. Technical report, Swiss Federal Office of Energie.

Shalaby, A. I. (1994). Estimating probable maximum flood probabilities1. *JAWRA Journal of the American Water Resources Association*, 30(2):307–318.

Shaw, L., Hamilton, P. A., and Kent, c. E. (1984). Temporal Distribution of Rainfall in Virginia. Technical report, Virginia Highway & Transportation Research Council.

Shaw, S. B., Royem, A. A., and Riha, S. J. (2011). The Relationship between Extreme Hourly Precipitation and Surface Temperature in Different Hydroclimatic Regions of the United States. *Journal of Hydrometeorology*, 12(2):319–325.

Singh, K. and Frevert, D. (2005). *Watershed Models, Chapter 7. USGS Modular Modeling System (MMS). Precipitation-Runoff Modeling System (PRMS) by Leavesley, G.H., Markstrom, S.L. and Viger, R. J.*, pages 159–177. CRC Taylor & Francis Group.

Singh, V. and Frevert, D. (2002a). *Mathematical Models of Small Watershed Hydrology and Applications*. Water Resources Publications.

Singh, V. and Frevert, D. (2002b). *Mathematical Models of Small Watershed Hydrology and Applications, Chapter 4, CASC2D: A two dimensional, physically based, hortonian hydrological model by Ogden, F. L. and Julien, P. Y.* Water Resources Publications, LLC.

Slade Jr, J. (1936). An asymmetric probability function. *Transactions of the American Society of Civil Engineers*, 101(1):35–104.

Smith, C. (1998). The PMF does have a frequency. *Canadian Water Resources Journal*, 23(1):1–7.

Stallings, E. A. (1987). Analysis of extraordinary flood events determination of design floods using storm data. *Journal of Hydrology*, 96(1):319–328.

Stedinger, J. R. and Griffis, V. W. (2008). Flood Frequency Analysis in the United States: Time to Update. *Journal of Hydrologic Engineering*, 13(4):199–204.

Stoffer, D. S. (1986). Estimation and Identification of Space-Time ARMAX Models in the Presence of Missing Data. *Journal of the American Statistical Association*, 81(395):762–772.

Stratz, S. A. and Hossain, F. (2014). Probable maximum precipitation in a changing climate: Implications for dam design. *Journal of Hydrologic Engineering*, 19(12):06014006.

Swain, R., England, J., Bullard, K., Raff, D., and Reclamation, U. S. B. o. (2006). *Guidelines for Evaluating Hydrologic Hazards*. U.S. Department of the Interior, Bureau of Reclamation.

SwissCOD (2011). *Dams in Switzerland: Source for Worldwide Swiss Dam Engineering*. Swiss Commitee on Dams.

Takara, K. and Loebis, L. (1996). Frequency analysis introducing probable maximum hydrologic events: preliminary studies in Japan and in Indonesia. *Proceedings of international symposium on comparative research on hydrology and water resources in Southeast Asia and the Pacific.*, pages 67–76.

Takara, K. and Tosa, K. (1999). Storm and Flood Frequency Analysis using PMP/PMF Estimates. *Proceedings of International Symposium on Floods and Droughts, Nanjing, China, 18-20 October*.

Tavares, L. V. and Da Silva, J. E. (1983). Partial duration series method revisited. *Journal of Hydrology*, 64(1):1–14.

Tobin, C., Rinaldo, A., and Schaefli, B. (2012). Snowfall limit forecasts and hydrological modeling. *Journal of Hydrometeorology*, 13(5):1507–1519.

USDA-SCS (2007). *Chaptre 16: Hydrology, National Engineering Handbook: Part 630, Hydrologic Engineering*. U.S. Department of Agriculture, Soil Conservation Service. Snider, Dean Woodward, D.E. Hoeft, Claudia C. Merkel, William H. Chaison, Katherine E. Fox Moody, Helen.

Utsumi, N., Seto, S., Kanae, S., Maeda, E. E., and Oki, T. (2011). Does higher surface temperature intensify extreme precipitation? *Geophysical Research Letters*, 38(L16708):1–5.

Veneziano, D. and Villani, P. (1999). Best linear unbiased design hyetograph. *Water Resources Research*, 35(9):2725–2738.

Vernieuwe, H., Vandenberghe, S., De Baets, B., and Verhoest, N. (2015). A continuous rainfall model based on vine copulas. *Hydrology and Earth System Sciences*, 19(6):2685–2699.

Vertessy, R. A., Hatton, T. J., O'Shaughnessy, P. J., and Jayasuriya, M. D. A. (1993). Predicting water yield from a mountain ash forest catchment using a terrain analysis based catchment model. *Journal of Hydrology*, 150(2–4):665–700.

Vogel, R. M. and Wilson, I. (1996). Probability Distribution of Annual Maximum, Mean, and Minimum Streamflows in the United States. *Journal of Hydrologic Engineering*, 1(2):69–76.

Walland, D., Meighen, J., Xuereb, K., Beesley, C., and Hoang, T. (2003). Revision of the generalised tropical storm method for estimating probable maximum precipitation. Technical report, Bureau of Meteorology Melbourne.

Wasko, C., Sharma, A., and Johnson, F. (2015). Does storm duration modulate the extreme precipitation-temperature scaling relationship? *Geophysical Research Letters*, 42(20):8783–8790.

Watt, W., Chow, K., and Lathem, K. (1986). A 1-h urban design storm for Canada. *Canadian Journal of Civil Engineering*, No. 13:293–300.

Weingartner, R. (1999). Regionalhydrologische Analyse - Grundlagen und Anwendungen. *Beiträge zur Hydrologie der Schweiz*, 37.

Westra, S., Alexander, L. V., and Zwiers, F. W. (2012). Global increasing trends in annual maximum daily precipitation. *Journal of Climate*, 26(11):3904–3918.

Westra, S., Fowler, H. J., Evans, J. P., Alexander, L. V., Berg, P., Johnson, F., Kendon, E. J., Lenderink, G., and Roberts, N. M. (2014). Future changes to the intensity and frequency of short-duration extreme rainfall. *Reviews of Geophysics*, 52(3):522–555.

WMO (2009). *Manual on Estimation of Probable Maximum Precipitation (PMP)*, volume WMO-No.1045. World Meteorological Organization, Geneva.

Yen, B. C. and Chow, V. T. (1980). Design hyetographs for small drainage structures. *ASCE Journal of the Hydraulics Division*, 106(6):1055–1076.

Zeimetz, F., Receanu, R., Schleiss, A., and Hernández, J. G. (2015). Extreme flood assessment in swiss alpine environment. *Proceedings of the 25th Int. Congress on Large Dams (Abstract book)*, Q.97(R.24):58–59.

Zeller, J. (1975). Berechnung der Abflusswassermenge. *Beilage zur Vorlesung "Wildbach- und Hangverbau", Abteilung VI, ETH Zürich*.

Zhang, Y. and Smith, J. A. (2003). Space–Time Variability of Rainfall and Extreme Flood Response in the Menomonee River Basin, Wisconsin. *Journal of Hydrometeorology*, 4(3):506–517.

Appendix Part

A Temporal rainfall distribution

A.1 Mean variation

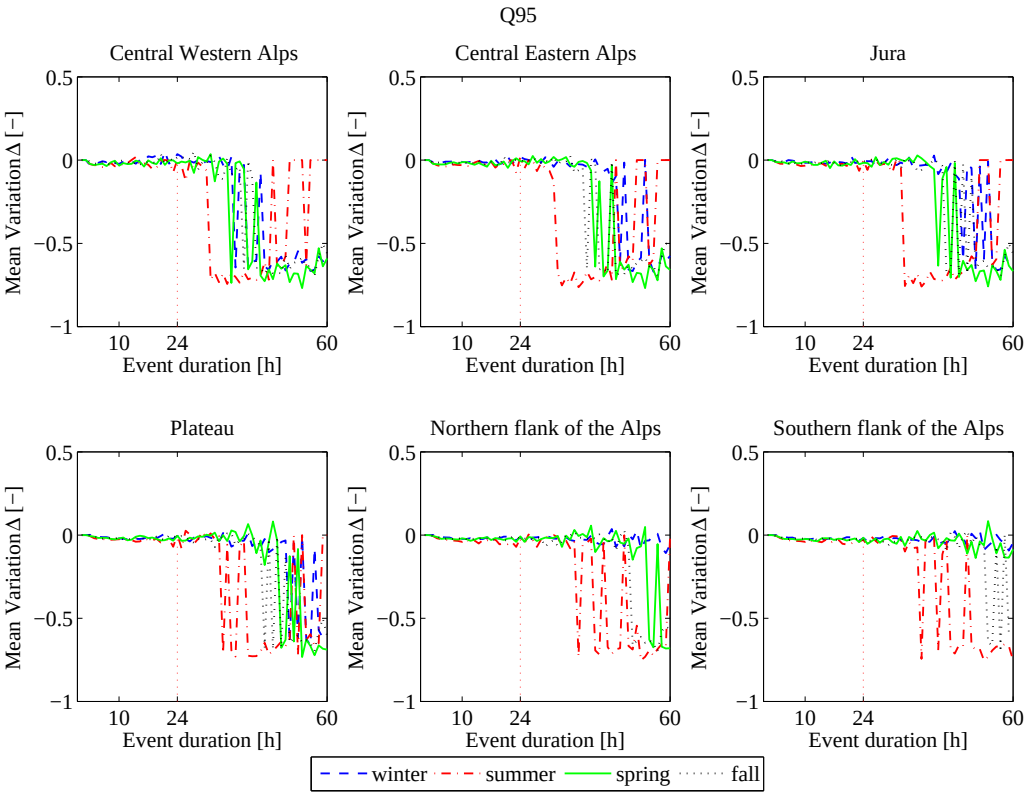

Figure A.1: Mean variation Δ of Huff curves from event definitions with 1h and 3h dry inter event periods for six Swiss regions, four seasons of the year and the 95% quantile of the Huff curves.

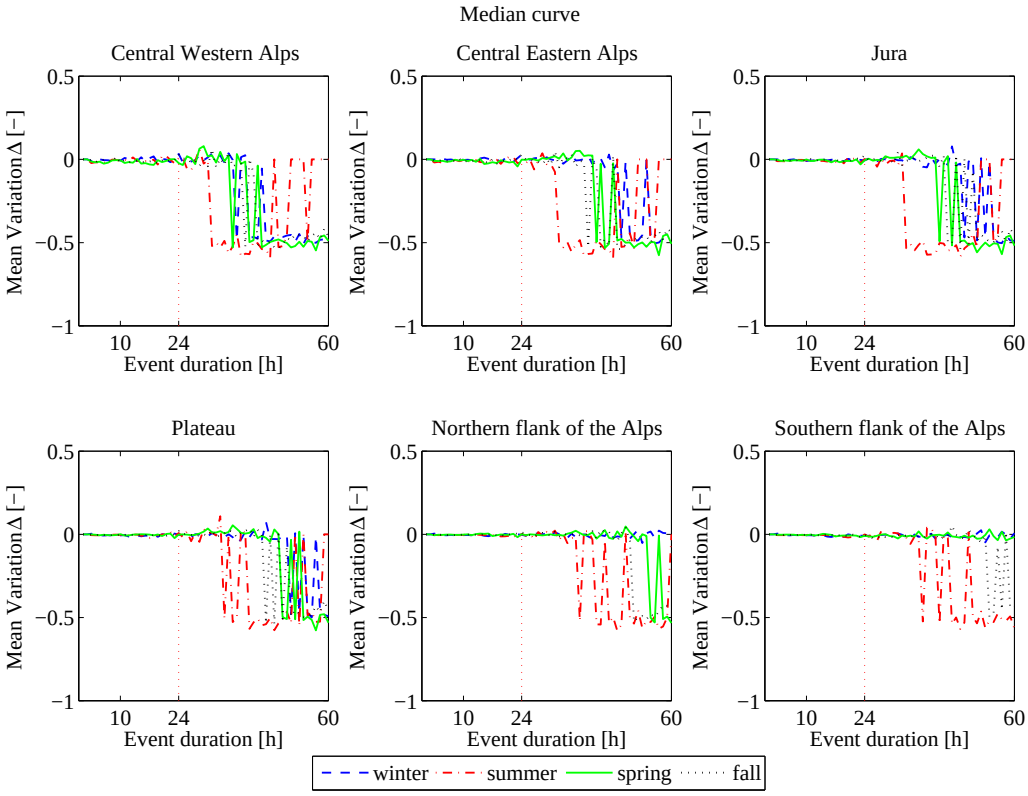

Figure A.2: Mean variation Δ of Huff curves from event definitions with 1h and 3h dry inter event periods for six Swiss regions, four seasons of the year and the 50% quantile of the Huff curves.

A.2 Regional variability

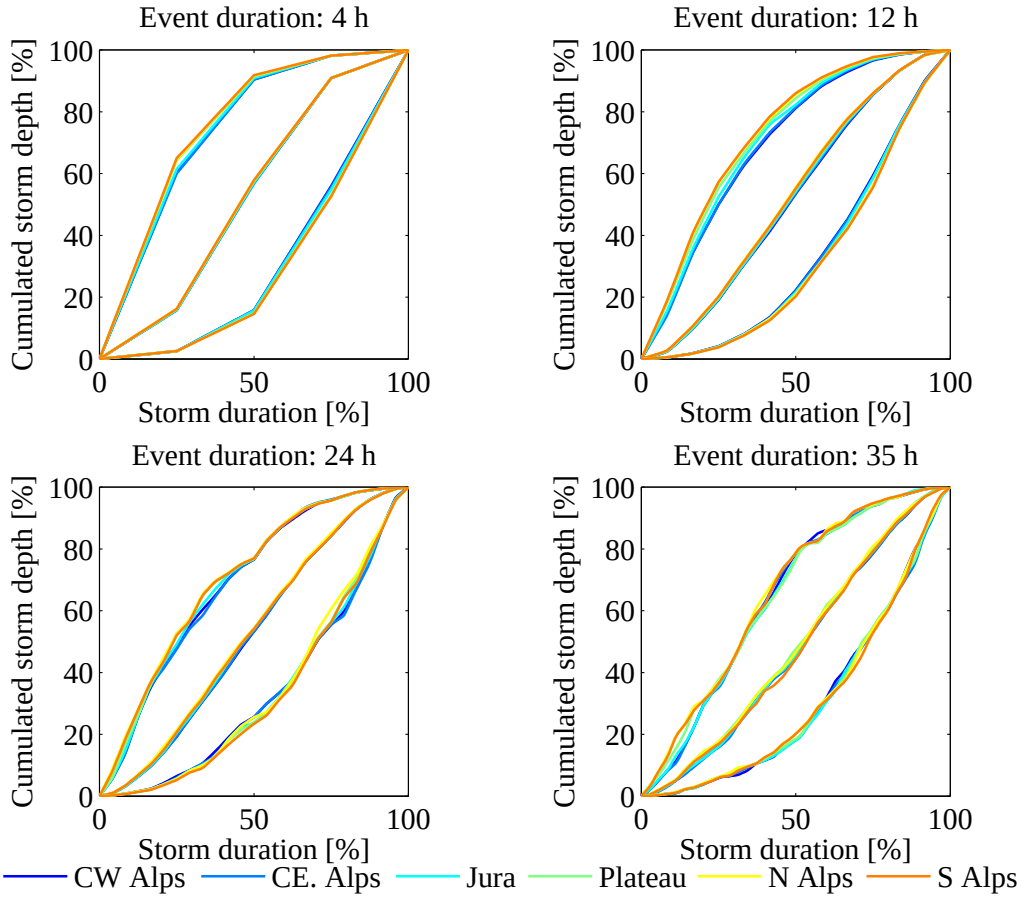

Figure A.3: Regional variation during spring for four different event durations. CW Alps = Central Western Alps, CE Alps = Central Western Alps, N Alps = Northern Alps, S Alps = Southern Alps.

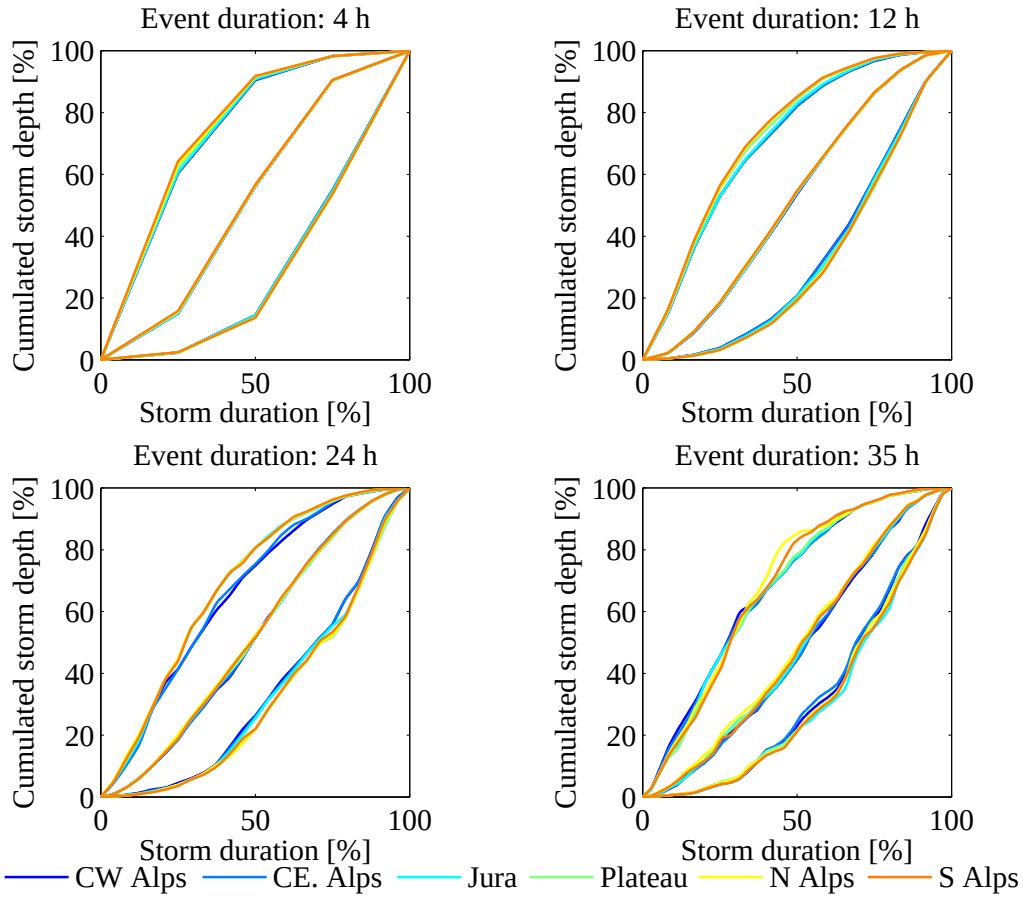

Figure A.4: Regional variation during fall for four different event durations.CW Alps = Central Western Alps, CE Alps = Central Western Alps, N Alps = Northern Alps, S Alps = Southern Alps.

A.3 Seasonal variability

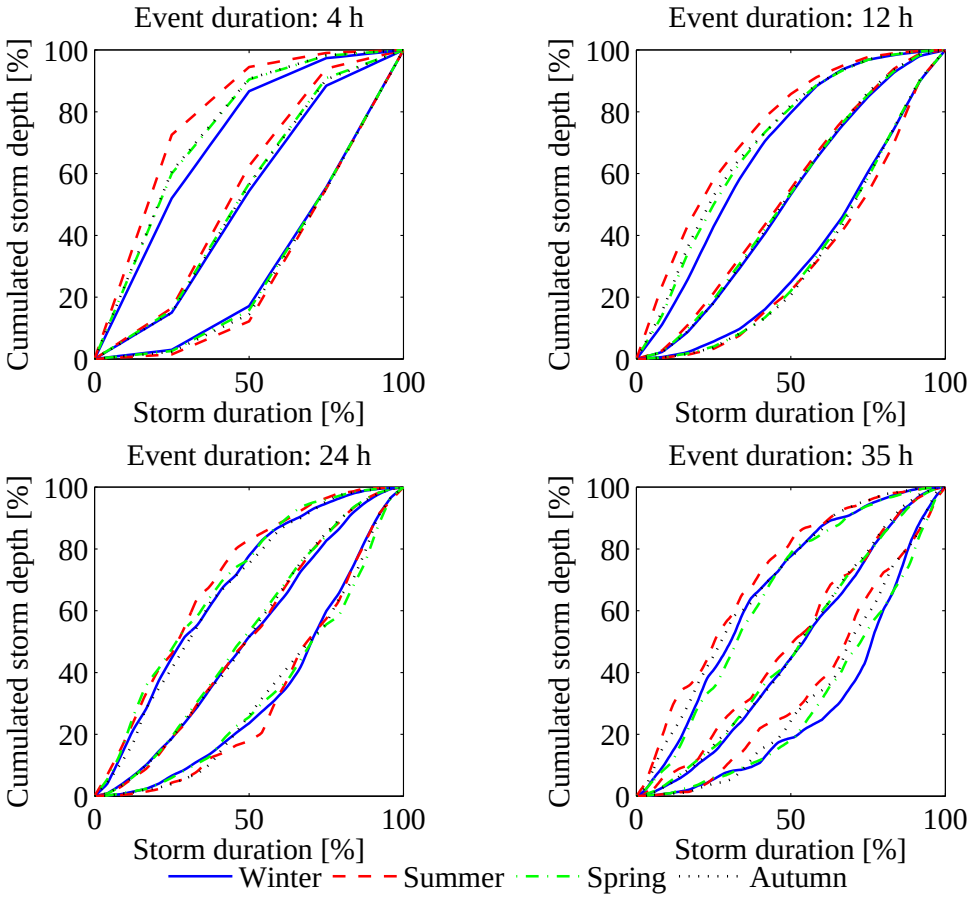

Figure A.5: Seasonality of the RMCs for the Central Eastern Alps for four different event durations.

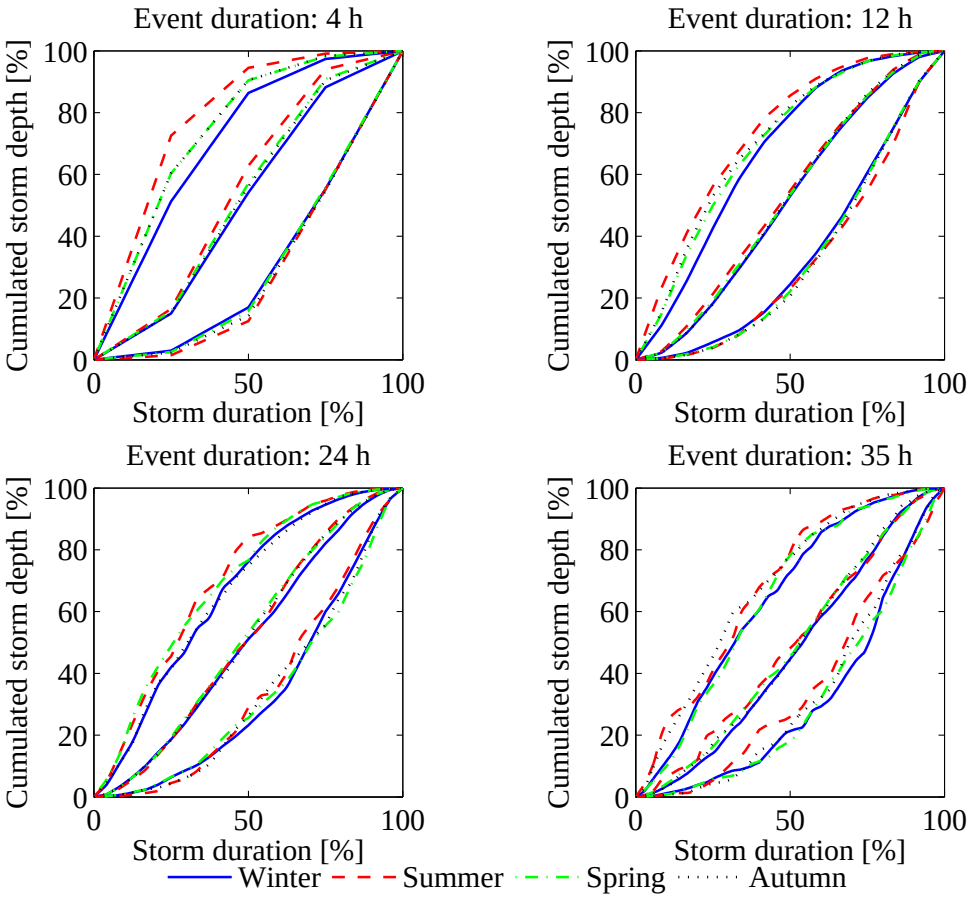

Figure A.6: Seasonality of the RMCs for the Central Western Alps for four different event durations.

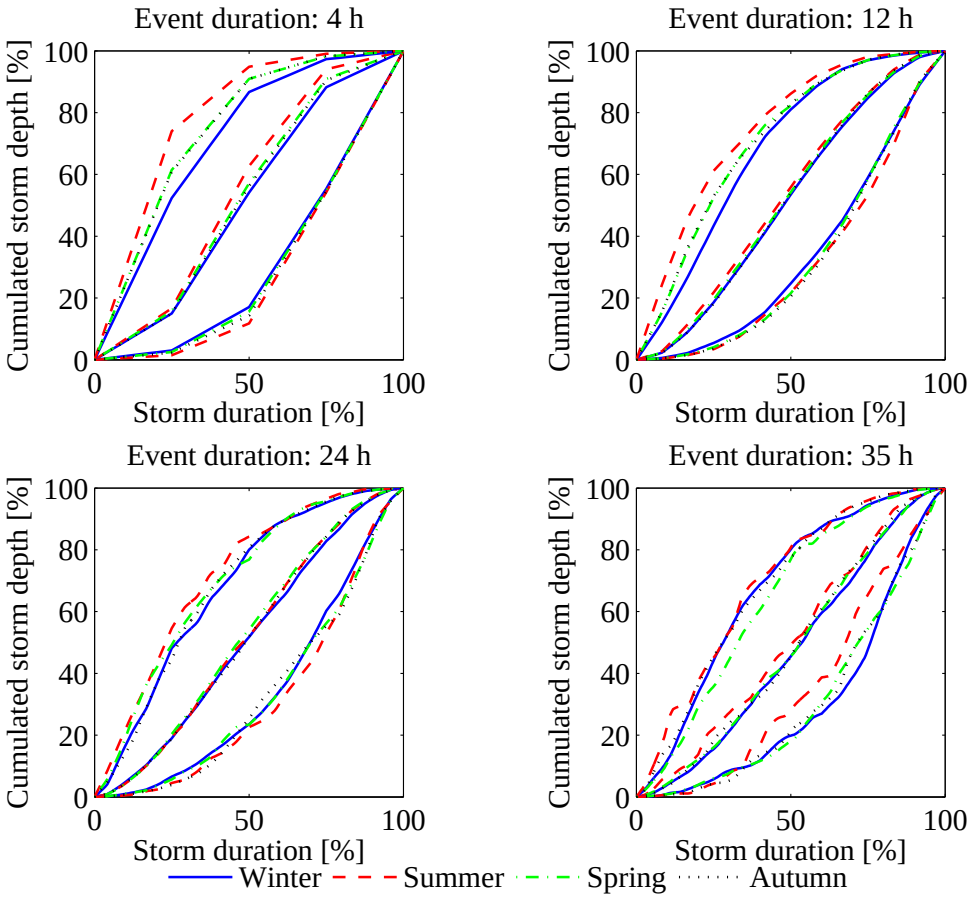

Figure A.7: Seasonality of the RMCs for the Jura for four different event durations.

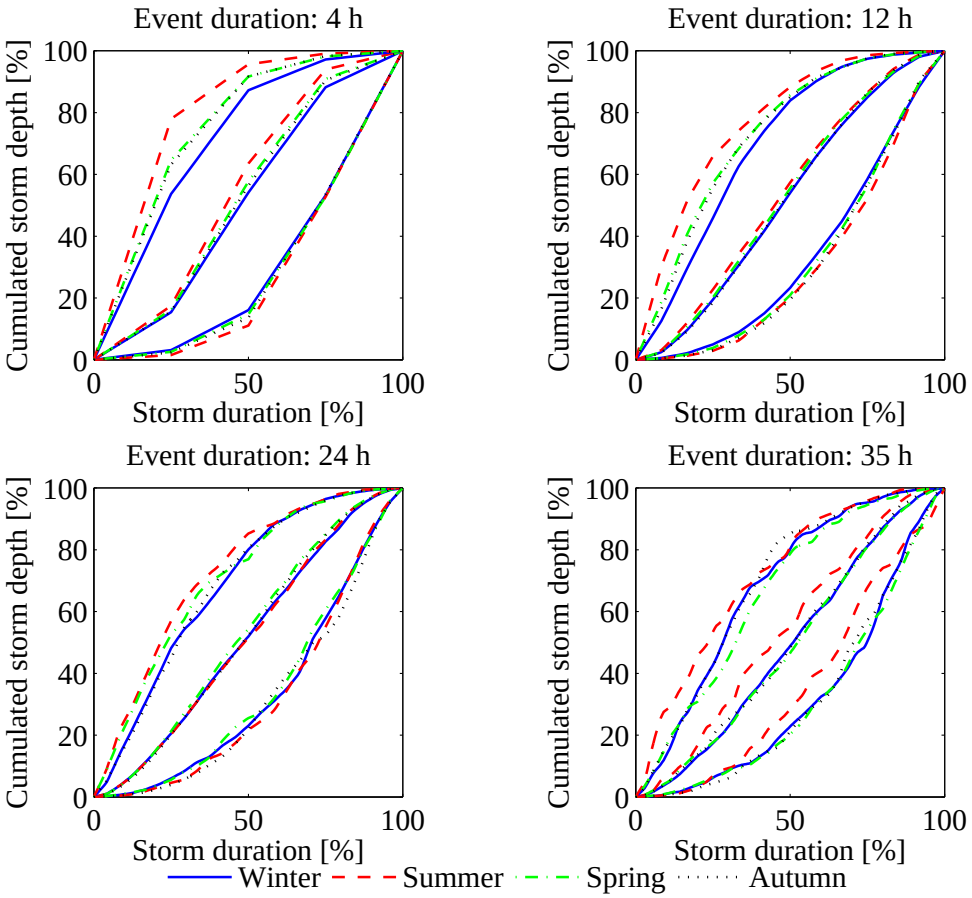

Figure A.8: Seasonality of the RMCs for the Northern Alps for four different event durations.

A.4 Dependence on event duration

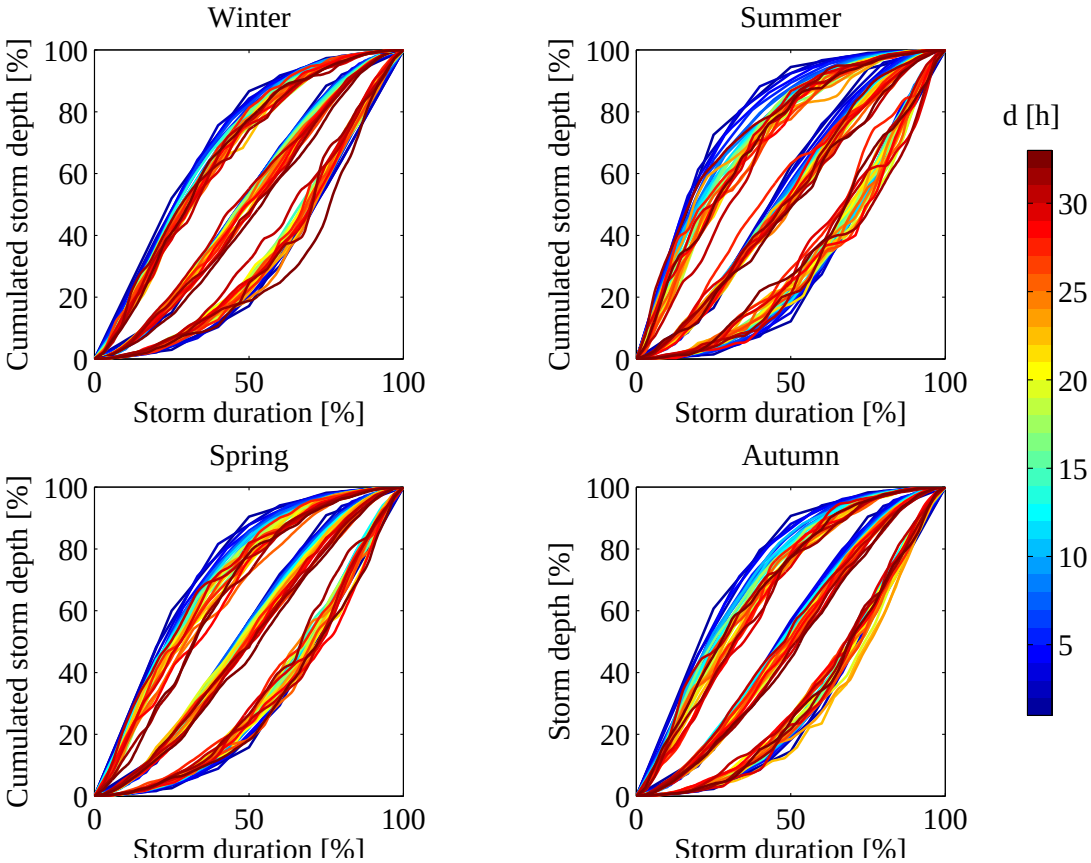

Figure A.9: Dependence on duration for the Central Eastern Alps for the four seasons.

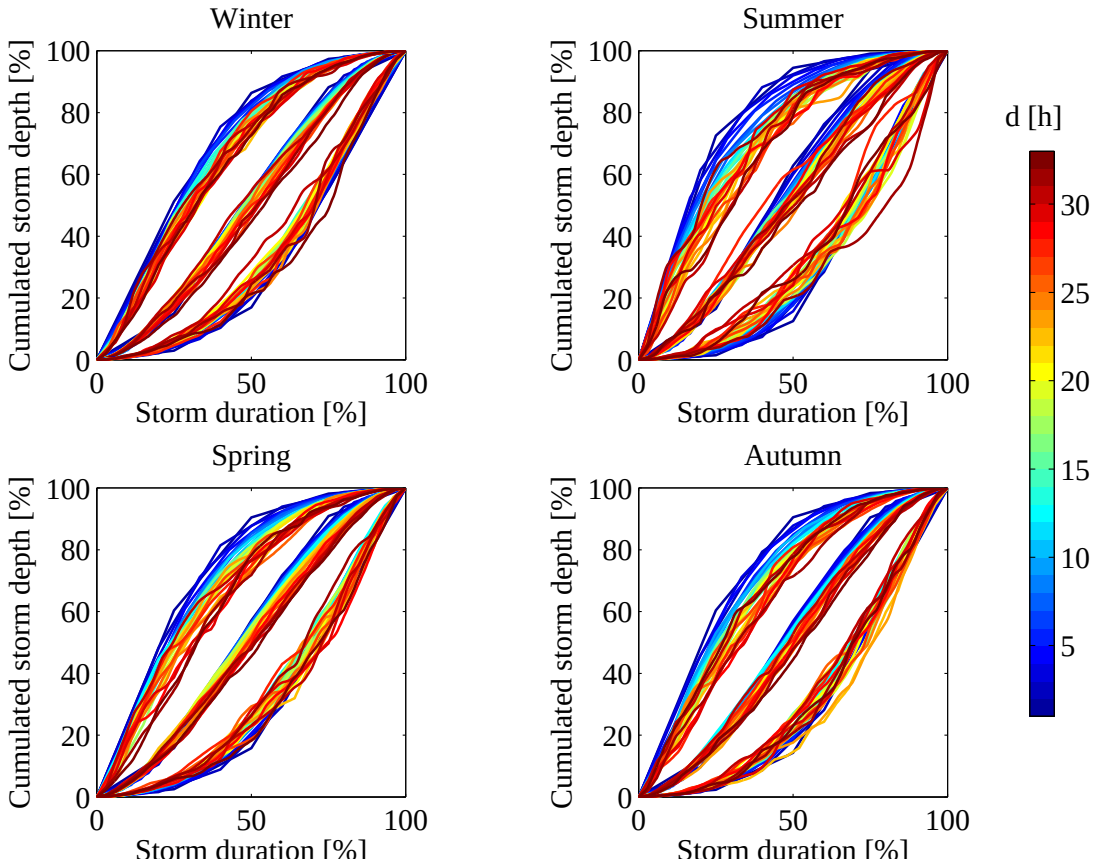

Figure A.10: Dependence on duration for the Central Western Alps for the four seasons.

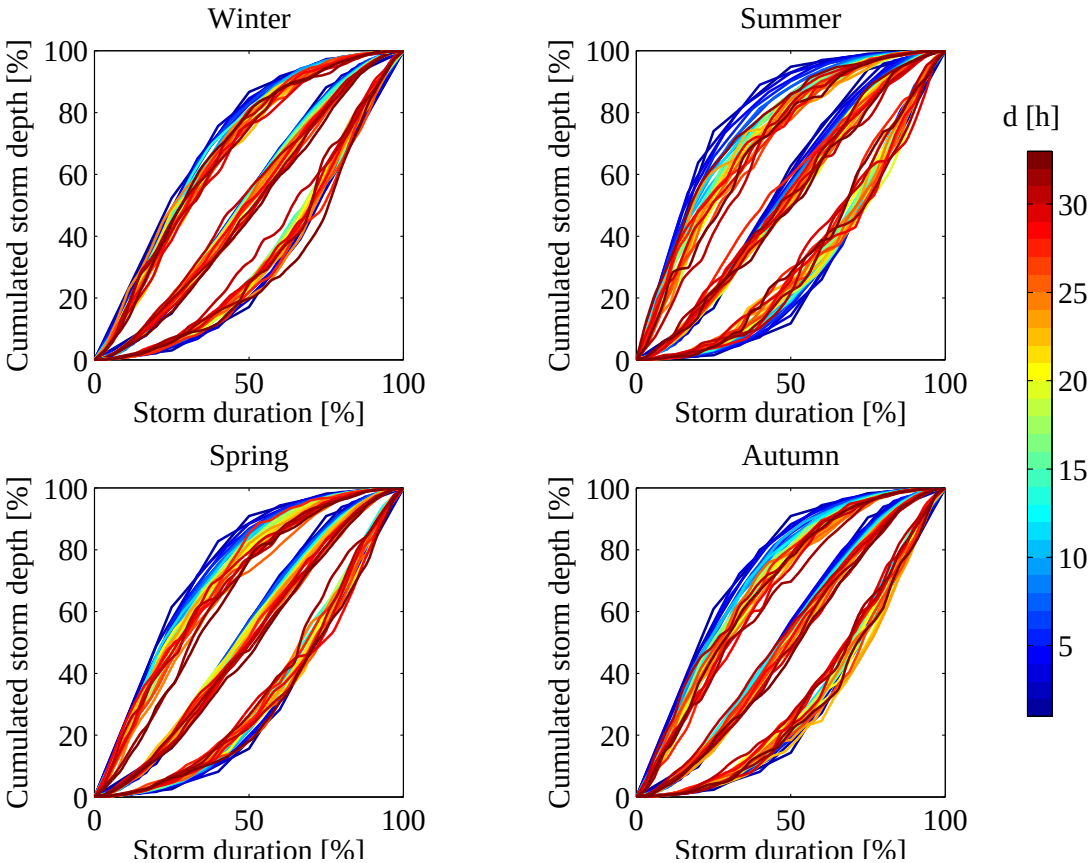

Figure A.11: Dependence on duration for the Jura for the four seasons.

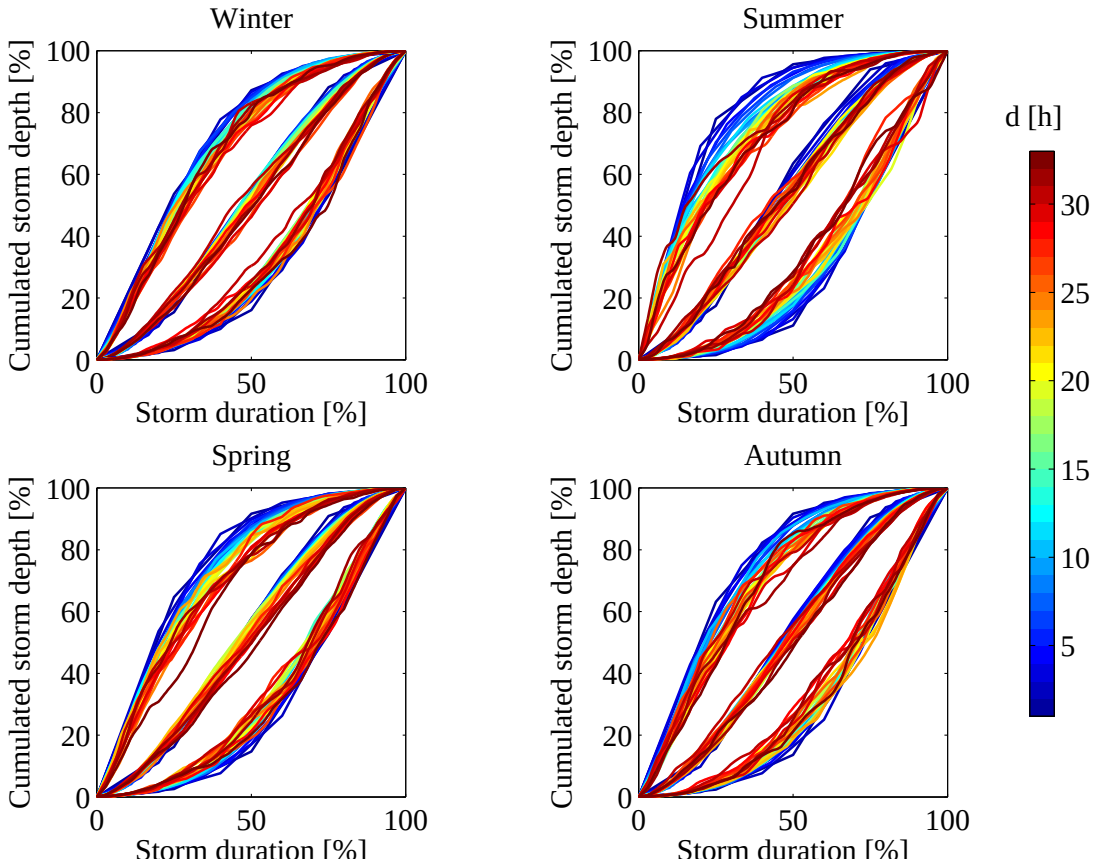

Figure A.12: Dependence on duration for the Northern Alps for the four seasons.

B Relevance of the correlation between precipitation and the 0° isothermal altitude

B.1 Criteria for the precipitation event definition

Figure B.1: Criteria for the event definition where one event can contain λ hours of precipitation free time, $\lambda \in \{0, 1, 2\}$.

B.2 Precipitation-temperature scalings

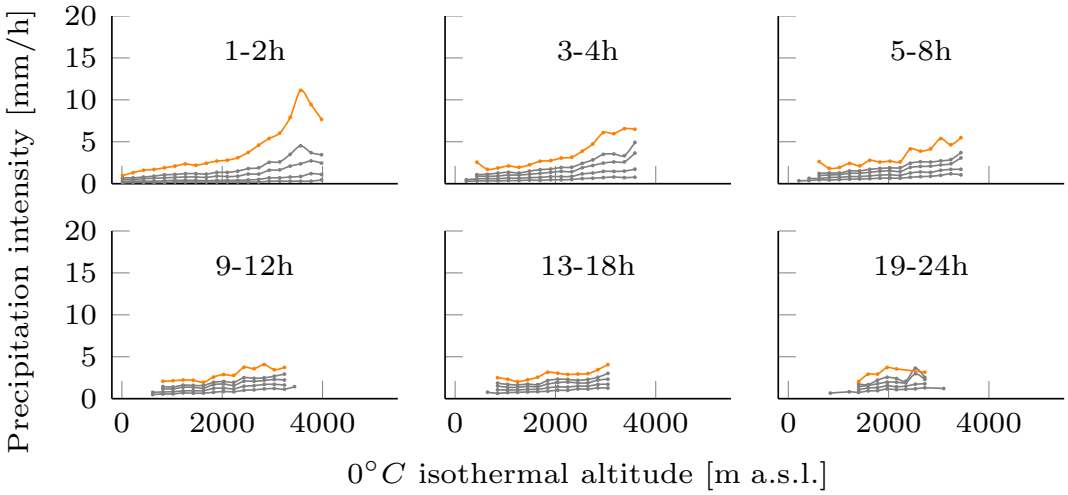

Figure B.3: 0.5, 0.75, 0.90, 0.95 and 0.99 quantiles of the different considered precipitation duration classes north of the Alps (Payerne meteorological soundings) and for the spring period (Mars-May) for $\lambda = 0$.

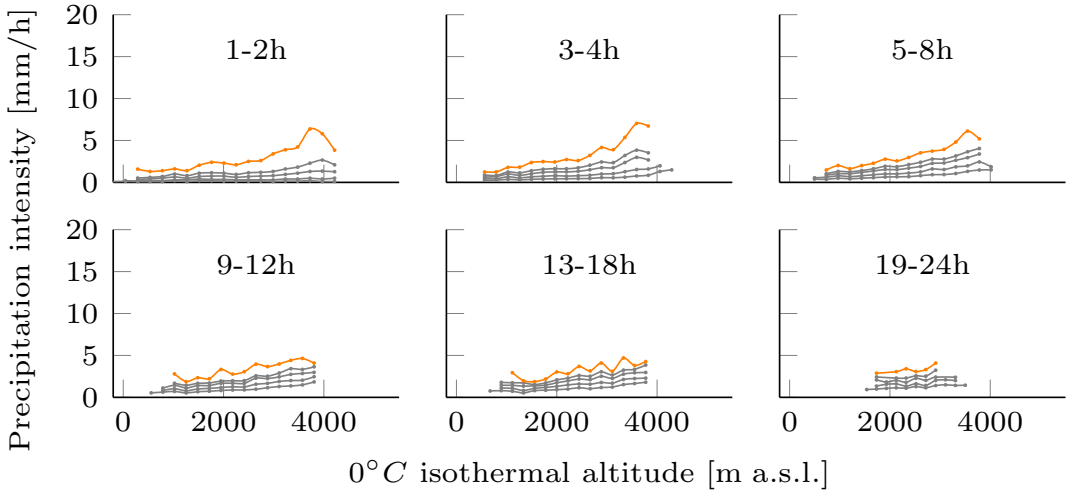

Figure B.2: 0.5, 0.75, 0.90, 0.95 and 0.99 quantiles of the different considered precipitation duration classes north of the Alps (Payerne meteorological soundings) and for the fall period (September-November) for $\lambda = 0$.

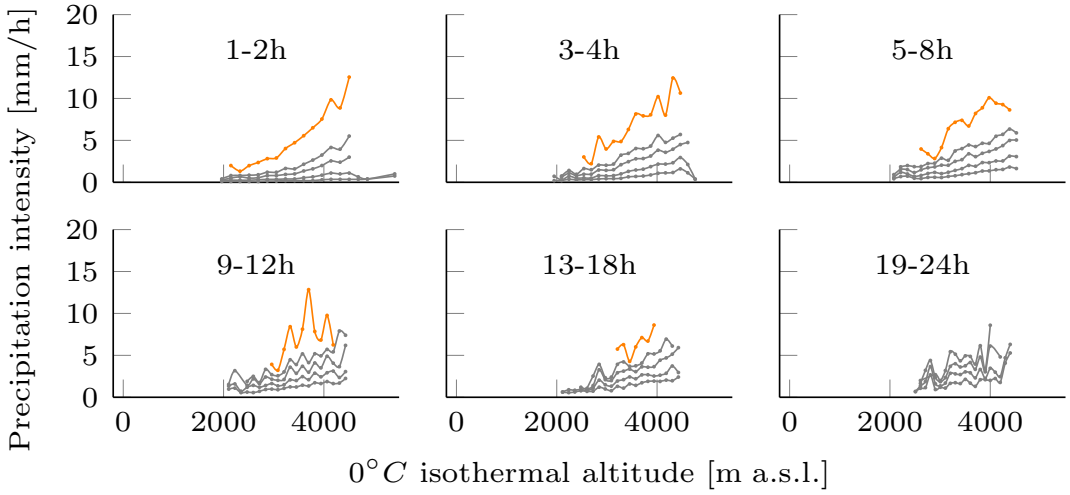

Figure B.4: 0.5, 0.75, 0.90, 0.95 and 0.99 quantiles of the different considered precipitation duration classes south of the Alps (Milan meteorological soundings) and for the summer period (June-August) for $\lambda = 0$.

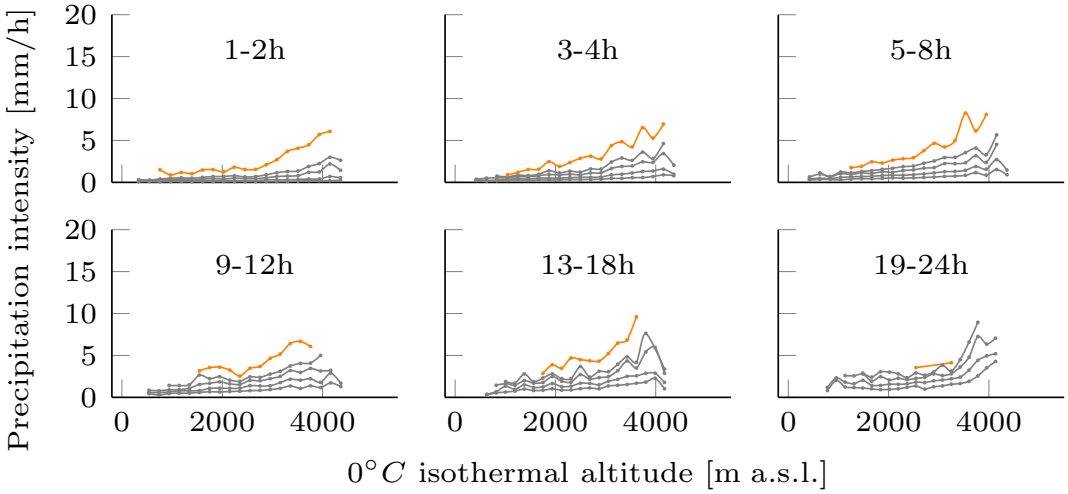

Figure B.5: 0.5, 0.75, 0.90, 0.95 and 0.99 quantiles of the different considered precipitation duration classes south of the Alps (Milan meteorological soundings) and for the fall period (September-November) for $\lambda = 0$.

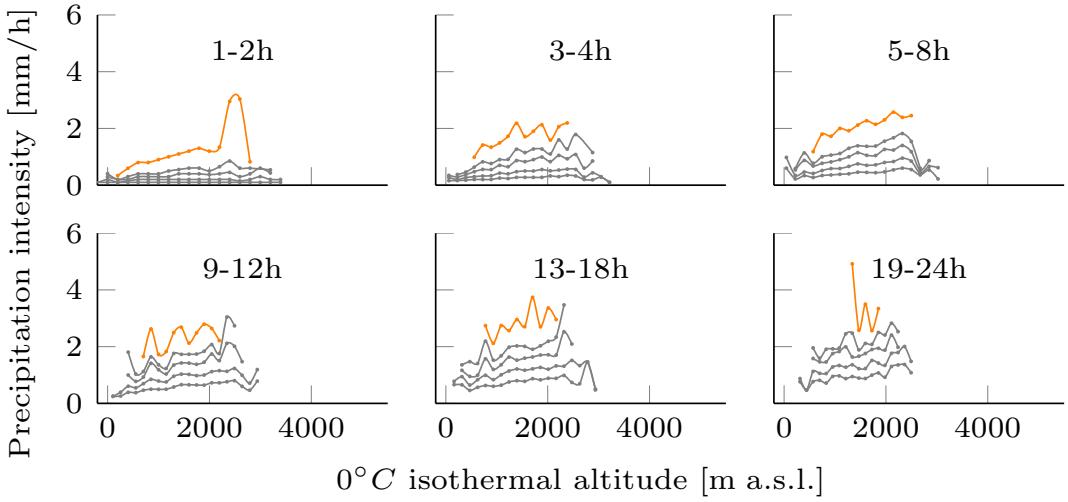

Figure B.6: 0.5, 0.75, 0.90, 0.95 and 0.99 quantiles of the different considered precipitation duration classes south of the Alps (Milan meteorological soundings) and for the winter period (December-February) for $\lambda = 0$.

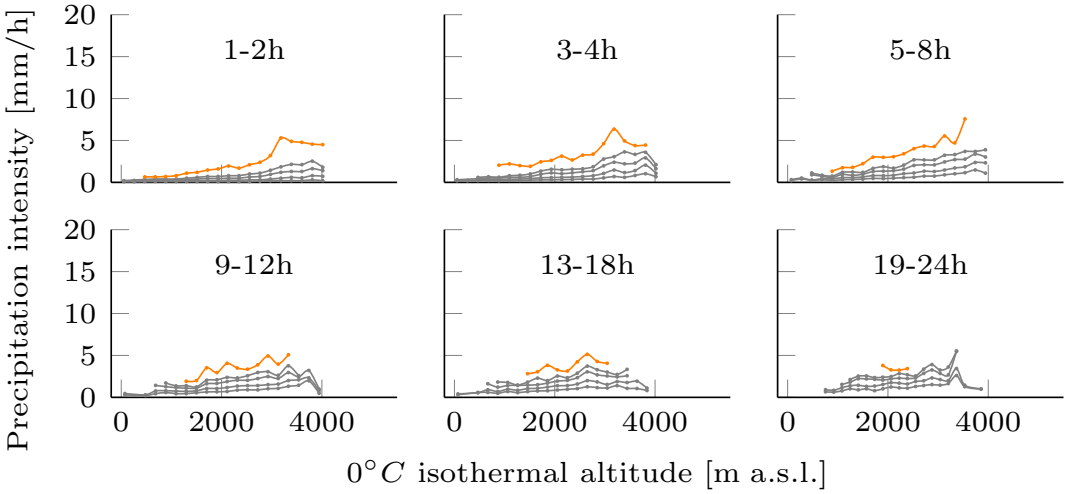

Figure B.7: 0.5, 0.75, 0.90, 0.95 and 0.99 quantiles of the different considered precipitation duration classes south of the Alps (Milan meteorological soundings) and for the spring period (Mars-May) for $\lambda = 0$.

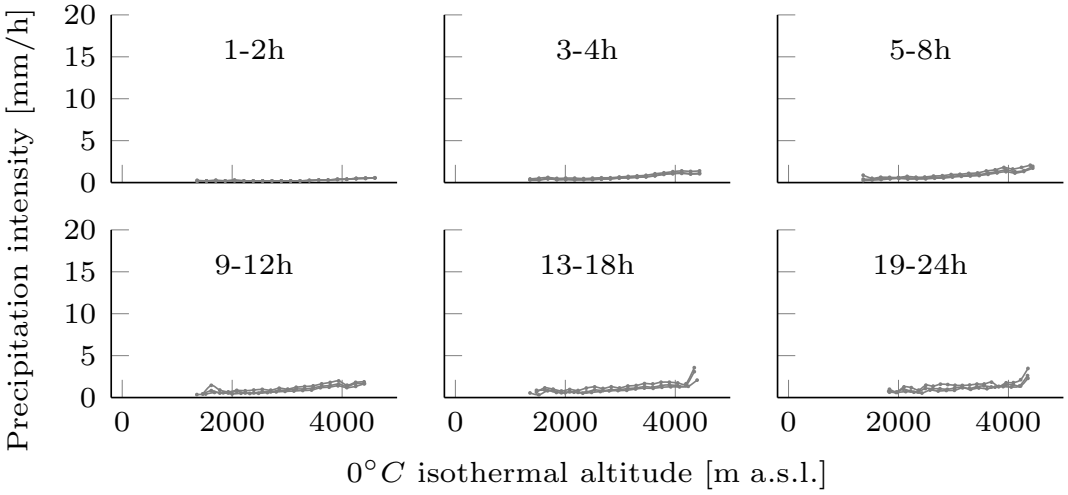

Figure B.8: Superposition of the results based on the three definitions (λ =0,1,2) for the precipitation events. Represented are the results for the soundings from Payerne during the summer period for the **0.50** quantile.

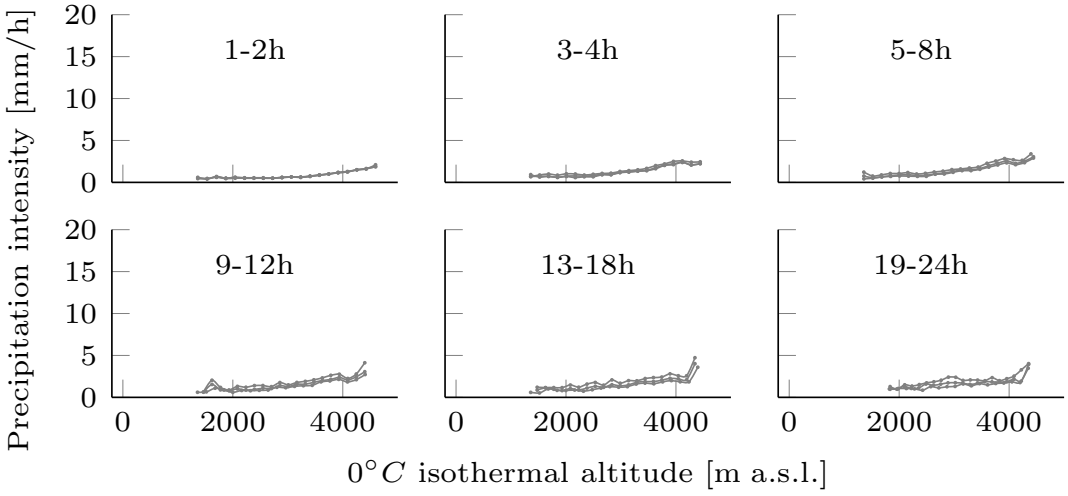

Figure B.9: Superposition of the results based on the three definitions (λ =0,1,2) for the precipitation events. Represented are the results for the soundings from Payerne during the summer period for the **0.75** quantile.

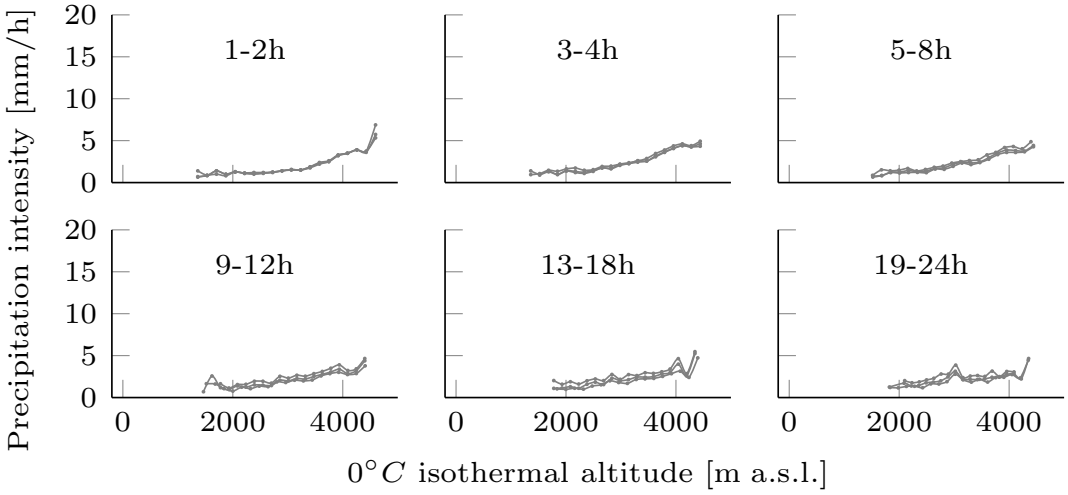

Figure B.10: Superposition of the results based on the three definitions (λ =0,1,2) for the precipitation events. Represented are the results for the soundings from Payerne during the summer period for the **0.90** quantile.

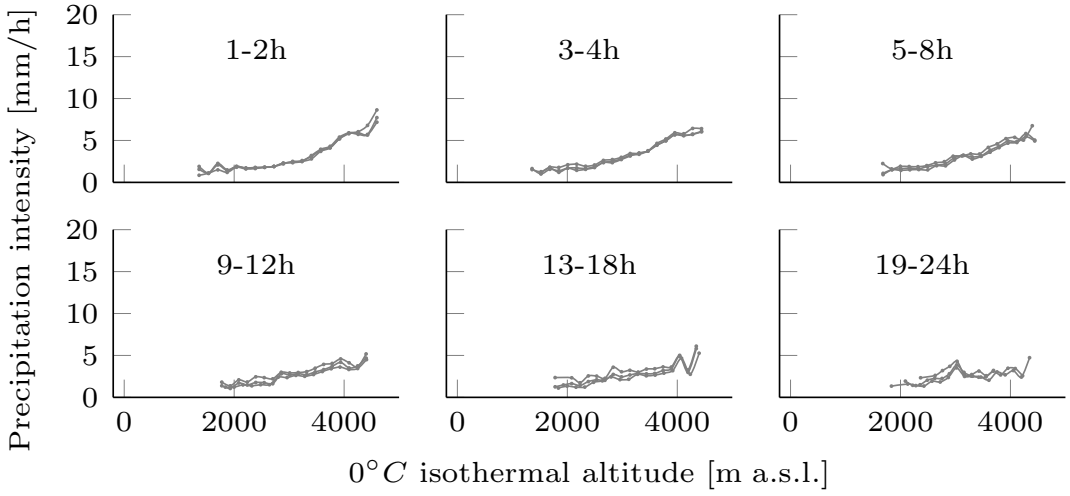

Figure B.11: Superposition of the results based on the three definitions (λ =0,1,2) for the precipitation events. Represented are the results for the soundings from Payerne during the summer period for the **0.95** quantile.

B.3 Parameters for linear relation application

In Chapter 4, a linear relation between the precipitation duration and the 0°C isothermal altitude could be derived. The parameters a and b of the relation $H = ad + b$, where H is the 0°C isothermal altitude and d is the precipitation duration in hours, are provided in Table B.1.

Table B.1: Parameters to apply the linear relation between the precipitation duration and the 0°C isothermal altitude for the four seasons of the years and two regions, i.e. north of the Alps and south of the Alps.

	North	South
Summer	$a = -8.352$, $b = 4521.7$	$a = -11.554$, $b = 4815.2$
Autumn	$a = -7.5411$, $b = 3109.3$	$a = -13.000$, $b = 4453.7$
Winter	$a = -15.505$, $b = 4389.3$	$a = -6.6532$, $b = 3085.8$
Spring	$a = -11.898$, $b = 3991.0$	$a = -11.187$, $b = 4066.1$

B.4 Hypsometric curve of Switzerland

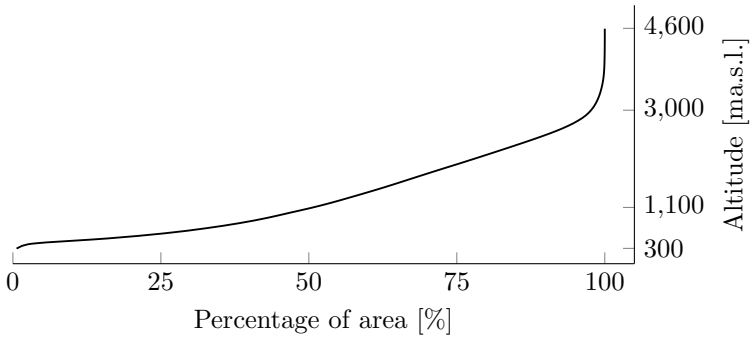

Figure B.12: Hypsometric curve of Switzerland

B.5 Hyetograph example

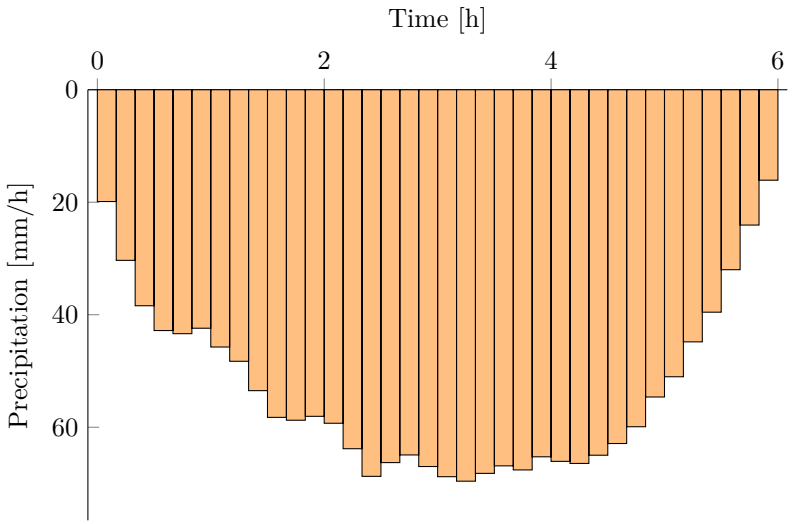

Figure B.13: Example of a 6h-PMP hyetograph.

C PMP maps upper surface limit

C.1 Study catchments on topographic maps

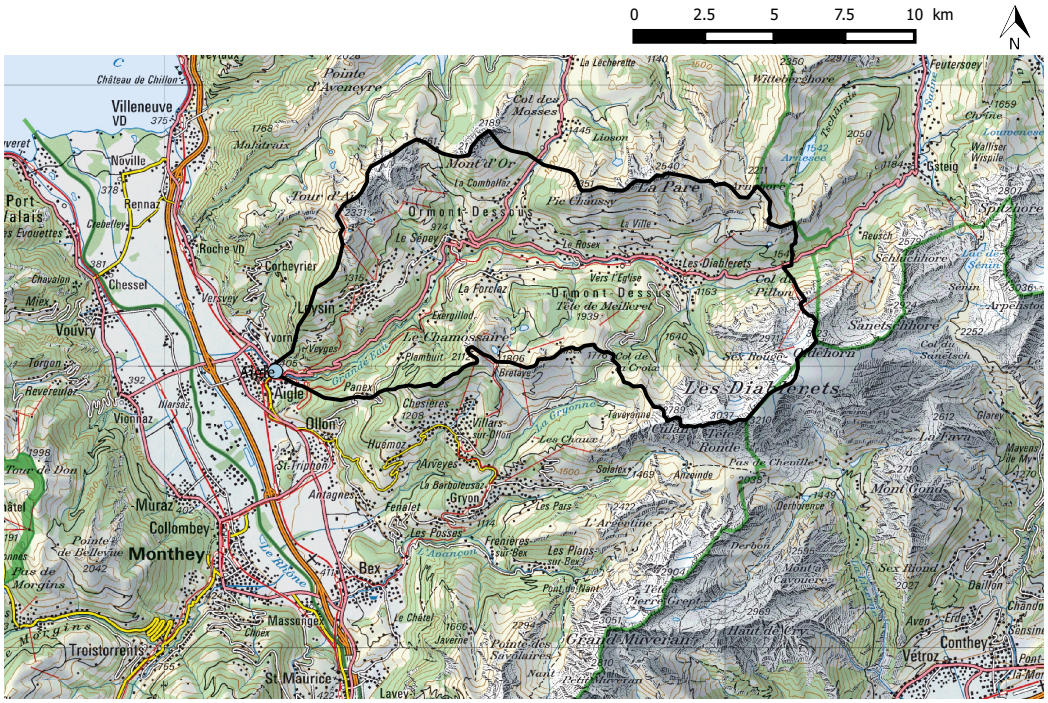

Figure C.1: Catchment of the *Grande Eau* river defined by the measurement station *Aigle*.

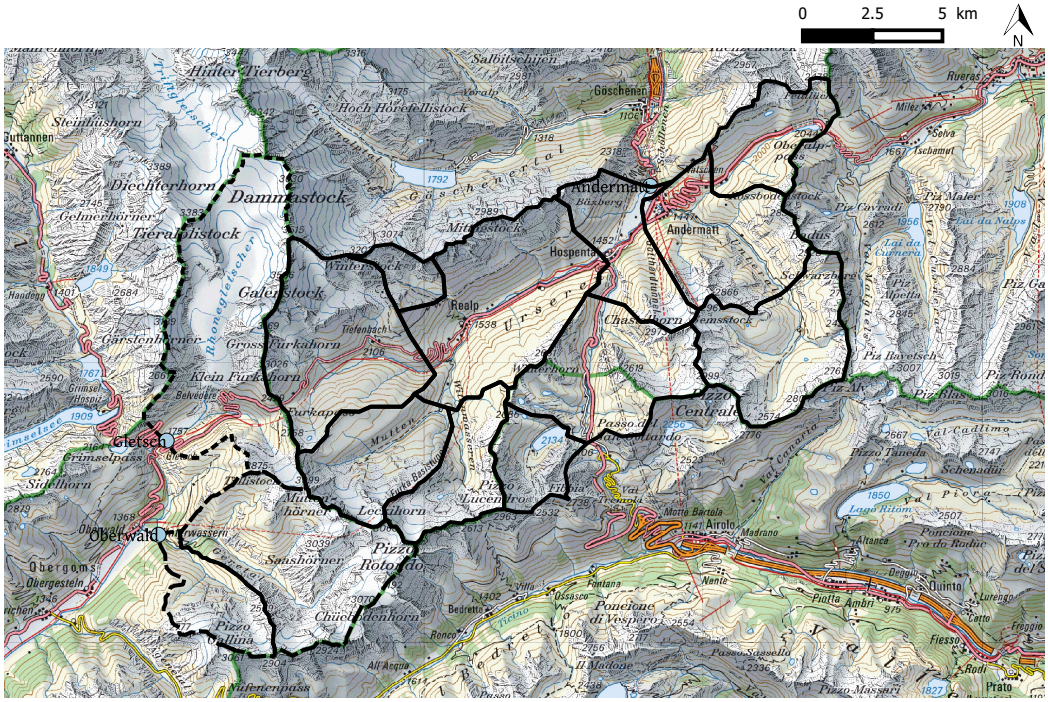

Figure C.2: Catchments of the *Reuss* river defined by the measurement station *Andermatt.*, the *Rhone* river defined by the measurement station *Gletsch* and the *Goneri* river defined by the measurement station *Oberwald*.

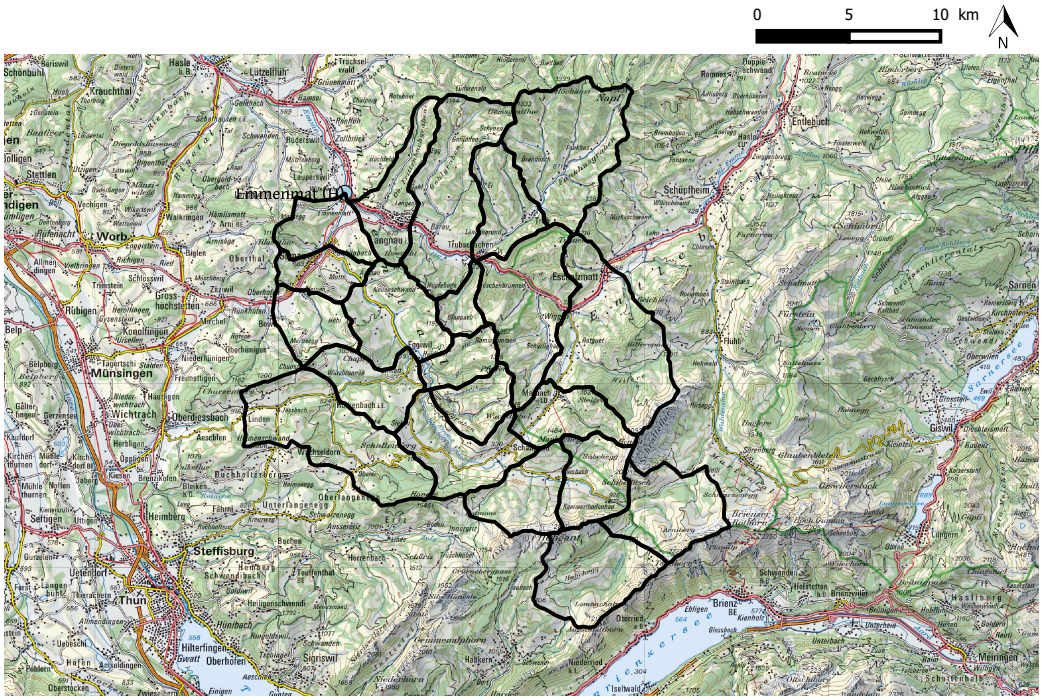

Figure C.3: Catchment of the *Emme* river defined by the measurement station *Emmenmatt*.

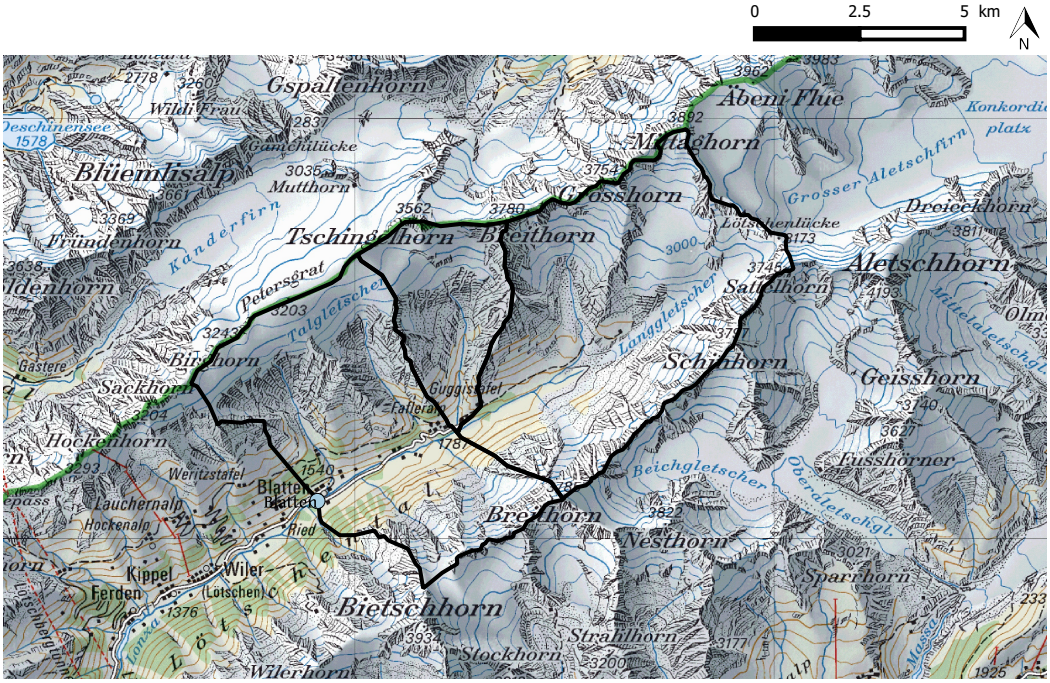

Figure C.4: Catchment of the *Lonza* river defined by the measurement station *Blatten*.

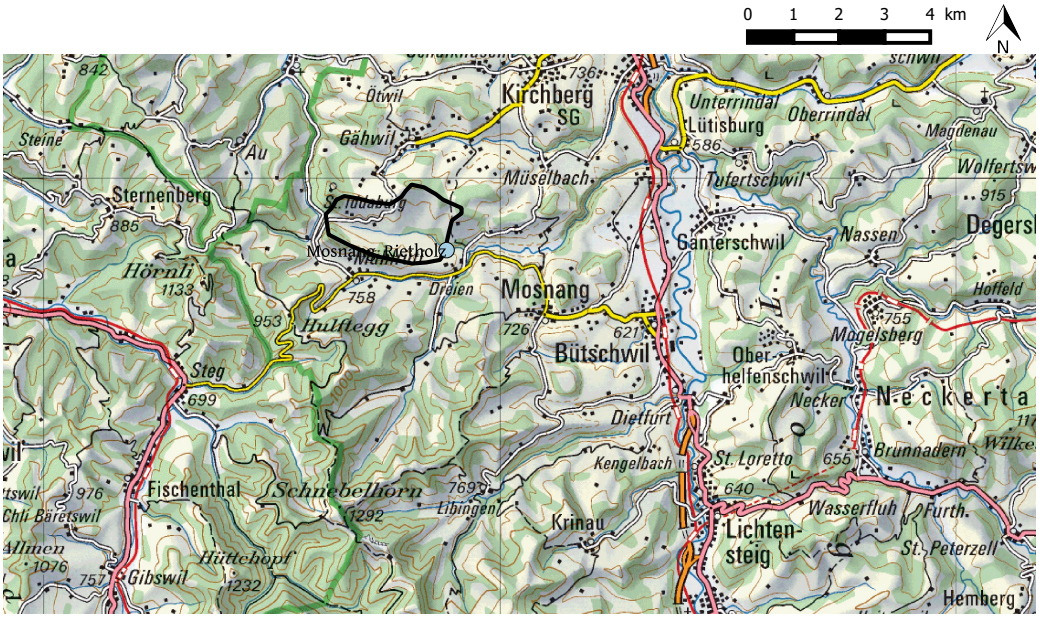

Figure C.5: Catchment of the *Rietholzbach* river defined by the measurement station *Mosnong/Rietholz*.

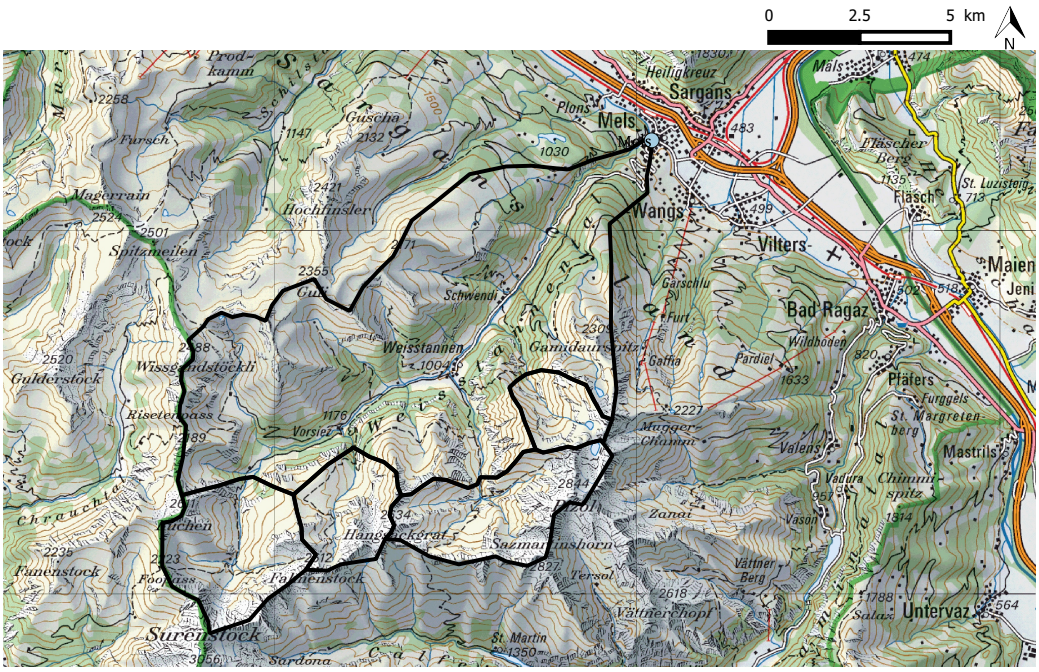

Figure C.6: Catchment of the *Seez* river defined by the measurement station *Mels*.

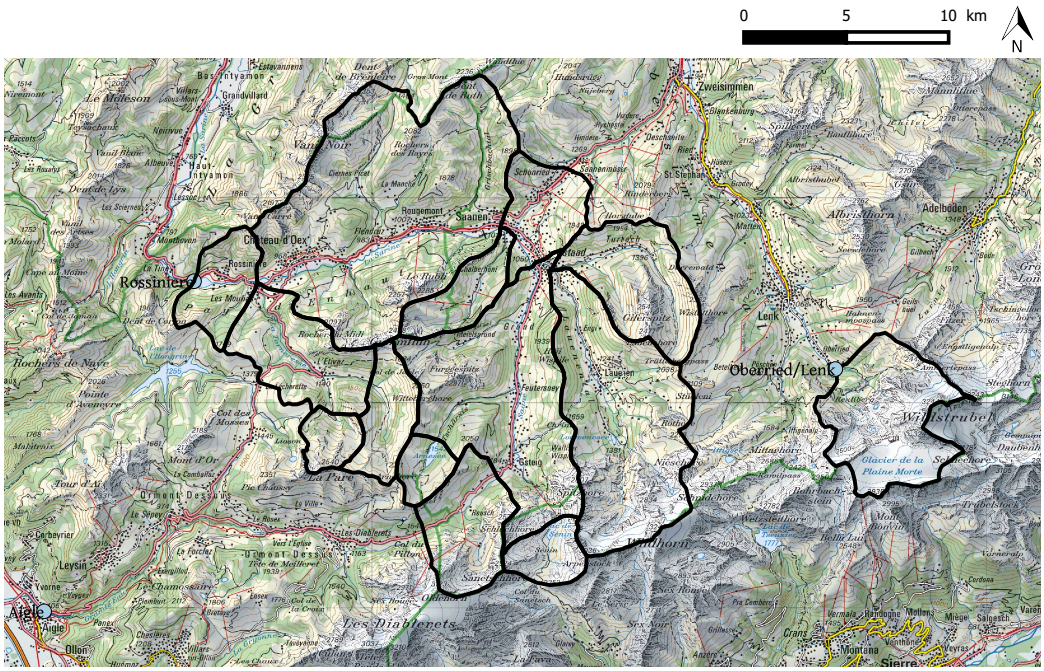

Figure C.7: Catchment of the *Sarine* river defined by the measurement station *Rossinière* and the *Simme* river defined by the measurement station *Oberried/Lenk*.

C.2 Study catchment surfaces

Table C.1: List of basins considered for the determination of the upper surface limit for the application of the Swiss PMP maps.

River name	Measurement station	Main catchment Surface [km^2]	Glacier cover [km^2]
Rietholzbach	Mosnang, Rietholz	3	0
Limmernbach	Limmernboden dam	17.5	2.2
Simme	Oberried/Lenk	36	12.6
Vispa	Mattmark dam	38	9.2
Rhone	Gletsch	39	20.3
Goneri	Oberwald	40	5.6
Lonza	Blatten	78	28.9
Seez	Mels	105	0.32
Grande Eau	Aigle	132	2.6
Reuss	Andermatt	192	11.5
Massa	Blatten bei Naters	195	128.7
Rhone	Reckingen	215	38.7
Vezasca	Contra dam	232	0
Sarine	Rossinière	295	11.8
Emme	Emmenmatt	443	0

C.3 Meteorological stations

C.3.1 Meteorological stations for the Aigle catchment

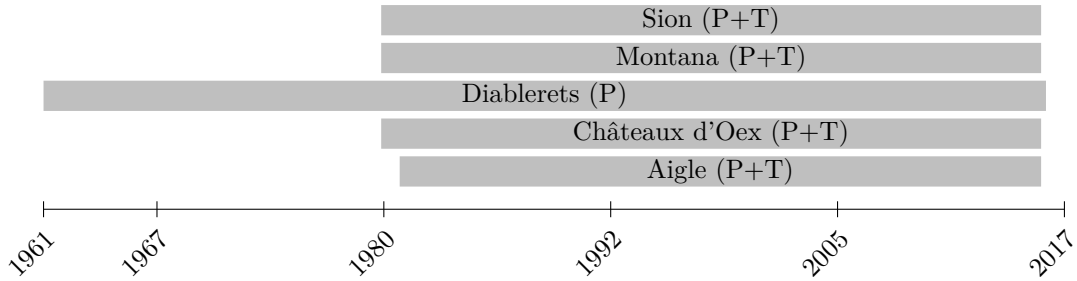

Figure C.8: Graphical data availability period representation for the meteorological stations considered for the calibration and validation for the basin defined by the discharge measurement station *Aigle*.

Table C.2: Detailed dates per meteorological station, taken into account for the calibration and validation for the basin defined by the discharge measurement station *Aigle*, with indication of the measured quantities.

Station	First value	Last value	Precipitation	Temperature
Aigle	01.01.1981 00:00	24.09.2015 23:00	✓	✓
Chateaux d'Oex	01.01.1980 00:00	24.09.2015 23:00	✓	✓
Diablerets	01.01.1961 00:00	30.12.2015 00:00	✓	
Montana	01.01.1980 00:00	24.09.2015 23:00	✓	✓
Sion	01.01.1980 00:00	24.09.2015 23:00	✓	✓

C.3.2 Meteorological stations for the Andermatt catchment

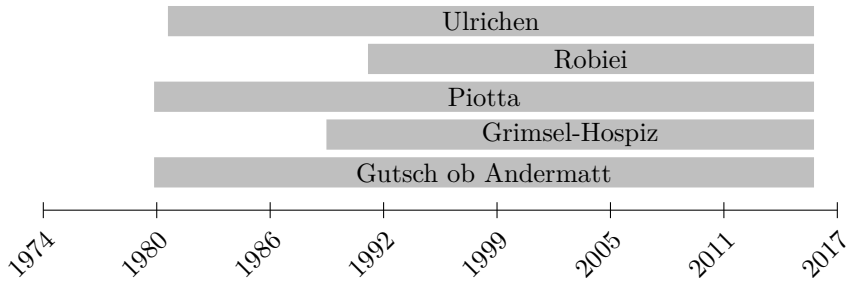

Figure C.9: Graphical data availability period representation for the meteorological stations considered for the calibration and validation for the basin defined by the discharge measurement station *Andermatt*.

Table C.3: Detailed dates per meteorological station, taken into account for the calibration and validation for the basin defined by the discharge measurement station *Andermatt*, with indication of the measured quantities.

Station	First value	Last value	Precipitation	Temperature
Gutsch ob Andermatt	01.01.1980 00:00	24.09.2015 23:00	✓	✓
Grimsel-Hospiz	01.05.1989 01:00	24.09.2015 23:00	✓	✓
Piotta	01.01.1980 00:00	24.09.2015 23:00	✓	✓
Robiei	01.08.1991 00:00	24.09.2015 23:00	✓	✓
Ulrichen	01.10.1980 01:00	24.09.2015 23:00	✓	✓
Disentis	24.09.1980 23:00	24.09.2015 23:00	✓	✓

C.3.3 Meteorological stations for the Blatten catchment

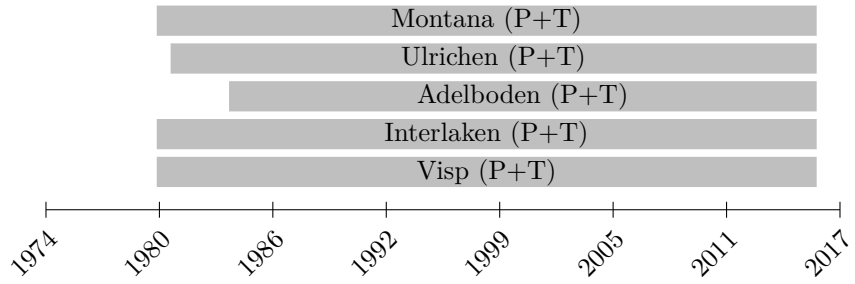

Figure C.10: Graphical data availability period representation for the meteorological stations considered for the calibration and validation for the basin defined by the discharge measurement station *Blatten*.

Table C.4: Detailed dates per meteorological station, taken into account for the calibration and validation for the basin defined by the discharge measurement station *Blatten*, with indication of the measured quantities.

Station	First value	Last value	Precipitation	Temperature
Visp	01.01.1980 00:00	24.09.2015 23:00	✓	✓
Interlaken	01.01.1980 00:00	24.09.2015 23:00	✓	✓
Adelboden	01.12.1983 00:00	24.09.2015 23:00	✓	✓
Ulrichen	01.10.1980 01:00	24.09.2015 23:00	✓	✓
Montana	01.01.1980 00:00	24.09.2015 23:00	✓	✓

C.3.4 Meteorological stations for the Contra dam catchment

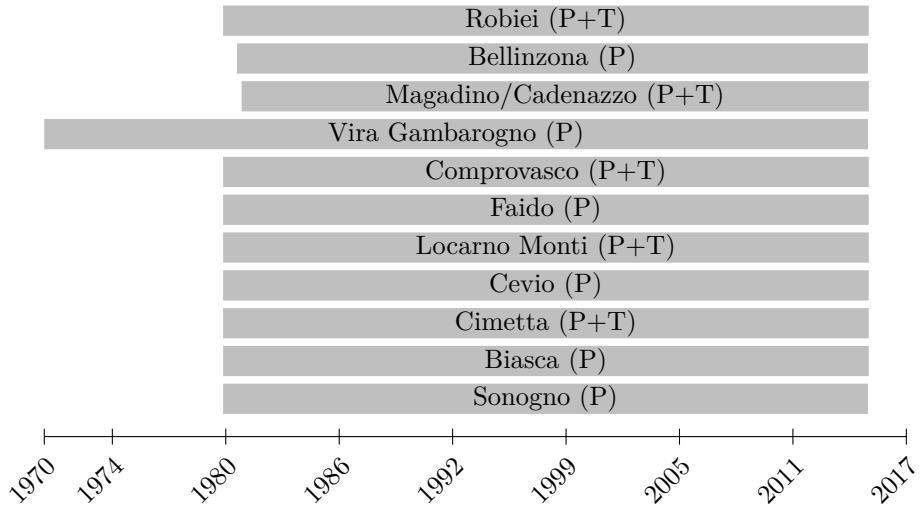

Figure C.11: Graphical data availability period representation for the meteorological stations considered for the calibration and validation for the *Contra dam*.

Table C.5: Detailed dates per meteorological station, taken into account for the calibration and validation for the basin of the *Contra dam*, with indication of the measured quantities.

Station	First value	Last value	Precipitation	Temperature
Sonogno	01.01.1980 00:00	01.12.2014 00:00	✓	
Biasca	01.01.1980 00:00	16.12.2014 00:00	✓	
Cimetta	01.01.1980 00:00	16.12.2014 12:00	✓	✓
Cevio	01.01.1980 00:00	16.12.2014 12:00	✓	
Locarno Monti	01.01.1980 00:00	16.12.2014 12:00	✓	✓
Faido	01.01.1980 00:00	16.12.2014 00:00	✓	
Comprovasco	01.01.1980 00:00	16.12.2014 12:00	✓	✓
Vira Gambarogno	01.01.1970 00:00	01.12.2014 00:00	✓	
Magadino/Cadenazzo	01.01.1981 00:00	16.12.2014 15:00	✓	✓

C.3.5 Meteorological stations for the Emmenmatt catchment

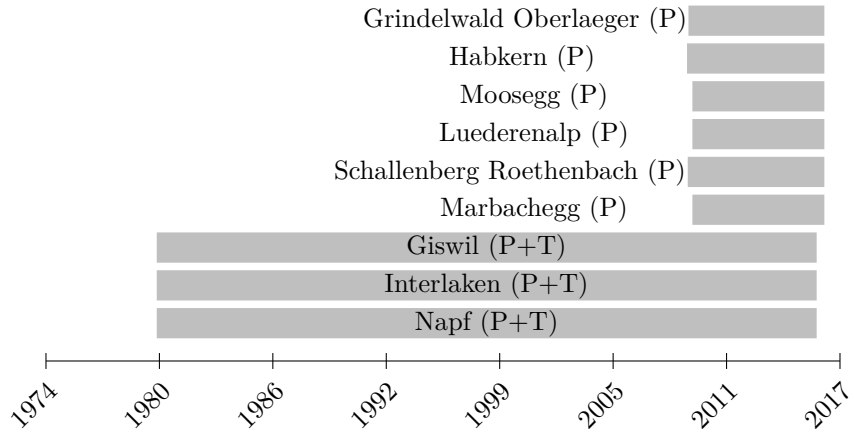

Figure C.12: Graphical data availability period representation for the meteorological stations considered for the calibration and validation for the basin defined by the discharge measurement station *Emmenmatt*.

Table C.6: Detailed dates per meteorological station, taken into account for the calibration and validation for the basin defined by the discharge measurement station *Emmenmatt*, with indication of the measured quantities.

Station	First value	Last value	Precipitation	Temperature
Napf	01.01.1980 00:00	24.09.2015 23:00	✓	✓
Interlaken	01.01.1980 00:00	24.09.2015 23:00	✓	✓
Giswil	01.01.1980 00:00	24.09.2015 23:00	✓	✓
Marbachegg	01.01.2009 00:00	23.02.2016 15:00	✓	
Schallenberg Roethenbach	01.10.2008 01:00	23.02.2016 15:00	✓	
Luederenalp	01.01.2009 00:00	23.02.2016 15:00	✓	
Moosegg	01.01.2009 00:00	23.02.2016 15:00	✓	
Habkern	17.09.2008 01:00	23.02.2016 15:00	✓	
Grindelwald Oberlaeger	15.10.2008 01:00	23.02.2016 15:00	✓	

C.3.6 Meteorological stations for the Gletsch catchment

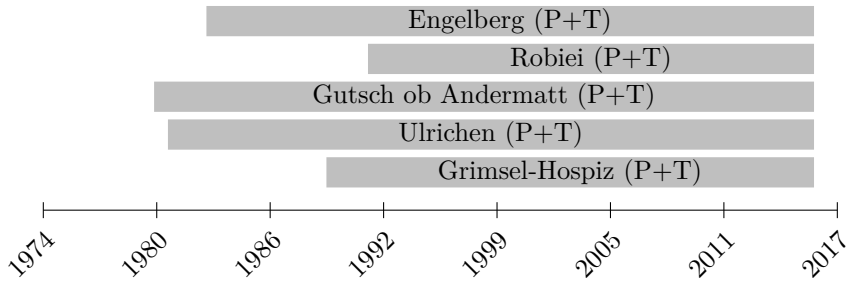

Figure C.13: Graphical data availability period representation for the meteorological stations considered for the calibration and validation for the basin defined by the discharge measurement station *Gletsch*.

Table C.7: Detailed dates per meteorological station, taken into account for the calibration and validation for the basin defined by the discharge measurement station *Gletsch*, with indication of the measured quantities.

Station	First value	Last value	Precipitation	Temperature
Grimsel-Hospiz	01.05.1989 01:00	24.09.2015 23:00	✓	✓
Ulrichen	01.10.1980 01:00	24.09.2015 23:00	✓	✓
Gutsch ob Andermatt	01.01.1980 00:00	24.09.2015 23:00	✓	✓
Robiei	01.08.1991 01:00	24.09.2015 23:00	✓	✓
Engelberg	01.11.1982 00:00	24.09.2015 23:00	✓	✓

C.3.7 Meteorological stations for the Limmernboden dam catchment

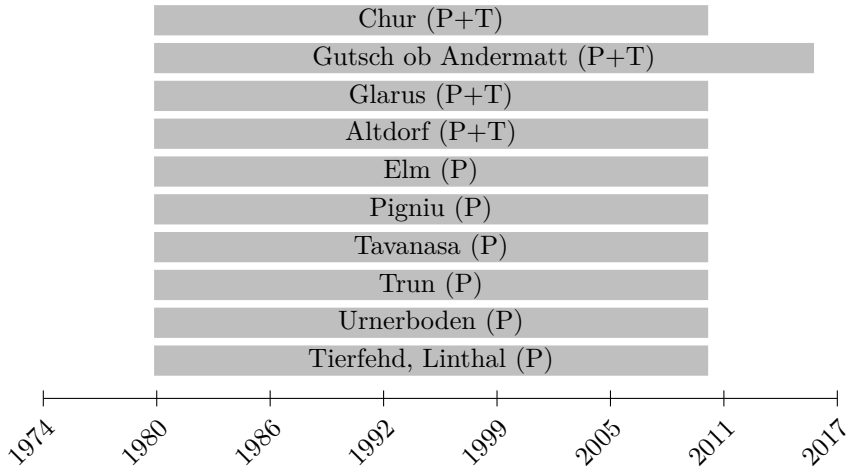

Figure C.14: Graphical data availability period representation for the meteorological stations considered for the calibration and validation for the *Limmernboden dam*.

Table C.8: Detailed dates per meteorological station, taken into account for the calibration and validation for the basin of the *Limmernboden dam*, with indication of the measured quantities.

Station	First value	Last value	Precipitation	Temperature
Tierfehd, Linthal	01.01.1980 00:00	31.12.2009 14:00	✓	
Urnerboden	01.01.1980 00:00	31.12.2009 14:00	✓	
Trun	01.01.1980 00:00	31.12.2009 17:00	✓	
Tavanasa	01.01.1980 00:00	31.12.2009 17:00	✓	
Pigniu	01.01.1980 00:00	31.12.2009 18:00	✓	
Elm	01.01.1980 00:00	31.12.2009 18:00	✓	
Altdorf	01.01.1980 00:00	31.12.2009 12:00	✓	✓
Glarus	01.01.1980 00:00	31.12.2009 11:00	✓	✓
Gutsch ob Andermatt	01.01.1980 00:00	24.09.2015 23:00	✓	✓
Chur	01.01.1980 00:00	31.12.2009 18:00	✓	✓

C.3.8 Meteorological stations for the Mattmark dam catchment

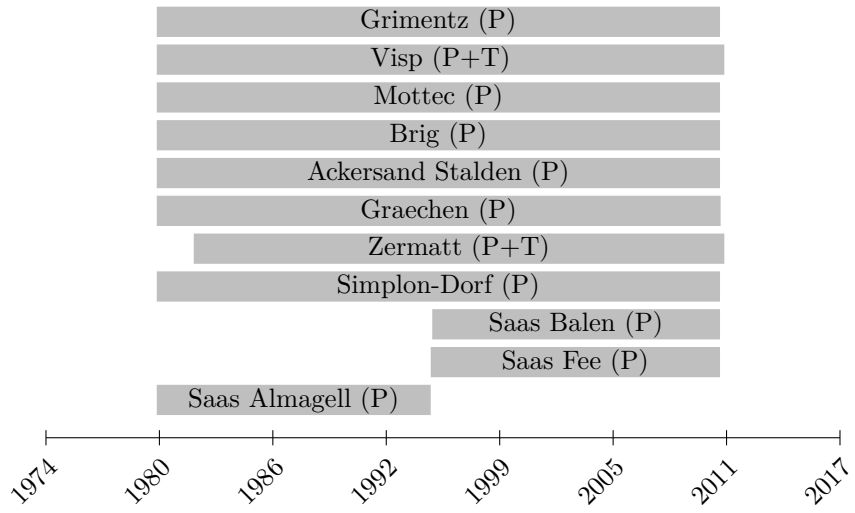

Figure C.15: Graphical data availability period representation for the meteorological stations considered for the calibration and validation for the *Mattmark dam*.

Table C.9: Detailed dates per meteorological station, taken into account for the calibration and validation for the basin of the *Mattmark dam*, with indication of the measured quantities.

Station	First value	Last value	Precipitation	Temperature
Saas Fee	01.11.1994 00:00	01.07.2010 06:00	✓	
Saas Balen	01.12.1994 00:00	01.07.2010 06:00	✓	
Saas Almagell	01.01.1980 00:00	01.09.1994 00:00	✓	
Simplon-Dorf	01.01.1980 00:00	01.07.2010 06:00	✓	
Zermatt	01.01.1982 00:00	24.09.2010 12:00	✓	✓
Graechen	01.01.1980 00:00	13.07.2010 06:00	✓	
Ackersand Stalden	01.01.1980 00:00	01.07.2010 06:00	✓	
Brig	01.01.1980 00:00	01.07.2010 06:00	✓	
Mottec	01.01.1980 00:00	01.07.2010 06:00	✓	
Visp	01.01.1980 00:00	24.09.2010 12:00	✓	✓
Grimentz	01.01.1980 00:00	01.07.2010 06:00	✓	

C.3.9 Meteorological stations for the Mels catchment

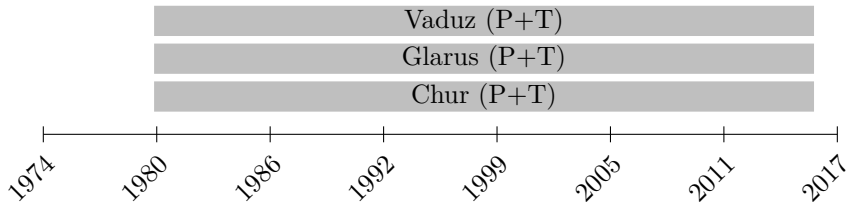

Figure C.16: Graphical data availability period representation for the meteorological stations considered for the calibration and validation for the basin defined by the discharge measurement station *Mels*.

Table C.10: Detailed dates per meteorological station, taken into account for the calibration and validation for the basin defined by the discharge measurement station *Mels*, with indication of the measured quantities.

Station	First value	Last value	Precipitation	Temperature
Chur	01.01.1980 00:00	24.09.2015 23:00	✓	✓
Glarus	01.01.1980 00:00	24.09.2015 23:00	✓	✓
Vaduz	01.01.1980 00:00	24.09.2015 23:00	✓	✓

C.3.10 Meteorological stations for the Oberried/Lenk catchment

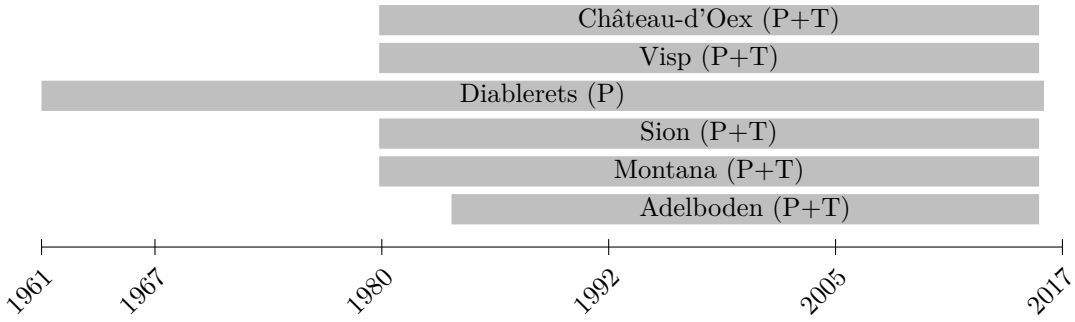

Figure C.17: Graphical data availability period representation for the meteorological stations considered for the calibration and validation for the basin defined by the discharge measurement station *Oberried/Lenk*.

Table C.11: Detailed dates per meteorological station, taken into account for the calibration and validation for the basin defined by the discharge measurement station *Oberried/Lenk*, with indication of the measured quantities.

Station	First value	Last value	Precipitation	Temperature
Adelboden	01.12.1983 00:00	24.09.2015 23:00	✓	✓
Montana	01.01.1980 00:00	24.09.2015 23:00	✓	✓
Sion	01.01.1980 00:00	24.09.2015 23:00	✓	✓
Diablerets	01.01.1961 00:00	30.12.2015 00:00	✓	
Visp	01.01.1980 00:00	24.09.2015 23:00	✓	✓
Château-d'Oex	01.01.1980 00:00	24.09.2015 23:00	✓	✓

C.3.11 Meteorological stations for the Oberwald catchment

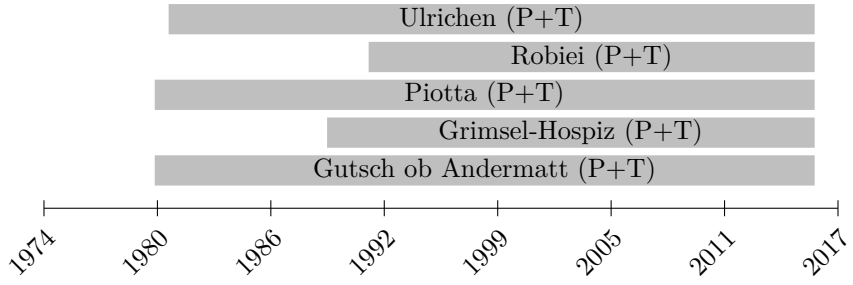

Figure C.18: Graphical data availability period representation for the meteorological stations considered for the calibration and validation for the basin defined by the discharge measurement station *Oberwald*.

Table C.12: Detailed dates per meteorological station, taken into account for the calibration and validation for the basin defined by the discharge measurement station *Oberwald*, with indication of the measured quantities.

Station	First value	Last value	Precipitation	Temperature
Gutsch ob Andermatt	01.01.1980 00:00	24.09.2015 23:00	✓	✓
Grimsel-Hospiz	01.05.1989 01:00	24.09.2015 23:00	✓	✓
Piotta	01.01.1980 00:00	24.09.2015 23:00	✓	✓
Robiei	01.08.1991 00:00	24.09.2015 23:00	✓	✓
Ulrichen	01.10.1980 01:00	24.09.2015 23:00	✓	✓

C.3.12 Meteorological stations for the Rossinière catchment

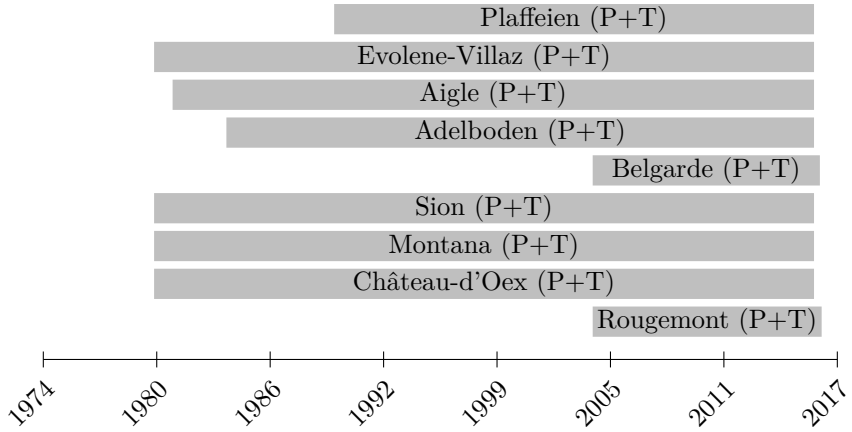

Figure C.19: Graphical data availability period representation for the meteorological stations considered for the calibration and validation for the basin defined by the discharge measurement station *Rossinière*.

Table C.13: Detailed dates per meteorological station, taken into account for the calibration and validation for the basin defined by the discharge measurement station *Rossinière*, with indication of the measured quantities.

Station	First value	Last value	Precipitation	Temperature
Rougemont	01.10.2003 00:00	23.02.2016 00:00	✓	✓
Château-d'Oex	01.01.1980 00:00	24.09.2015 23:00	✓	✓
Montana	01.01.1980 00:00	24.09.2015 23:00	✓	✓
Sion	01.01.1980 00:00	24.09.2015 23:00	✓	✓
Belgarde	01.10.2003 00:00	19.01.2016 00:00	✓	✓
Adelboden	01.12.1983 00:00	24.09.2015 23:00	✓	✓
Aigle	01.01.1981 00:00	24.09.2015 23:00	✓	✓
Evolene-Villaz	01.01.1980 00:00	24.09.2015 23:00	✓	✓
Plaffeien	01.10.1989 01:00	24.09.2015 23:00	✓	✓

C.3.13 Summary of the time series length and subdivision in calibration and validation periods

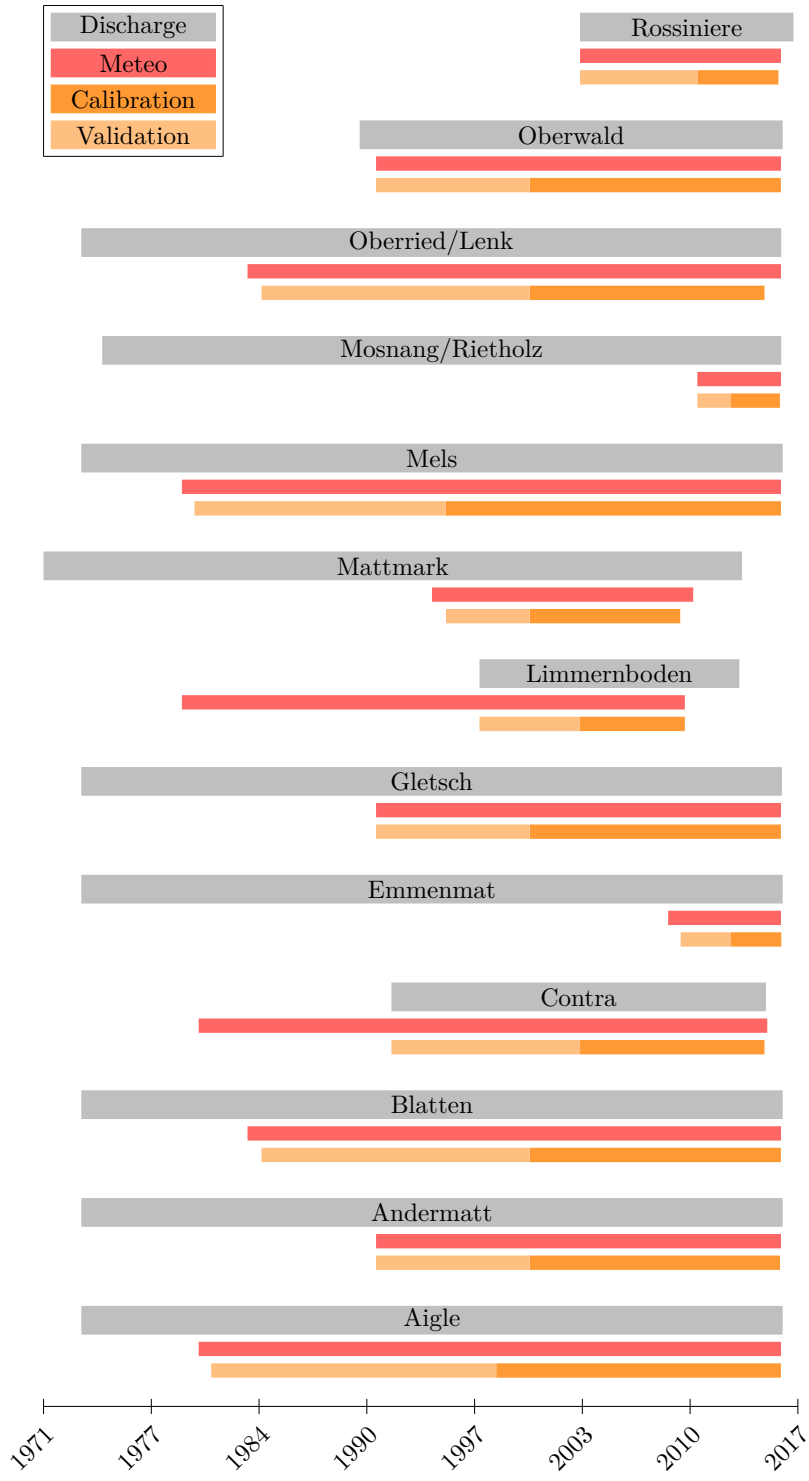

Figure C.20: Illustration of the periods for which the meteorological and discharge data are available as well as the calibration and validation period.

C.4 PMF estimates

C.4.1 Aigle catchment

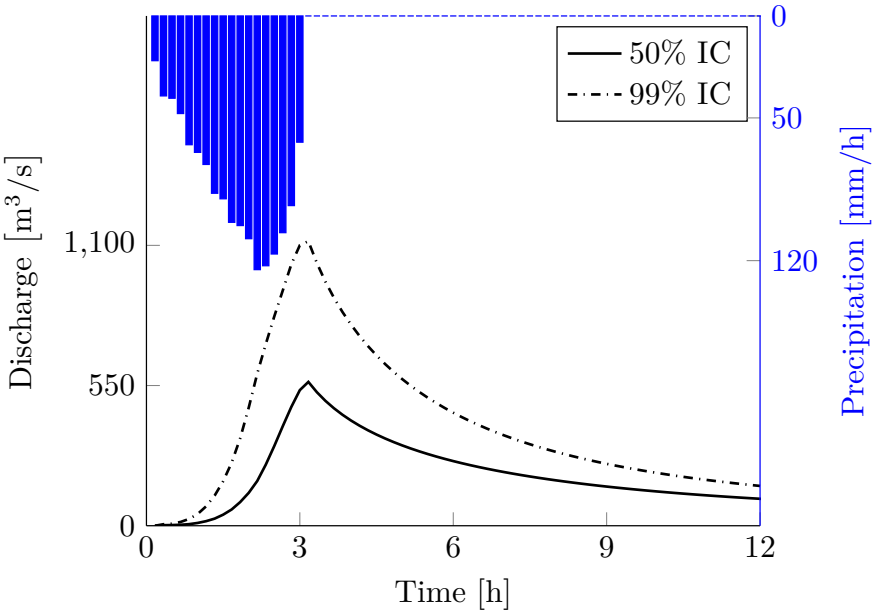

Figure C.21: PMF estimate for the Aigle catchment.

C.4.2 Andermatt catchment

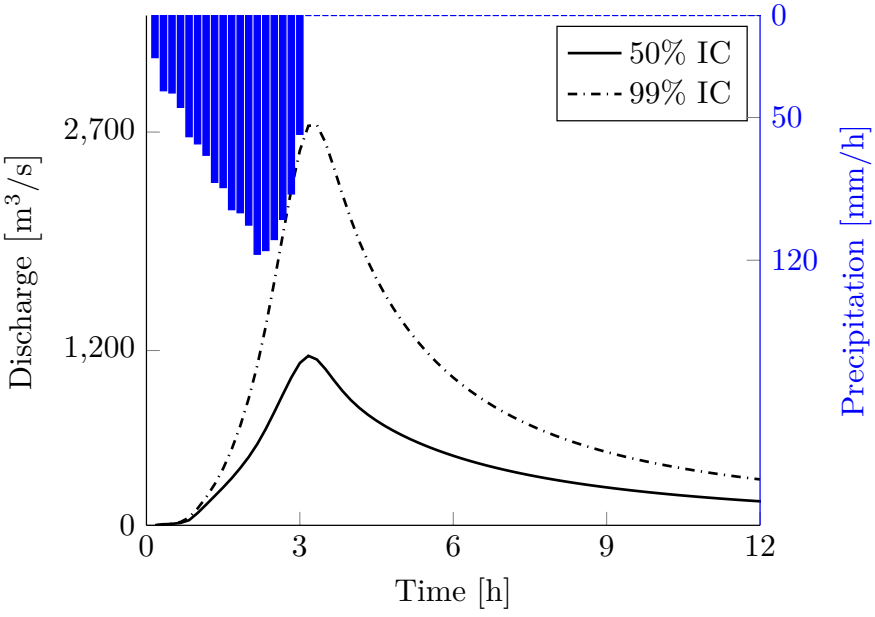

Figure C.22: PMF estimate for the Andermatt catchment.

C.4.3 Blatten catchment

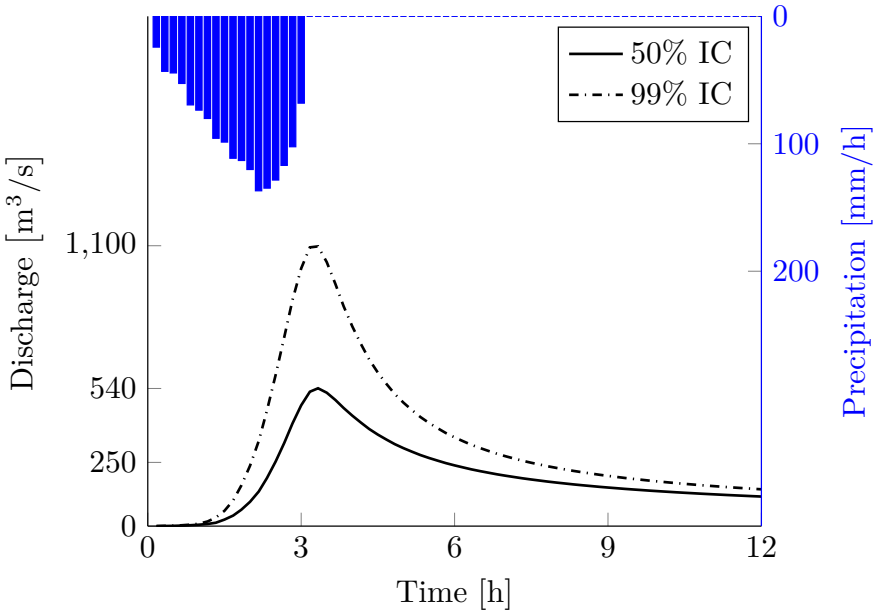

Figure C.23: PMF estimate for the Blatten catchment.

C.4.4 Contra catchment

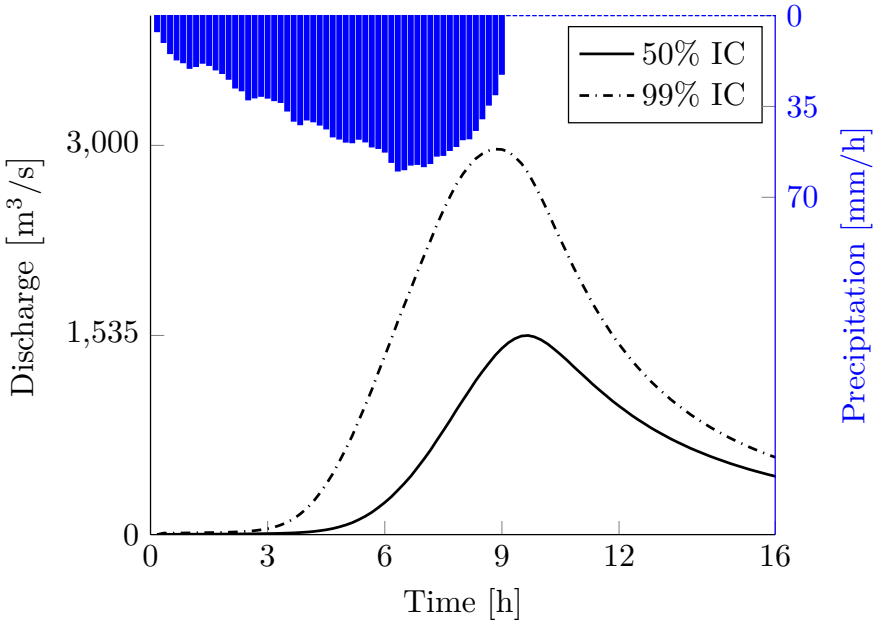

Figure C.24: PMF estimate for the Contra dam catchment.

C.4.5 Emmenmatt catchment

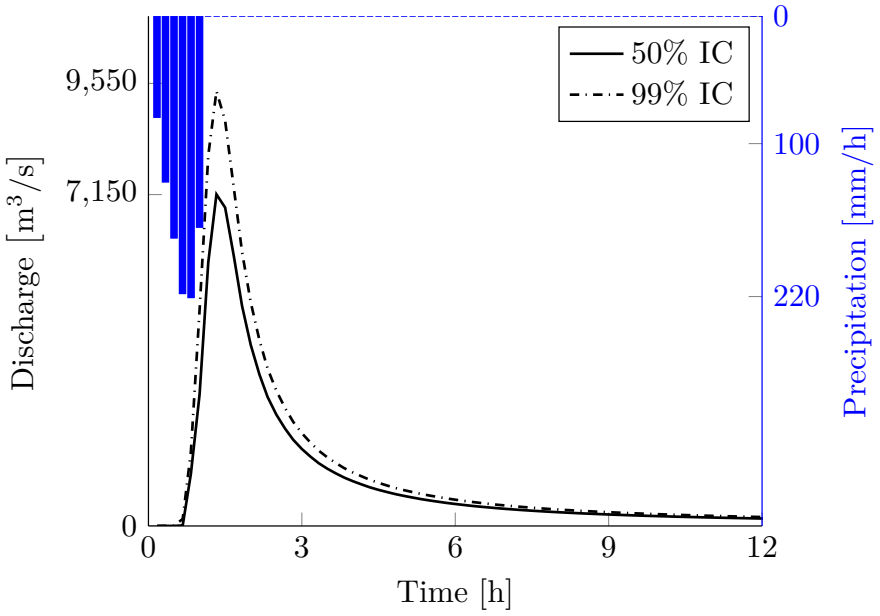

Figure C.25: PMF estimate for the Emmenmatt catchment.

C.4.6 Gletsch catchment

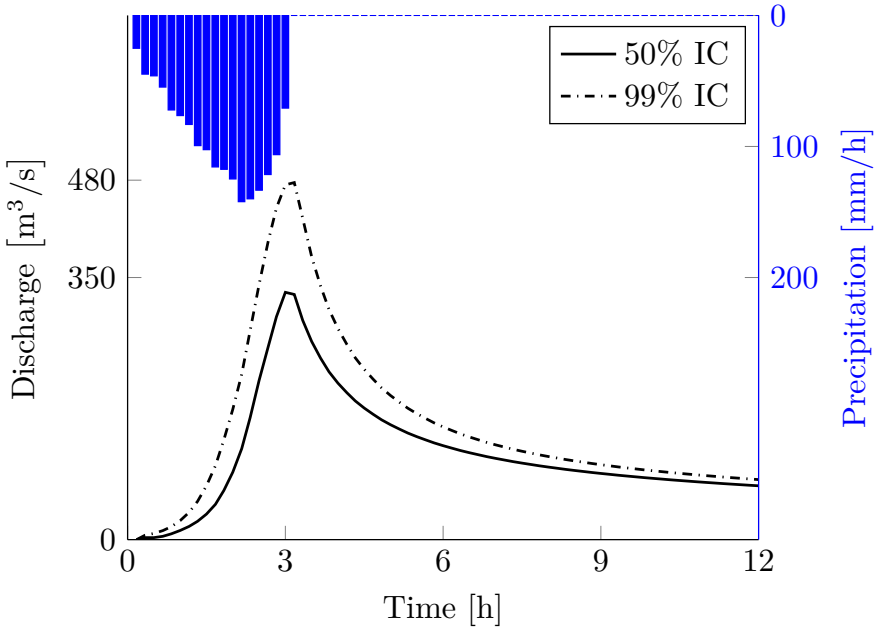

Figure C.26: PMF estimate for the Gletsch catchment.

C.4.7 Limmernboden dam catchment

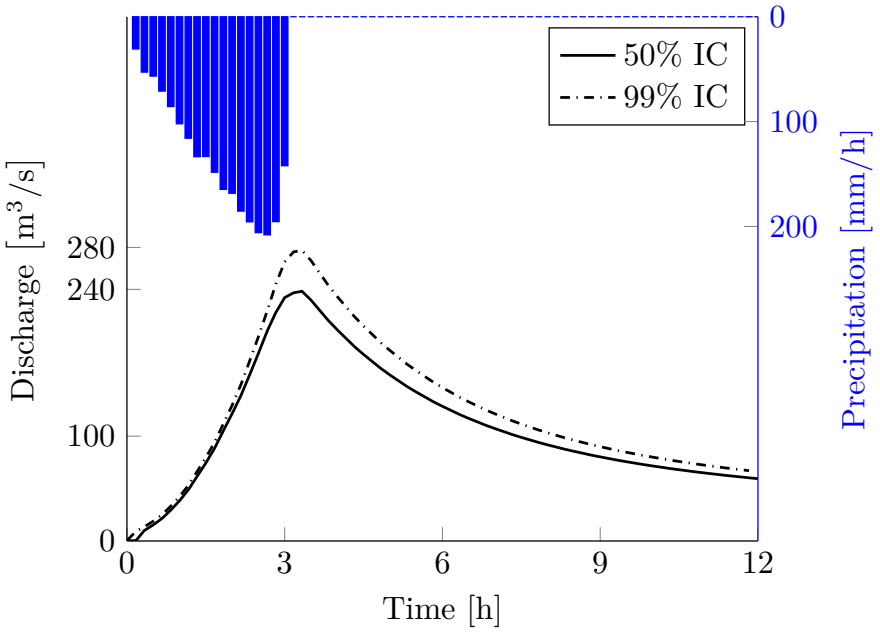

Figure C.27: PMF estimate for the Limmernboden dam catchment.

C.4.8 Mattmark dam catchment

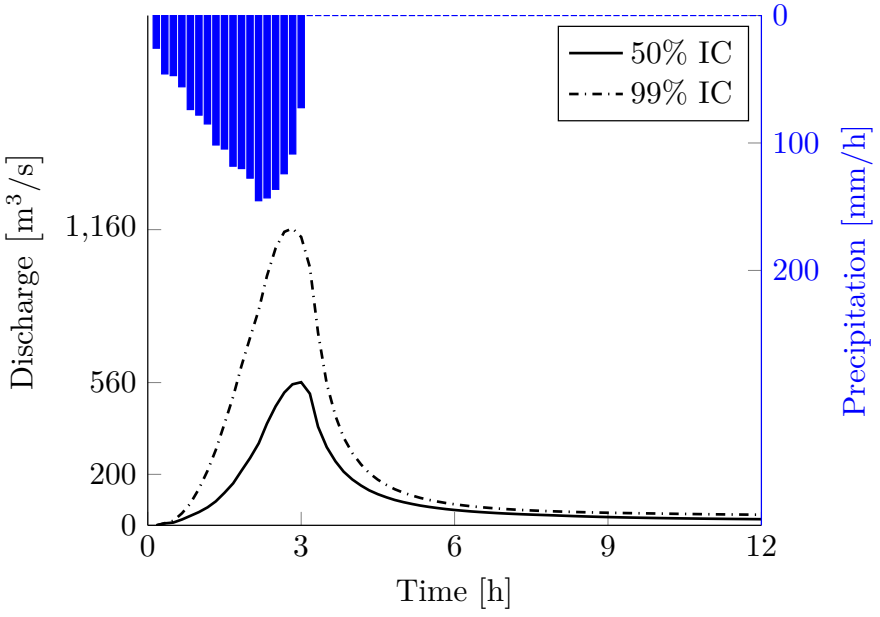

Figure C.28: PMF estimate for the Mattmark dam catchment.

C.4.9 Mels catchment

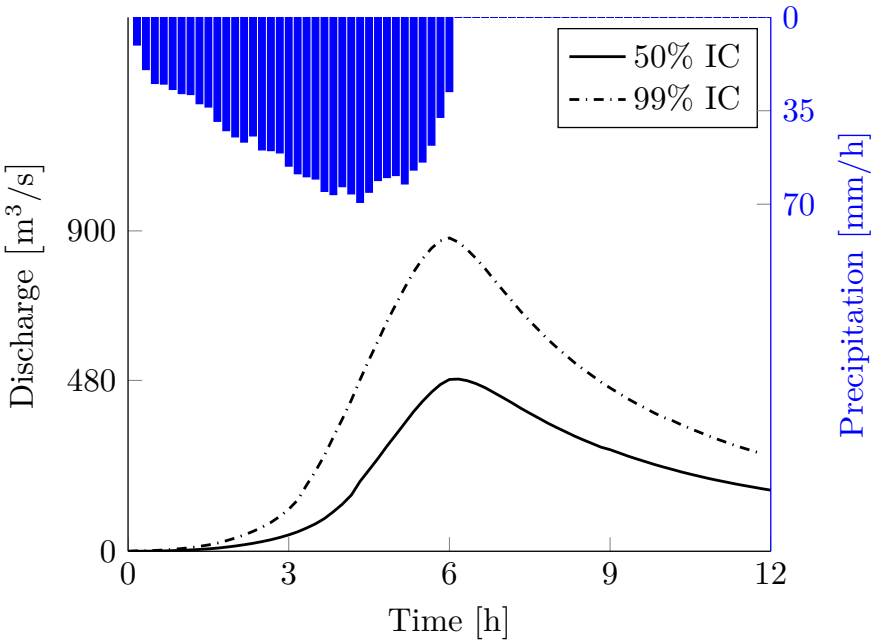

Figure C.29: PMF estimate for the Mels catchment.

C.4.10 Mosnang/Rietholz catchment

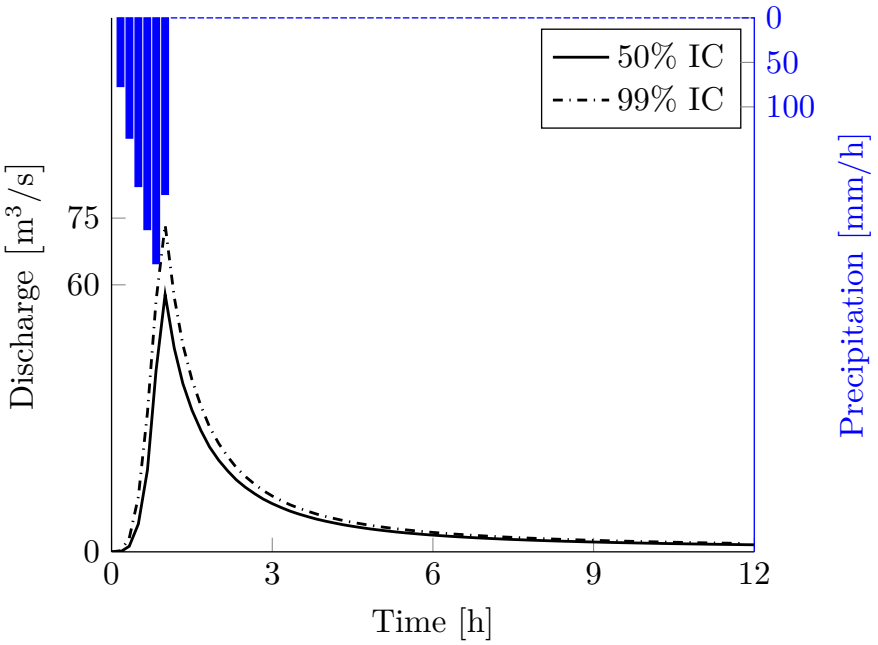

Figure C.30: PMF estimate for the Mosnang/Rietholz catchment.

C.4.11 Oberried/Lenk catchment

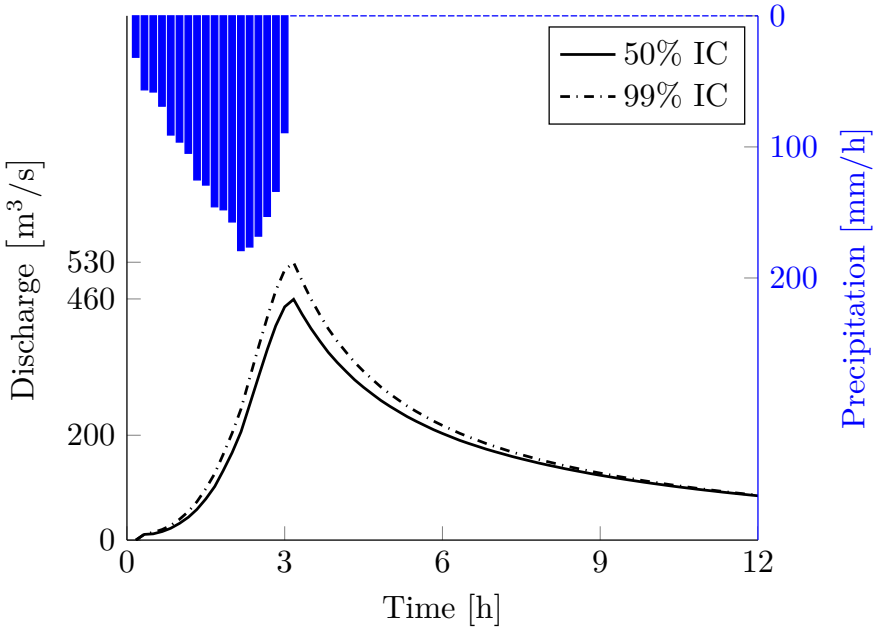

Figure C.31: PMF estimate for the Oberried/Lenk catchment.

C.4.12 Oberwald catchment

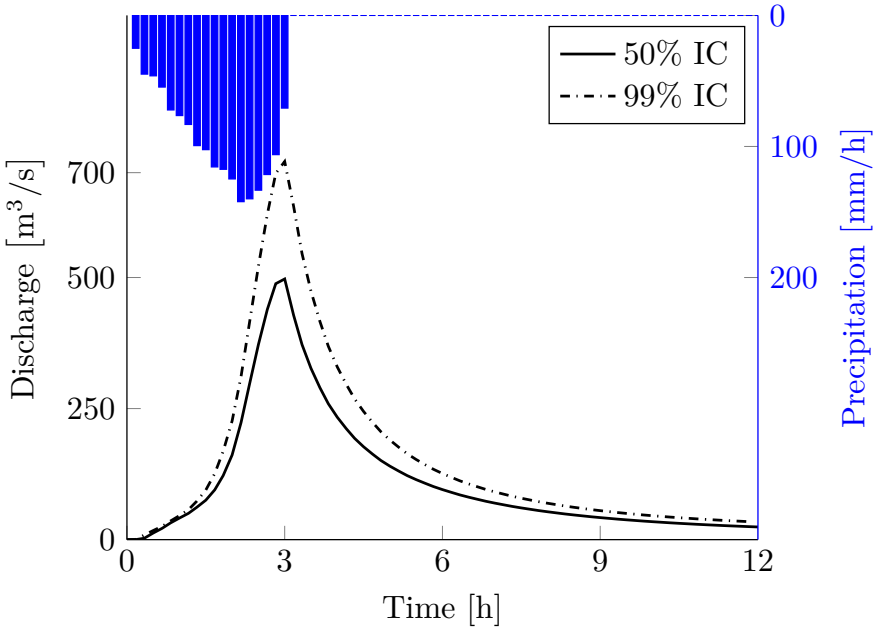

Figure C.32: PMF estimate for the Oberwald catchment.

C.4.13 Rossinière catchment

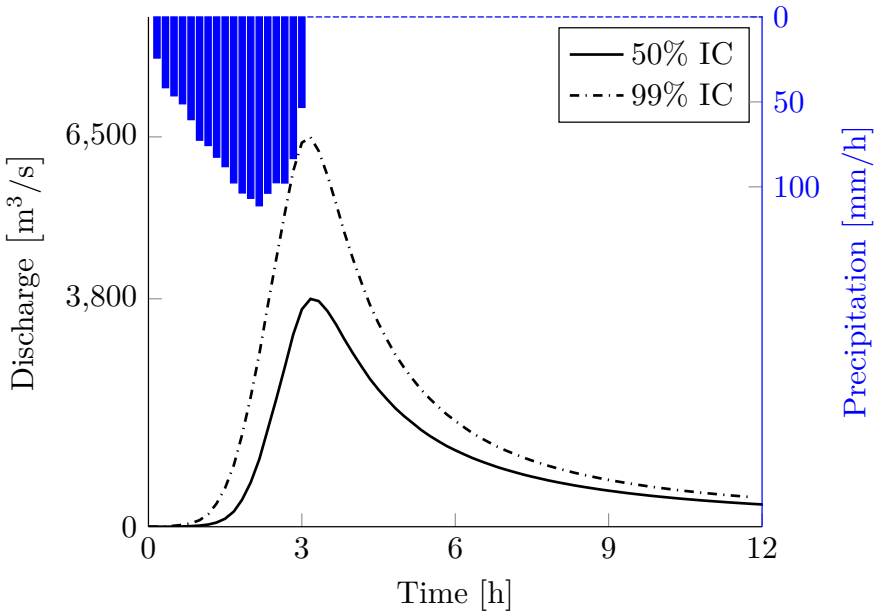

Figure C.33: PMF estimate for the Rossiniere catchment.

D Upper bounded distribution analysis

D.1 Example of a permuted time series

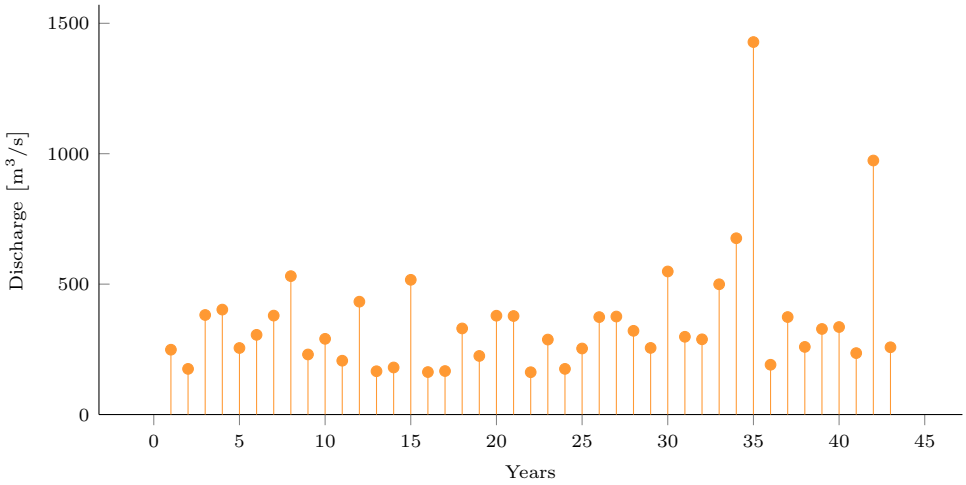

Figure D.1: Permuted time series used for the GEV and EV4 distribution fit shown on Figure 7.6.

D.2 Statistical distributions used for comparison

GEV distribution

The cumulative density function of the GEV is given by equation D.1. Equation D.2 is the expression of the probability density function of the GEV distribution.

$$F(x) = \exp\left\{-\left[1+\xi\left(\frac{x-\mu}{\sigma}\right)\right]^{-1/\xi}\right\} \tag{D.1}$$

$$f(x) = \frac{1}{\sigma}\left(1+\xi\frac{x-\mu}{\sigma}\right)^{-\frac{1}{\xi}-1}\exp\left[-\left(1+\xi\frac{x-\mu}{\sigma}\right)^{-\frac{1}{\xi}}\right] \tag{D.2}$$

where μ is the location parameter, σ the scale parameter, ξ the shape parameter.

Two parameter log-normal distribution

$$F(x) = \Phi\left[\frac{\ln(x-\mu)}{\sigma}\right] \tag{D.3}$$

$$f(x) = \frac{1}{\sqrt{2\pi}(x-\mu)\sigma}\exp\left[-\frac{1}{2}\left(\frac{\ln(x-\mu)}{\sigma}\right)^2\right] \tag{D.4}$$

where μ is the location parameter, σ the scale parameter and Φ the cumulative distribution function of the normal distribution.

E Methodology application

E.1 POT method

For the peak over threshold (POT) method, the Generalized Pareto distribution (GPD) is used. The expression of the cumulative density function and the probability density function are given by Equations E.1 and E.2 respectively.

$$F(x) = 1 - \left(1 + \xi \frac{x-s}{\sigma}\right)^{-1/\xi} \tag{E.1}$$

$$f(x) = \frac{1}{\sigma}\left(1 + \xi \frac{x-s}{\sigma}\right)^{-1/\xi - 1} \tag{E.2}$$

where $x > s$, s is the threshold and ξ is the shape parameter, σ the scale parameter.

The conversion of the quantiles into occurrence probabilities per year is explained in the following lines:

$n_o = \frac{n_d}{n_a}$ and $\zeta_s = \frac{n_s}{n_d}$

where n_d is the number of flood event data in the sample, n_a is the number of years, n_s the number of values above the threshold.

The Generalized Pareto distribution is fitted to the data above the chosen threshold. The quantiles corresponding to a certain return period T are then calculated by

$$x(T) = \begin{cases} s + \frac{\sigma}{\xi}\left[(T n_o \zeta_s)^{\xi} - 1\right] & if\ \xi \neq 0 \\ s + \sigma \ln(T n_o \zeta_s) & if\ \xi = 0 \end{cases}$$

E.2 Model performance coefficients

The Nash-Sutcliffe efficiency of defined by Equation E.3.

$$NS = 1 - \frac{\sum_{t=1}^{T}(Q_o^t - Q_s^t)^2}{\sum_{t=1}^{T}(Q_o^t - \overline{Q_o})^2} \tag{E.3}$$

where Q_o^t is the observed discharge at time t, Q_s^t is the simulated discharge at time t and $\overline{Q_o}$ is the mean observed discharge.

The Kling-Gupta efficiency is estimated by Equation E.4.

$$KGE = r^2(2\alpha - \alpha^2 - \beta^2) \tag{E.4}$$

where $r = \frac{\sum_{t=1}^{T}(Q_o^t - \overline{Q_o})(Q_s^t - \overline{Q_s})}{\sqrt{\sum_{t=1}^{T}(Q_o^t - \overline{Q_o})^2 \sum_{t=1}^{T}(Q_s^t - \overline{Q_s})^2}}$, $\alpha = \frac{\sum_{t=1}^{T}(Q_s^t - \overline{Q_s})^2}{\sum_{t=1}^{T}(Q_o^t - \overline{Q_o})}$ and $\beta = \frac{\overline{Q_s} - \overline{Q_o}}{\sum_{t=1}^{T}(Q_o^t - \overline{Q_o})}$. $\overline{Q_s}$ is the mean simulated discharge.

The volume ration is calculated with Equation E.5.

$$VR = \frac{V_s}{V_o} \tag{E.5}$$

Where V_s is the simulated volume and V_o the observed volume.

E.3 Application to the Limmernboden dam catchment

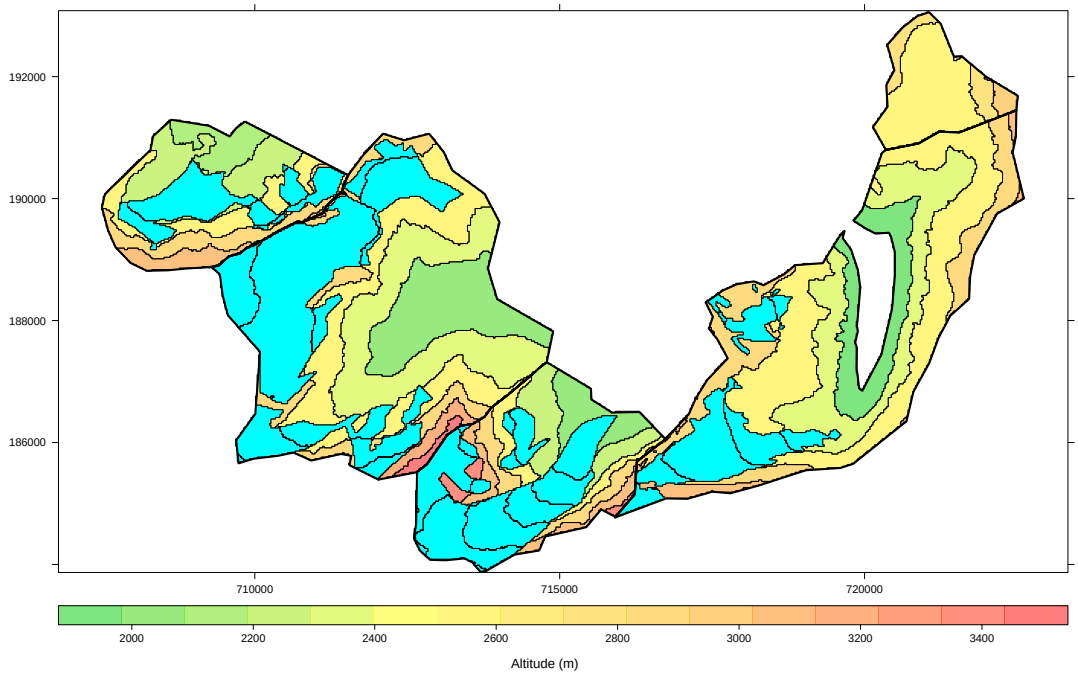

Figure E.1: Subdivision of the Limmernboden dam catchment in altitude bands with a vertical resolution of 300m. The glacier cover is shown in blue-green.

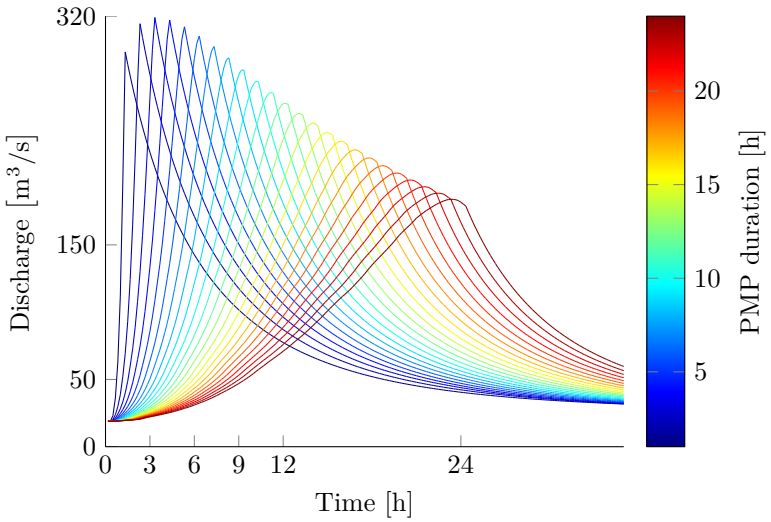

Figure E.2: Hydrograph estimates for the Limmernboden dam derived from different PMP events with wind sector "north". The simulation has been made with a 10 minutes time step and 99% quantile initial values.

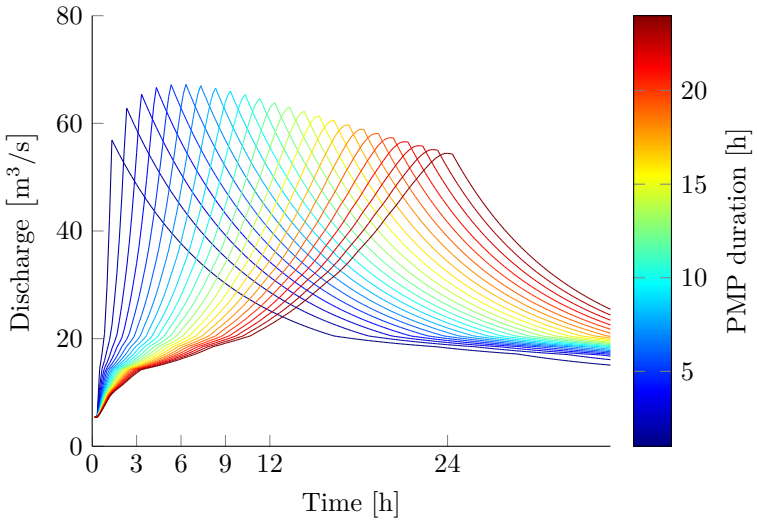

Figure E.3: Hydrograph estimates for the Limmernboden dam derived from different PMP events with wind sector "north". The simulation has been made with a 10 minutes time step and 50% quantile initial values.

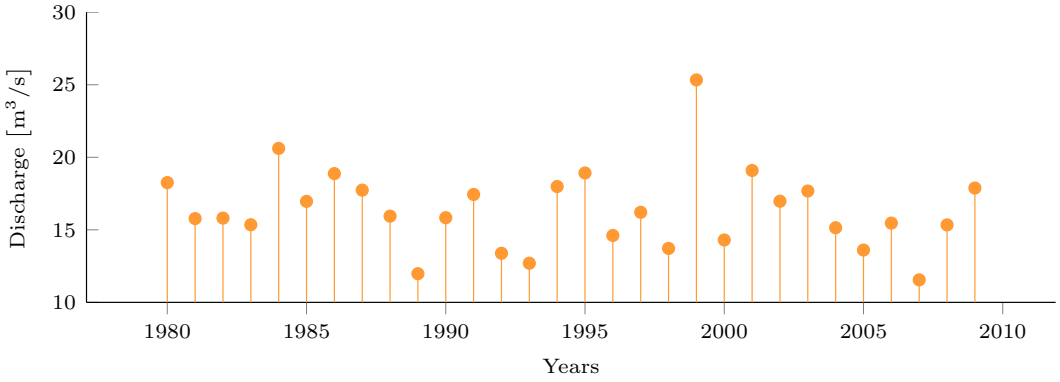

Figure E.4: Maximum annual discharges generated with the hydrological model with an hourly temporal resolution for the catchment of the Limmernboden dam.

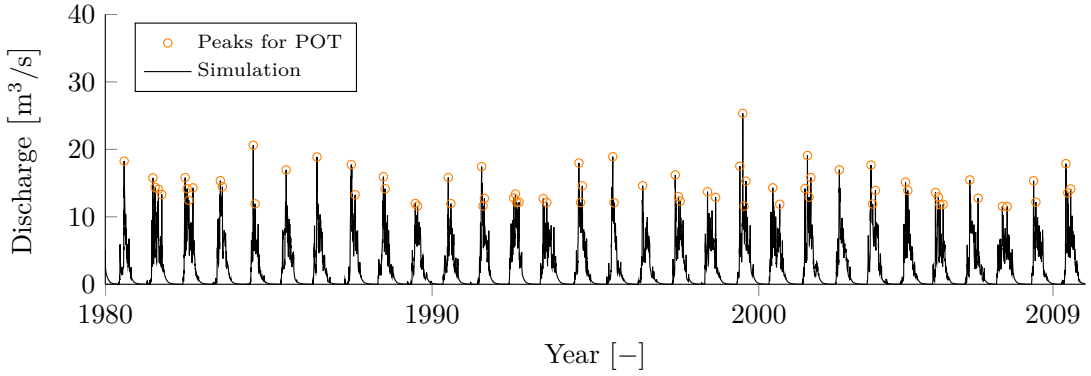

Figure E.5: Peak discharges over the threshold $u = 11.5\,\mathrm{m}^3/\mathrm{s}$ generated with the hydrological model with an hourly temporal resolution for the catchment of the Limmernboden dam.

Table E.1: Parameters of the distribtuions estimated to fit the generated extremes for the Limmernboden dam. GP stands for General Pareto, the distribution used in the case of the POT method.

GEV	GP	log-normal	LN4
$\mu = 15.182$	$\sigma = 3.353$	$\mu = 2.781$	$\mu_Y = -2.775$
$\sigma = 2.362$	$\xi = -0.136$	$\sigma = 0.165$	$\sigma_Y = 0.173$
$\xi = -0.082$			$a = 0$

E.4 Application to the Mattmark dam catchment

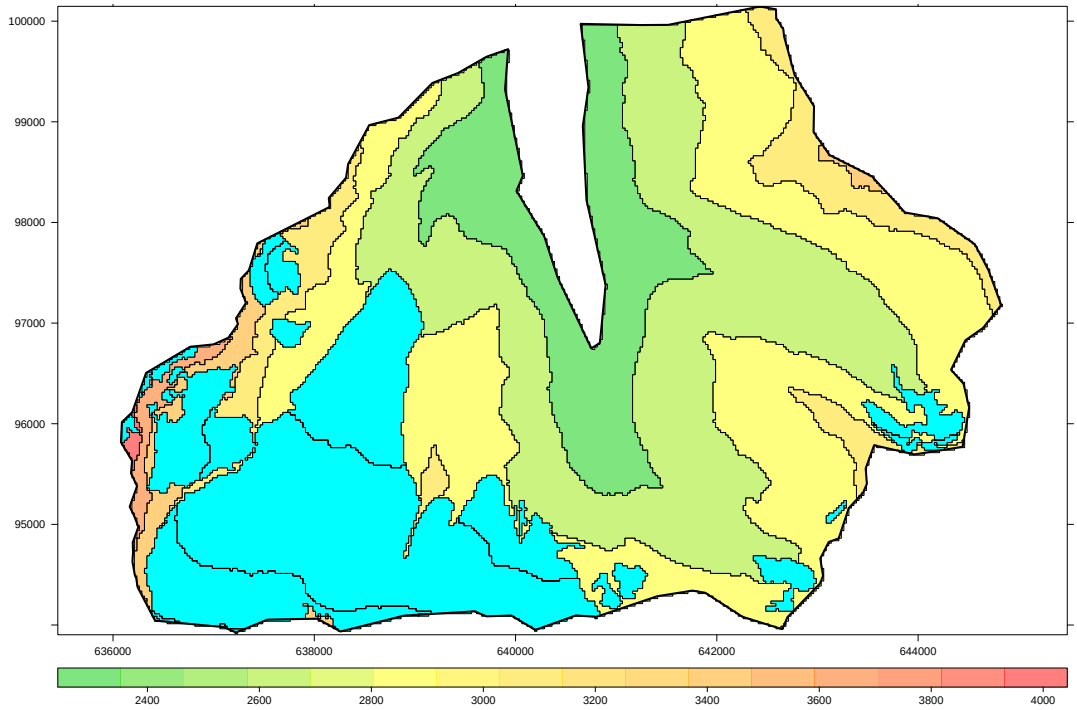

Figure E.6: Subdivision of the main Mattmark dam catchment in altitude bands with a vertical resolution of 300m. The glacier cover is shown in blue-green.

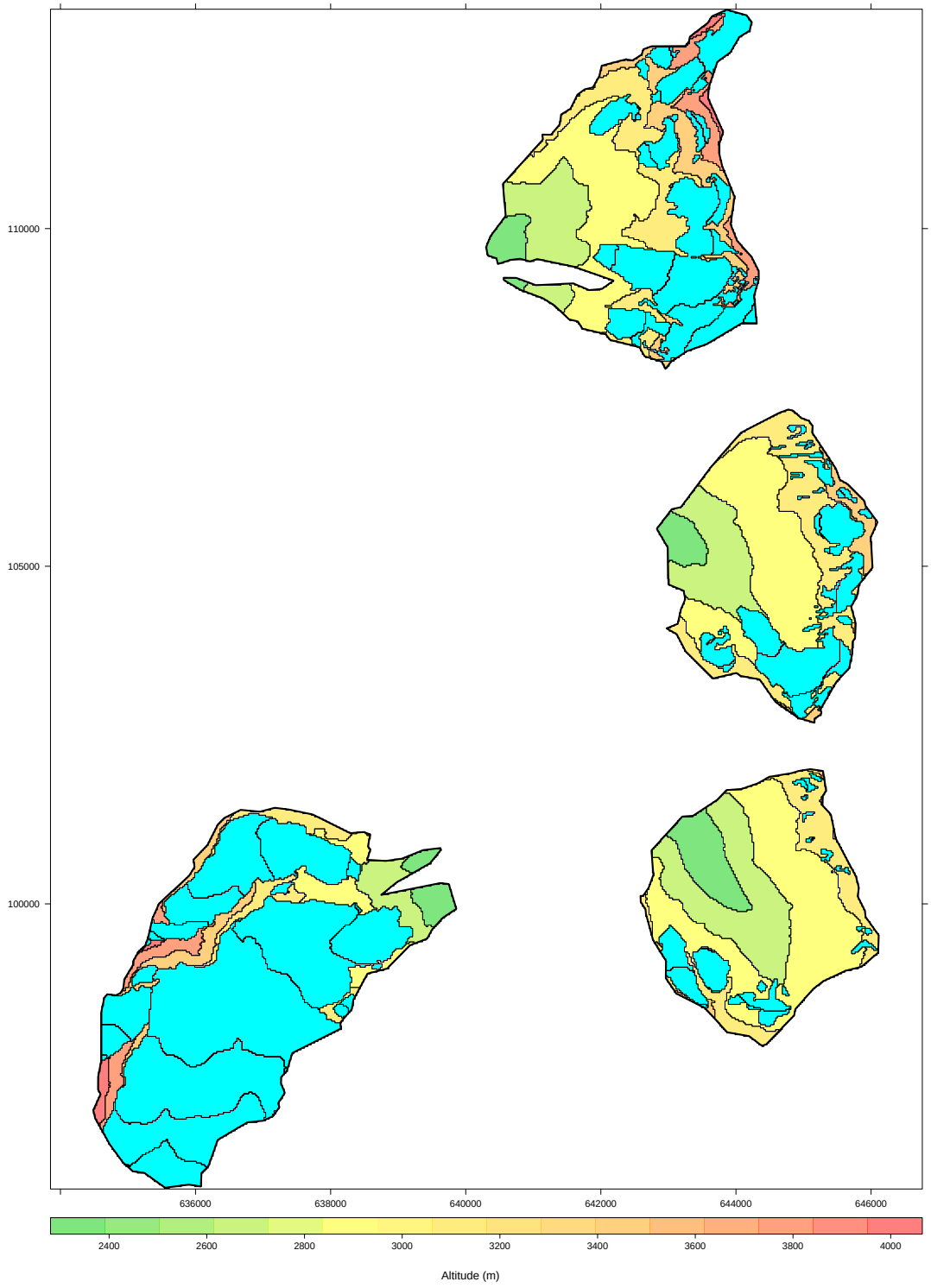

Figure E.7: Subdivision of the lateral Mattmark catchments in altitude bands with a vertical resolution of 300m. The glacier cover is shown in blue-green.

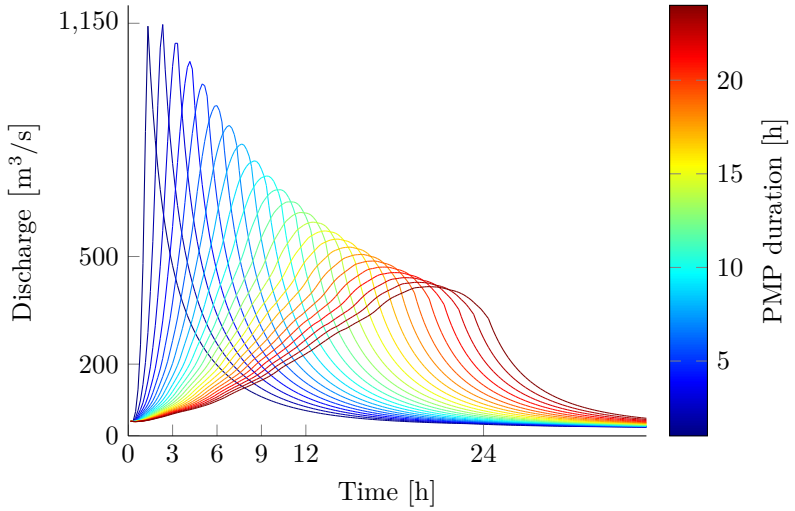

Figure E.8: Hydrographs derived from different PMP events with wind sector "south". The simulation has been made with a 10 minutes time step and 99% quantile initial values.

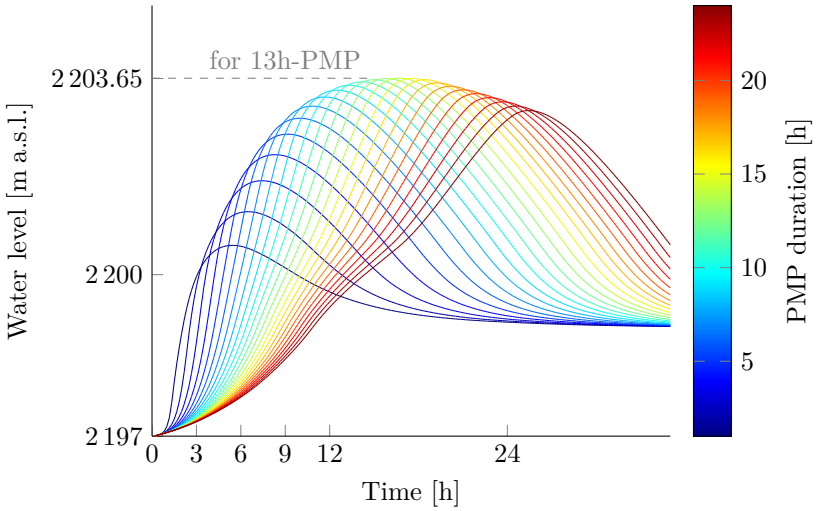

Figure E.9: Mattmark dam lake water level estimates for different PMP events (wind sector "south") for 99% quantile initial values. The maximum level is reached for a 13h-PMP event.

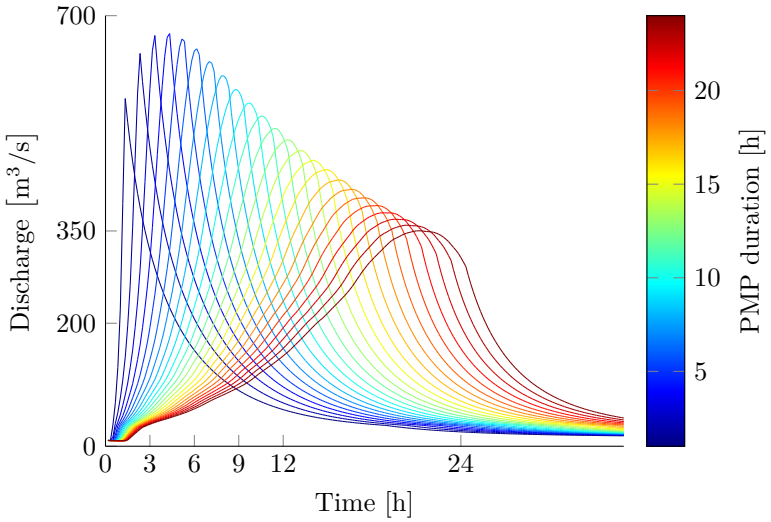

Figure E.10: Hydrographs derived from different PMP events with wind sector "south". The simulation has been made with a 10 minutes time step and 50% quantile initial values.

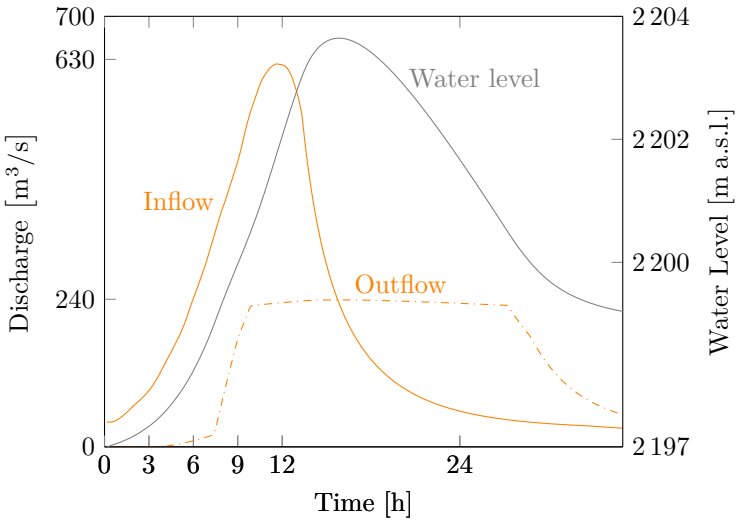

Figure E.11: Lake water level for different PMP events (wind sector "south") for 99% quantile initial values. The maximum level is reached for a 13h-PMP event.

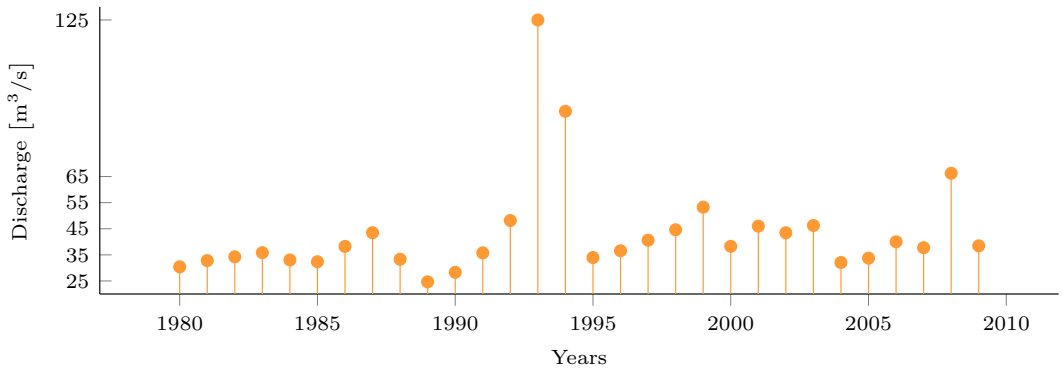

Figure E.12: Maximum annual discharge generated with the hydrological model with an hourly temporal resolution for the Mattmark dam.

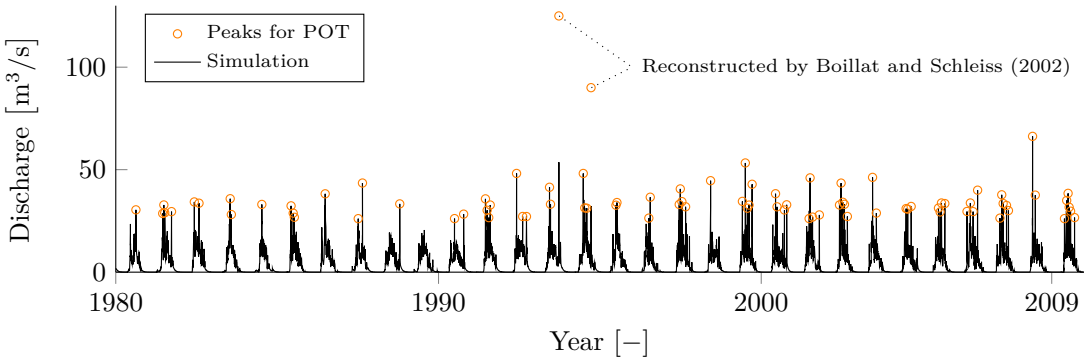

Figure E.13: Peak discharges over the threshold $u = 26\,\mathrm{m}^3/\mathrm{s}$ generated with the hydrological model with an hourly temporal resolution for the catchment of the Mattmark dam.

Table E.2: Parameters of the distributions estimated to fit the generated extremes for the Mattmark dam. GP stands for Generalized Pareto, the distribution used in the case of the POT method.

GEV	GP	log-normal	EV4
$\mu = 35.24$	$\sigma = 7.741$	$\mu = 3.653$	$\nu = 36.87$
$\sigma = 7.712$	$\xi = 0.169$	$\sigma = 0.2096$	$k = 3.287$
$\xi = 0.283$			$a = 9.1$

E.5 Application to the Contra dam catchment

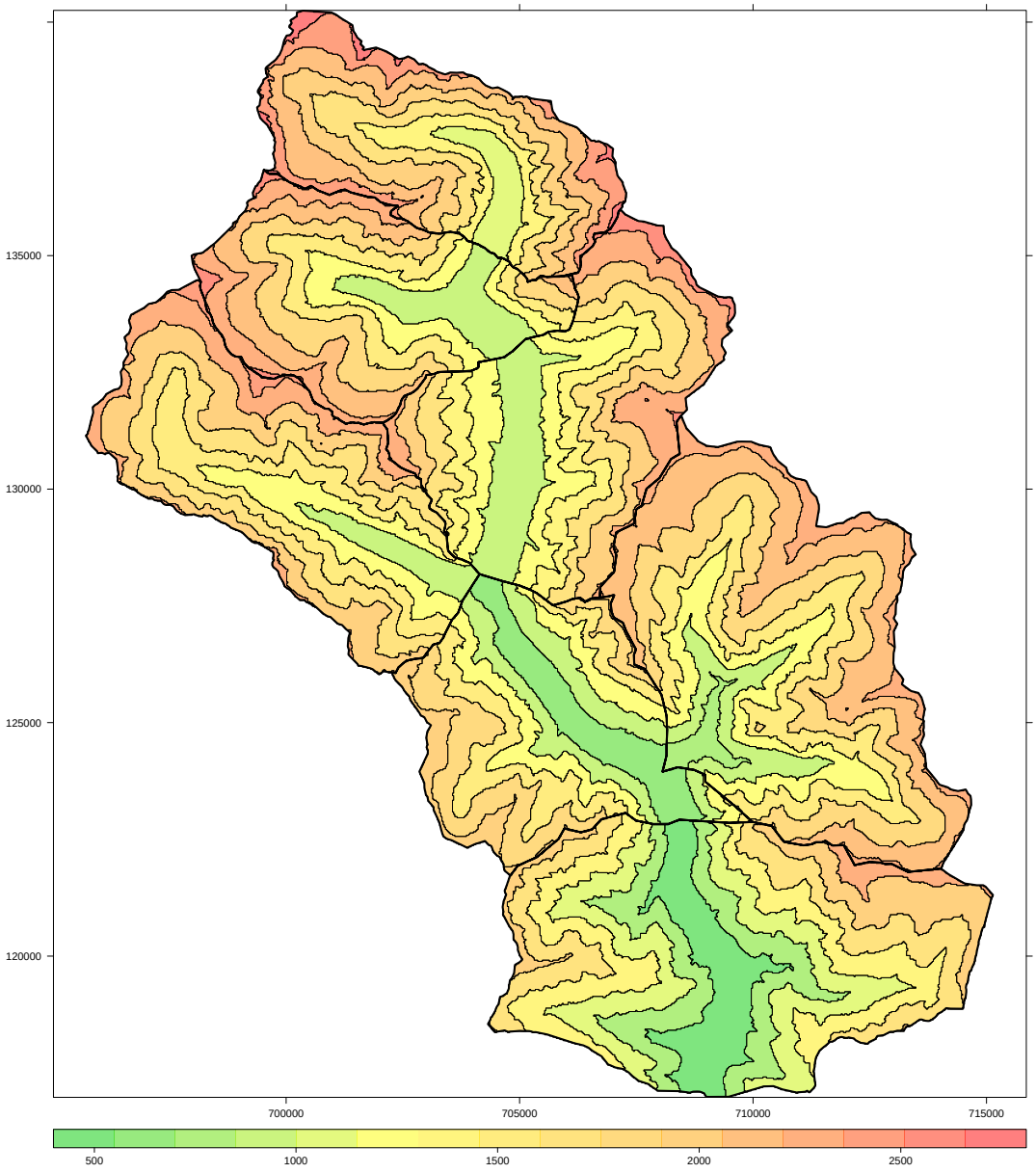

Figure E.14: Subdivision of the Contra dam catchment in altitude bands with a vertical resolution of 300m.

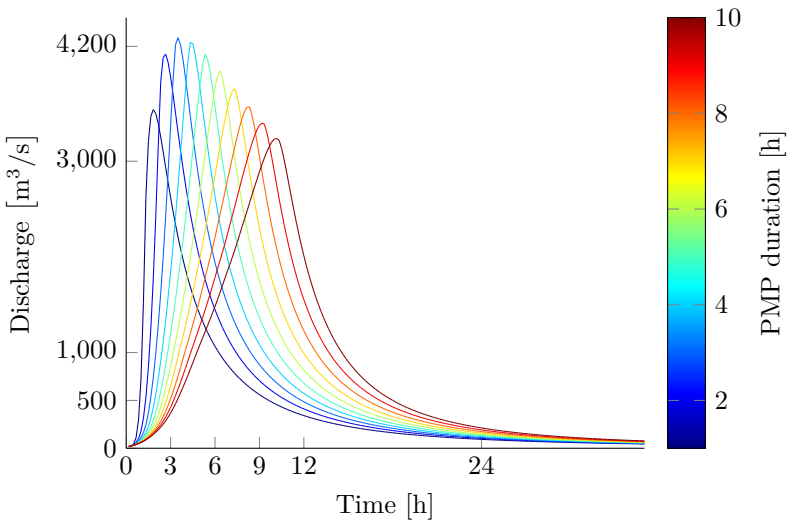

Figure E.15: Hydrographs derived from different PMP events with wind sector "south". The simulation has been made with a 10 minutes time step and 99% quantile initial values for the Contra dam catchment.

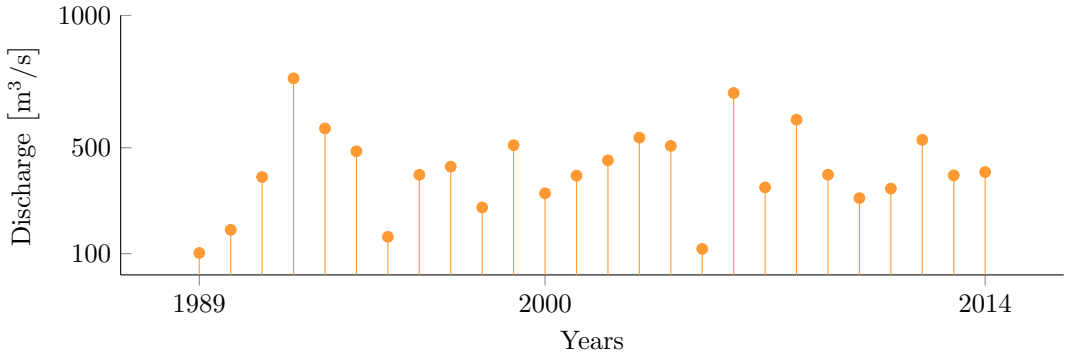

Figure E.16: Maximum annual discharge for the Contra dam catchment derived by scaling the discharges observed at the measurement station Campioi-Lavertezzo with a factor of $\sqrt{\frac{A_{tot}}{A_{CL}}} = 1.12$ ($A_{tot} = 233\ km^2$ is the total catchment area and $A_{CL} = 186\ km^2$ is the catchment area upstream of the Campioi-Lavertezzo observation station).

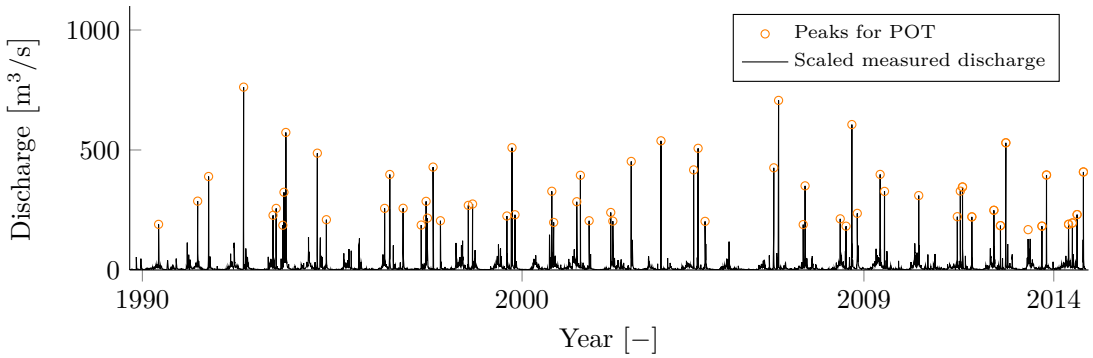

Figure E.17: Peak discharges over the threshold $u = 180\,\mathrm{m}^3/\mathrm{s}$ generated by scaling the discharges observed at the measurement station Campioi-Lavertezzo with a factor of $\sqrt{\frac{A_{tot}}{A_{CL}}} = 1.12$ ($A_{tot} = 233\ km^2$ is the total catchment area and $A_{CL} = 186\ km^2$ is the catchment area upstream of the Campioi-Lavertezzo observation station).

Table E.3: Parameters of the distributions estimated to fit the scaled observed extremes for the Contra dam. GP stands for Generalized Pareto, the distribution used in the case of the POT method.

GEV	GP	log-normal	LN4
$\mu = 353.34$	$\sigma = 147.812$	$\mu = 5.917$	$\mu_Y = -2.295$
$\sigma = 159.91$	$\xi = -0.0511$	$\sigma = 0.498$	$\sigma_Y = 0.530$
$\xi = -0.276$			$a = 0$

Acknowledgements

The writing of the acknowledgements is certainly one of the most difficult tasks of a doctoral thesis, but one of the most satisfying at that. Getting to this point means that the accomplishment of this four years' endeavour is near.

A few years ago, I participated in a bet to remember 500 decimals of the famous mathematical constant π. To my utter surprise, I succeeded. Does this mean that my memory cannot fail? Certainly not! Today, I can only recall seven decimal places (π=3.1415926). I forgot most of it. The human memory is naturally intermittent. For instances, neuroscientists know that emotionally painful moments are far easier to remember than agreeable ones. I thus serenely recognize my incapability to remember all of the great people that deserve to be mentioned here. If life is like music, then remembering people is like remembering a symphony. Without any problem, you can recall the melody. Yet, citing the harmony, that gives the music its taste and uniqueness, is far more difficult. Even so, one has no problem to recognize it. Nietzsche's statement about the bright side of the intermittency of the human memory deploys its full significance when comparing it to music.

> *The advantage of a bad memory is that one enjoys several times the same good things for the first time.*
>
> — Friedrich Nietzsche

First of all, I would like to sincerely thank the Swiss Federal Office of Energy (SFOE), represented by Dr. Georges Darbre and Dr. Markus Schwager, for funding this research work.

I would like to express my special appreciation and thanks to Prof. Dr. Anton J. Schleiss for his precious advices, his encouragements, his trust in me, his permanent availability and the pleasant ambiance he created at the Laboratory of Hydraulic Constructions (LCH).

Cordial thanks are due to the scientific collaborators Dr. Javier García Hernández from *Centre de recherche sur l'environnement alpin (CREALP)* as well as Dr. Fred Jordan and Dr. Guillaume Artigue from the consulting firm *e-dric.ch*, Dr. Jacques-André Hertig, who unfortunately passed away during the project, and Dr. Jean-Michel Fallot from the consulting firm *Hertig & Lador SA* and Dr. Ramona Receanu from *LCH*. I also thank the president of the jury, Prof. Christophe

Ancey, and the examiners, Prof. Bettina Schaefli, Prof. Peter Molnar and Dr. Georges Darbre for their interesting discussion of the work presented herein.

I have the same gratitude towards my colleagues from *LCH* of whom I would like to mention some in particular: Alain, Ana Clara, Ana Margaritha, Azin, Bettina, Carmelo, Caroline, Cédric, David, Davide, Dora, Emilie, Felix, Gesualdo, Giovanni, Guillaume, Irene, Iria Rita, Ivan, Marc-Eric, Mário, Matthias, Michael, Michel, Mona, Nicolas, Paloma, Pedro, Pierre, Raphaël, Sabine, Sara, Scarlett, Sebastian, Sebastian G., Severin, Stéphane, Tamara, Theodora, Violaine.

I would also like to thank Alex, a very good friend, with whom I finally spend 9 years at EPFL, first as civil engineering students, then as flatmate and colleague at LCH. Special thanks are also due to my three office mates Elena, Rafael and Zé (José Pedro Matos). We had a very good time with lots of helpfulness and fun.

A great thank is also due to the designers of the CRUEX++ logo from *Fondation Le Relais*.

E ganz groussen Merci gëllt natierlech och menge Lëtzebuerger Frënn, déi ech hei zu Lausanne kenne geléiert hunn. Si ware fir vill Motivatioun a schéi Momenter verantwortlech. Ech si frou, datt ech ëmmer op si ziele kann!

Och wann e puer Zeilen net duergi fir e Merci auszedrécken deen deem gerecht gëtt woufir ë steet, geet dach dee gréisste Merci u meng Famill. Nëmmen duerch si all konnt ech esou wäit kommen. Si hu mech ëmmer an Allem ënnerstëtzt a mech motivéiert. Näischt wa hinnen ze vill wann ech emol e schwéiere Moment während menge Studien hat, an dat obwuel et och fir si net einfach wa, datt eng Häerd Kilometeren tëschent eis waren. Si waren ëmmer fir mech do.

Zu gudder Lescht, dann elo dat Bescht. Jessica, je te remercie infiniment, pour ton soutien, ta douceur et ton amour, que tu m'as fait découvrir au cours de ces dernières années. Avec ta façon motivante et ton attitude positive, tu m'as poussé vers la réussite de ce travail. Je t'aime beaucoup.

Lausanne, 06 October 2016 F. Z.

Communications du Laboratoire de Constructions Hydrauliques ISSN 1661-1179
Ecole Polytechnique Fédérale de Lausanne
Editeur: Prof. Dr A. Schleiss

N° 55 2013 E. Person
Impact of hydropeaking on fish and their habitat

N° 56 2013 T. Cohen Liechti
Influence of dam operation on water resources management under different scenarios in the Zambezi River Basin considering environmental objectives and hydropower

N° 57 2014 A. M. da Costa Ricardo
Hydrodynamics of turbulent flows within arrays of circular cylinders

N° 58 2014 T. Ghilardi
Sediment transport and flow conditions in steep rivers with large immobile boulders

N° 59 2014 R. Duarte
Influence of air entrainment on rock scour development and block stability in plunge pools

N° 60 2014 J. P. Matos
Hydraulic-hydrologic model for the Zambezi River using satellite data and artificial intelligence techniques

N° 61 2015 S. Guillén Ludeña
Hydro-morphodynamics of open-channel confluences with low discharge ratio and dominant tributary sediment supply

N° 62 2016 M. Jafarnejad Chaghooshi
Time-dependent failure analysis of large block size riprap as bank protection in mountain rivers

N° 63 2016 S. Terrier
Hydraulic performance of stepped spillway aerators and related downstream flow features

N° 64 2016 M. Ostad Mirza
Experimental study on the influence of abrupt slope changes on flow characteristics over stepped spillways

N° 65 2016 I. Almeida Samora
Optimization of low-head hydropower recovery in water supply networks

N° 66 2016 D. Ferràs Segura
Fluid-structure interaction during hydraulic transients in pressurized pipes: experimental and numerical analyses

N° 67 2016 E. Battisacco
Replenishment of sediment downstream of dams: Erosion and transport processes

N° 68 2017 F. Zeimetz
Development of a methodology for extreme flood estimations in alpine catchments for the verification of dam safety

ISSN 1661-1179

DOI: 10.5075/epfl-lchcomm-68

Prof. Dr A. Schleiss
Laboratoire de constructions hydrauliques - LCH
EPFL, Bât. GC, Station 18, CH-1015 Lausanne
http://lch.epfl.ch
e-mail: secretariat.lch@epfl.ch